Université d'Ottawa · University of Ottawa

Steady State Behaviour of Sands and Limitations of the Triaxial Test

Huiming Zhang, B. Sc., M. Sc.

A Dissertation
Submitted to School of Graduate Studies
Under the supervision of

Dr. Vinod K. Garga, P. Eng., F. EIC.

in partial fulfillment of the requirements for the degree of

Doctor of Philosophy in Civil Engineering

Department of Civil Engineering
University of Ottawa
Ottawa, Ontario
Canada K1N 6N5

March 1997

The Doctor of Philosophy in Civil Engineering is a joint program between Carleton University and University of Ottawa, which is administered by the Ottawa-Carleton Institute for Civil Engineering

0-612-21979-8

To my children

Jieling, Eileen and Vincent

ACKNOWLEDGMENTS

The author would like to express his sincere appreciation to his research advisor, Dr. Vinod K. Garga, for his continuous support, generous advice, invaluable guidance throughout this program of research. The author also wishes to sincerely thank Dr. K. Tim Law, Dr. Erman Evgin and Dr. B. H. Fellenius for serving as members on various examination committees during this study.

The financial supports from the University of Ottawa and from the Natural Sciences and Engineering Research Council of Canada (NSERC) are gratefully acknowledged.

Thanks to all support staff in the Department of Civil Engineering, especially to Mr. Richard J. Moore, for his excellent technical support in the experimental program.

The author would like to especially thank his previous advisor, Professor Zhao-Jun Lu, and his teachers, Professors Jing Zhou and Chanwen Yang, of the China Academy of Railway Sciences, who gave the author the invaluable training in Geotechnical Engineering.

The author is indebted to his parents for their encouragement, support and understanding throughout his education. Many thanks are also extended to his brothers and sisters, particularly to Muzhen and her husband, Chiyao, for their support and encouragement.

Finally, it is the author's wife, Hong, whose encouragement, patience and understanding made this PhD study successful. The supports from his parents-in law are also appreciated.

ABSTRACT

Steady state strength is an important parameter in evaluating the stability of sand deposits against flow sliding. Most loose sands exhibit the so called quasi-steady state behaviour in undrained triaxial tests, in which no unique ultimate shear resistance can be reached. This study focused on why the quasi-steady state behaviour occurs and how to determine the steady state strengths of sand samples with the quasi-steady state behaviour in triaxial tests. The main contributions in this study are as follows:

- The quasi-steady state behaviour may not be an inherent behaviour of sands, but is primarily caused by end restraint which results from the friction between end platens and sample. The main effect of end restraint in triaxial tests on sands is decreasing pore pressure under undrained loading or increasing sample volume under drained loading. The QSS behaviour may also result from volume change during undrained loading.

- There are four deformation stages in an undrained triaxial test on a loose sand sample: initial stage, collapse stage, critical stress stage and post failure stage. The strain rate in the test remains constant in a deformation stage, but is different in various deformation stages. The steady state strength occurs in the collapse stage.

- A modified definition of the steady state of deformation is suggested as follows

  The steady state of deformation for any mass of particles is that state in which the mass is continuously deforming at constant volume, constant normal effective stress, constant shear stress, and constant velocity. **The constant shear stress is the minimum strength of the mass, which is dependent on the local void ratio within shear zone.**

- The steady state strength should be determined, based on the modified definition of the steady state, by considering all test information including shear stress, pore pressure, strain rate, and effective stress path under undrained loading condition or volume change under drained loading condition.

- The error in steady state strengths determined in triaxial tests is affected by the coefficient of uniformity of a sand. The error for a sand with a 2.5 coefficient of uniformity can be 5 times that for a sand with a coefficient of uniformity lower than 1.8.

- The volume changes of a moist tamped sand sample during saturation can be over 0.025 in terms of void ratio for the Unimin sand.

- The volume change of a sand sample during undrained loading results from the compression of pore fluid and the variation of membrane penetration. The volume change due to the variation of membrane penetration is about 4 times that due to pore fluid compression.

- A new method of area correction in triaxial tests was developed. The average diameter over the middle portion of a sample is dependent on axial strain, volumetric strain, end radial strain, and the length of the middle portion. A middle third average diameter is suggested to be used in the calculation of deviator stress in triaxial tests. The error in deviator stress due to using the conventional area correction can be over 10 % at large axial strain under fixed end condition.

TABLE OF CONTENTS

LIST OF TABLES

LIST OF FIGURES

NOTATIONS

A_m	Peripheral area of a sample
A_{mc}	Peripheral area of a sample at consolidation
α	The angle between vertical direction and major stress direction
α_{us}'	The angle of failure envelop at steady state, = arctan (τ_s / p_s')
b	Length factor, = L / H
B	Skempton's pore pressure coefficient
CAU	Consolidated anisotropically undrained test
CIU	Consolidated isotropically undrained test
C_c	Compressibility of soil skeleton
CSR	Cyclic stress ratio, = cyclic shear stress / initial vertical effective stress
C_u	Uniformity coefficient
C_v	Compressibility of pore fluid
C_w	Compressibility of water
d	Diameter of a sample
D_0	Initial diameter
D_{50}	Average grain diameter
D_b	Average diameter over middle portion (L = bH) with $\varepsilon_e = 0$
$D_b(\varepsilon_e)$	Average diameter over middle portion (L = bH) with end radial strain = ε_e
D_{ave}	Average diameter
D_e	Diameter at ends of a sample
D_m	Maximum diameter of a sample
Dr_c	Relative density at consolidation
ΔD	Diameter change at ends of sample
e	Void ratio
e_g	granular void ratio, = {volume of voids - volume of soil}/{volume of solid phase}
e_{max}	Maximum void ratio
e_{min}	Minimum void ratio

Er	Error in deviator stress
ε_a	Axial strain
ε_e	End radial strain
ε_v	Volumetric strain
ϕ_{us}'	Effective residual angle of friction
h	The height at calculated point
H	The height of a sample for a given strain
H_0	Initial height of a sample
H_{mold}	The depth of a mold
ΔH	Axial deformation
HRDT	Hall effect radial displacement transducer
G_s	Gravity of soil grains
I_B	Bittleness, $= (S_{up} - S_{ur}) / S_{up}$
κ	Parameter, $= H^2 / \{4(D_m - D_e)\}$
Kc	Consolidation ratio, $= \sigma_{1c}' / \sigma_{3c}'$
L	The length of the middle portion of a sample
L_p	Liquefaction potential, $= (\sigma_{3i}' - \sigma_{3f}') / \sigma_{3f}'$
n	Porosity of soil
$(N_1)_{60}$	Dynamic standard penetration test blow count corresponding to a combined efficiency of 60% normalized to effective overburden pressure of 100 kPa
P	Axial load
p'	Effective mean stress, $= (\sigma_1' + 2\sigma_3') / 3$
p_s'	Mean effective stress at steady state
PT	Phase transformation
q	Deviator stress, $= (\sigma_1 - \sigma_3)$
SSL	Steady state line
S_{up}	Undrained peak strength
S_{ur}	Undrained residual strength
S_{us}	Steady state strength from undrained test
σ_{3i}'	Initial effective minor principal stress

σ_{3f}'	Effective minor principal stress at steady state
τ	Shear stress
τ_{cy}	Cyclic shear stress
τ_p	Peak shear stress, $= \tau_s + \tau_{cy}$
τ_s	Shear stress at steady state
τ_s	Static shear stress
u	Pore pressure
$\mu(\sigma)$	Unit membrane penetration
Δu	Induced pore pressure
V	Volume of a sample
V_0	Initial volume of a sample
ΔV	Volume change of a sample
ΔV_c	Volume change of triaxial cell
ΔV_{crp}	Volume change due to the creep deformation of triaxial cell and cell water
ΔV_m	Volume change due to membrane penetration
ΔV_p	Volume change of cell water due to the movement of loading piston
ΔV_t	Total volume change of cell water
ΔV_w	Volume change of pore fluid

CHAPTER 1

INTRODUCTION

1.1 Statement of the problem

Numerous flow failures due to liquefaction have been reported in literature (Seed et al., 1975, 1978; Seed, 1979b; De Alba et al., 1988; Ishihara, 1993; etc.). Liquefaction of loose, saturated granular soil during earthquakes or other loading sources will continue to be a major cause of destruction of constructed facilities. Under appropriate static or cyclic loading condition, a saturated sand mass may suffer a rapid drop in its shear resistance to a minimum value, the steady state strength, which remains constant with further strain. Thus, there are two important aspects in the undrained behaviour of sands: the triggering condition of the collapse and the undrained residual shear strength. By the middle of 1980s, most of the laboratory investigations on liquefaction of sandy soils were focused on the triggering condition in pore pressure development under undrained cyclic loading. Seed (1987) stated, however, that it may be adequate and economically advantageous to simply ensure the stability of a slope or embankment against flow failure after collapse has been triggered, rather than to prevent triggering. Evaluating the stability of sand mass requires a knowledge of undrained residual strength which sandy soils can mobilize after collapse.

Published data reports the existence of three different stress-strain behaviours of saturated sands in undrained static triaxial tests: strain hardening behaviour, steady state behaviour, and quasi-steady state behaviour (Fig. 1.1). The strain hardening behaviour usually occurs in dense sands, the shear resistance always increases with axial strain. In the steady state behaviour, the shear stress of a sand sample rapidly decreases once its collapse is triggered, and then remains constant with further axial strain. The constant shear stress at the steady state is considered as the undrained residual strength, or the so-called steady state strength of the sample. For a given sand, the steady state strength is only a function of void ratio, independent of sample preparation methods, loading modes, strain rate and drainage condition. Furthermore, the steady state strengths from undrained static loading and from undrained cyclic loading are the same for a given void ratio (Castro et al, 1982; Alarcon-Guzman et al, 1988). The steady state of sands is thus well defined.

In the quasi-steady state behaviour, the shear stress also rapidly decreases after peak and drops to a minimum value; however it remains at this minimum value for a short period and then increases with further strain. In other words, no unique ultimate shear resistance exists in this type of behaviour. The question arises: what is the undrained residual shear strength in this case and why does the shear stress continuously increase at large strain? Furthermore, most loose sands display the quasi-steady state behaviour (Ishihara, 1993; Poulos et al., 1988). From a practical view point, a comprehensive examination of the quasi-steady state behaviour therefore appears to be necessary.

1.2 Research objectives

The main objectives of this experimental study were:

(1) To study the volume changes of sand samples during saturation, consolidation and undrained loading.

(2) To study the error of steady state strength due to the conventional cross-sectional area correction.

(3) To investigate why the quasi-steady state of sands occurs in undrained triaxial tests.

(4) To develop an approach to evaluate the undrained residual strength for sand samples which exhibit quasi-steady state behaviour.

(5) To examine the limitations of the triaxial tests on sands.

1.3 Scope of research

In order to accomplish the research objectives, experimental work was undertaken on the following aspects:

1. Develop devices to improve the accuracy of the void ratio measurement of a sand sample and to provide some apparatus required in this research.

2. Investigate the accuracy of the estimate of void ratio.

4. Conduct membrane penetration tests to investigate the effect of membrane thickness on the membrane penetration during consolidation.

5. Conduct water-air mixture compression tests and B value tests to investigate the degree of saturation of sand samples.

6. Conduct undrained triaxial tests with volume measurement to examine the effect of undrained volume change on steady state strength.

7. Discuss the limitation of constant volume triaxial shear tests and the problems about the post-testing correction of membrane penetration on pore pressure.

8. Develop a new correction approach to correct the cross-sectional area during shear. Three diameter measurement tests were carried on for this purpose.

9. Examine the quasi-steady state behaviour. Undrained and drained triaxial tests on sand samples with regular end platens or lubricated end platens were conducted.

10. Examine the sensitivity of steady state strength. The scatters of steady state lines obtained in this study and in the literature were compared.

11. Discuss the limitations of triaxial tests on sands.

1.4 Outline of thesis

Chapter 2 gives the detail literature review on previous studies made on liquefaction and undrained behaviour of sands.

Chapter 3 describes the developed devices, test programs and some considerations on sample preparation and deviator stress calculation.

Chapter 4 presents the sample volume changes in undrained triaxial tests, including the error of void ratio due to dimension measurement, volume changes during saturation, consolidation and during undrained loading. B value and the degree of saturation of water pluviated samples and moist tamped samples are also discussed.

Chapter 5 presents the derivation of average diameter with the failure zone of a triaxial sample, and the error in shear strength due to conventional area correction.

Chapter 6 describes the critical examination of the quasi-steady state behaviour which is only a test induced behaviour, caused mainly by the effect of end restraint. The effect of lubricated end platens on steady state strength is also presented in this chapter.

Chapter 7 presents the determination of steady state strength of sand samples with quasi-steady state behaviour. The definition of steady state is modified, based on the comparison of the basic concepts with laboratory behaviour. Four deformation stages during triaxial shear (initial stage, steady state stage, critical stress state and post failure stage) are described and the steady state strength is suggested to be determined in the steady state stage. The scatter of steady state lines for different sands is also given in this chapter.

Chapter 8 describes the limitations of the triaxial tests on sands.

Chapter 9 presents the conclusions of this study, and provides some recommendations for further research and development.

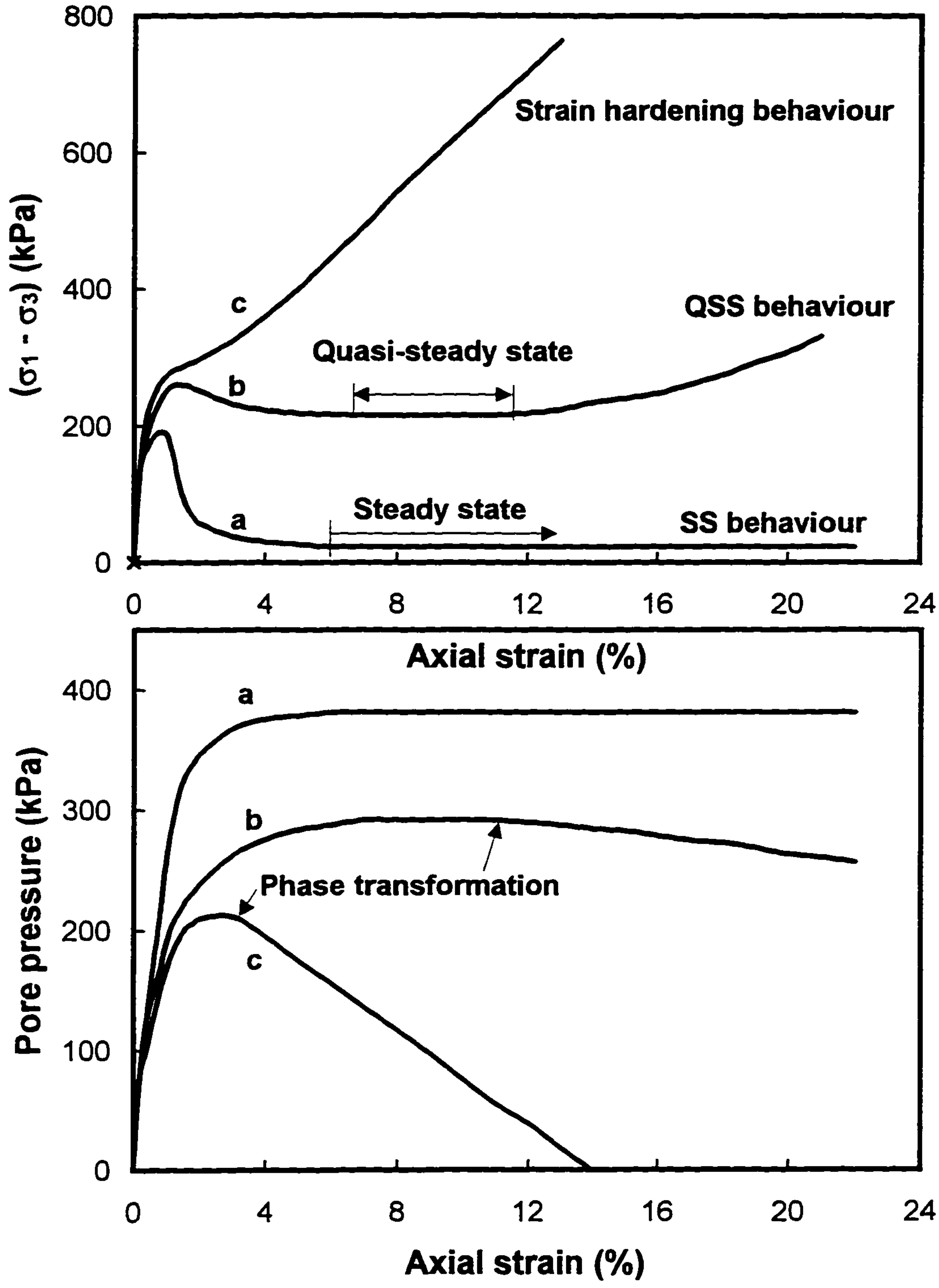

Fig. 1.1 Undrained behaviour of sands in triaxial tests

CHAPTER 2

LITERATURE REVIEW

2.1 Definitions

2.1.1 Liquefaction

The phenomenon of a sand changing its behaviour from a solid state to a fluid state was recognized early this century. In 1920, Hazen had used the term " liquefies" to describe the flow slide failure of the hydraulic fill sands in Calaveras Dam in California (as cited in Castro 1969). In their classical text book "Soil Mechanics in Engineering Practice", Terzaghi and Peck (1948) indicated that a slight disturbance such as a mild shock can cause an important decrease in volume at unaltered value of overburden pressure in very loose fine sand. If this decrease takes place below the water table, it is preceded by a temporary increase in pore water pressure to a value almost equal to the overburden pressure, thus the effective overburden pressure becomes almost zero and the sand flows like a viscous fluid. This phenomenon was defined as "spontaneous liquefaction." Since then, various definitions of the liquefaction phenomenon have proposed by different researchers.

Casagrande (1975) presented the following definitions:

1. **Actual liquefaction** is the response of loose, saturated sand when subjected to strain or shock that results in substantial loss of strength and in extreme cases leads to flow slides.

2. **Cyclic liquefaction** is the response of a test specimen of dilative sand to cyclic loading in a triaxial test when the peak pore pressure rises momentarily in each cycle to the confining pressure.

Seed (1979) presented the following definitions:

1. **Liquefaction**: denotes a condition where a soil will undergo continued deformation at a constant low residual stress, due to the buildup and maintenance of high pore water pressures, which reduce the effective confining pressure to a very low value; the pore pressure buildup leading to liquefaction may be due either to static or cyclic stress applications and the possibility of its occurrence will depend on the void ratio or relative density of a sand and the confining pressure; it may also be caused by a critical hydraulic gradient during an upward flow of water in a sand deposit.

2. **Peak cyclic pore pressure ratio of 100%:** denotes a condition where, during the course of cyclic stress applications, the residual pore water pressure on completion of any full stress cycle becomes equal to the applied confining pressure; the development of a peak cyclic pore pressure ratio of 100% has no implications concerning the magnitude of the deformation that the soil might subsequently undergo; however, it defines a condition that is a useful basis for assessing various possible forms of subsequent soil behaviour.

3. **Peak cyclic pore pressure ratio of 100% with limited strain potential or cyclic mobility**: denotes a condition in which cyclic stress applications develop a peak cyclic pore pressure ratio of 100% and subsequent cyclic stress applications cause limited strains to develop either because of the remaining resistance of the soil to deformation or because the soil dilates, the pore pressure drops, and the soil stabilizes under the applied loads. Cyclic mobility may also be used in a broader sense to describe the cyclic straining that may occur even with pore pressure ratios less than 100% in which case the actual peak value of pore pressure ratio may simply be stated.

Castro et al (1982) presented the following definitions:

1. **Liquefaction** is a phenomenon wherein a mass of soil loses a large percentage of its shear strength, when subjected to undrained monotonic, cyclic or shock loading, and flows in a manner resembling a liquid until the shear stresses acting on the mass are as low as the reduced shear resistance.

2. Cyclic mobility is the progressive softening of a saturated soil when subjected to cyclic loading at constant void ratio. The softening is accompanied by high pore pressure, increasing cyclic deformation, and in some cases, permanent deformation, but it does not lead to loss in shear strength nor to continuous deformation, both of which are essential aspects of liquefaction.

Based on the understanding of the behaviour of cohesionless soils within the last decade, Robertson (1994) suggested the following modified definitions:

1. Flow liquefaction:

-- Requires strain softening response in undrained loading resulting in constant shear stress and effective stress, (i.e. ultimate steady or critical state).

-- Requires that in-situ shear stress is greater than undrained residual or steady state shear strength.

-- Flow liquefaction can be triggered by either monotonic or cyclic loading,

-- For failure of a soil structure to occur, such as a dam or a slope, a sufficient volume of material must show strain softening response. The resulting failure can be a slide or a flow depending on the material characteristics and slope geometry. The resulting movements are due to internal causes and can occur after the trigger mechanism.

--Flow liquefaction can occur in saturated, very loose granular deposits, very sensitive clays and loose loess deposits.

2. Cyclic liquefaction:

-- Requires undrained cyclic loading where shear stress reversal or zero shear stress can develop (i.e. where in-situ static gravitational shear stress is low compared to cyclic shear stress).

-- Requires sufficient undrained cyclic loading to allow effective confining stress to essentially reach zero.

-- At point of zero effective confining stress no shear stress can exist, when shear stress is applied, pore pressure drops and a very soft initial stress strain response can develop resulting in large deformations. Soil will strain harden with increasing shear strain.

-- Deformations during cyclic loading when effective stress is approximately zero can be large, but deformations generally stabilize when cyclic loading stops. The resulting movements are due to external causes and only occur during the cyclic loading. Subsequent movements can occur due to pore pressure redistribution. However, this will depend on ground condition and soil stratigraphy.

-- Can occur in almost all sands provided size and duration of cyclic loading is sufficiently large. For dense sands, the size and duration of cyclic loading will be large and hence, the condition of zero effective confining stress may not always be achieved.

-- Clays can experience cyclic liquefaction but deformations at zero effective stress are generally small due to the possible cohesive strength at zero effective stress and deformation are often controlled by rate effects (creep).

3. Cyclic mobility:

-- Requires undrained cyclic loading where shear stress is always greater then zero, i.e. no shear stress reversal develops.

-- Zero effective stress does not develop.

-- Deformation during cyclic loading will essentially stabilize. The resulting movements are due to external causes and only occur during the cyclic loading.

-- Can occur in almost any sand provided size and duration of cyclic loading is sufficiently large and no stress reversal occurs. Can also occur in dense sand with shear stress reversal provided cyclic loading is not sufficient to cause zero effective stress to develop.

-- Clays can experience cyclic mobility but deformations are often controlled by rate effects (creep).

A comparison of the above definitions indicates that the terms liquefaction, actual liquefaction and flow liquefaction in fact indicate the same phenomenon: a large deformation occurs very rapidly in a mass of saturated soil deposit due to a loss of the shear strength resulting from the buildup of high pore pressure. This implies that the necessary conditions of "**flow liquefaction**" are: (1) the soil deposit is saturated so that the pore pressure in the soil mass can increase rapidly to a very high value to cause a flow liquefaction under some condition. In unsaturated soils, the high compressibity of the air occupying in the pore of the soil mass can alleviate the rapid increase in the pore pressure and thus prevent flow liquefaction. The coarse nature of the soil deposit is not necessary, for the flow liquefaction can occur in very sensitive clays, even though its mechanism may not be exactly the same as that in cohesionless soils; (2) the soil deposit is loose (contractive) so that the undrained residual strength is less than the in-situ shear stress. The undrained residual strength is the minimum resistance of the loose soil deposit under undrained loading condition. Thus the flow liquefaction will never occur if the shear stress is less than the undrained residual strength; (3) The triggering source is sufficiently large to activate flow liquefaction. It can be monotonic, cyclic or shock loading, and generally under undrained condition. The soil structure in very sensitive clays might be damaged due to the change in component of the pore liquid. Such a damage in soil structure might also trigger a flow liquefaction in very sensitive clays.

In the case of **cyclic liquefaction**, the pore pressure can build up to the value of initial effective confining pressure under undrained cyclic loading, but no flow liquefaction occurs, because the shear stress (static) is less than the undrained residual strength of the soil mass. Large deformations can result from the soft initial stress-strain response of the soil deposit, but cannot develop further due to the strain-hardening behaviour of the soil. The deformations will stabilize when cyclic loading stops. Shear stress reversal or zero shear stress may not be necessary for cyclic liquefaction to happen, since the produced pore pressure during undrained cyclic loading depends not only on the static and cyclic shear stresses, but also on the density of the soil mass.

Cyclic liquefaction generally occurs in dense (dilative) soils under undrained cyclic loading , in which zero effective confining pressure does not develop, and the deformation during cyclic loading essentially stabilizes.

2.1.2 Ultimate states

Critical void ratio

Casagrande (1936) defined the critical void ratio as one at which a cohessionless soil can undergo any amount of deformation without volume change under drained condition. This critical void ratio can be reached from either a loose or dense state. For undrained condition, dense sands generally obtain greater strength when volume changes are prevented during shear, and loose sands lose strength. The critical void ratio is one at which shearing under constant volume condition leads to no strength change (Taylor, 1948).

Flow structure

Based on the observation of the sliding failure of the Fort Peck dam, Casagrande developed the hypothesis of flow structure in which each grain is constantly rotating in relation to all surrounding grains so as to offer a minimum frictional resistance. He postulated that such a structure (1) spreads by a chain reaction, (2) exists only during flow, and (3) that at the moment flow stops, the grains rearrange themselves and revert into a static structure which, after the excess water has drained, will be slightly denser then the static structure before liquefaction occurred. After a flow structure is fully developed, the sand has lost all memory of its past stress-strain history (Casagrande, 1975). In other words, flow structure is a flowing state of a soil mass, in which the soil mass exhibits the minimum friction resistance that is not affected by the stress-strain history.

Steady state of deformation

The concept of the steady state of deformation is an extension of Casagrande's concepts of the critical void ratio and the flow structure. Poulos (1971, 1981) described the concept as follows:

> The steady state of deformation for any mass of particles is that state in which the mass is continuously deforming at constant volume, constant normal effective stress, constant shear stress, and constant velocity. The steady state of deformation is achieved only after all particle orientation has reached a statistically steady state condition and

after all particle breakage, if any, is complete, so that the shear stress needed to continue deformations and the velocity of deformation remain constant.

The steady state is not a static state of a soil, but rather occurs only during continuous deformation at constant velocity. Poulos (1981) illustrated that the steady state of deformation can occur in any particular mass and for any loading and drainage conditions that can break down the original structure into a flow structure. For example, the steady state of deformation can occur during undrained tests on saturated loose sands when liquefaction has occurred, and in drained tests on sands at large strains. The steady state of deformation also occurs in drained shear when the residual shear strength is reached at very large strains, and in undrained tests in soft clays at large strains. The steady state of deformation can also be achieved by monotonic or cyclic loading.

The remolded strength of undisturbed clays as determined by the vane shear test is nearly a steady state shear strength (Poulos, 1981). In the shear zone a statistically constant structure is achieved if the vane is rotated at a constant rate. However, since drainage takes place away from the shear zone during the vane tests on soft clays, the strength measured in that test may be somewhat higher than it would be without any drainage. The effect of this drainage may be much large for sands.

Steady state line

The steady state line is a graphical representation of the locus of all steady states of deformation for a particular soil. It should be described in a three dimensional plot since the full description of the steady state of a soil consists of three elements: an effective normal stress, a shear stress, and a void ratio or density. However, since there is a firm relation between the effective normal stress and the shear stress at the steady state of deformation, the steady state line (SSL) can be conveniently represented by a pair of two dimensional plots: $e \sim \log p'$ or $e \sim \log \tau$. Generally the steady state line in $e \sim \log p'$ (or $\log \tau$) is a straight line within the normal stress range of about 1000 kPa.

Critical state

Roscoe et al. (1958) extended the concept of the critical void ratio to the concept of the critical state (critical void ratio state):

> In a drained test, the critical void ratio state can be defined as that ultimate state of a sample at which any arbitrary further increment of shear distortion will not result in any change of voids ratio. In any series of drained tests the set of critical void ratio points so defined can be expected to lie in or near a line on the drained yield surface.
>
> In an undrained test, the sample remains at a constant void ratio, but the effective stress will alter to bring the sample into an ultimate state such that the particular void ratio, at which it is compelled to remain during shear, becomes a critical void ratio. In any series of undrained tests the set of critical void ratio points so defined can be expected to lie in or near a line on the undrained yield surface.

This definition implies that an element of soil undergoing uniform shear distortion can eventually reach a critical state at which it can continue to deform without further change of void ratio and the effective stresses q' and p' (Roscoe and Burland, 1968). The critical state points from drained and undrained tests lie on a unique line (called the critical state line) (Roscoe et al., 1958, 1963).

Steady state and critical state

The concept of a steady state of deformation is closely analogous to the critical state , both of them originate from Casagrande's concept of critical void ratio. Steady state of deformation is mainly used to describe the collapse behaviour of sands and is accepted widely in the evaluation of liquefaction. The critical state is usually used for clays and is used as an important concept in Critical Soil Mechanics. Both concepts in fact indicate the same ultimate state, at which the mass is continuously deforming at constant void ratio, constant normal effective and shear stresses (Poulos, 1981 on the steady state); or any further increment of shear distortion will not result in any change of void ratio, and the critical points will lie in or near a unique line on a yield surface (Roscoe et al., 1958 on the critical state). Sladen et al.

(1985) and Been et al. (1991) considered that there is no clear distinction between the steady state and the critical state, the difference between the two concepts seems only in the statement of the definitions. Poorooshasb et al. (1991) considered that the definition of the critical state in critical state theory includes Poulos' definition of the steady state of deformation, both concepts are in fact equivalent.

Phase transformation

Many investigators have reported that for the undrained triaxial tests on a medium loose sand sample, the pore pressure increases in the initial stage of shearing up to a maximum value at a small strain, and then continuously decreases until the sample fails. Ishihara et al. (1975) called this temporary state of transition from increase to decrease in pore pressure as the **phase transformation** (Fig. 1.1).

Quasi-steady state

Castro (1969) found that in undrained triaxial tests on a medium loose sample, the shear stress increases to the peak at small strain, then the sample suddenly deforms to a large strain, along with approximately constant shear stress and pore water pressure; thereafter, further straining causes the pore pressure to decrease and the sample regains strength. Alarcon-Guzman et al. (1988) called this temporary steady state of deformation as **quasi- steady state** (Fig. 1.1).

2.1.3 Onset states

Collapse surface

Fig. 2.1(a) indicates schematically the undrained behaviour of several sand samples with same void ratio but at different initial confining stresses. If its initial state lies above the steady state line, a sand sample will collapse when the stress path reaches a peak, accompanied by a rapid deformation and a sudden increase in pore pressure. Samples with different initial confining stresses will collapse at different stress state points (e.g. points c, d, e in Fig. 2.1(a)). The collapse stress state points appear to fall on a straight line which passes through the origin of a p'-q space (Vaid and Chern, 1985). For samples with initial states below the steady state line, no collapse will occur (samples A and B in Fig. 2.1(a)). Thus, Kramer (1996) suggested a collapse line as shown in Fig. 2.1(b). Sladen et al. (1985) defined a collapse line through a steady state point. All the collapse lines for different void ratios will form a collapse surface. In other words, **the collapse surface is defined as the locus of the maximum shear stress in p'-q space, at which collapse will be initiated.**

State boundary surface

A sand sample always exhibits contractive behaviour at low shear stress or very low strain level. The pore pressure of a sand sample can thus increase with the number of loading cycles under undrained cyclic loading condition. The sample will collapse once its stress state reaches the post-peak part of the effective stress path which is obtained from an undrained monotonic test on a sample with the same void ratio (Alarcon et al, 1988 and Ishihara, 1991, Sasitharan et al., 1993, 1994). **The post-peak part of the monotonic effective stress path is termed as state boundary surface, at which a sand sample may collapse under cyclic loading condition** (Fig. 2.2).

2.1.4 State parameter

The difference between the consolidation void ratio of a soil element and the void ratio at steady state corresponding to the mean consolidation effective stress applied on the soil element is termed as the state parameter of the soil element (Fig, 2.3). Hvorslev (1937) first presented the concept of state parameter. Roscoe et al. (1963) extended this concept and postulated that samples with same state parameter will exhibit similar behaviour. This hypothesis has been shown to be valid for dense sands (Cole, 1967) and for loose sands (Sladen et al. 1985). Been and Jefferies (1985) used this state parameter to relate the behaviour of loose sands and found that many engineering design parameters are dependent on this state parameter.

2.2 Undrained behaviour of sands

Before Castro's pioneering work in 1969, undrained tests on sands had been carried out by Taylor (1939), Bishop and Eldin (1950, 1953), Bishop et al (1965), Hvorslev (1950), Bjerrum et al (1961). However, these early investigations mainly paid attention to the dense sand samples and could only reveal the dilation behaviour of sands. Based on the concepts of the critical void ratio and the flow structure, Castro (1969) carried out undrained triaxial tests on very loose sands (relative density Dr less than zero) and found the most important behaviour related to the liquefaction of sandy soils: the sand samples could collapse, accompanied by large deformation and significant decrease in shear strength, within a small fraction of a second under static or cyclic undrained loading conditions. Since then, numerous investigations have been conducted on the undrained behaviour of loose sands.

2.2.1 Undrained stress-strain curves

There are three typical stress-strain curves in undrained triaxial tests on saturated sands: contractive (or strain softening) curve, dilative (or strain hardening) curve and partly contractive (or partly strain softening) curve. As shown in Fig. 2.4, in the initial stage of shearing, a sand sample always exhibits increase in deviator stress and in pore pressure independent of its initial state. Then, at the same initial σ', the sample may behave as a strain-softening or strain-hardening material, depending on its density.

Strain-softening curve

For a loose sample, both the deviator stress and the pore pressure increase to a small axial strain. Suddenly, the sample collapses, accompanied by a large decrease in shear resistance and a rapid increase in pore pressure. The sample thereafter continuously deforms under constant shear stress and constant pore pressure to a very large strain in very short period (e.g. sample a in Fig. 2.4).

Strain-hardening curve

For a dense sand sample, both the pore pressure and the deviator stress increase with axial strain until phase transformation is reached; subsequently, the pore pressure continuously decreases with further strain, accompanied by the increase in the deviator stress, and the stress path follows a straight failure envelope (e.g. sample c in Fig. 2.4).

Partly strain-softening curve

For a medium loose sand sample, the deviator stress as well as the pore pressure increases with axial strain until the stress path reaches collapse surface; then a rapid deformation suddenly occur, accompanied by an increase in pore pressure and a decrease in deviator stress. With further straining, the pore pressure decreases with increase in deviator stress, and the stress path follows along a straight line failure envelope (e.g. sample b in Fig. 2.4)

2.2.2 Steady state behaviour

Steady state line

An important undrained behaviour of sands is that for a given sand, the shear strength at steady state is only the function of void ratio (Casagrande, 1975, Castro, 1969, Castro et al., 1982, Poulos et al., 1988, etc.). The steady state is an ultimate deforming state which often exists during the rapid collapse of loose sand. The continuous large deformation at steady state can erase all difference in the initial fabric structures of a sand and the stress or strain history. Therefore, the steady state strength of the sand can be uniquely determined from its void ratio, regardless of sample preparation methods, loading modes, strain rate, stress path (Poulos et al., 1985). The steady state strength is the minimum shear strength for a given sand condition, because during the continuous deformation at the steady state, each grain is constantly rotating in relation to all surrounding grains so as to provide a minimum resistance (Casagrande, 1975). The relationship between steady state strength and void ratio is a straight line (steady state line) in an e-logp' or e-logq plot in the general stress range in practical engineering for many sands.

The liquefaction potential of a sand can be estimated from the position of its state relatively to the steady state line. Casagrande (1975) suggested a parameter $L_p = (\sigma_{3i}' - \sigma_{3f}') / \sigma_{3f}'$ to express the liquefaction potential, where σ_{3i}' is the consolidation effective minor principal stress and σ_{3f}' is the effective minor principal stress at steady state. Casagrande defined three zones for the potential behaviour of a sand: dilative zone, contractive zone and "E" zone (Fig. 2.5). If the initial state of a sand is along the steady state line, the liquefaction potential L_p is zero. In the dilative zone which is below the steady state line, L_p would be negative, and negative pore pressures would develop under undrained shear condition and additional strength would be mobilized. The contractive zone may be far above the steady state line, with a high liquefaction potential (over 6 ~ 10 for the Banding sand in Fig. 2.5). The sand in this zone will always develop a distinctly contractive response when strained and flow liquefaction is expected. The E zone is between the contractive and dilative zones. Casagrande considered that in the E zone, dilative or contractive response is possible depending on the strain rate, and also depending on how close to the steady state line the initial state is located. F line, E_{sc} line and E_u line are the ultimate state lines of the Banding sand obtained from stress-controlled and strained-controlled undrained tests, and drained tests, respectively.

Collapse behaviour

Another important undrained behaviour of sands is the collapse behaviour in which a large deformation can occur very rapidly, accompanied by an increase in pore pressure and a decrease in shear resistance. Thus, a disastrous liquefaction failure may occur without obvious premonition, such as the flow liquefaction of the Lower San Fernando Dam (Seed et al., 1973 and 1975). The occurrence of a collapse depends on the initial state of a sand and the disturbing source. It is seen in Fig. 2.6 (Sladen et al., 1985) that all stress states above collapse surface are unstable, flow liquefaction may occur under static loading. If a stress state is below collapse surface but the shear stress level is larger than the steady state strength, flow liquefaction may occur in response to some external cause of excess pore pressure, such as cyclic loading. If shear stress level is lower than the steady state strength, flow liquefaction is impossible. It should be noted that collapse surface may not pass through a steady state point (Kramer, 1996).

Cyclic steady state behaviour

The **cyclic strength** of a sand is defined as the cyclic shear stress needed to reach a specified value of the accumulated strain, which is the maximum axial strain measured from the beginning of cyclic loading, in a given number of uniform stress cycles (Lee and Seed, 1967). This cyclic strength is affected by many factors, including the steady state strength of a sand, consolidation confining stress, initial shear stress, cyclic shear stress, the specified strain level and cycle number (Lee and Seed, 1967, Vaid and Chern, 1983, Mohamad and Dobry, 1985, Alarcon-Guzman and Leonards, 1988, etc.). It may be also affected by the non-uniform deformation which develops during cyclic undrained loading (Casagrande, 1975).

A cyclic undrained test can provide the same steady state strength as a static undrained test for a given void ratio. Once a collapse is initiated in a cyclic undrained test on a sand sample, the collapse deformation may be much faster than the frequency of cyclic loading, so that a steady state of deformation can be reached as in a static test. This may explain why the effective stress path during collapse in a undrained cyclic test is similar to that in a static undrained test for a given void ratio (Alarcon-Guzman and Leonards, 1988); and why the steady state strengths from static undrained tests and cyclic undrained tests are the same (Castro, 1969, Castro et al., 1982, Konrad, 1989).

A sand sample may or may not collapse under undrained cyclic loading condition, depending on its steady state strength S_{us}, static shear stress τ_s, cyclic shear stress τ_{cy} and peak shear stress $\tau_p = \tau_s + \tau_{cy}$:

(1) If the static shear stress is larger than the steady state strength, $\tau_s > S_{us}$, the pore pressure increases during undrained cyclic loading until the effective stress path reaches the state boundary surface of the sample; subsequently, a collapse is initiated and a steady state of deformation develops (Castro, et al., 1982, Mohamad and Dobry, 1986).

(2) If the static shear stress is less than the steady state strength, $\tau_s < S_{us}$, collapse deformation is not possible in many cases. It was observed that most of the failures of earth dams occurred

in several hours after the earthquakes, rather than during earthquake motion (Seed, 1979b). This indicates that although an earthquakes can trigger the buildup of pore pressure, the presence of seismically-induced shear stress is not required to drive a collapse deformation or a flow failure. A static shear stress larger than the steady state strength should be the necessary condition to initiate flow failures. Experimental results also show that if static shear stress is less than the steady state strength, no collapse deformation occurs except for the presence of shear stress reversal (i.e. $\tau_{cy} > \tau_s$).

(a) If $\tau_p = \tau_s + \tau_{cy} < S_{us}$ and $\tau_{cy} < \tau_s$, both accumulated strain and induced pore pressure are small even after over hundreds cycles of loading. The effective stress path cannot reach the state boundary surface, so that collapse deformation is impossible (Castro, et al., 1982).

(b) If $\tau_p = \tau_s + \tau_{cy} < S_{us}$ and $\tau_{cy} > \tau_s$, the effective stress path cannot reach the state boundary surface and no collapse deformation occurs. However, the extension-reversal ($\tau_{cy} > \tau_s$) may cause larger accumulated strain than nonreversing cyclic loading (case (a)) (Mohamad and Dobry, 1986 and Alarcon-Guzman and Leonards, 1988).

(c) If $\tau_p = \tau_s + \tau_{cy} > S_{us}$ and $\tau_{cy} < \tau_s$, both pore pressure and strain continue to accumulate with each loading cycle, so that significant strain may exist at large loading cycles; but no collapse deformation occurs (Castro, et al., 1982).

(d) If $\tau_p = \tau_s + \tau_{cy} > S_{us}$ and $\tau_{cy} > \tau_s$, collapse deformation may occur at **extension side** of cyclic loading. Alarcon-Guzman and Leonards (1988) found that under undrained cyclic torsional loading with $\tau_s = 0$, the pore pressure of Ottawa 20-30 sand samples continued to accumulate with loading cycles, while the accumulated shear strains were low, about 0.3 % even at the onset of collapse. When the effective stress path reached the state boundary surface at extension side ($\tau < 0$), large shear strains suddenly occurred with a rapid increase in pore pressures.

The above mentioned cyclic undrained behaviours indicate that liquefaction potential of sands can be easily evaluated by comparing steady state strengths with static shear stress and cyclic shear stress. The cyclic strength may not be an appropriate parameter to be used in the evaluation of liquefaction potential, since it is complexly determined and is affected by many factors.

2.2.3 Quasi-steady state behaviour

In the quasi-steady state behaviour, the pore pressure in a sand sample gradually increases during undrained loading until the effective stress path reaches collapse surface, subsequently, collapse deformation suddenly occurs, accompanied by an increase in pore pressure and a decrease in deviator stress. However, after **phase transformation (PT)**, the pore pressure decreases and the deviator stress increases with further strain. This behaviour has been observed and reported by many investigators (Bishop et al, 1965; Castro, 1969; Hanzawa, 1980; Been et al, 1991; Vaid et al., 1990; Georgiannou et al., 1991, etc.).

Compared with the steady state behaviour, the major different character in the quasi-steady state behaviour is its **post-PT increase in shear resistance** which follows a large collapse deformation. Ishihara (1994) considered that the steady state behaviour and the quasi-steady state behaviour should be placed in one category, for both the behaviours are characterized by large collapse deformation with minimum mobilized shear resistance. Finno et al. (1996) attempted to find the difference between the two behaviours by using stereophotogrammetry to determine the local void ratio change during undrained plane-strain loading. Their test results in fact indicate that there is no significant difference between the two behaviours for masonry sand. The steady state points and the quasi-steady state points were located essentially on one line; the volumetric strains inside shear band for both the behaviours were close and essentially remained constant after phase transformation; and the development of the strain within shear band was similar in both cases.

2.2.4 Monotonic strength envelope

During steady state deformation, the mean effective stress p_s' and the shear stress τ_s are constant, and thus define a steady state or undrained residual strength envelope of angle α_{us}' =

arctan (τ_s / p_s'). The relations among various drained and undrained strength envelopes for Banding sand are shown in Fig. 2.7 (Mohamad and Dobry, 1986). In drained tests, the peak strength envelope depends on initial void ratio, the corresponding angle α_d is equal to 32.7° for very dense samples (Dr = 95 - 98 %), and decreases to 26.5° for loose samples. In undrained tests on loose sand samples, the residual strength envelope coincides with the drained peak envelope, with α_{us} = 26.5°. The undrained peak envelope lies below the undrained residual envelope, with α_{up} = 21.5°. For different sands, the undrained residual friction angle, ϕ_{us}' increases consistently as the grains become more angular, equal to 30° for several rounded and subrounded sands, and equal to 35° for angular tailings sands (Mohamad, 1984).

2.3 Factors affecting undrained behaviour of sands

2.3.1 Soil type

Liquefaction is a state of suspension of particles, which results from a release of contacts between soil particles due to the buildup of pore water pressure. Thus, the soil type most susceptible to liquefaction is one in which the resistance to deformation is mobilized by friction resistance (Ishihara, 1985). The contribution from the friction to resist deformation generally tapers off as the grain size becomes smaller, and the contribution from the permeability to resist the buildup of pore water pressure gradually increases when the grain size becomes larger. Thus, there appears a boundary in terms of grain size to separate potentially liquefiable sandy soils from fine-grained soils and coarse-grained soils. Fig. 2.8 shows such boundaries proposed by Tsuchida (1970) and modified by Ishihara (1989).

Fine grained soils

The effect of fines content on the behaviour of fine-grained soils depends on the plasticity of the fines. Troncoso and Verdugo (1985) found that an increase in low plasticity fines content tends to considerably reduce the undrained cyclic strength of sand at a constant initial void ratio. Erten and Maher (1995) investigated the effect of fines on pore water pressure of sandy soils and concluded that the adding silt will accelerate the pore pressure buildup of the soil.

Ishihara and Koseki (1989) carried out a systematic triaxial tests on reconstituted specimens with varying fines content and varying plasticity index values, and showed that the cyclic strength of the fine-containing sands increases with the increase in the plasticity index of the fines. Therefore, it is concluded that plastic fines increase the cyclic strength of the fine-grained sand, but the nonplastic fines reduce the strength of the fine-grained sand (Ishihara, 1993).

Considering the effect of fine content on the liquefaction potential of the soils, Seed et al. (1985) modified their liquefaction assessment chart to relate cyclic stress ratio τ_{av} / σ_o' and SPT value $(N_1)_{60}$ (Fig. 2.9). It is seen that the fines increase the resistance against liquefaction, the cyclic stress ratio in soils with 15% fine is much larger than that with 5% fine. However, it should be mentioned that the apparent increase in the cyclic resistance due to the effect of fines as demonstrated in Fig. 2.9 is valid only when the fines have higher plasticity value. If the sand contains non-plastic fines, the cyclic strength mobilized in the sand may decrease with fines. Chameau and Sutterer (1994) also considered that the SPT based procedures do not adequately account for the effect of fines since fabric, plasticity, and clay content are not considered.

Sladen et al. (1985) carried out undrained triaxial tests on three Nerlerk sands with varying fines content from 0 to 12 percent. Their results show that on the plot of q versus p' at steady state condition, all the data for the three sands fall in a straight line regardless of the fines content; but on an e-logp' plot, the steady state line for Nerlerk sand with 12% fines is much lower than that for Nerlerk sands with 0 and 2% fines (Fig. 2.10).

Georgiannou et al.(1990, 1991a) found that for the same granular void ratio e_g (note: e_g = {volume of voids - volume of clay}/{volume of granular phase}, Mitchell, 1976) and increasing clay content up to 10 percent, the peak strength remained approximately the same, and the steady state strength decreased (Fig. 2.11). Their results also show that the sand sample with higher clay content exhibits higher undrained brittleness (defined as $I_B = (S_{up} - S_{ur}) / S_{up}$, where S_{up} and S_{ur} are peak and residual undrained shear strengths, respectively, Bishop, 1967), and this trend reversed for clay content from 20 to 30 percent.

Pitman et al. (1994) carried out monotonic undrained triaxial tests on loose sand samples prepared with varying percentages of both plastic fines (kaolinite) and nonplastic fines (crushed silica fines and 70-140 silica sand), and found that the undrained brittleness decreases as the fines content, for both plastic and nonplastic types, increases. However, the plasticity of the fines affects the volume change during saturation and consolidation, and the location of the steady state line appears to change with the percentage and plasticity of the fines. They also found that a fines content of 20% in a sand sample seems to mark the transition between the soil structure dominated by sand grain to sand grain contact and one dominated more by the fines matrix. Kuerbis and Vaid (1989) also found that up to a 20% fines content the fines would occupy the void spaces and would not contribute to large change in undrained behaviour.

Gravelly soils

It is usually considered that gravelly soils are far less susceptible to liquefaction when compared to sandy soils due to their higher permeability, higher positive dilatancy and greater stiffness (Wong et al. 1975). However, several liquefaction-induced failures in gravelly soils have been reported in last decades (Coulter et al., 1966, Ishihara, 1974, Andrus et al, 1987, Endo et al. 1988).

The field evidence has shown that most liquefied gravelly soils are comprised of both sand and gravel (Evans and Harder, 1993), thus the gravel content may play an important role on the undrained behaviour of gravel-sand composites. Siddiqi (1984) found that prototype soils with 2 in. diameter maximum particles and their finer matrix soil fractions passing the 1/2 in. sieve have similar cyclic loading resistance if tested at the same relative density. Conversely, Wang (1984) found that the liquefaction resistance of sand-gravel composites increased with the inclusion of gravel particles. Evans and Zhou (1995) found that the liquefaction resistance of sand-gravel composites may increase significantly with increasing gravel content. This increase was observed even for composite specimens tested at the same relative density.

Uniformity of soil particles

Castro et al. (1982) used five different gradations of Banding sand to examine the effect of gradation on the steady state behaviour of sands. They found that the five steady state lines are nearly parallel but plot at lower void ratio as the uniformity coefficient c_u increases.

Grain angularity

Fig. 2.12 shows the steady state lines for a variety of sands, from subrounded to angular (Castro et al. 1982). It is seen that all of the subround and subround to subangular sands have nearly linear and relatively flat steady state lines, and the angular to subangular and angular sands have significantly nonlinear and generally much steeper steady state lines. The steady state lines for the more angular sands generally vary from relatively flat at low stresses to relatively steep at higher stresses.

2.3.2 Initial conditions

Void ratio

Void ratio may be the most important factor affecting the undrained behaviour of cohesionless soils. The effect of void ratio on the undrained behaviour depends on its position relatively to the critical void ratio for the same confining pressure applied on the sample. If the initial void ratio of the sample is much larger than the critical void ratio, or in other words, its initial state is much above the steady state line, the sample will exhibit contractive behaviour under undrained loading condition, and a high induced pore pressure and a collapse failure are to be expected; if the initial void ratio is less than the critical void ratio, the sample will exhibit dilative behaviour, and no strain softening would occur (Casagrande, 1975).

Confining pressure

The critical void ratio for a given soil varies with the confining stress, the higher the effective confining stress, the lower the critical void ratio. For a given void ratio, a sample under lower confining stress may exhibit dilative behaviour, but may show contractive behaviour under high confining stress (Casagrande, 1975). The steady state line for sub-angular or subrounded sands is frequently approximated by a straight line in e - logp space in a stress range of 10 to 500 kPa. For wider stress range, Been et al. (1991) found that the steady state line of a subrounded sand (Erksak sand) curves abruptly at a stress level of about 1 MPa (Fig. 2.13). The authors considered that the break in the steady state line is indicative of a change in mechanism of shearing at high stress levels: at large stress level, the effect of grain breakage may become significant. At low stress level (10 kPa) the steady state line at stress levels seems to become flatter (Tatsuoka et al. 1986).

Initial shear stress or consolidation stress ratio

It is a common situation that the stress condition in a soil element in the ground is anisotropic and there is likely to be a shear stress on a potential failure surface prior to earthquake shaking or static loading. Thus the effects of initial shear stress on the cyclic and steady state behaviour of sand have attracted much attention (Castro, 1969, Seed and Lee, 1966; Lee and Seed, 1967; Seed et al., 1973; Yoshimi et al., 1975; Yoshimi et al., 1978; Vaid and Finn, 1979; Vaid and Chern, 1983; Castro et al., 1982; Mohamad and Dobry, 1986).

Seed and co-workers (Lee and Seed, 1967; Seed et al., 1973) conducted undrained cyclic tests on anisotropically consolidated samples to investigate the effect of static shear stress on cyclic strength, and concluded that the cyclic strength of sands increases with initial shear stress. Conversely, similar investigations by using ring torsional apparatus (Yoshimi et al., 1975) and shaking table (Yoshimi et al., 1978) indicated that the cyclic strength decreases or remains unchanged with increase in initial static shear stress. Vaid and Chern (1983) found that the presence of initial shear stress increase or decrease the cyclic strength, depending on the relative density, magnitude of the initial static shear stress and the specified level of strain development.

Castro et al. (1982) investigated the effect of initial shear stress on the cyclic strength of sands in the terms of the steady state of deformation in triaxial tests and found that the presence of initial shear stress greater than the undrained steady state strength is a necessary condition for cyclic loading to produce a liquefaction failure. The higher the initial shear stress, the more susceptible the soil is to liquefaction failure. Mohamad and Dobry (1986) also used the concept of steady state to study the undrained cyclic behaviour of anisotropically consolidated specimens. They found that for contractive samples, if there is stress reversal and the peak shear stress is small than the steady state strength, the cyclic strength increases with the initial shear stress; however, if the peak shear stress is larger than the steady state strength, the cyclic strength may increase or decrease with the static shear stress. If there is no shear stress reversal, the cyclic strength always decreases with increasing static shear stress. For dilative specimens, the cyclic strength always increases with the static shear stress.

Castro and Troncoso (1989) proposed a ratio of steady state strength to vertical effective stress to determine the steady state strength, for as the vertical pressure σ'_{1c} increases, the void ratio decreases and thus the steady state strength S_{us} increases. This may provide a simple approach for the determination of the steady state strength. Dobry and co-workers (Baziar, et al., 1992; Baziar and Dobry, 1995; Dobry, 1995) followed this approach and found that the ratio of S_{us} / σ'_{1c} seems to increase as the consolidation ratio, $Kc = \sigma_1' / \sigma_3'$, increases. However, this conclusion may not be correct due to the void ratio change during the application of the initial deviator stress ($\Delta\sigma_c = \sigma_{1c}' - \sigma_{3c}'$) in their tests. For a given void ratio, the steady state strength is independent of the anisotropic consolidation ratio Kc (Castro, 1969, Castro, et al., 1992, Poulos et al., 1988).

2.3.3 Sample preparation

There are several preparation methods: moist tamping, air pluviation and water pluviation, generally used to produce sand samples for studying the behaviour of sand deposits in laboratory. Moist tamping method may be one of the oldest laboratory techniques to reconstitute a sand sample (Lambe, 1951). This method consists of placing consecutive soil layers of specified thickness into a sample mold, and tamping each layer flat with a specified force, and then next layer is placed and tamped. This moist tamping method best models the soil fabric of rolled construction fills. Air pluviation method consists of pluviating air-dry sand through air into a sample mold, keeping the height of fall constant. Different density values can be obtained by changing the height of fall. Air pluviation best models the natural deposition process of wind blown aeolian deposits. Water pluviation method is similar to the air pluviation method, but sand is pluviated through de-aired water rather than air and sometimes the sand sample is boiled in water before pluviating. The terminal velocity of soil particles in water is reached in mere 0.2 cm (Vaid and Negussey, 1988), so that the fall distance does not affect the density of the specimen. The specimen can be densified to a desired density by vibrating. This method is not valid to form a uniform sample of poorly-graded or silty sand, for the different settling velocity of different sized grains may result in particle segregation. For example, Baziar and Dobry (1995) found that the steady state strength of a silty sand from the remolded homogeneous samples was much less than that from the remolded layered samples, which were prepared by pouring the material into a triaxial preparation mold and waiting enough time for full sedimentation to occur before pouring the next layer. In order to overcome this problem, some other methods, such as slurry deposition method, have been developed (Kuerbis and Vaid, 1988). The water pluviation technique simulates the deposition of sand through water found in many natural environments and mechanically placed hydraulic fills (Oda et al., 1978).

The moist tamping method can be used to prepare a sand sample with a void ratio even larger than the maximum void ratio of the sand which is determined from a standard method (Ishihara, 1993). The maximum void ratio which can be reached in the water pluviation and the air pluviation methods is less than that in the moist tamping method, while the minimum void ratios from the three methods are close.

The sample preparation methods may significantly affect the cyclic strength of sands. Ladd (1974) employed moist tamping method and air-vibration method to prepare sand samples to the same density and sheared them in triaxial cell under undrained cyclic loading. He found that the samples prepared by the dry-vibration method were significantly weaker during cyclic loading than the samples prepared using the moist tamping method. Mulilis et al. (1977, 1978) used eleven different procedures to compact sand samples and obtained similar results. They also showed that the magnitude of the effect of preparation method is a function of the type of sand. Tatsuoka et al. (1986) showed that among the four sample preparation methods: air-pluviation, wet-tamping, wet-vibration and water-vibration, the wet-vibration method generally provides the strongest samples and the air-pluviation method generally gives the weakest samples; but the other two methods also provide the strongest or the weakest samples in some cases.

The initial fabric formed by different preparation methods seems to have no influence on the steady state strength of sands, for the large deformation at steady state erases the initial fabric completely (Castro, et al., 1982, Poulos et al., 1988). Been et al. (1991) found that the steady state strengths of Erksak sand were the same from the samples prepared by using the moist tamping method and the water pluviation method. Ishihara (1993) provided similar results for Toyoura sand. Negussey and Islam (1994) prepared sand samples with inclined bedding by mounting the sample mold on a tilt plane and sheared the samples under triaxial undrained loading condition. They found that the steady state line was independent of the bedding orientation.

2.3.4 Loading condition

Loading or strain rate

Comparing the results of stress-controlled (or load-controlled) and strain-controlled triaxial tests on Banding sand by Castro (1969), Casagrande (1975) noted that the steady state line "E_{sc} line" from the undrained strain-controlled tests was much higher than the "F line" from the undrained stress-controlled tests (Fig. 2.5). He attributed the large difference in the steady state lines to the difference in the strain rates: the strain rate during the steady state deformation in the stress-controlled tests was 20,000 times faster than the constant strain rate in the strain-controlled tests. Thus, he suspected that a wide range of E_{sc} lines could be achieved with widely differing rates in strain-controlled tests.

However, Castro, et al. (1982) found that the steady state points resulting from several strain-controlled tests on three sands (Banding sand #6, Sand #19 and mine tailings) were close to the steady state line from the stress-controlled tests. Similar results were provided for Erksak sand by Been, et al. (1991) (Fig. 2.13). Therefore, these investigators concluded that there may be insignificant difference between the results from stress-controlled and strain-controlled tests.

Bolton et al. (1994) found that loading rate may or may not affect the undrained behaviour of sandy soils, dependent on the content of fine grains. They used shock testing apparatus and quasi-static testing apparatus to examine the one-dimensional behaviour of induced pore pressure of Bonny silt, Monterey No. 0/30 sand and a mixture of the two soils. They found that the rate of loading had a large effect on an induced pore pressure ratio for Bonny silt and the silty sand mixture, but little or no effect on the induced pore pressure ratio for the Monterey sand.

Stress path

Symes et al. (1984) employed a hollow cylinder apparatus to investigate the anisotropy and the effects of principal stress rotation on Ham River sand. Water pluviation method with a baffle board below a siphon tube was used to prepare the sand samples with initial anisotropic structure. The results of the undrained tests with fixed major stress directions (the angle between vertical and major stress directions, $\alpha = 0°, 24.5°, 45°$) indicate that the conventional tests ($\alpha = 0°$) gave the maximum values of initial modulus, peak strength and residual strength; and with the increase in the angle α, these values decreased (Fig. 2.14). The results of the undrained tests with different major stress directions show that the undrained strength of the sand depends mainly on the loading direction, and little on the rotation of the major stress direction.

The effects of stress paths in compression and extension triaxial tests, or simple shear tests on the undrained behaviour of sands have drawn much attention (Miura and Toki, 1982; Vaid, Chung and Kuerbis, 1990; Vaid and Thomas, 1994, 1995; Vaid and Sivathayalan, 1996; Been et al., 1991; Negussey and Islam, 1994; Pillai and Stewart, 1995; Hyodo et al., 1994). It is observed that for a given void ratio, the undrained extension strength may be less than the undrained compression strength (Hanzawa, 1980; Miura and Toki, 1982; Vaid et al., 1990; Negussey and Islam, 1994; Hyodo et al., 1994; Pillai and Stewart, 1995); or both the strengths are the same (Been et al., 1991).

Vaid and coworkers (Vaid, Chung and Kuerbis, 1990; Vaid and Thomas, 1994, 1995; Vaid and Sivathayalan, 1996) also found that the friction angle mobilized at steady state or at phase transformation state is unique, independent of both the initial state (void ratio, confining pressure, and shear stress) and the loading mode (compression or extension). The steady state line of the sand is unique for compression; the extension steady state line is parallel to but below the compression steady state line, with the amount of shift increasing with increase in deposition void ratio. The results similar to the extension tests were also observed in their simple shear tests under constant volume condition. The collapse in compression is triggered at a unique critical stress ratio line; a unique critical stress ratio line in extension is independent of the consolidation stress state, but associated with each deposition void ratio. Negussey and Islam (1994) found that for a mine tailing sand, both the steady state lines for compression and extension are unique, respectively; but the extension steady state line is lower than and is not parallel to the compression steady state line. Been et al. (1991) observed that for Erksak sand, the compression steady state line coincides with the extension one.

Drainage condition

Liquefaction failure of sands can occur also under drained shearing condition. Lindenberg and coworkers (Begemann et al., 1977; Lindenberg et al., 1981) sheared sand samples, along the stress path $p' = (\sigma_1' + 2\ \sigma_3')$ = constant, at a very slow rate so that no excess pore pressure occurred; and found that the samples collapsed with sudden increase in pore pressure. Liquefaction failures were also observed in a sand deposit during modeling the hydraulic fill procedure in a long flume (Bezuijen and Mastbergen, 1989), and in a series of model tests on coking coal by increasing the water level in the coal stockpiles (Eckersley, 1990).

In triaxial tests, it was observed that the steady state points from drained tests were located on or near the steady state line from undrained tests for Syncrude Tailings (Poulos et al., 1988) and for Erksak sand (Been et al., 1991). Conversely, Alarcon and Leonards (1988) re-examined the results of the triaxial tests on Banding sand by Castro (1969), and found that the undrained steady state strength might be considerably smaller than the strength obtained from drained test at the same void ratio. However, among the three sands used by Castro, the undrained and drained steady state points were located on the same lines for two of the sands. Only in sand B appeared that four of the six steady state points from the drained tests were above the undrained steady state line, along with two of the steady state points on that line.

2.3.5 Influence of testing details

Dimension measurement

The undrained steady state strength of sands may be affected by the errors in dimension measurements, since the undrained behaviour of sands is sensitive to void ratio. The error of the initial void ratio of a sand sample may result from the dimension measurement and the weight measurement. Generally, the weight of a specimen can be measured to ± 0.01 g. Comparing with the sample weight of more than 200g, the error in measurement of weight by 0.01 is negligible. For a 36 mm × 53 mm triaxial sample, its diameter and height can be measured to 0.01 mm and 0.05 mm with calipers, respectively. Thus Castro et al. (1982) concluded that the error in the measurement of diameter by +0.01 mm and of height by +0.05 mm results in a maximum error in void ratio of +0.001. However, they did not consider the potential error which may occur in the measurement.

Volume change during saturation

Moist tamping method is usually used to prepare very loose sand samples in determining the steady state behaviour of the sand. A moist tamped sample is saturated by flushing CO_2 gas and then water through the sample and applying back pressure. The dimensions of the sample are measured before the water flushing or the application of the back pressure; and the void ratio calculated from these measured dimensions, and deducting the void ratio change during consolidation, is often used as the void ratio before shear. Thus, the volume change during saturation is usually ignored. Castro (1969) considered that the volume of the sample might increase during saturation, for the saturation decreases the surface tension and consequently the effective stress in the sample. Conversely, Sladen and Handford (1987) found that the back pressure saturation may densify a loose sample by 0.15 in terms of void ratio for Syncrude tailings sand. This void ratio change can result in significant error in the undrained steady state strength of the sand.

Sample size

Cyclic behaviour of uniform clear sand from large scale simple shear tests is close to that from small scale simple shear tests (De Alba et al., 1976). Castro et al. (1982) found that in undrained triaxial tests, there was no significant difference between the steady state points from 3.6 cm samples and from 7.1 cm samples for Banding Sand #1 and Banding Sand #6; while the steady state line of Sand #19 was always lower from 7.3 cm samples than from 3.6 cm samples. The difference between the Banding Sands #1 and #6 and Sand #19 is that the Banding sands are subrounded, uniform (C_u = 1.53 to 1.70), containing little fines (0.2%), and the Sand No. 19 is subrounded to angular, well-graded (C_u = 2.89), containing more fines(18%).

Non-uniform deformation

Non-uniform deformation in triaxial sand samples may develop due to the formation of shear bands, the effect of end restraint, or sample necking under extension loading.

The occurrence of shear bands may depend on test types, soil types and sample density. Desrues et al (1996) found, using computed tomography technique, that in triaxial tests on sand, shear bands occurred mainly in dense samples; for a loose sample with void ratio less than critical, no significant contrast between shear zone and the rest of the sample could be observed even at large strain. In plane strain shear tests on a masonry sand, obvious shear band were observed even in very loose samples which exhibited steady state behaviour or quasi-steady state behaviour (Finno et al., 1996). Once a shear band develops in a sand sample, the void ratio within the shear band will be larger than the global void ratio of the sample. Thus, the steady state points of a sand from drained triaxial tests on dense samples are always lower than those from loose samples (Verdugo and Ishihara, 1996). The effect of shear band can be eliminated by using loose sand samples in triaxial tests (Desrues et al, 1996), or the results can be corrected by measuring the local void ratio within the shear band (McRoberts and Sladen, 1992).

Sample necking is a serious problem in triaxial extension tests on sands. Roscoe et al. (1963b) found that strain localization can occur at small strain in the extension tests, and consequently, almost all of the further shearing occurs in a narrow localized zone. This strain localization can result in large underestimation of the deviator stress (Fig. 2.16). Similar results were provided by Lade (1982) and Yamamuro and Lade (1995). These results may explain why the extension strength is less than the compression strength (Vaid et al., 1990; Negussey and Islam, 1994; etc.).

Similar necking may also occur in the triaxial cyclic tests on sands. Casagrande and coworkers (Castro, 1969; Casagrande, 1975) found that the upper zone of a cyclic sample became soft in the first few loading cycles, and gradually this zone deformed by alternate necking and bulging (Fig. 2.17). The density profile of the sample indicates that the upper zone was much looser than the rest of the sample. Casagrande also used gyratory shear apparatus to study the strain localization under cyclic loading condition and obtained the same conclusion: non-uniform deformation is particularly remarkable within cyclic samples.

Effect of end restraint

The end restraint effect had been recognized in 1900s by Foppal (as cited by Timoshenko, 1953). He reported that the end restraint in the compression tests on solid specimens can be minimized by using paraffin wax on the ends of the solid specimen. In triaxial tests on soil samples, the end restraint may cause nonuniform deformation and then affect the pore pressure or the volume change, the stress-strain behaviour and the shear strength of the samples (Shockley and Ahlvin, 1960; Rowe, 1962; Rowe and Barden, 1964; Duncan and Dunlop, 1968; Lee, 1978; Lee and Frank, 1978; Goto and Tatsuoka, 1988; Ueng et al., 1988).

The lubricated end platen developed by Rowe (1962) is widely accepted as a practical and useful approach to minimize the effect of end restraint. The results of the drained triaxial tests on sands with lubricated end (LE) platens and non-lubricated or regular end (RE) platens indicate that the strength was always larger with RE platens than with LE platens. Before the peak strength was reached, the dilation volume change with RE platens might be larger than that with LE platens (Rowe and Barden, 1964; Bishop and Green, 1965; Ueng et al., 1988), or less than that with LE platens (Lee, 1978). In undrained triaxial tests on sands, the samples with RE platens exhibited higher pore pressure and lower peak shear strength than those with LE platens (Lee, 1978); but the steady state strength was the same for a given void ratio, regardless of the platen types.

Membrane penetration

In a triaxial sand sample, the membrane may penetrate into the interstices of the soil grains at the boundary of the sample under effective confining pressure. This membrane penetration may overestimate the volume change during consolidation, and thus result in an underestimation of the void ratio of the sample before shear (Newland and Allely, 1957). In an undrained triaxial test on a sand sample, the membrane penetration may also affect the sample volume due to the variation of pore pressure during undrained loading (Newland and Allely, 1959).

Many studies have been carried out on (1) how to measure and estimate the membrane penetration (Roscoe, Schofield and Thurairajah, 1963; Raju and Sadasivan, 1974; Baldi and Nova, 1984; Vaid and Negussey, 1984; Kramer et al., 1989; Ohara and Yamamoto, 1991; Tanaka et al., 1991; Nicholson et al., 1993a); (2) its effects on the drained and undrained behaviour of granular materials, and how to eliminate or correct such effects (Pockering, 1973; Kiekbusch and Schuppener, 1977; Lade and Hernandez, 1977; Martin et al., 1978; Molenkamp and Lugerm 1981; Ramana and Raju, 1981; Baldi and Nova, 1984; Tokimatsu and Nakamura, 1986; Seed, et al., 1989; Evans et al., 1992; Nicholson et al., 1993b; Ansal et al., 1996).

The factors influencing the membrane penetration in a granular material sample include: (1) effective confining pressure; (2) the grain size, shape, gradation of the material, and the density and circumferential area of the sample; (3) the rubber membrane thickness and its extension modulus. Nicholson et al. (1993a) critically reviewed the experimental and theoretical approaches of estimating the membrane penetration, and proposed a new estimating method in which the membrane penetration is only the function of effective confining stress, the D_{20} grain size of tested material and the circumferential area of a sample. However, such a simple method may not be appropriate to accurately estimate the membrane penetration in an individual test.

Constant volume systems have also been developed and modified in attempts to eliminate the effect of membrane penetration on the results of undrained triaxial tests on granular materials (Ramana and Raju, 1981, Seed and Anwar, 1986, Seed et al., 1989; Nicholson et al., 1993b). Seed et al. (1989) and Nicholson et al. (1993) found that the steady state points of the conventional undrained tests on loose sand samples (D = 7.1 cm) were higher than that from the constant volume (with injection) tests; while the conventional steady state points with volume correction coincided with the steady state points from the tests on large samples (D = 30.5 cm), for which membrane penetration effects are small, and from the constant volume tests (Fig. 2.18). It is also noted in Fig. 2.18 that for the dense samples with a given initial void ratio, the steady state strength from the constant volume test was even larger than that from the conventional undrained test. These results indicate an important problem in the "constant volume" approach: how can the steady state strength from the constant volume tests be less in some cases, but larger in other cases than that from the conventional undrained tests?

2.4 Summarizing remarks

The steady state strength has been extensively investigated for many years, since it is the minimum strength which a soil mass can mobilize for a given density (Poulos et al., 1985). The reported investigations were mainly focused on the uniqueness of the steady state line of a sand and the accuracy of the steady state strength determined from laboratory tests and in-situ tests.

2.4.1 Uniqueness of steady state line

Based on the concepts of the critical void ratio and the steady state of deformation, there should be a unique steady state line in a density-effective stress plot for a given sand. The critical void ratio of a sample depends only on the effective normal stress under drained loading condition, or the effective stress at steady state depends only on the void ratio under undrained loading condition (Casagrande, 1975; Taylor, 1948; Roscoe et al., 1958, Poulos et al., 1985). Investigations have proven that for a given void ratio, the steady state strength is independent of sample preparation methods (Castro et al., 1982, Poulos et al., 1988; Been et al., 1991; Ishihara, 1993; Negussey and Islam, 1994); independent of drainage conditions (Poulos et al., 1988; Been et al., 1991; Verdugo and Ishihara, 1996; Riemer and Seed, 1997); and independent of consolidation stress ratio (Castro, 1969, Poulos et al, 1988, Castro et al, 1992).

However, it was also found that the steady state strength may or may not be affected by strain rate, stress path and effective consolidation stress prior to shear. Casagrande (1975) found that the steady state line from undrained strain-controlled tests was much higher than that from undrained stress-controlled tests; while Castro et al. (1982) and Been et al. (1991) noted that the steady state lines from the strain- and stress-controlled tests were close. There seems a *limiting strain rate* beyond which the undrained behaviour of a sand may be independent of the strain rate (Alarcon and Leonards, 1988). Been et al. (1991) observed that the steady state strengths from undrained compression tests and from undrained extension tests were the same; while other investigators found that the undrained extension steady state strength was always less than the corresponding compression strength (Hanzawa, 1980; Miura and Toki, 1982; Vaid et al., 1990; Negussey and Islam, 1994; Hyodo et al., 1994; Pillai and Stewart, 1995; Riemer and Seed, 1997). Riemer and Seed (1997) and Konrad (1990 a, b) also found that the steady state strength was affected by effective consolidation stress. For a given void ratio, the higher the consolidation stress, the larger the steady state strength.

The results of laboratory tests on sands can be affected by end restraint (Rowe and Barden, 1964; Bishop and Green, 1965; Ueng et al., 1988; Lee, 1978). The end restraint is caused by the friction between a sample and end platens, which is dependent on normal effective stress. Thus, the difference between the test results under different consolidation stresses may also result from the end restraint. Necking deformation is a serious problem in triaxial extension tests. This non-uniform deformation can occur at small strain in an extension test on a sand sample. Consequently, almost all further shearing occurs in a narrow localized zone (Roscoe et al., 1963b; Lade, 1982; Yamamuro and Lade, 1995), accompanied by a lower density and a smaller average area in the localized zone than the global density and the overall average area of the sample, respectively. As a result, the extension strength of the sample may be underestimated. Therefore, it is not clear whether the steady state line is affected by effective consolidation stress and by effective stress path.

2.4.2 Accuracy of steady state strength

The steady state line is often very flat in a log p' - e plot, a small error in estimating void ratio may result in a significant error in steady state strength. In laboratory tests, the uncertainties of void ratio can result from dimension measurement, saturation, membrane penetration, and non-uniform deformation. The error in void ratio due to measurement is affected by the resolutions in measuring dimensions and mass, the amount of void ratio, the size of a sample, and observer's skill. The error in the void ratio of a 50 × 100 mm sand sample can be over 0.01 due to the resolutions of measuring devices (Vaid and Sivathayalan, 1996). The observer's error in void ratio is different from different testers and may be large in the case of very loose sand samples.

The void ratio of a sand sample is often overestimated due to ignoring the densification during saturation. Sladen and Handford (1987) found that back pressure saturation could result in the void ratio of a very loose Syncrude tailings sand sample 0.15 lower than that calculated from dimension measurements. Newland and Allely (1957) observed that the membrane penetration into the interstices of the soil grains at a sample boundary can overestimate the volume change of the sample during consolidation, and thus lead an underestimated void ratio. The membrane penetration may also affect the volume of a sand sample during undrained loading (Newland and Allely, 1959; Seed et al., 1989).

The steady state strength of a sand sample depends mainly on the void ratio in its shear zone. Non-uniform deformation may develop during shear due to the formation of shear band or due to end restraint. Shear band often develops in dense sand samples during drained or undrained loading, resulting in the void ratio within shear zone larger than the global void ratio (Desrues et al., 1996). The end restraint in a triaxial sand sample can also affect its volume change or volume change tendency during shear (Raju et al., 1972; Lee, 1978; Ueng et al., 1988). Thus, the non-uniform deformation may significantly affect the steady state strength of sands in some cases.

2.4.3 Quasi-steady state behaviour

The partly strain-softening response or quasi-steady state response (Fig. 2.4, curve b) is possibly a more commonly observed behaviour than the steady state response (Fig. 2.4, curve a) for most loose sands (Poulos et al., 1988; Ishihara, 1993; Riemer and Seed, 1997). No ultimate steady state strength can be reached in an undrained triaxial sand sample with quasi-steady state behaviour, and its minimum strength is usually used as the undrained residual strength in engineering practice. The quasi-steady state behavior has led some researchers to suggest a term of **limited liquefaction** or **flow with limited deformation** (Ishihara, 1993). Based on the concept of the steady state of deformation, a steady state strength should be reached after all particle orientation has reached a statistically steady state condition and after all particle breakage is complete. Thus, it is difficult to understand why after phase transformation, a sample with quasi-steady state behaviour can exhibit a continuous increase in shear resistance and maintain this tendency even at very large strain.

Review of literature suggests that further research on the following is desirable, and has been undertaken in this study:

1. The evaluation of void ratio of sand samples in triaxial tests.
2. Why the quasi-steady state behaviour can occur in undrained triaxial tests.
3. The limitations of the triaxial tests on sands.

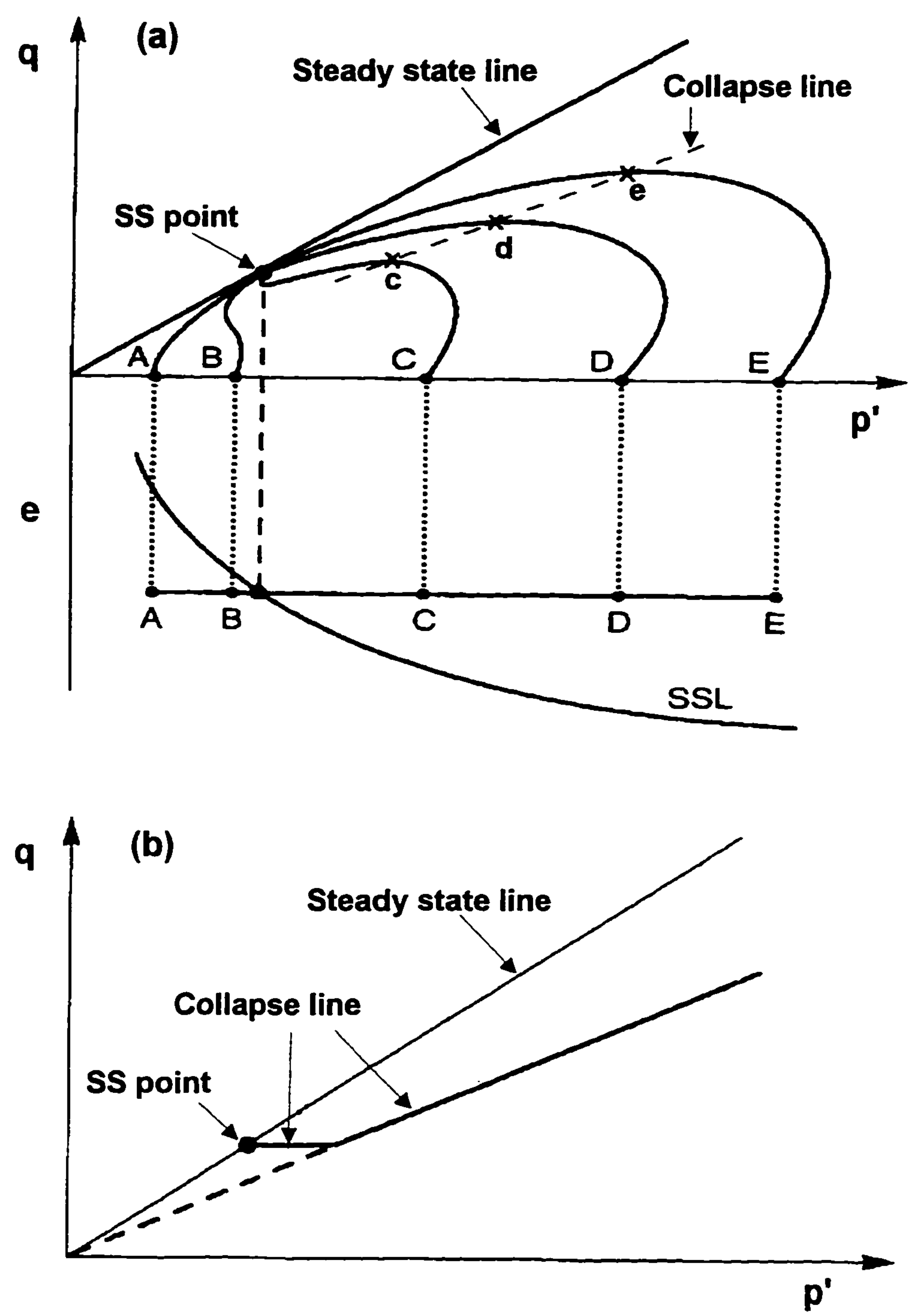

Fig. 2.1 Schematic illustration of collapse surface (after Kramer, 1996)

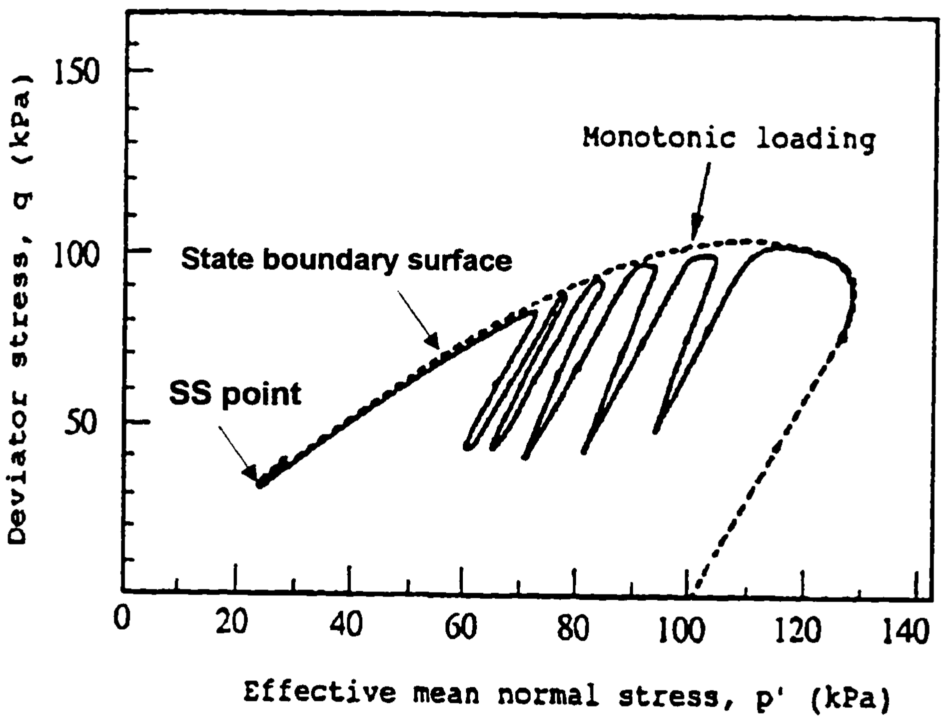

Fig. 2.2 Illustration of state boundary surface (After Sasitharan et al, 1994)

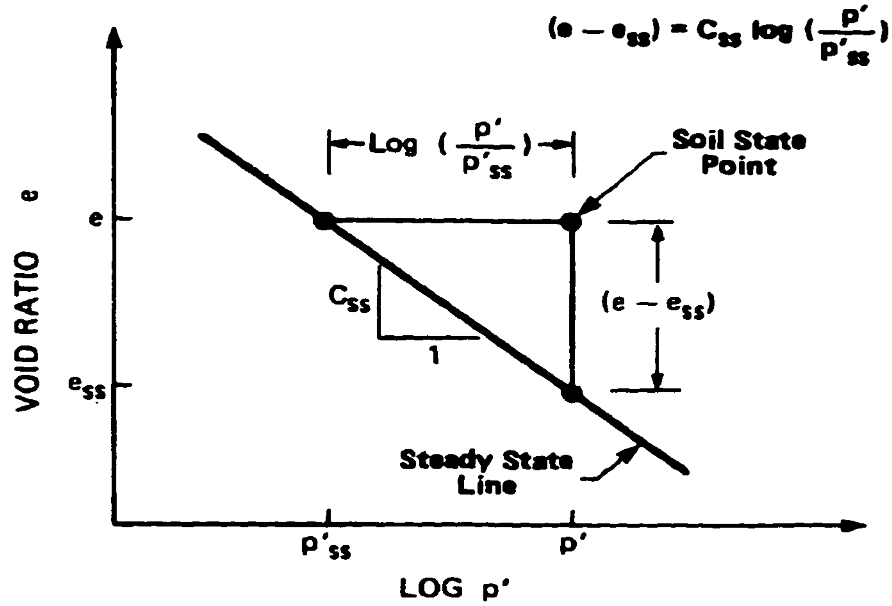

Fig. 2.3 Schematic illustration of state parameter (after Been et al., 1985)

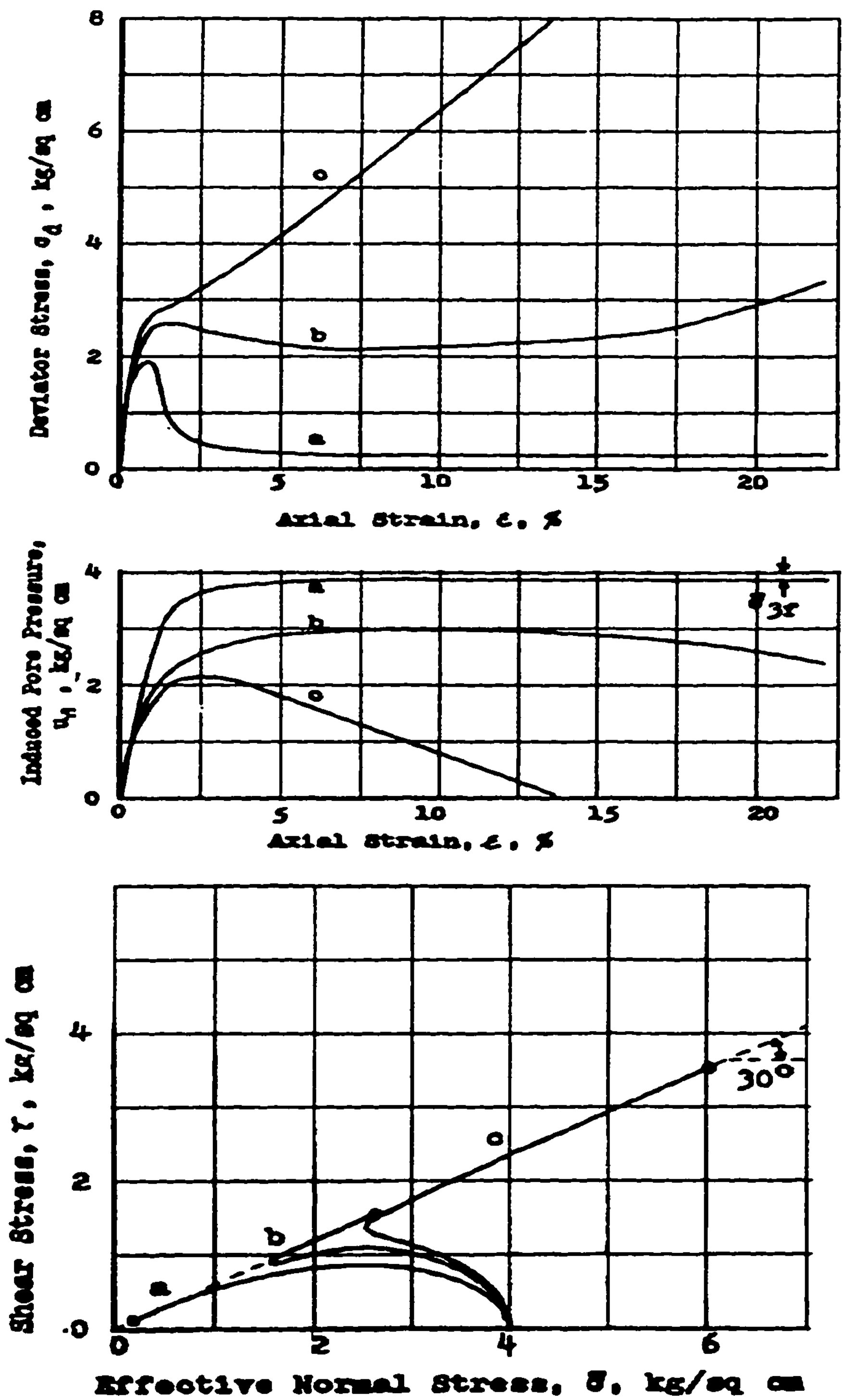

Fig. 2.4 Three types of stress-strain curves in undrained triaxial tests (after Castro, 1969)

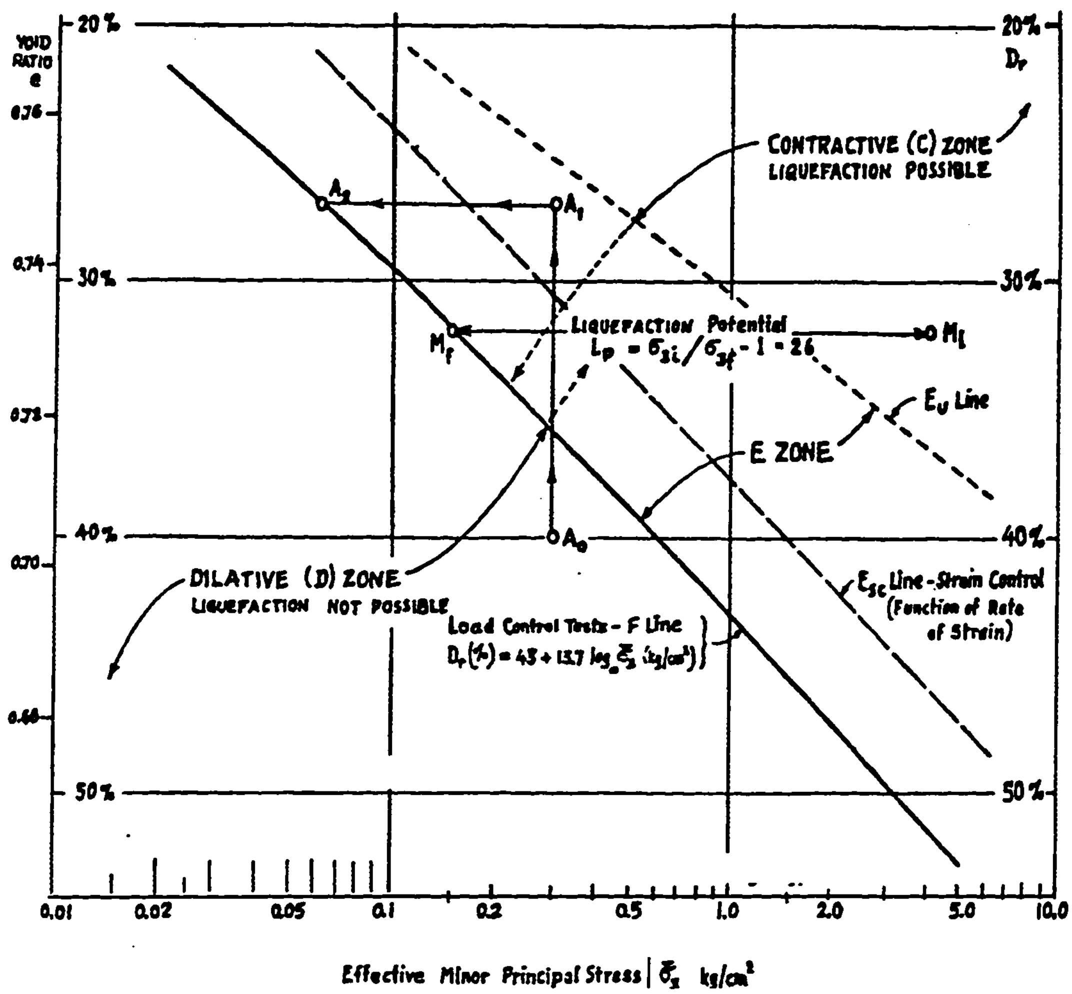

Fig. 2.5 Variable controlling potential for actual liquefaction of Banding sand (after Casagrande, 1975)

ZONE	LIQUEFACTION POTENTIAL
A	Impossible
B	Possible Under Cyclic Loading
C	Possible Under 'Static' Loading

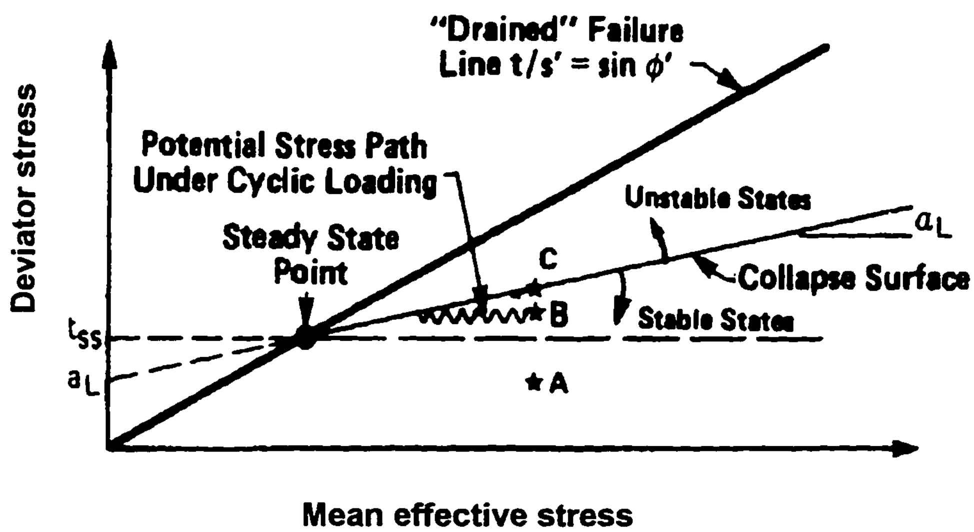

Fig. 2.6 Effect of soil state on liquefaction potential
(after Sladen et al., 1985)

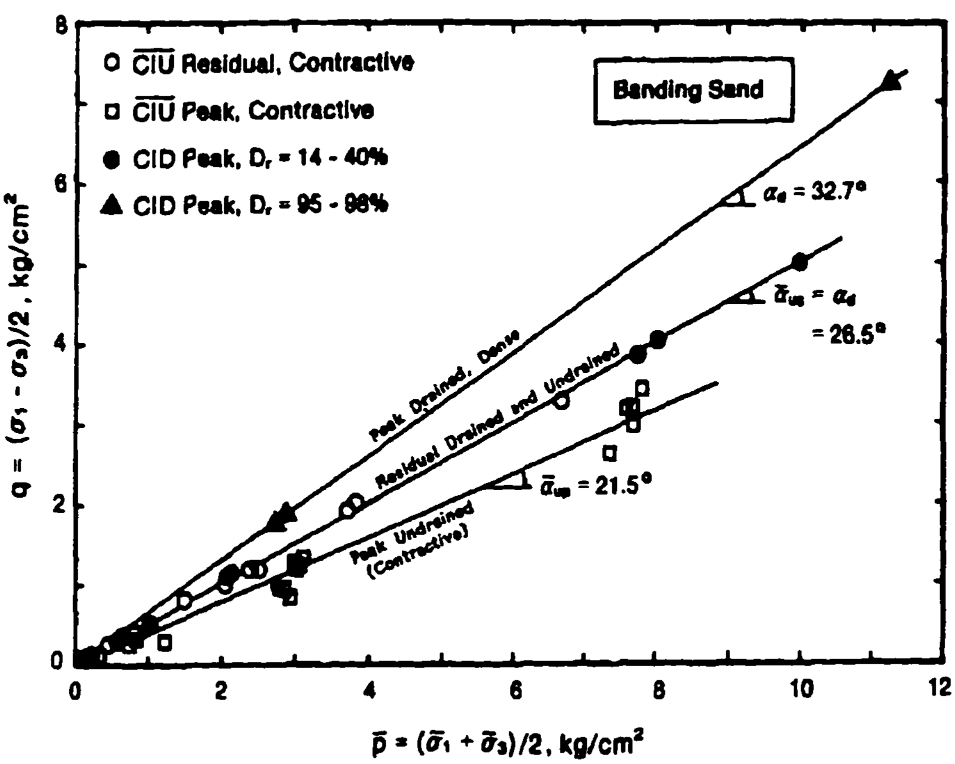

Fig. 2.7 Various strength envelopes for Banding sand (data from Castro, 1969) (after Mohammed et al., 1986)

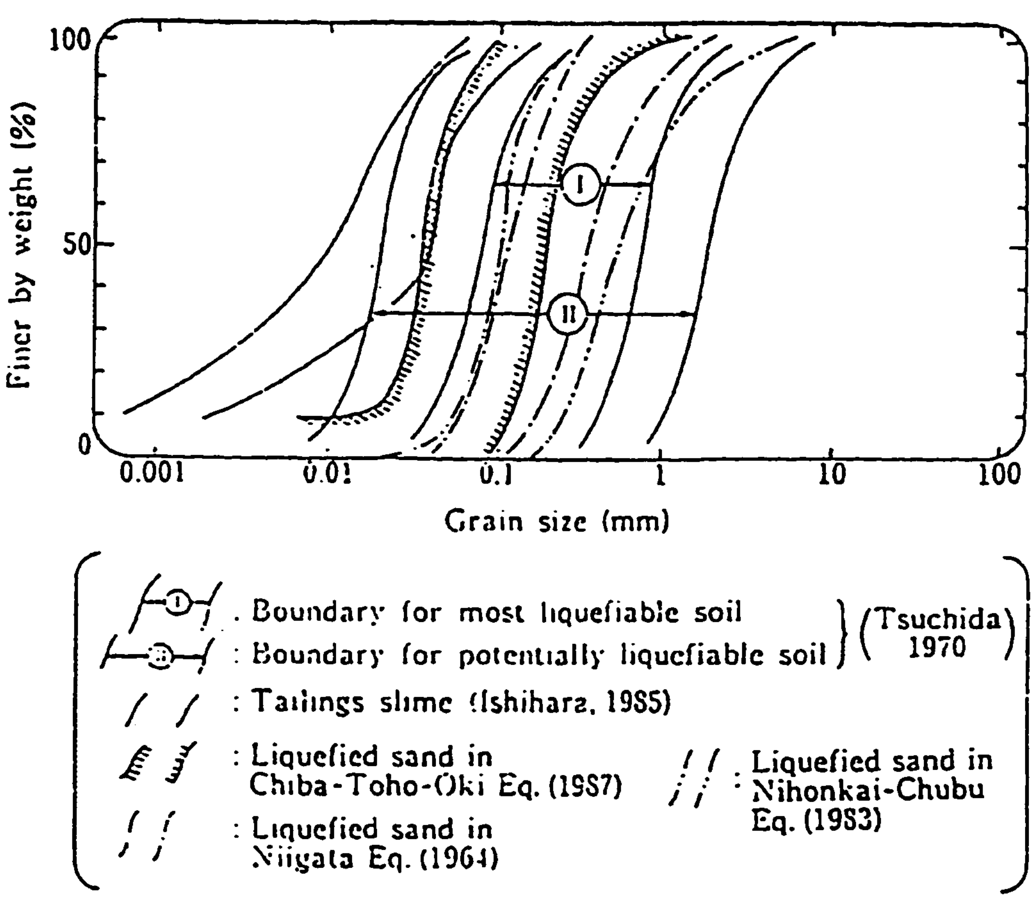

Fig. 2.8 Various grain size distributions of liquefied soils (after Ishihara et al., 1989)

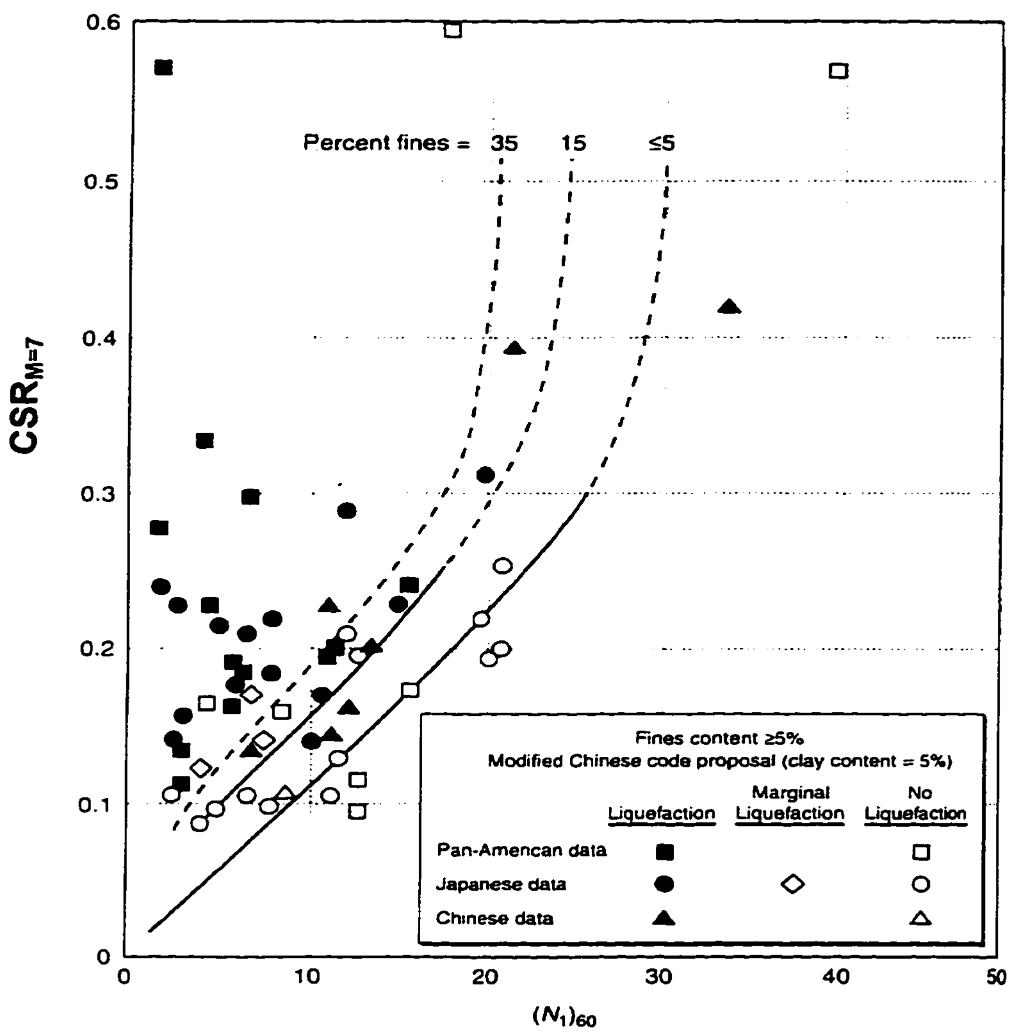

Fig. 2.9 Liquefaction-causing stress ratio versus $(N_1)_{60}$ value for silty sands for M = 7.5 earthquake (after Seed et al, 1985, shown in Kramer, 1996)

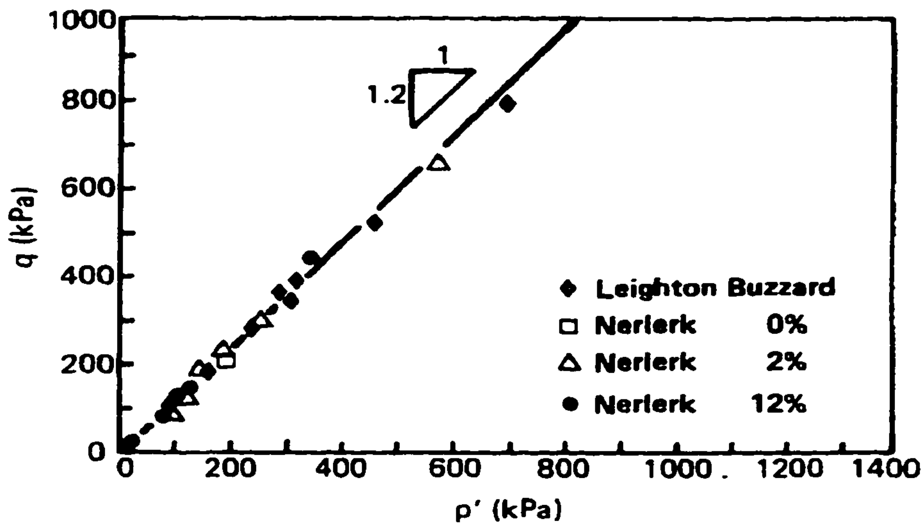

(a) Steady state lines in p'-q plot

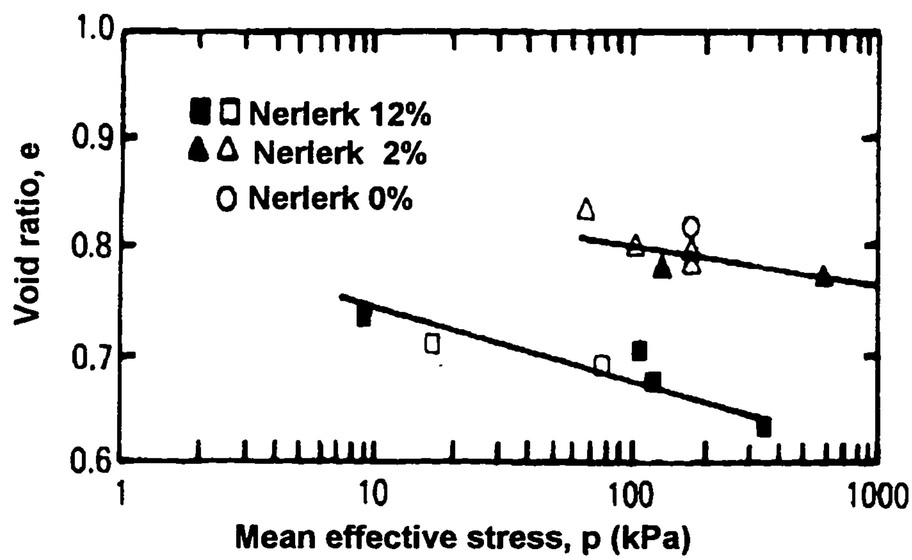

(b) Steady state lines in p'-e plot

Fig. 2.10 Effect of silt content on steady state lines (after Sladen et al., 1985)

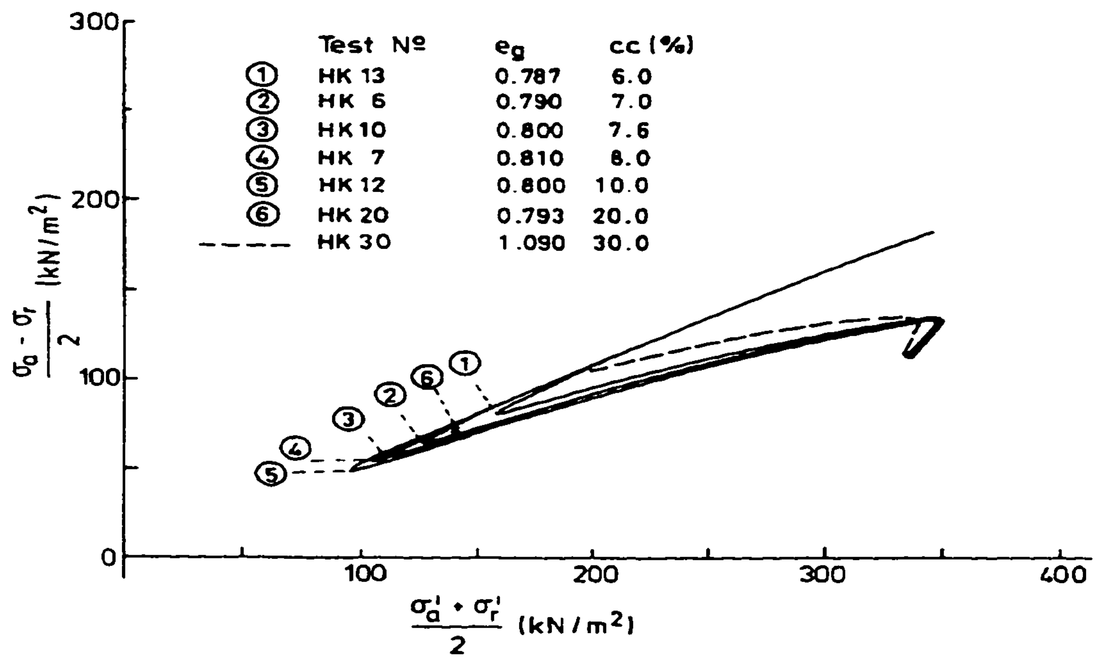

Fig. 2.11 Effective stress paths for undrained triaxial tests on sands with varying clay content (after Georgiannou et al., 1990)

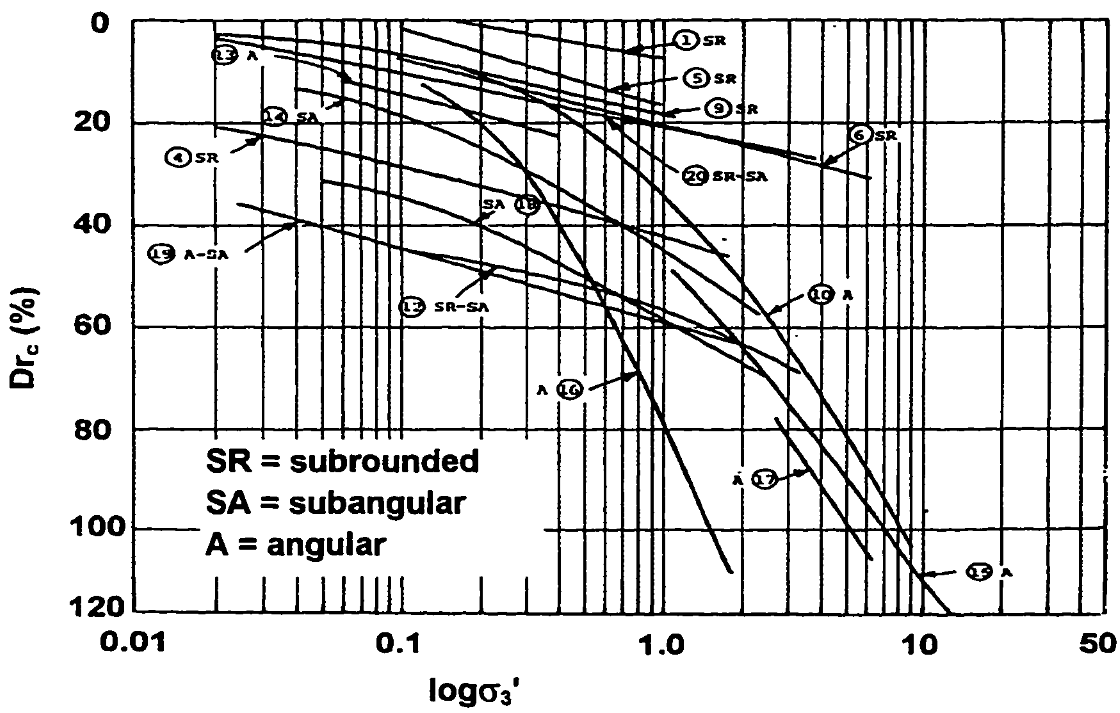

Fig. 2.12 Steady state lines for different sands (after Castro et al., 1982)

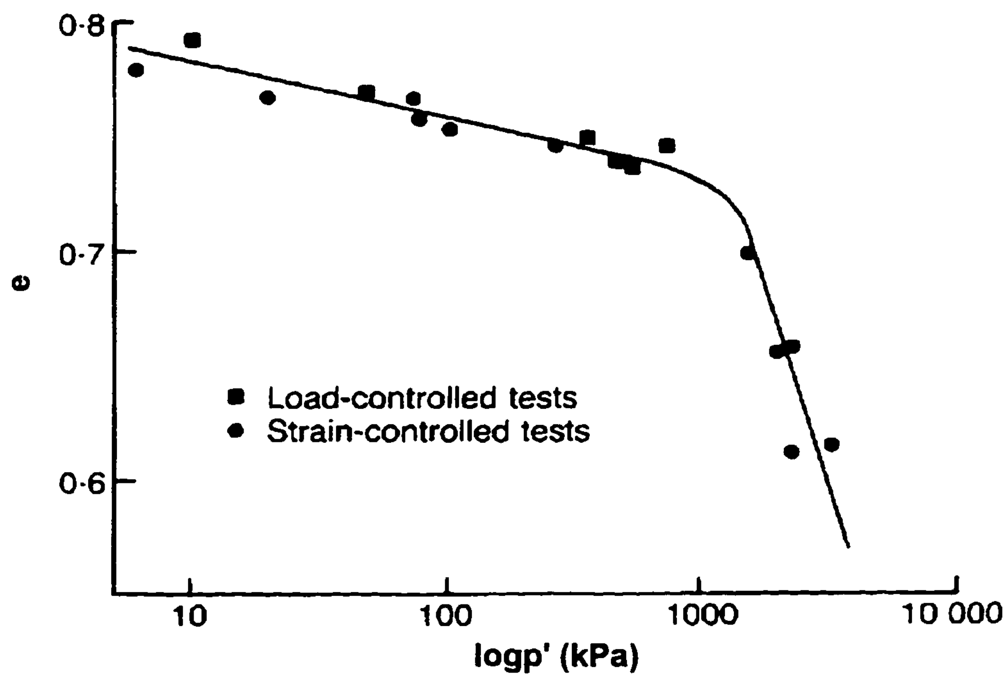

Fig. 2.13 Steady state line of Erksak sand under different loading modes (after Been et al., 1991)

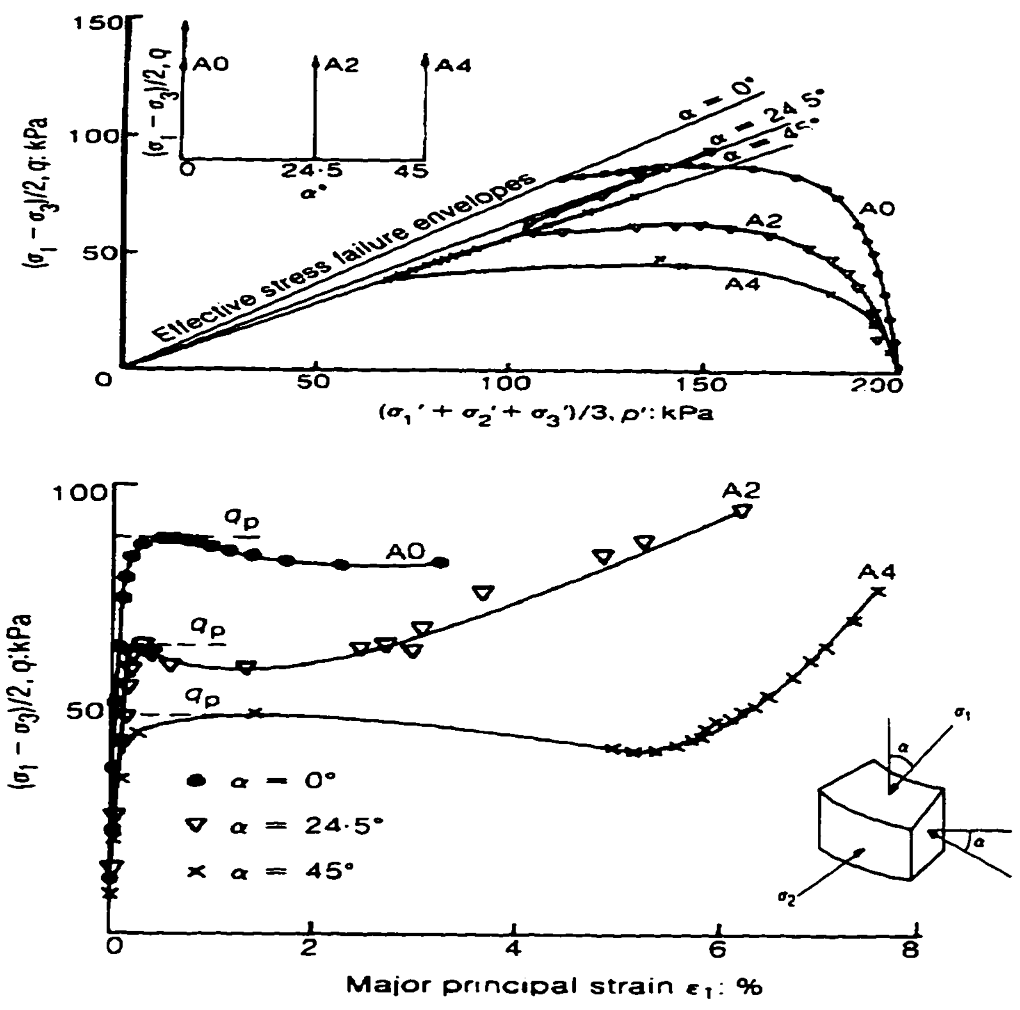

Fig. 2.14 Stress-strain behaviour of undrained hollow cylinder tests on Ham river sand (after Symes et al., 1984).

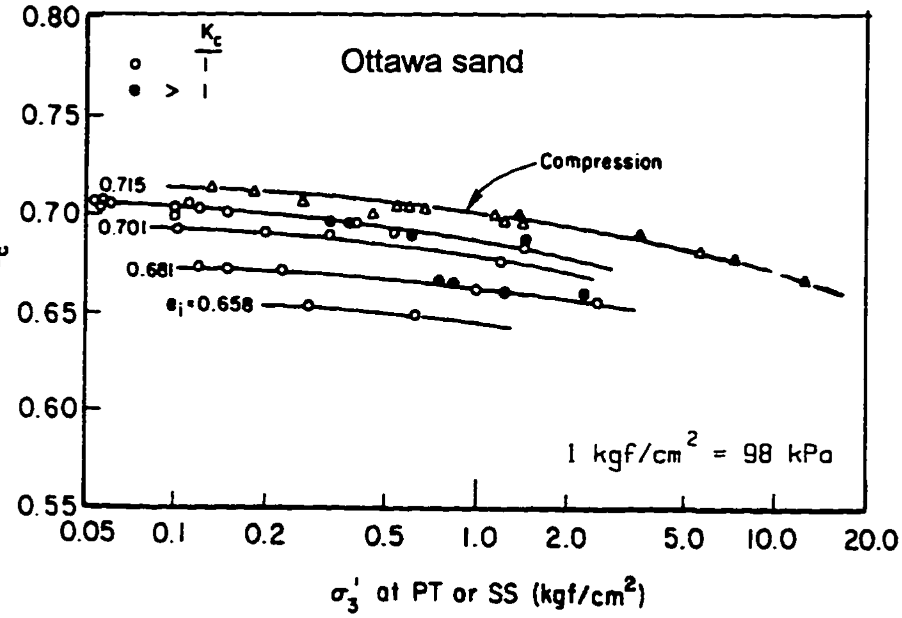

Fig. 2.15 Steady state or quasi-steady state lines in extension and compression loading (Vaid et al., 1990)

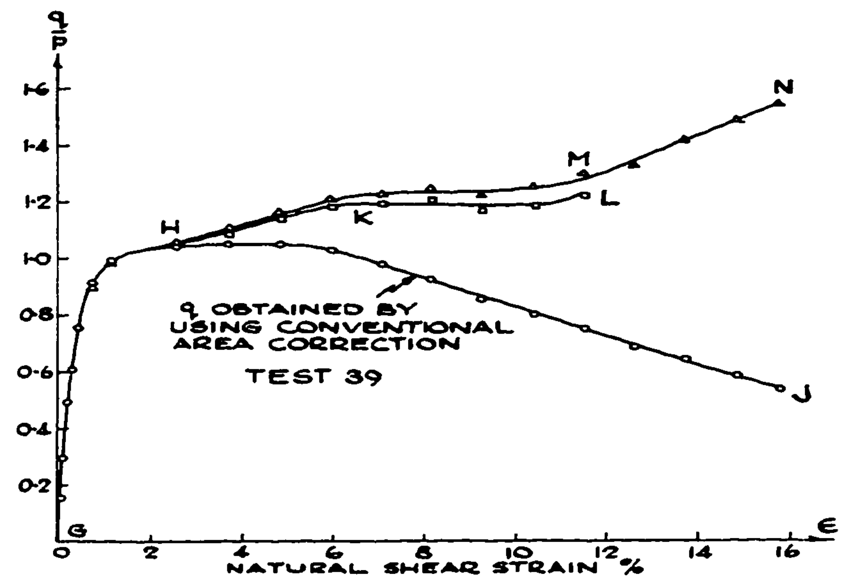

Fig. 2.16 Non-uniform deformation in drained triaxial extensio test on sand (Roscoe et al., 1963)

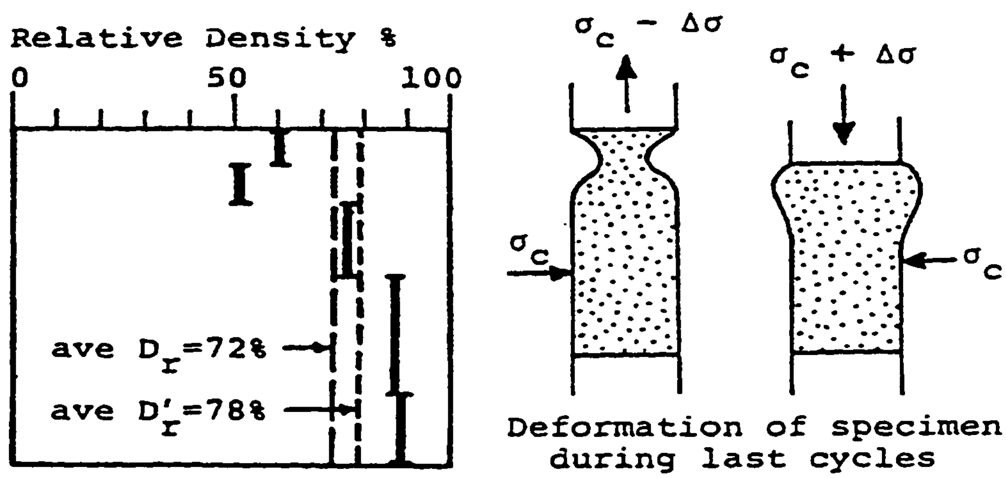

Average Relative Density of Specimen:

1) As prepared and during cyclic test $D_r = 72\%$
2) After reconsolidation under σ_c at end of test $D'_r = 78\%$

Test Procedure:
After 14 load cycles, which produced 14% total strain amplitude, specimen was reconsolidated under σ_c, then frozen, cut into segments and water contents determined. The corresponding relative densities are shown by the heavy vertical bars.

Fig. 2.17 Redistribution of density in cyclic triaxial spencimen (Casagrande, 1975)

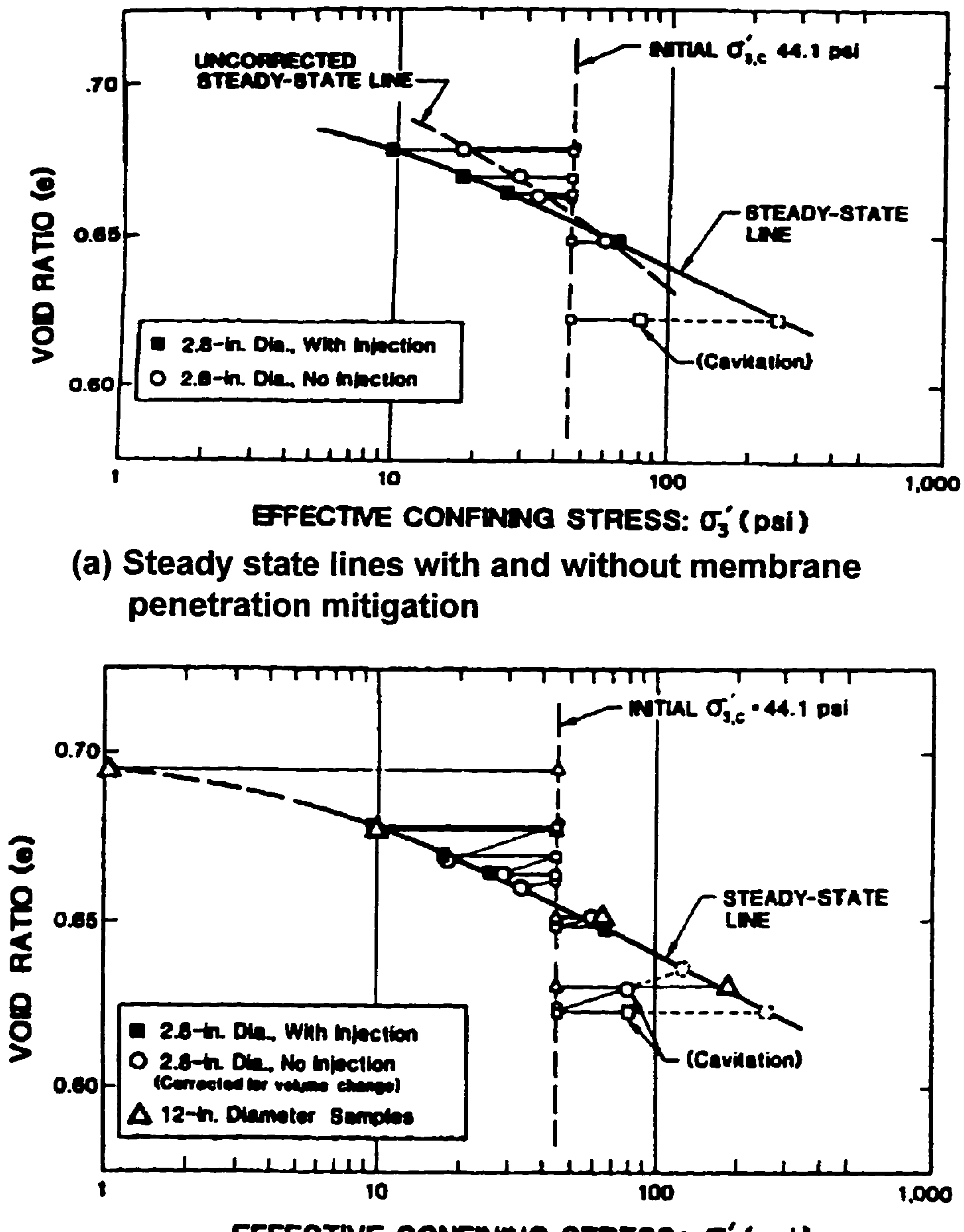

(a) Steady state lines with and without membrane penetration mitigation

(b) Steady state lines from small and large triaxial tests

Fig. 2.18 Effect of membrane penetration on steady state line (after Seed et al., 1989)

CHAPTER 3

EXPERIMENTAL INVESTIGATION

The laboratory apparatuses which have been developed during the course of this research include Hall Effect radial displacement transducer, height gauge, tamping device, water compression device, high water pressure system, and membrane checker. Two volume gauges were used in the undrained triaxial tests to measure the volume changes during consolidation and during shearing.

3.1 Apparatus development

3.1.1 Hall Effect radial displacement transducer (HRDT)

A Hall Effect radial displacement transducer (HRDT) was improved, from a radial strain measuring device (RSMD) developed by Clayton et al. (1989), to measure the radial deformation of a sample during both saturation and consolidation. The main modifications in the HRDT were that two adjustable screws were used and that the close supporting frame in the RSMD was replaced by an open one. Because of these modifications, the HRDT can be very easily installed on a triaxial sample and can be adjusted to a desired initial reading. The HRDT consists of two bar magnets, one Hall effect sensor, two curved pads, two adjusted screws, and one spring (Fig. 3.1). Its linear range is about 1.5 mm with a resolution of 0.01 mm. The procedure of installing the HRDT is (1) smear a thin layer of silicon grease on the insides of the curved pads; (2) place the curved pads on the middle height of the sample; (3) place the HRDT on the curved pads; and (4) adjust the initial position of the HRDT in the valid measurement range and take the initial reading. This is a useful and economic device. A set of the Hall effect sensor and magnets for one HRDT costs just about CN$30. The present HRDT can accurately measure only one direction change in diameter.

3.1.2 Height gauge

The height of a triaxial sample can be measured by using a caliper (e. g. Castro et al., 1982), or by using a dial gauge (e.g. Sasitharan et al., 1993). In the dial gauge method, the height is determined by comparing the dial gauge reading for the sample with a reference taken by placing a dummy sample of known height. Following this idea, a height gauge was developed. The height gauge consists of a dial gauge fixed in a gauge head, a cylinder and a cap button (Fig. 3.2). A straight calibration curve can be obtained by using the height gauge to measure several dummy samples with known heights. Then the height of a triaxial sample could be easily measured to 0.01 mm by taking one reading with this height gauge.

3.1.3 Tamping device

A new tamping device, consisting of a tamper assembly and a tamper cylinder, was developed in this study. The tamper assembly consists of a tamper, a tamper lock, a stopper and a bearing guide. The tamper cylinder is used to adjust the position of the tamper for each layer, consisting of a cylinder, a cylinder lock, a piston, a base and five equal-height guide blocks (for five-layer samples) (Fig. 3.3). The procedure of using the tamping device to prepare a moist sample was as follows: (1) determine the mass of a sand sample based on its desired density; (2) weigh five equal parts (each equal to fifth of the mass) of the material and pour them into five beakers, respectively; (3) mix the material with water (water content equal to 3 % for the Unimin sand and 1 % for the Ottawa sand); (4) install a split mold on the pedestal of a triaxial cell; (5) place the tamper into the mold and fix it by using the tamper lock. The distance between the bottoms of the guide plate and the tamping foot is thus equal to the depth of the mold, H_{mould}; (6) place the tamper into the tamper cylinder, adjust the depth of the cylinder equal to H_{mould}; (7) remove the tamper and place one guide block into the cylinder; (8) place the tamper into the cylinder, unlock and then lock the tamper. Thus the position of the tamper for this layer of the sample is set up; (9) pour the material into the mold and level the surface; (10) tamp the material in a circular pattern until the tamper lock touches the stopper (hammer fall = 0); (11) repeat steps (7) to (10) for the other layers of the samples; (12) install cap platen and seal the sample with an "O" ring; (13) apply low suction (15 - 20 kPa) to the sample and remove the mold; (14) measure the dimensions of the sample; (15) install HRDT, triaxial cover, LVDT, and fill the triaxial cell with deaired water.

3.1.4 Water pressure system

The pressure system used in this study, consisted of source air pressure, air pressure amplifier, servo control panel, bladder cell and pressure booster, is shown in Fig. 3.4. The bladder cell is used to transfer air pressure to water pressure. The source air pressure supplied from the power plant of the university is about 600 kPa, less than the maximum water pressure of 1500 kPa required in the triaxial tests. The 1:5 ratio air pressure amplifier (Model AAD-5, Haskel Inc., California, USA) was employed to increase the air pressure. However, the limit pressure in the servo control system was only about 850 kPa, so higher air pressure could not be applied to the system. A water pressure over 850 kPa was applied by the pressure booster which consists of a small cylinder filled with water and a large cylinder connected to the servo control panel. The ratio of the area of the large cylinder to that of the small cylinder is 2.5, so the maximum water pressure provided by the pressure booster is equal to $2.5 \times 600 = 1500$ kPa if the source air pressure is used.

3.1.5 Membrane checker

A membrane checker was developed to check the leakage of a rubber membrane. It consists of a cylinder, an air pressure tube and two O ring seals (Fig. 3.5). The procedure of using the checker is (1) a rubber membrane is installed on the cylinder and is secured with the O ring seals; (2) a low air pressure is applied to the membrane; (3) the membrane is immersed into water. The membrane is not damaged if no continuous air bubbles appear.

3.1.6 Lubricated end platens

Lubricated end platens shown in Fig. 3.6 were used for most triaxial samples in this study. It consists of end platen with a thin (0.04 - 0.06 mm) smear of silicon grease covered by a latex membrane (0.3 mm thick). Since developed by Rowe in 1962, lubricated end platens have been widely used to reduce end restraint in triaxial samples. The lubrication effect depends on the thickness of silicon grease; the thicker the silicon grease, the less is the friction between end platens and sample. However, it should be noted that the use of generous smear of silicon grease may result in significant error in void ratio of a sample due to the extrusion of the silicon grease (Castro et al, 1982). Furthermore, the deformation of the membrane in the lubricated end platens may not be negligible, and should be deducted from the total vertical deformation measured by LVDT to improve the accuracy of void ratio estimation. For example, for a consolidation pressure of 500 kPa, two 0.30 mm thick membranes in the end platens of a sample can deform by $\frac{500}{1400} \times (2 \times 0.3) = 0.21\,\mathrm{mm}$ (the Young's modulus of latex membrane is equal to 1400 kPa (ASTM, 1993b)). This vertical deformation can overestimate the void ratio of a 50 × 100 mm sand sample by 0.04.

3.2 Triaxial test system

A UBC type triaxial apparatus was used in this study (Fig. 3.7). The axial load can be applied in stress-controlled mode or in strain-controlled mode (except collapse deformation) by a double chamber bellofram actuator. A bedded bushing was installed in the cell cap to eliminate the friction between the piston and the cell cap. Besides a load cell, a LVDT, three pressure transducers and a volume gauge, which are usually used in conventional triaxial tests, a HRDT and another volume gauge were also used in this triaxial system. The HRDT was used to measure the radial deformation of a sample during saturation and consolidation, and the second volume gauge was used to measure the volume change of pore fluid during undrained loading under constant cell pressure.

The triaxial apparatus is controlled by a personal computer (model 486 DX4 100) through a data acquisition and control system. The data acquisition and control system (LabMate, Sciemetric Inc., Ottawa, Ontario) is capable of reading up to sixteen analog to digital (A/D) channels and two digital to analog (D/A) channels. A custom-optional controller board was added to the original LabMate to operate three stepper motors which control axial load, cell and back pressures separately. The LabMate converts analog signals from various transducers to digital signals which are fed to the computer for further control on the load or the pressures and for processing the data. The computer analyzes the received data, compares with the desired stress or strain level and operates a stepper motor, if required, to achieve the desired stress or strain level. The frequency of data acquisition in this system is about one cycle per second. A dynamic signal analyzer (HP 35670A, Hewlett-Packard Company, Washington, USA) was also used to record the data during a rapid collapse. The detail of operating this triaxial test system is described in "Manual of operation of automatic stress-path control system" (Khan, 1993).

3.3. Materials tested and sample preparation

3.3.1 Materials tested

The main material tested was the Unimin sand 2010, an angular medium crushed quartz sand obtained from St-Canut, Quebec. Ottawa sand (C190) was also used in some tests. Their physical properties are given in Table 3.1 and Fig. 3.8. The minimum and maximum void ratios were determined according to the ASTM test methods D 4253-93 (Method 1A) and D 4254-91 (Method A), respectively.

3.3.2 Sample preparation

There are numerous preparation methods: moist tamping, air pluviation and water pluviation, used to prepare sand samples. Moist tamping method may be one of the oldest laboratory techniques to reconstitute a sand sample (Lambe, 1951). This method consists of pouring consecutive soil layers of specified thickness into a sample mold, and tamping each layer flat with a specified force, and then next layer is placed and tamped. This moist tamping method best models the soil fabric of rolled construction fills. Air pluviation method consists of pluviating air-dry sand through air into a sample mold, keeping the height of fall constant. Different density values can be obtained by changing the fall height. Air pluviation best models the natural deposition process of wind blown aeolian deposits. Water pluviation method is similar to the air pluviation method, but sand is pluviated through de-aired water rather than air and sometimes the sand sample is boiled in water before the pluviating. The terminal velocity of soil particles in water is reached in mere 0.2 cm (Vaid and Negussey, 1988), so that the fall distance does not affect the density of the specimen. A water pluviated sand sample can be densified to a desired density by vibrating. The water pluviation technique simulates the natural alluvial sands and mechanically placed hydraulic fills (Oda et al., 1978).

The moist tamping method was employed to prepare all the sand samples except for a few samples which were used in the investigation of membrane penetration. The reasons for this selection are (1) the difference in the initial fabrics of sand samples due to different preparation methods does not affect the steady state strength of sands, since the large deformation at steady state can erase the initial fabric (e. g. Been et al., 1991, Ishihara, 1993 and Negussey et al., 1994); (2) for a well-graded sand, the water pluviation method produces a segregated or layered sample in which the top portion contains more finer grains than the lower portion. Such a sample may exhibit steady state strengths different to that of a homogeneous sample (Baziar and Dobry, 1995), since the steady state strength is very sensitive to the grain size distribution of the material within the shear zone of the sample (Castro et al., 1982); (3) the moist tamping method can produce sand samples with void ratios over a large range.

In the moist tamping method, the compaction of each succeeding layer can further densify the material in the layers below it (Chen, 1948). Ladd (1978) developed an undercompaction tamping method to correct the over densification in the lower layers of tamped sand samples. Each layer of a sample is compacted to a lower density than the final desired value in this tamping method. The percent undercompaction U_n, defined as {(desired density - tamped density) / desired density}, is assumed to linearly vary from the maximum value at the bottom (first) layer to zero at the top layer. In other words, it is assumed that the effects of the compaction of top layer on the previous layer and on the first layer would be the same. This assumption however may not be valid.

Without a better method, a zero drop tamping method (the hammer fall height equal to zero) was used to reduce the over densification in the lower layers of a tamped sand sample in this study. The main steps to prepare a moist sample in this study are described in section 3.1.3.

3.3.3 Saturation

Water flushing and back pressure saturation were used to saturate a tamped sand sample in this study. Following the step 15 in sample preparation (Section 3.1.3), the saturating procedures are as follows: (1) apply low cell pressure (about 25 kPa) and then release the suction in the sample; (2) flush carbon dioxide gas from the bottom to the top of the sample for 15 minutes. The gas pressure on the bottom was less than 3 kPa; (3) flush deaired water from the bottom to the top of the sample until all visible gas bubbles are pushed out. The water pressure at the bottom is maintained at a value less than 3 kPa; (4) apply back pressure and cell pressure, and maintain the difference between the back and the cell pressures constant. A B value over 0.98 can be reached under a back pressure of 300 kPa for the Unimin sand.

3.4. Membrane and calculation of deviator stress

3.4.1 Membrane leakage

Leakage may occur under consolidation pressure for some poor quality membranes. It was found that in a sand sample sealed with a brand new membrane (0.30 mm thick, used three months after manufacture) under an effective confining pressure of 200 kPa, the measured water volume squeezed out of the sample increased continuously, or the pore pressure increased rapidly if the back pressure valve was closed. However, the membrane was checked before and after the test by using the membrane checker, and no leakage occurred. In order to find the source of the leakage under a pressure of 200 kPa, a dummy aluminum sample sealed with the membrane and a thicker membrane (0.70 mm thick) were installed in the triaxial cell, respectively, in a manner similar to a sand sample. It was found that no leakage occurred for the thicker membrane even under an effective confining pressure of 800 kPa; while leakage appeared under an effective confining pressure of 100 kPa for the thinner membrane, and became faster under higher effective confining pressure. All the other membranes (thickness = 0.3 - 0.4 mm) in the same package were also found to leak under an effective confining pressure of 100 kPa. However, some other thin membranes (about 0.3 mm thick) did not leak even under high effective pressure. It is interesting that both the good and the poor membranes were supplied by the same supplier (Precision Dippings Marketing Ltd.) and might be made by the same manufacturer. Thick latex membranes (thickness = 0.60 - 0.75 mm) were therefore used in all the tests in this study except for some of the membrane penetration tests.

3.4.2 Effect of membrane on shear strength

The restraining of latex membrane on a sample may increase its shear strength. This restraining effect is significant for a sample which exhibits brittle failure (Blight, 1967; La Rochelle, 1967); but is insignificant in plastic failure (no obvious shear band appears) (Wesley, 1975; Gens, 1982). All the loose to medium dense Unimin sand samples display plastic failure. According to the correction suggested by ASTM (1993c), the deviator stress induced due to membrane restraining in the Unimin sand samples with 0.75 mm thick membrane is about 13 kPa at an axial strain of 15 %. However, it was observed that a latex membrane along a Unimin sand sample wrinkled at large strain during shear. This indicates that a membrane cannot support any axial stress at large strain. Therefore, no membrane restraining correction was applied when determining the steady state strength of the Unimin sand.

3.4.3 Calculation of deviator stress

The deviator stress in a triaxial sample is equal to axial load divided by the average cross-sectional area of the sample. The average cross-sectional area is corrected during shear. A new area correction was developed (see Chapter 5) and was used in the calculation of deviator stress in this study.

3.5. Tests conducted

The experimental programs in this study were as follows: (1) developing the apparatuses required in the consequent tests; (2) investigating the error in void ratio estimation; (3) developing a new method of correcting cross-sectional area of a triaxial sample; (4) investigating the quasi-steady state behaviour of sands; (5) discussing the limitations of triaxial tests on sands. The tests conducted in (2) to (4) are listed in Table 3.2.

Table 3.1. Index properties of the sands

Name	G_s	D_{50} (mm)	C_u	e_{min}	e_{max}
Unimin sand	2.665	0.87	2.00	0.655	1.037
Ottawa sand	2.670	0.70	1.26	0.496	0.674

Table 3.2 List of tests conducted in this study

	Test	Apparatus	Material	No	Note
1	Dimension measurement	Triaxial system Caliper Perimeter tape Height gauge	Dummy aluminum samples	4	
2	Saturation	Triaxial system LVDT, HRDT	Unimin sand	9	Moist tamped samples
3	Membrane penetration	Triaxial system LVDT, HRDT	Unimin sand Ottawa sand	4	Water pluviated samples
4	Water compression	Hydraulic consolidation cell	Water Air	4	
5	Air dissolution	Nold DeAeriator Oxygen meter	Water Air	1	
6	B value & degree of saturation	Triaxial system	Unimin sand Ottawa sand	4	
7	Diameter measurement test	Triaxial system	Unimin sand Ottawa sand	3	Moist tamped samples
8	CIU shear test	Triaxial system	Unimin sand	23	
9	CAU shear test	Triaxial system	Unimin sand	21	Kc = 1.5, 2
10	Drained shear test	Triaxial system	Unimin sand	9	
CIU = consolidated isotropically undrained, CAU = consolidated anisotropically undrained.					

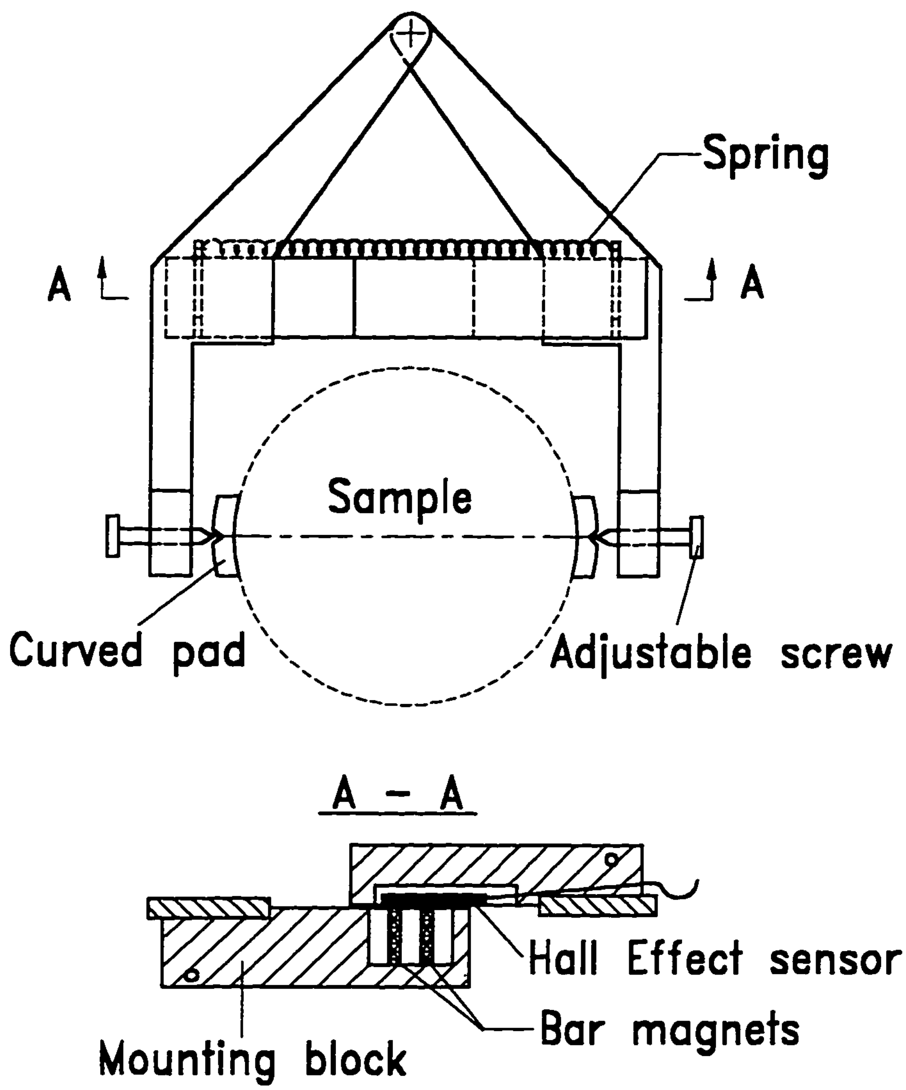

Fig. 3.1 Schematic diagram of HRDT

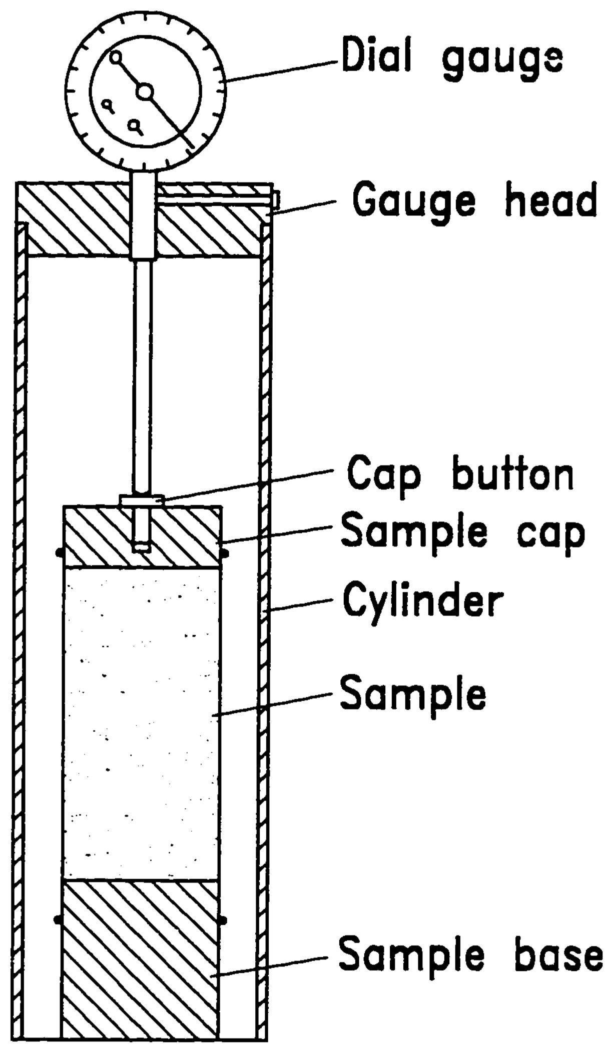

Fig. 3.2 Schematic diagram of height gauge

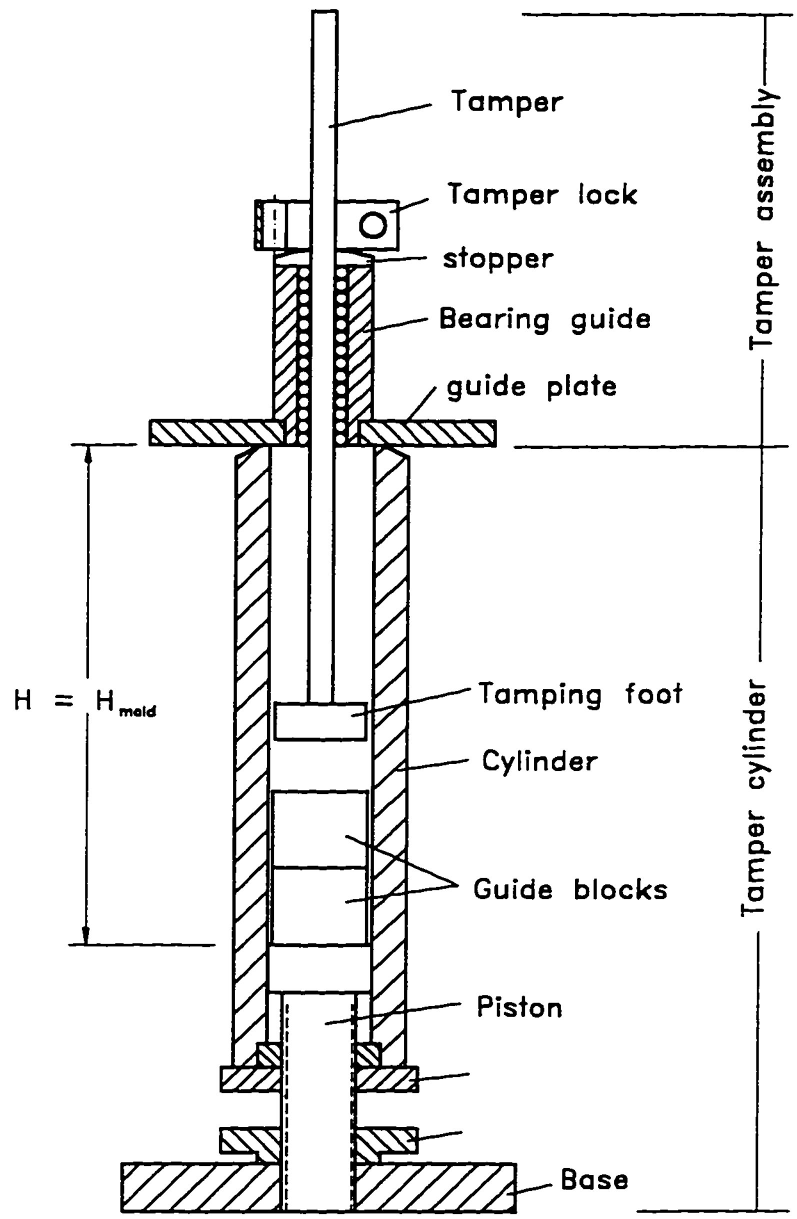

Fig. 3.3 Schematic diagram of tamping device

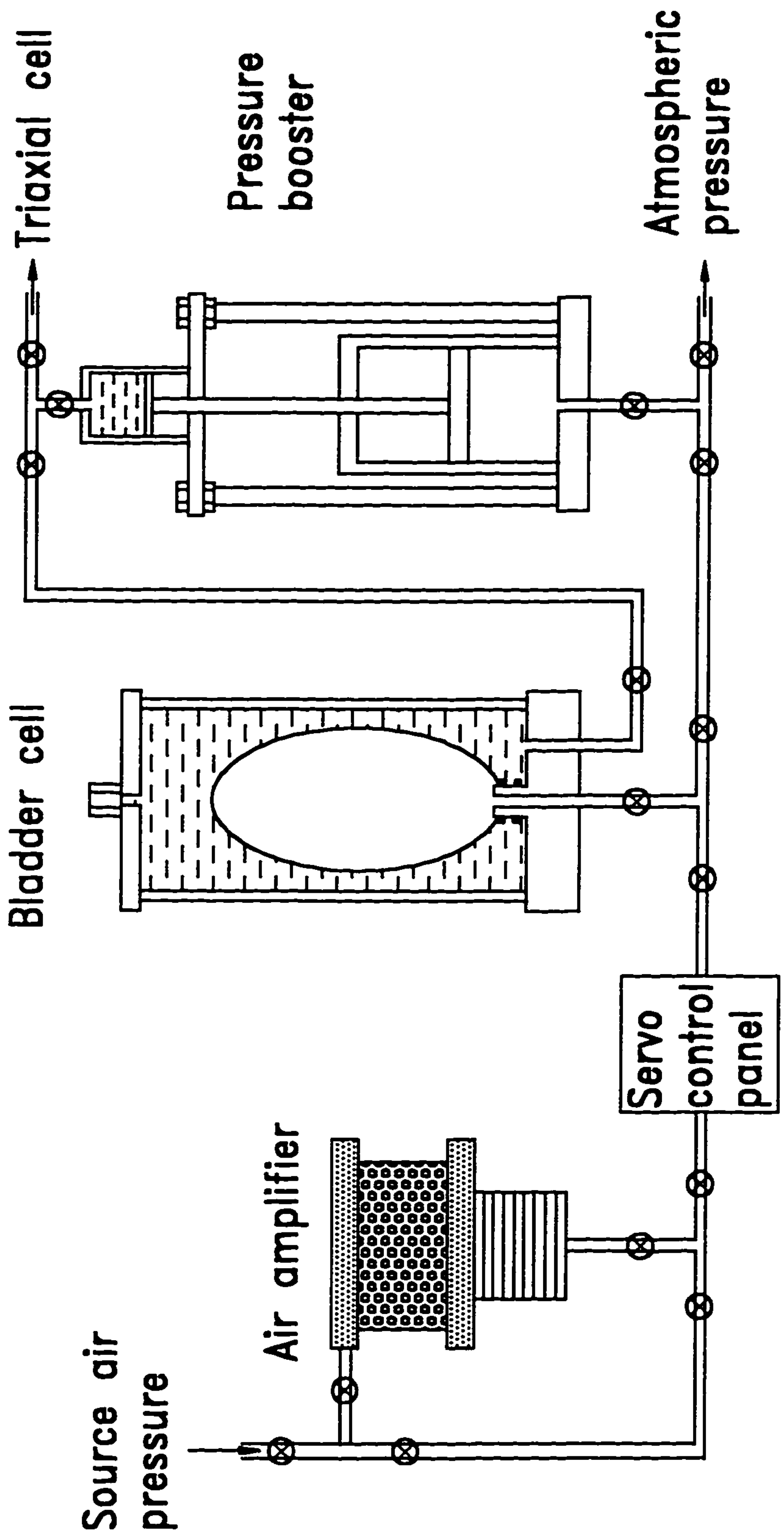

Fig. 3.4 Cell pressure system

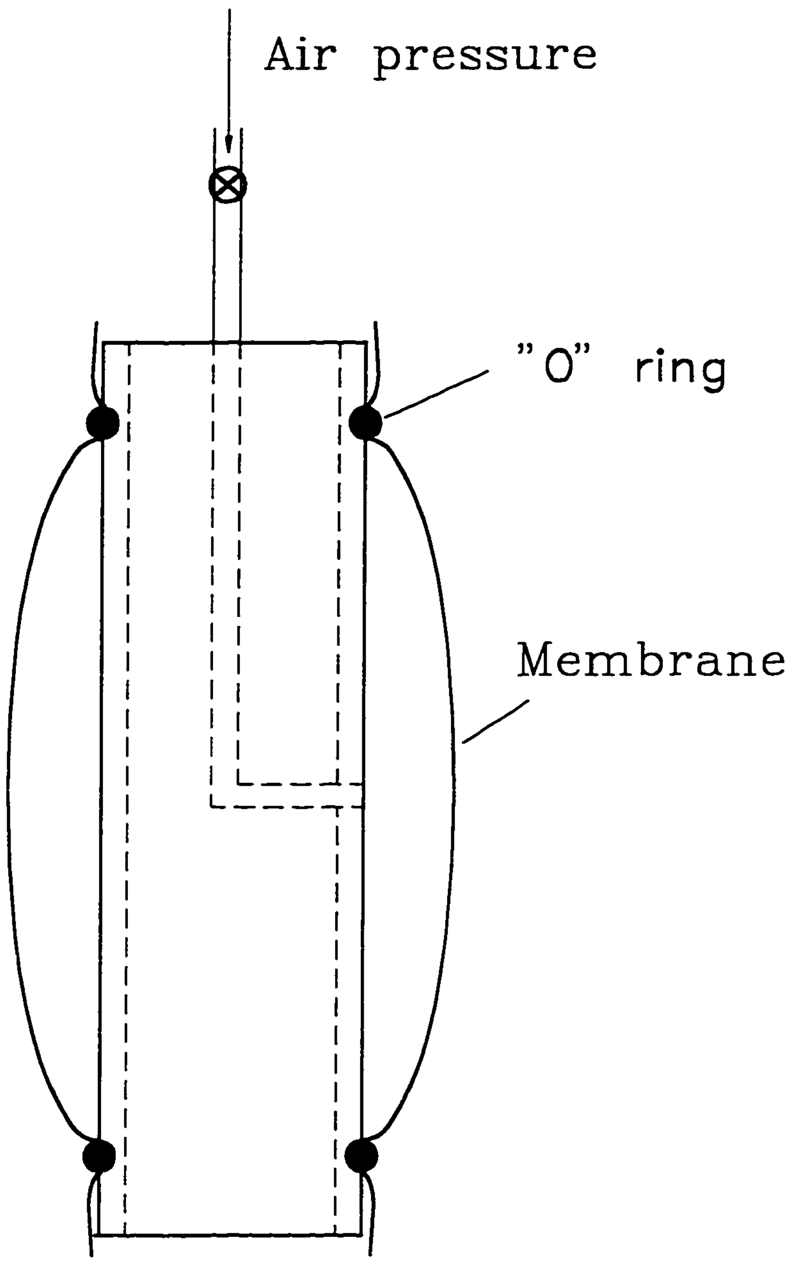

Fig. 3.5 Membrane checker

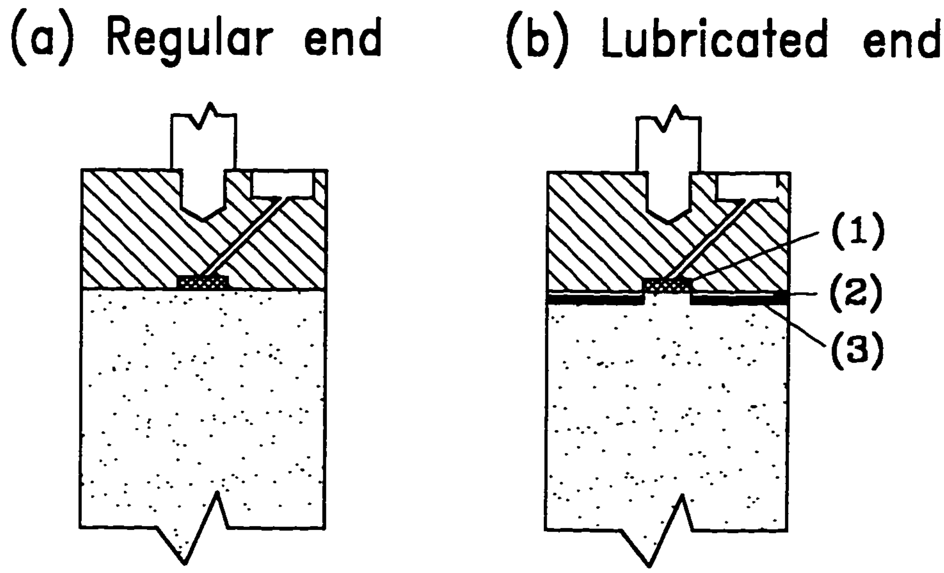

(1) Sintered bronze

(2) Silicon grease (0.04–0.06 mm)

(3) Circular rubber membrane (0.3 mm)

Fig. 3.6 Schematic diagram of end platens

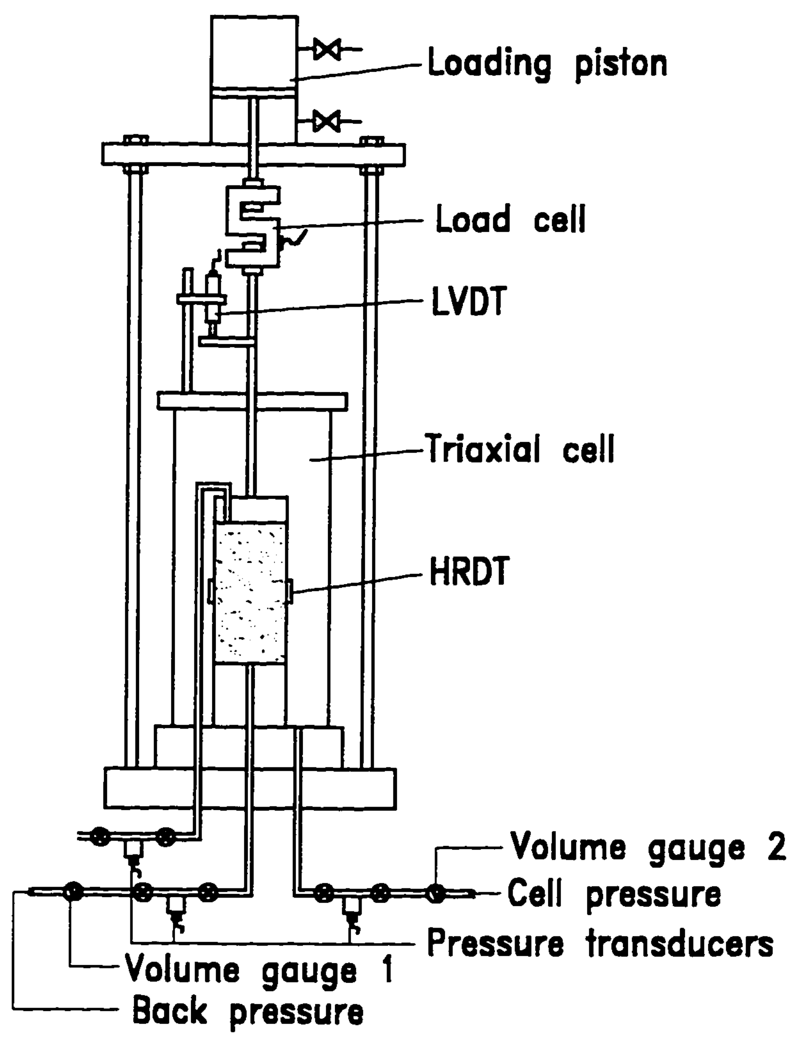

Fig. 3.7 Schematic diagram of triaxial apparatus

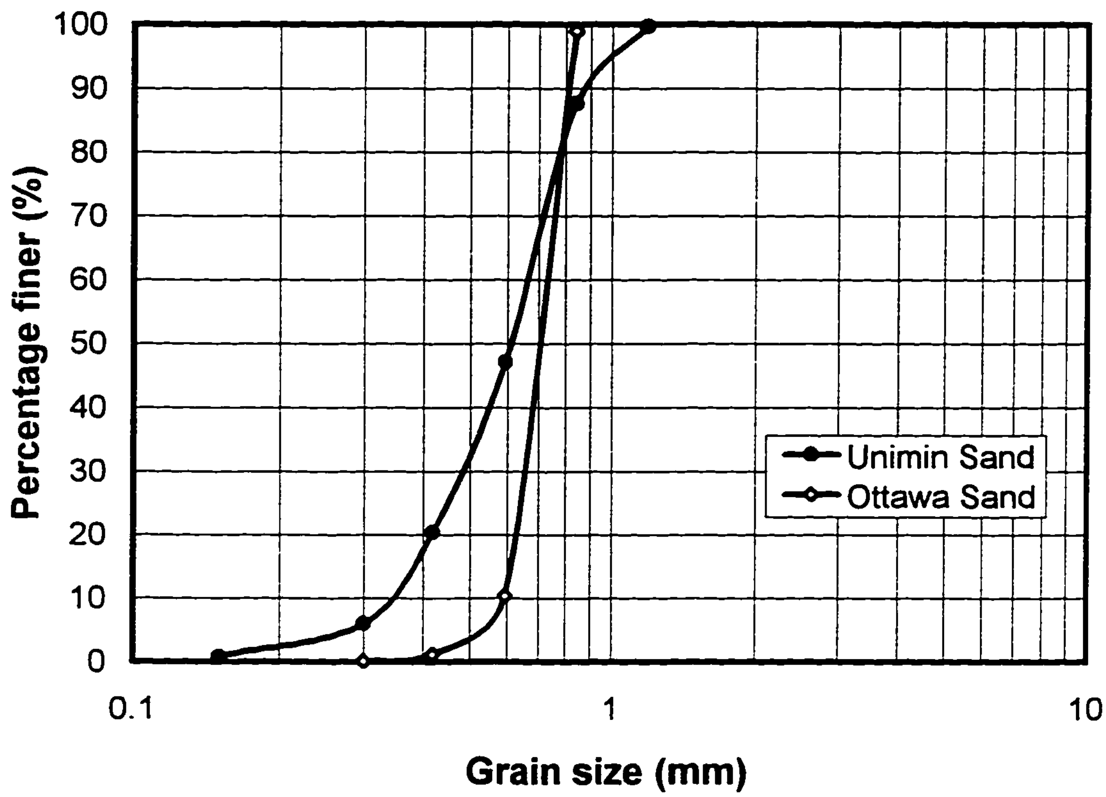

Fig. 3.8 Grain size distribution curves

CHAPTER 4

*VOLUME CHANGES IN UNDRAINED TRIAXIAL TESTS**

4.1 Introduction

The steady state line relates the void ratio and the effective stresses at the steady state (as defined by Poulos, 1981) in undrained triaxial tests or other shear tests on sands (Castro, 1969, Casagrande, 1975). This steady state line is unique for a given sand under undrained triaxial compression condition, regardless of the initial conditions of the sand samples (Castro et al., 1982, Poulos et al., 1985, Vaid et al., 1985, 1990, Sladen et al., 1985, Been et al., 1991, McRoberts et al., 1992, Negussey et al., 1994, etc.). However, the steady state line is often so flat within the normal range of in-situ stresses that a small change in the void ratio can result in a large change in the steady state strength. This may be one of the reasons why often the steady state, in practice, is not located along a unique line, but on a wide band for a given sand (e.g. Konrad, 1990 (a), (b)). As an important factor affecting the undrained behaviour of sands, void ratio may be altered substantially due to sample volume changes which occur in triaxial tests. Hence, it is of interest to investigate the potential volume changes of a sand sample in conventional undrained triaxial tests on saturated sands.

In laboratory tests, uncertainties of sample volumes can result from initial dimension measurement, sample saturation, membrane penetration and loading procedure. The error in initial void ratio of a sample may be caused by dimension measurement and weight measurement. The error in weight measurement, usually less than 0.01%, is negligible. Castro et al. (1982) considered that the error in dimension measurement should be less than $\pm$0.001

---

* A version of this chapter has been submitted for publication: Volume changes in undrained triaxial tests on sands. Canadian Geotechnical Journal.

in terms of void ratio. However, this was only the error estimated from the resolution of the measurement tools. Observer error in void ratio determination may be much larger than the resolution error.

It is often necessary to prepare a loose sand triaxial sample with strain-softening behaviour in unsaturated state, for example by using the moist tamping method (Castro et al., 1982), in which the surface tension between soil particles is employed to maintain a very loose sand structure. This type of structure can result in sample volume change during saturation. However, the volume change occurring during saturation is usually ignored due to the difficulty in measuring radial deformation of the sample. Sladen and Handford (1987) found that a very loose sample may be densified significantly during back pressure saturation. The potential error resulting from ignoring this densification was reported as much as 0.15 in terms of void ratio for the Syncrude tailings sand. Also, the volume change of a sand sample during saturation, which occurs after the dimension measurement and is usually ignored in triaxial tests, may be different for different saturation procedures.

Newland and Allely (1957) first observed that the membrane penetration into the interstices of the soil grains at a sample boundary under cell pressure can lead to erroneous volume measurement. Since then, many investigators have studied the measurement of, and correction due to the membrane penetration (e. g. Roscoe et al., 1963; Raju et al., 1974; Vaid et al., 1984; Ohara et al., 1991; Tanaka et al., 1991, Nicholson et al., 1993a, etc.). However, the membrane penetration can be affected by many factors including the effective confining pressure; grain size, shape, gradation, and density of the sample; characteristics of the rubber membrane such as thickness and extension modulii; and the surface area of the sample in contact with the rubber membrane (Raju and Sadasivan, 1974). Hence no single approach can consider all the factors and can be used to accurately estimate the membrane penetration for different sands

The volume of a saturated sand sample is not constant during undrained shear due to membrane penetration (Newland and Allely, 1959). This undrained volume change may significantly affect the undrained behaviour of sands. Thus, the correction of the membrane penetration effect, or its elimination have drawn much attention (e.g., Pickering, 1973; Kiekbusch et al., 1977; Lade et al., 1977; Martin et al., 1978; Molenkamp et al., 1981; Ramana et al., 1981; Baldi et al., 1984; Tokimatsu et al., 1986; Seed et al., 1989; Evans et al., 1992, Nicholson et al., 1993(b), Ansal et al., 1996, etc.). Seed et al. (1989) and Nicholson et al. (1993b) used a technique of injection/removal compensation to investigate the undrained behaviour of a sand. Their results showed that a partly strain-softening response without the injection compensation could become a strain-hardening response with the compensation. The use of their compensation scheme may overestimate the undrained strength of the sand samples with partly strain-softening behaviour.

A potential problem, which has been ignored to date, is whether the pore water volume can be changed during undrained loading on a saturated sand sample. It is a generally accepted assumption that the pore water within the sample is incompressible, because of the low compressibility of deaired water. However, the sample may not be completely saturated with water, particularly in the case of moist tamped samples. The compressibility of pore water in such a sand sample may not be negligible and may affect the undrained behaviour of sands.

The objective of this chapter is to investigate the errors in sample dimension measurements, the membrane penetration during consolidation, and in the sample volume changes during saturation and during undrained triaxial tests on sand samples. Further, the limitation of the constant volume triaxial tests is also explored.

4.2 Laboratory Investigation

The experiments in this study consisted of sample dimension measurement, saturation tests, consolidation tests, B value tests, undrained triaxial compression tests, deaired water compression tests and air dissolution tests. A height gauge was developed to measure the height of a triaxial sample (Fig. 3.2). A calibration curve can be obtained by using the height gauge to measure several aluminum dummy samples with known heights. Then the height of a sample can be easily measured to 0.01 mm with this height gauge. A Hall effect radial displacement transducer (HRDT) was improved, from the concept described by Clayton et al.

(1989), to measure the radial deformation of a triaxial sample during saturation and consolidation (Fig. 3.1). The HRDT has an effective linear range of about 2 mm, with a resolution of 0.01 mm. Two bellofram type volume gauges with resolution of 0.02 cm^3 were also used in the triaxial apparatus system (Fig. 3.7). One was connected to base of the sample in the usual manner, while the other was connected to the triaxial chamber in order to measure the volume change of the sample pore fluid, under constant cell pressure, during undrained loading.

The main material tested was the Unimin sand, an angular medium crushed quartz sand obtained from St-Canut, Quebec. Ottawa sand (C190) was also used in some tests. Their index properties are given in Table 3.1. The minimum and maximum void ratios were determined according to the ASTM test methods D 4253-93 (Method 1A) and D 4254-91 (Method A), respectively. Triaxial specimens, 50 mm in diameter × 100 mm in height, were prepared by water pluviation and moist tamping methods.

4.3 Dimension measurements

In order to investigate the measurement error, four dummy aluminum samples, whose dimensions (D = 48.86 ~ 50.76 mm, H = 100.54 ~ 111.25 mm) were previously measured by a caliper with resolution of 0.01 mm, were fully installed on the triaxial base, in a manner similar to a sand sample. Their heights were again measured by two different methods: caliper method (as used by Castro et al., 1982) and the height gauge method. In the caliper method, four readings of a sample height in different directions were taken, and their average was used as the measured height of the sample. In the height gauge method, only one reading was taken. The caliper method (as used by Castro et al., 1982) and perimeter tape method (as used by Sasitharan, 1994 and Verdugo and Ishihara, 1996) were also used to measure the diameters of the aluminum samples. In the caliper method, the diameters at the top, middle and bottom of a sample were measured over a membrane in two orthogonal directions. The average of the six readings, and deducting twice the thickness of the membrane, was used as the measured diameter. The perimeter of the sample was also measured by a perimeter tape with resolution of 0.5 mm. However, the corresponding accuracy, equal to $0.5/\pi = 0.15$ mm, was too poor to be acceptable for the measurement of the sample diameter (D = 50 mm) used in this study. Instead, the perimeter readings were taken by marking the circumferential connecting points on the tape with a fine pencil and measuring the linear distance between the connection points with a caliper. In this way, the perimeter readings at the top, middle and bottom of the sample were taken; and their average, divided by π and then deducting twice the thicknesses of the membrane and the perimeter tape, was taken as the measured diameter of the sample.

The errors in measurement are shown in Table 4.1. The error in height measurement by using the caliper method was large, from 0.09 to 0.23 mm. This error results mainly from the caliper inclination and the observer's error to distinguish the boundaries between a sample and the end platens. A two degree inclination of the caliper can make the measured length 0.06 mm longer than the nominal vertical length of 100 mm. The sample boundaries are usually not very distinct, particularly when observed from outside of a membrane. The height gauge method provided better results, with insignificant observation error. Its average relative error was only 0.02%, much less than that in the caliper method.

The error in diameter measurement by using a caliper was from 0.01 to 0.03 mm, less than that by using the perimeter tape. The average relative errors were 0.04% and 0.11% for the caliper method and the perimeter method, respectively. The limitations of the perimeter method are the low resolution of the perimeter tape and the difficulty of determining the contact points of the tape. The potential error in void ratio of a nominal 50 × 100 mm Unimin sand sample with Dr = 30% would be 0.006 and 0.003 by using a caliper to measure both the diameter and height of the sample, and by using a caliper to measure the diameter and using a height gauge to measure the height, respectively.

It should be noted that the measured volumetric error may be much higher in sand samples than in the aluminum dummy samples. The primary problem lies in the diameter measurement: how to contact a caliper or a perimeter tape on the surface of a sand sample accurately? A 0.1 mm or higher error in diameter measurement is possible; the corresponding error in void ratio for a 50 × 100 mm sand sample is over 0.008. The looser the sand sample, the higher the potential error. Unfortunately, the sand samples for the determination of the steady state line are often very loose. In order to increase the accuracy of the diameter measurement, it appears necessary to develop a better measurement device, or to apply a higher suction on the samples to reduce the uncertainty in the diameter measurement.

4.4 Volume change during saturation

Saturation of moist tamped samples is usually undertaken in two stages: water flushing and back pressure saturation. Two water flushing methods are commonly used. In the first method (e.g. Sladen et al., 1987), carbon dioxide gas followed by deaired water is flushed through the sample; then the sample top cap is seated and the membrane is secured with O-rings. At this step, the sample dimensions are measured after applying a low suction on the sample and removing the mold. In the second method (e.g. Sasitharan, 1994), the sample dimension is first measured under a low suction (about 20 kPa in this study) before carbon dioxide gas and water are flushed through the sample. In conventional triaxial tests, the volume change during back pressure saturation in the first method or during water flushing and back pressure saturation in the second method is often ignored.

In the first method in which sample dimension is measured after water flushing, no suction is applied during water flushing and so soil grains can move to a state approximating that in a water pluviated sample. Thus a loose sample prepared by moist tamping method will be formed close to the loosest density which can be reached in the water pluviation method. For example, two Unimin sand samples with initial relative densities of 7% and 19% were densified to relative densities of 25% and 26%, respectively (the loosest relative density for Unimin sand in water pluviation method is about 30%). Therefore, in order to obtain a larger density range, all other moist tamped samples in this study were flushed by using the second method only .

The procedure to prepare a saturated sand sample in this study was carried out in the following steps: (1) tamp a sample in five layers; (2) apply a suction (20 kPa) on the sample and measure its dimensions; (3) install the HRDT, the triaxial cell cover and the external LVDT; (4) fill the cell with water and apply a low cell pressure (25 kPa) on the sample; (5) remove suction and flush carbon dioxide gas and deaired water through the sample; (6) apply the desired back pressure and cell pressure. All displacements after the initial dimension measurement, except the vertical deformation during the installation of the triaxial cell, were monitored with the HRDT and the LVDT.

The test results of sample volume changes occurring in steps (4) to (6) are shown in Table 4.2 and Fig. 4.1. The results indicate that for the Unimin sand, the volume changes under a cell pressure increase of 25 kPa were small and did not vary significantly with relative density. During water flushing, the volume change was large at low densities (as high as 1.78 cm^3 for the sample with initial Dr = 1.9 %; but decreased rapidly up to a relative density of 30 %. During back pressure saturation, the volume change ranged from 0.27 to 0.92 cm^3. The entire saturation procedure resulted in a volume change of 0.026 to 0.008 in terms of void ratio; the looser the sample, the larger the volume change. This indicates that the error in void ratio due to ignoring the volume change during saturation can be over 0.020 for the loose Unimin sand samples. The steady state line is often very flat for many sands (Castro et al., 1982) and is usually determined based on the undrained tests on very loose samples. Thus, the high void ratio error in loose sand samples may significantly overestimate the undrained steady state strength for a given sand. For example, for the Unimin sand sample with a relative density of 30 %, an error in void ratio of 0.02 may overestimate its steady state strength from 101 kPa to 183 kPa.

Sladen and Handford (1987) showed that a very high error of 0.15 in terms of void ratio occurred in Syncrude tailing sand due to ignoring sample densification during back pressure saturation. Compared with the maximum void ratio changes of 0.026 during the entire saturation procedure and 0.009 during the back pressure saturation for the Unimin sand samples, the above mentioned 0.15 void ratio error appears to have been overestimated, since both Syncrude and Unimin sands have the same (e_{max} - e_{min}) difference value of 0.38. A void ratio change of 0.15 would make a loose Unimin sand sample become very dense. In the reported tests on the Syncrude sand, the final volumes of the samples were determined indirectly by measuring the moisture content of these samples subsequent to undrained shear. Thus the high estimated volume change reported by Sladen and Handford (1987) may result not only from the back pressure saturation, but also from the volume change during undrained shearing and lack of 100 % saturation of the samples.

4.5 Volume change due to membrane penetration

Volume change due to membrane penetration occurs when a latex membrane penetrates into the surface irregularities of a sand sample when applying effective confining stress to the sample during consolidation. It is equal to the difference between the total water volume expelled out of the sample and the volume change of the soil skeleton. In this study, only the effect of the membrane thickness on the penetration was investigated. The expelled water volume was measured by a precise volume gauge, and the skeleton volume change was determined from the vertical and radial deformations of the sample measured by the LVDT and the HRDT, respectively. Thus, the membrane penetration could be directly determined for each sample.

Water pluviated Unimin sand and Ottawa sand samples were used to determine membrane penetrations with thin (0.33 mm) and thick (0.62 mm) membranes. The initial relative densities of the Unimin sand and the Ottawa sand samples were about 33% and 17%, respectively. The test results are shown in Fig. 4.2. Clearly, the membrane thickness significantly affects the membrane penetration in both sands. The thinner the membrane, the higher the volume change due to the membrane penetration. The membrane penetration for the 0.33 mm membrane was 2 - 3 times that for the 0.62 mm membrane.

These results, as well as published data, indicate that it is questionable to apply a constant membrane penetration correction for different membranes and test conditions.

4.6 Compressibility of air-water mixture and B value

The compressibility of a fully deaired, i.e. "pure" water is equal to 4.58 × 10^{-7} (kPa^{-1}) (Fredlund and Rahardjo, 1993). When water pressure increases from 0 to 500 kPa, the volume change of the pore water in a fully saturated sand sample with typical dimensions of 50 × 100 mm is very small, equal to about 0.02 cm^3. However, the pore water in a "saturated" sand sample often contains some dissolved air and possibly even free air in some cases. The compressibility of water with dissolved air is approximately two orders of magnitude greater than that of pure water, and the inclusion of even 1 % free air in the voids is sufficient to significantly increase the pore fluid compressibility (Fredlund and Rahardjo, 1993). Hence, the pore fluid volume change in a saturated sand sample may be large enough to affect the undrained behaviour of sands, and therefore merited further examination.

4.6.1 Compressibility of air-water mixture

The water compression tests were conducted in a hydraulic consolidation cell (Garga and Khan, 1991). The compressibility of deaired water was obtained from the difference between the total volume changes of two deaired water samples with different volumes subjected to the same pressure. Then, the system volume change was calibrated by deducting the volume change of the deaired water from the total volume change of each of the two deaired water samples. Next, the compressibility of three water samples with different but known free air content was determined. The known free air content was introduced by using a syringe to draw the desired volume of water from the cell which was initially full of freshly deaired water.

The test results are shown in Fig. 4.3 and Table 4.3. It can be seen that the volume change of the fresh deaired water sample was very small, its volumetric strain was less than 0.1 % even at a pressure of 1500 kPa (Fig. 4.3). Its compressibility was equal to 13.7 - 3.4 × 10^{-7} kPa^{-1} in a pressure range of 0 - 1500 kPa (Table 4.3), close to that of pure water. However, the volumetric strain increased rapidly with increase in the initial free air content, changing from 0.03 % at a pressure of 400 kPa for the freshly deaired water, to 1.48 %, 3.35 % and 7.41 % for the initial air contents of 1.8 %, 4.2 %, 9.3 %, respectively (Fig. 4.3). The compressibility of the air-water mixture was, at low pressure, two orders of magnitude greater than that of the deaired water, and decreased with water pressure. Even at a water pressure of 500 kPa, the air-water mixture still exhibited high compressibility, 1.19×10^{-5} (1 / kPa), for an initial air content of 4.2 % (Table 4.3). This indicates that even using a high back pressure, the volume change of the pore fluid in a "saturated" sand sample may not be negligible during undrained loading, particularly in the case of moist tamped samples.

4.6.2 Solution of air in deaired water

It was noted during set up of sand samples that when a suction was adjusted before it was applied to a sample, numerous air bubbles appeared in the water in the tubing which was deaired only three hours back. This indicated that air could rapidly dissolve in the deaired water. In order to investigate the rate of air dissolution in deaired water, an oxygen meter (Model 860, manufactured by Orion Research Incorporated, Germany) was employed. In these tests, distilled water was filled into the tank of a Nold DeAeriator and was deaired under a suction of 97 kPa for 40 minutes. Next, the deaired water was drained into a 300 ml beaker after flushing the drainage line. The oxygen content in the deaired water was then measured at different times. The test results are shown in Fig. 4.4. It can be seen that the oxygen content in the fresh deaired water was 2.2 mg/l, and increased rapidly to 4.4 mg/l in 10 minutes. Two hours later, the deaired water had regained its original air content of 6.3 mg/l. This implies that, if assuming that air dissolves into the deaired water at the same rate as oxygen, and if the deaired water is used two hours after exposed to air in a small container, the deairing effect may be eliminated. One day later, the deaired water had an oxygen content of 9.0 mg/l, almost the same as that of tap water after waiting for ten hours. The oxygen content of the deaired water, kept in the Nold reservoir but exposed to air, increased to 4.4 mg/l in 12 hours, much lower than that of the deaired water contained in a beaker. It was also noted that the water deaired under high suction remains at an oxygen content of 2.2 mg/l. Thus, even the fresh deaired water is not fully deaired, and the compressibility of deaired water is larger than that of "pure" water.

4.6.3 Back pressure, B value and degree of saturation

Skempton's pore pressure coefficient B is usually used to verify the degree of saturation of a sample. In the 1980s, the sample was assumed to be saturated if the B value was equal to or larger than 0.95 (e.g. Castro et al., 1982); currently, a higher B value (0.99) is targeted (e.g. Sasitharan, 1994).

The B value tests on water-pluviated samples were conducted to investigate the volume change of pore water. The samples were prepared by pluviating boiled sands under freshly deaired water. The volume change in the measuring system due to pressure change was calibrated prior to the application of the back pressure. The water volume introduced into the samples due to back pressure change could then be obtained from the volume and deformation measurements. The test results shown in Fig. 4.5 indicate that the B values at zero back pressure were low, equal to 0.68 for Unimin sand and 0.72 for Ottawa sand. In order to reach a high B value of over 0.99, the required back pressure was 600 and 500 kPa, and the water volume introduced in the soil was 1.06 cm^3 and 0.98 cm^3 for Unimin sand and Ottawa sand samples, respectively. The compressibility of the pore water in the samples was equal to about 1.9×10^{-5} (kPa^{-1}), 21 times that of the freshly deaired water. This higher compressibility in the pore water may result from some tiny air bubbles which could have been caught between the membrane and the sample cap or base, or from the compression of the pore water.

The B value tests on moist tamped Unimin sand samples were also carried out to investigate the relationships between the back pressure and B value or the degree of saturation. The samples were flushed with or without carbon dioxide gas before flushing water. The final degree of saturation of the samples was obtained from the final dimensions and the final water content of the sample. Then, the degree of saturation could be determined based on the deformations, introduced water volume and the final degree of saturation. The test results are shown in Fig. 4.6. For the CO_2 flushed sample, the degree of saturation was equal to 94% at zero back pressure, and its B value was as high as 0.934 under a back pressure of 100 kPa. When the degree of saturation was increased to 99.7 %, a B value of 1.011 was obtained. In the sample without CO_2 flushing, the degree of saturation was equal to 74 % at zero back pressure, much less than that for the CO_2 flushed sample, and could attain a value of only 98 % under a back pressure of 700 kPa. Its B value was low, equal to 0.502 and 0.98 under back pressures of 100 and 700 kPa, respectively. Therefore, in order to obtain a highly saturated sand sample, it is necessary to flush carbon dioxide gas through the sample before flushing deaired water.

Even a high B value, over 0.99, may not indicate a sand sample to be fully saturated in some cases. Skempton (1954) derived the pore pressure coefficient, B, as a function of the porosity n, the compressibility of pore fluid C_v and the compressibility of soil skeleton C_c: $B = \frac{\Delta u}{\Delta \sigma_3} = \frac{1}{1 + nC_v / C_c}$. This expression indicates that the B value would be always less than unity. When the voids in a soil sample are fully saturated with water, the void fluid compressibility nC_v is equal to the water compressibility nC_w, much less than that of the soil skeleton. Thus the B value is close to, but less than unity. It is in fact assumed in the derivation of the formula that the volume change of the soil skeleton could be caused only by the variation in effective confining stress. However, in the case of sandy soils, the skeleton volume change can occur under constant effective confining stress due to the application of back pressure (Sladen and Handford, 1987 and previous section in this paper). If under undrained condition, the skeleton volume change is close to or larger than that of the pore fluid due to application of the cell pressure, the B value can be close to or over unity, even though the sample may not be completely saturated.

4.7 Volume change during undrained loading

4.7.1 Consideration of sample volume change

The volume change of a soil sample results from its void volume change, which consists of two components. The first component is due to the fluid drainage out of or into the soil skeleton and the second component is due to the compression of the pore fluid. No pore fluid is drained out of the sample under undrained loading condition. Since the membrane penetration varies with the change in effective confining stress, the pore fluid can however migrate into or from the sample peripheral boundary. This migration can result in a change of the sample skeleton volume (Newland and Allely, 1959). The application of a vertical stress may also cause a further compression of the pore fluid. Therefore, the volume change of a saturated sand sample during undrained loading can be expressed as follows:

$$\Delta V = \Delta V_m + \Delta V_w \tag{4-1}$$

In which, ΔV = Volume change of a sample (compression as positive).

ΔV_m = volume change due to membrane penetration.

ΔV_w = Volume change of pore fluid.

If the effective confining stress varies from the consolidation stress σ_{3c}' to some value σ_3' due to the buildup of the pore pressure in the sample during undrained loading, the volume change due to membrane penetration is given by:

$$\Delta V_m = A_{mc}\mu(\sigma_{3c}') - A_m\mu(\sigma_3') \tag{4-2}$$

where, $\mu(\sigma)$ is the unit membrane penetration, dependent on the effective confining stress for a given sample. It can be predetermined at the consolidation stage for each sample. A_{mc} and A_m are the sample peripheral areas corresponding to σ_{3c}' and σ_3', respectively. Based on the relationship between diameter and height of a triaxial sand sample at axial strain ε_a and volumetric strain ε_v during loading (Chapter 5), the peripheral area, A_m, can be expressed as follows:

$$A_m = \frac{1}{6} A_{mc}(1-\varepsilon_a)\left\{\sqrt{\left[\frac{30(1-\varepsilon_v)}{(1-\varepsilon_a)} - 5\right]} + 1\right\} \tag{4-3}$$

The volumetric strain ε_v is usually less than 0.01 under undrained loading, and may be negligible. Therefore,

$$\frac{A_m}{A_{mc}} = \frac{1}{6}\left[\sqrt{5(5+\varepsilon_a)(1-\varepsilon_a)} + (1-\varepsilon_a)\right] \qquad (4\text{-}4)$$

The volume change of the pore fluid, ΔV_w can be determined by measuring the cell water volume change during undrained loading:

$$\Delta V_w = \Delta V_t - \Delta V_c - \Delta V_{crp} + \Delta V_p \qquad (4\text{-}5)$$

where, ΔV_t = total volume change of the cell water, measured by a volume gauge connected to the triaxial cell;

ΔV_c = volume change of the triaxial cell, equal to zero when cell pressure is constant;

ΔV_p = volume change of the cell water due to the movement of the loading piston, equal to the vertical deformation times the area of the piston;

ΔV_{crp} = volume change due to the creep deformation of the triaxial cell and the cell water. It is usually negligible if the undrained test is conducted after 40 minutes or longer subsequent to the application of the cell pressure in the system used in this investigation.

4.7.2 Test results of undrained volume change

The results of conventional undrained triaxial tests on Unimin sand are showed in Figs 4.7 to 4.9 and in Table 4.4. For a loose Unimin sand sample, its deviator stress and induced pore pressure gradually increased up to a small strain (less than 1 %), then a sudden collapse occurred with a significant decrease in the deviator stress and a large increase in the induced pore pressure. Following this collapse, with further axial strain, the deviator stress continuously increased accompanied by a decrease in the pore pressure (Fig. 4.7). It is noted that the post-collapse behaviour was observed for all loose Unimin sand samples. The medium dense Unimin sand sample exhibited a typical strain-hardening behaviour as shown in Fig. 4.8.

The tests on samples with dilative behaviour show that the pore fluid compression increased with strain at initial stage of undrained loading, reaching a peak at about the phase transformation (Ishihara et al., 1975), and then slightly decreased or remained constant (Fig. 4.8). In a loose sample with contractive behaviour, the volume of the pore fluid decreased during initial straining and collapse, and then slowly increased or remained essentially constant with further strain (Fig. 4.7).

The membrane penetration volume change was estimated from the pore pressure, hence its tendency was similar to that of the pore pressure (Figs 4.7 and 4.8). The penetration volume change during undrained loading is mainly dependent on the change of the effective confining stress. The higher the consolidation stress of a sand sample, the larger its penetration volume change at the onset of collapse and at the phase transformation (Table 4.4). The results in Fig. 4.7 show that prior to the collapse, the effective confining stress decreased from the consolidation stress of 200 kPa to 76 kPa, and caused a total volume change of 0.57 cm^3. During collapse, the effective stress dropped rapidly to 10 kPa and the membrane penetration volume change increased to 1.41 cm^3. The membrane penetration volume change continued to decrease with further strain due to subsequent decrease in pore pressure.

Table 4.4 and Fig. 4.9 show a summary of the volume changes during undrained loading in twelve samples of the Unimin sand tested at different relative densities. The volume change due to the pore fluid compression during undrained loading varied from 0.05 to 0.23 cm^3 at the onset of collapse and from 0.08 to 0.39 cm^3 at the phase transformation. The compressibility of the pore fluid in these samples varied between 3 ~ 14 $\times$ 10^{-6} (1/kPa), which are within the range of compressibility of the deaired water as shown in Table 4.3. The membrane penetration volume change was large, about six times the pore fluid volume change. It resulted in a change of 0.003 to 0.020 in void ratio at the onset of collapse and from 0.009 to 0.027 at the phase transformation stage (Fig. 4.9).

4.7.3 Effect of undrained volume change on steady state strength

Seed et al. (1989) and Nicholson et al. (1993b) found that the variation of membrane penetration during undrained shear in a conventional undrained triaxial test may significantly affect the steady state line of a sand. They further stated that this effect on the steady state line may be eliminated by conducting constant volume triaxial tests or undrained triaxial tests on large samples, or by deducting the variation of membrane penetration from the consolidation volume of a sample in a conventional undrained triaxial test.

The steady state lines for the Unimin sand both with and without volume correction are shown in Fig. 4.10. The steady state line (SSL1) at which the total volume change at the onset of collapse is corrected, is much lower than the steady state line (SSL) without any volume correction. For the Unimin sand, the difference in mean effective stress between SSL and SSL1 is 5 kPa for very loose samples, and over 100 kPa for medium dense samples. If the total volume change at phase transformation (PT) is corrected, the steady state line of the sand (SSL2) is even lower. For a given void ratio, the steady state stress p' determined from SSL2 is only approximately 76% of that determined from the steady state line without volume change. Therefore, the steady state strength of a sand may be significantly overestimated in conventional undrained triaxial test due to the variation of membrane penetration during undrained shear.

The induced pore pressure during undrained shear reflects the global volume change tendency of a sample, which may be also affected by the sample end restraint (Chapter 6) and the formation of shear band (Finno et al., 1996). Thus, care should be exercised to correct the induced pore pressure or to carry out the constant volume tests. For example, in some cases, the corrected pore pressure could be larger than the cell pressure in a conventional undrained triaxial test (Ansal et al., 1996). Also, for a sand sample with quasi-steady state behaviour, its undrained strength under "constant volume condition" could be much larger than that under conventional undrained triaxial shear condition (Seed et al., 1989, Nicholson et al., 1993b). Furthermore, if the "constant volume tests" are stress- or strain-controlled by utilizing a servo loading system, the volume change of a loose sand sample resulting during rapid collapse may not be eliminated. The increase in pore pressure during the collapse of the sample is faster than the response of most servo activated systems.

Further evidence is necessary to determine whether the membrane penetration correction should be applied at the onset of collapse or at the phase transformation for obtaining the real steady state line.

4.8 Conclusions

1. Volume change during saturation and membrane penetration during consolidation can be easily determined by directly measuring axial and radial dimensional changes of a sample.

2. The volume changes due to flushing water through a moist tamped sand sample (nominally 50 mm in diameter and 100 mm in height) and due to back pressure saturation can reach 1.78 and 0.92 cm^3, respectively; and the total volume change during the entire saturation procedure can be 2.79 cm^3 for the Unimin sand.

3. A high B value may not necessarily imply that a sample is completely saturated. Evaluating the void ratio from the final water content after shear may result in large error in void ratio.

4. Air can dissolve in deaired water rapidly. The compressibility of pore water in a saturated sample is much larger than that of pure water. For the water pluviated sand samples, the average compressibility of pore water was about 20×10^{-6} (1/kPa) in the pressures range of 0 to 500 kPa. The compressibility of the pore water in moist tamped samples was from $3 \sim 14 \times 10^{-6}$ (1/kPa) during undrained loading.

5. The volume change of a sand sample during undrained loading consists of two components: the compression of pore fluid and the penetration volume change. The pore fluid volume change varied from 0.08 to 0.39 cm^3 at the phase transformation, mainly depending on pore pressure and density of the samples. It reached a peak at about the phase transformation. The

penetration volume change varied from 0.30 to 1.73 cm^3 at the onset of collapse and from 0.77 to 2.20 cm^3 at the phase transformation, depending on the induced pore pressure.

6. Different steady state lines were obtained from volume corrections applied at the onset of collapse and at phase transformation.

Table 4.1. Error in dimension measurement

	Error in Height		Error in Diameter	
	Height Gauge M.	Caliper Method	Perimeter Method	Caliper Method
Error Range (mm)	-0.02 ~ 0.03	0.09 ~ 0.23	-0.07 ~ 0.06	-0.01 ~ 0.02
Ave. Relative Error (%)	0.02	0.14	0.11	0.04
Note: Ave. Relative Error = Σ{measured dimension - known dimension} / Σ{known dimension}				

Table 4.2 Volume changes during saturation (Unimin sand)

Initial D_r (%)	ΔV_{CP} (cm^3)	ΔV_{water} (cm^3)	ΔV_{BP} (cm^3)	Total ΔV (cm^3)	Total Δe	B value
1.9	0.34	1.78	0.50	2.79	0.026	1.014
4.3	0.25	1.68	0.27	2.18	0.023	1.006
6.9	0.31	1.33	0.35	1.99	0.020	1.004
14.7	0.24	0.78	0.89	1.90	0.019	1.011
17.0	0.34	0.34	0.92	1.60	0.016	1.018
28.1	0.26	0.12	0.43	0.81	0.008	0.997
33.4	0.12	0.16	0.71	0.99	0.009	
45.1	0.24	0.22	0.43	0.89	0.009	
54.7	0.12	0.08	0.67	0.87	0.008	
Note: ΔV_{CP}, ΔV_{water} and ΔV_{BP} are the volume changes due to application of 25 kPa cell pressure, flushing water through sample, and back pressure saturation (BP = 500 kPa), respectively.						

Table 4.3. Compressibility of water (10^{-7} 1 / kPa)

Pressure (100 kPa)	0 ~ 1	1 ~ 2	2 ~ 4	4 ~ 6	6 ~ 8	8 ~ 10	10 ~ 13	13 ~ 15
Initial air content								
0 %	13.7	8.9	6.9	5.6	4.7	4.0	3.4	3.4
1.8 %	867	334	140	58	38	21	21	21
4.2 %	2027	703	311	119	79	48	34	21
9.3 %	4413	1671	665	280	157	119	59	48

Table 4.4. Undrained volume changes of loose Unimin sand samples

D_{rc} (%)	σ_{3c} (kPa)	at onset of collapse				at phase transformation			
		σ_3' (kPa)	ΔV_w (cm^3)	ΔV_m (cm^3)	ΔV (cm^3)	σ_3' (kPa)	ΔV_w (cm^3)	ΔV_m (cm^3)	ΔV (cm^3)
13.9	100	62	0.05	0.30	0.33	5	0.08	0.77	0.85
15.5	200	71	0.13	0.53	0.66	7	0.22	1.08	1.30
17.4	200	76	0.10	0.57	0.67	10	0.17	1.41	1.58
21.1	200	94	0.17	0.95	1.12	15	0.24	1.31	1.55
25.2	399	163	0.14	0.94	1.08	34	0.24	1.43	1.67
26.7	200	93	0.07	0.32	0.39	15	0.12	1.00	1.12
28.5	500	187	0.07	0.98	1.06	36	0.13	1.65	1.78
29.3	398	166	0.11	0.52	0.63	39	0.19	1.42	1.61
37.5	601	211	0.18	1.35	1.68	84	0.33	1.88	2.21
39.6	806	354	0.15	1.25	1.40	118	0.26	2.05	2.31
41.4	997	349	0.19	0.92	1.11	155	0.32	1.53	1.85
45.1	1092	380	0.23	1.73	1.96	195	0.39	2.20	2.59

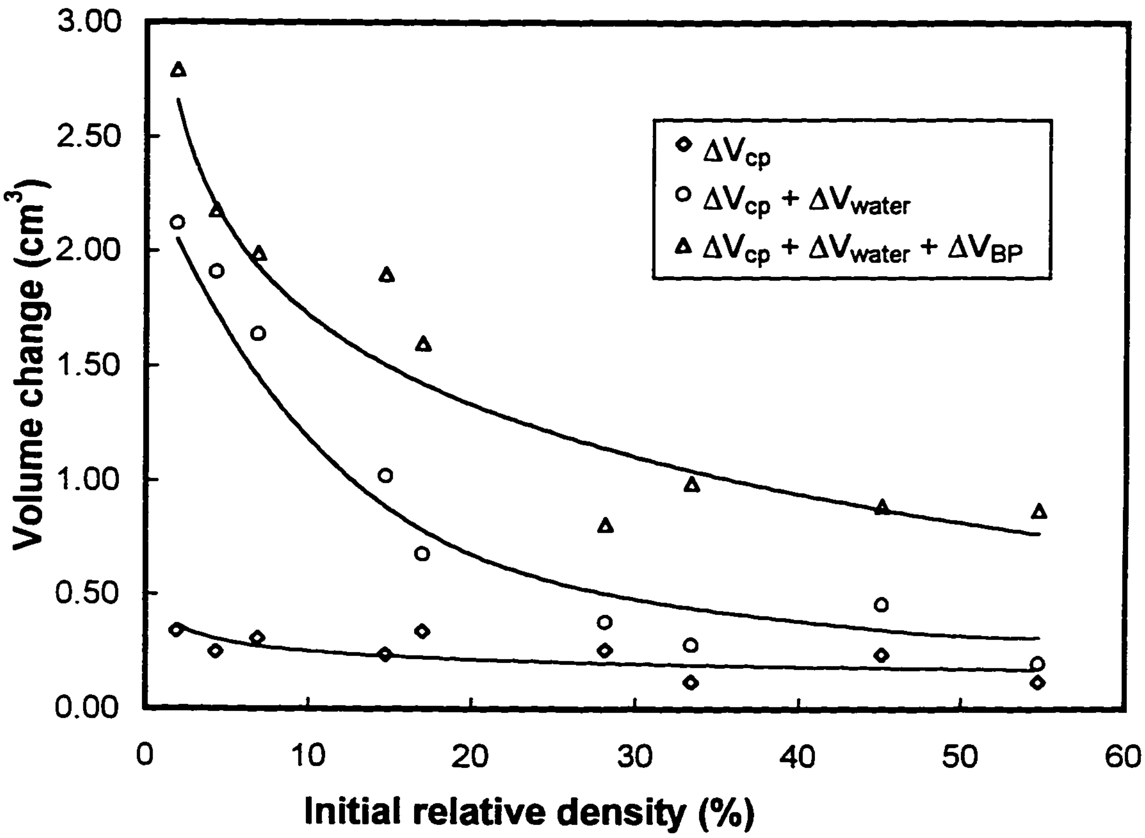

Fig. 4.1 Volume change during saturation (Unimin sand)

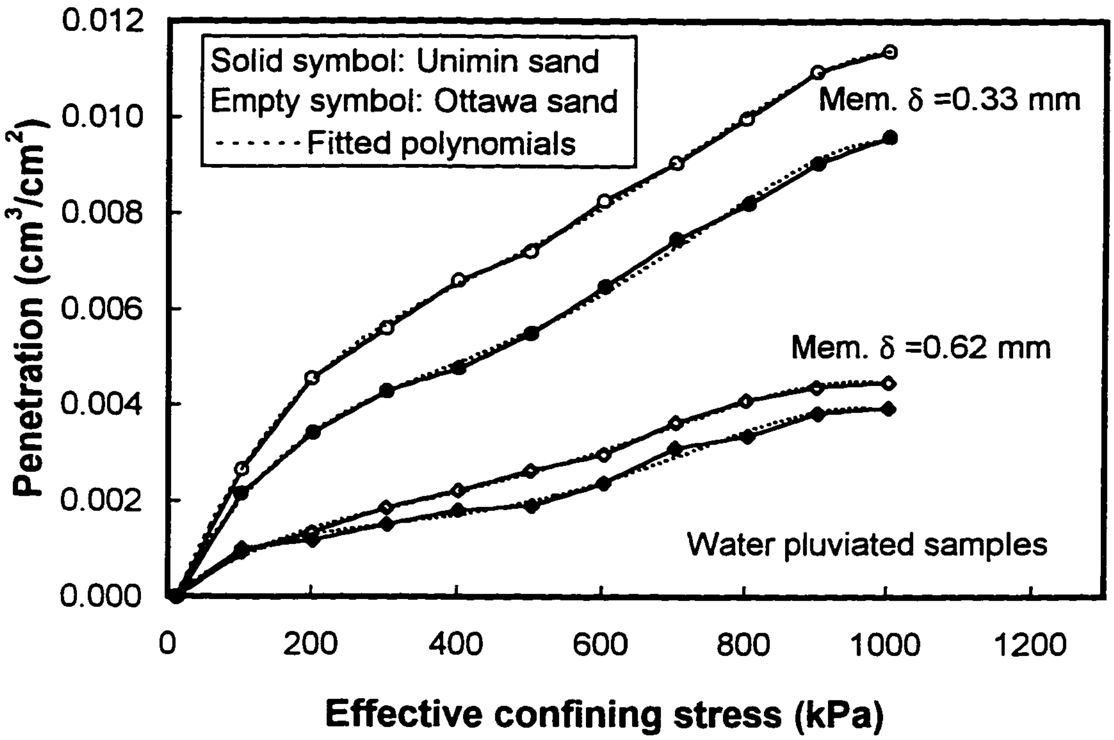

Fig. 4.2 Membrane penetration

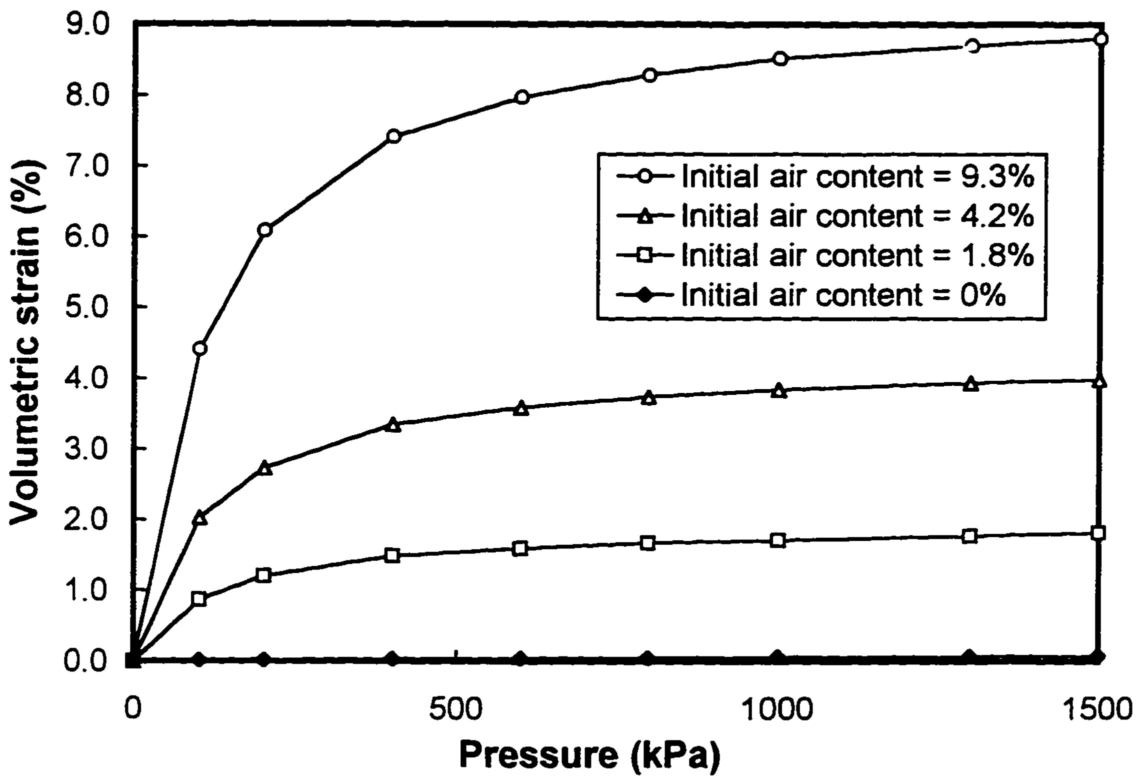

Fig. 4.3 Compression of air-water mixture

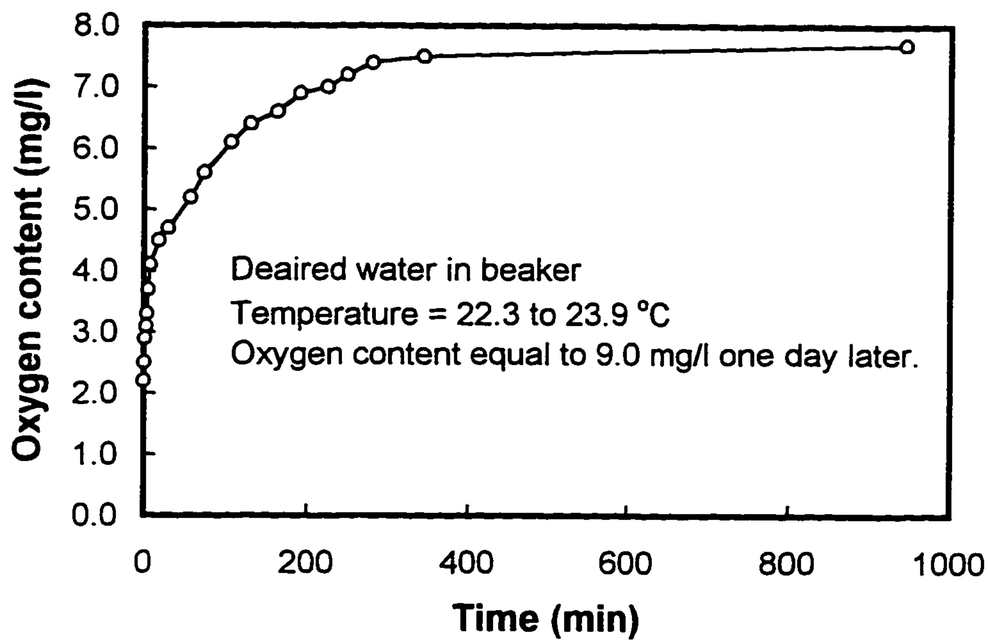

Fig. 4.4 Air dissolution test results

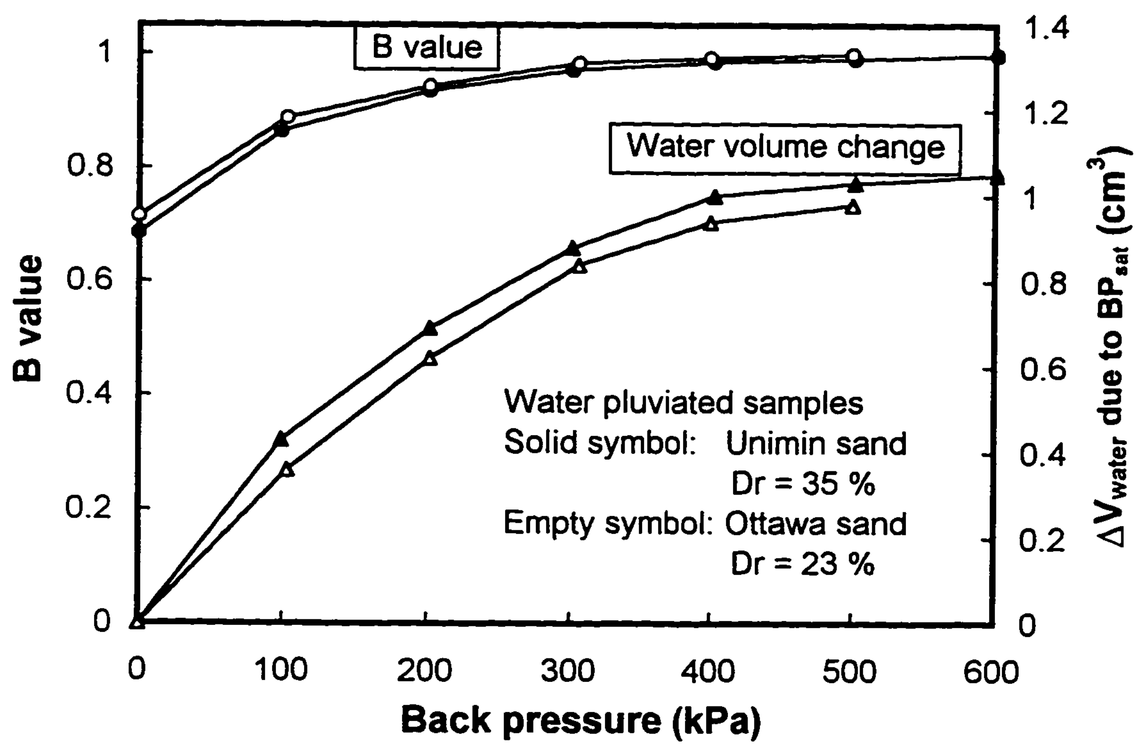

Fig. 4.5 Relationship between Back P. and B value

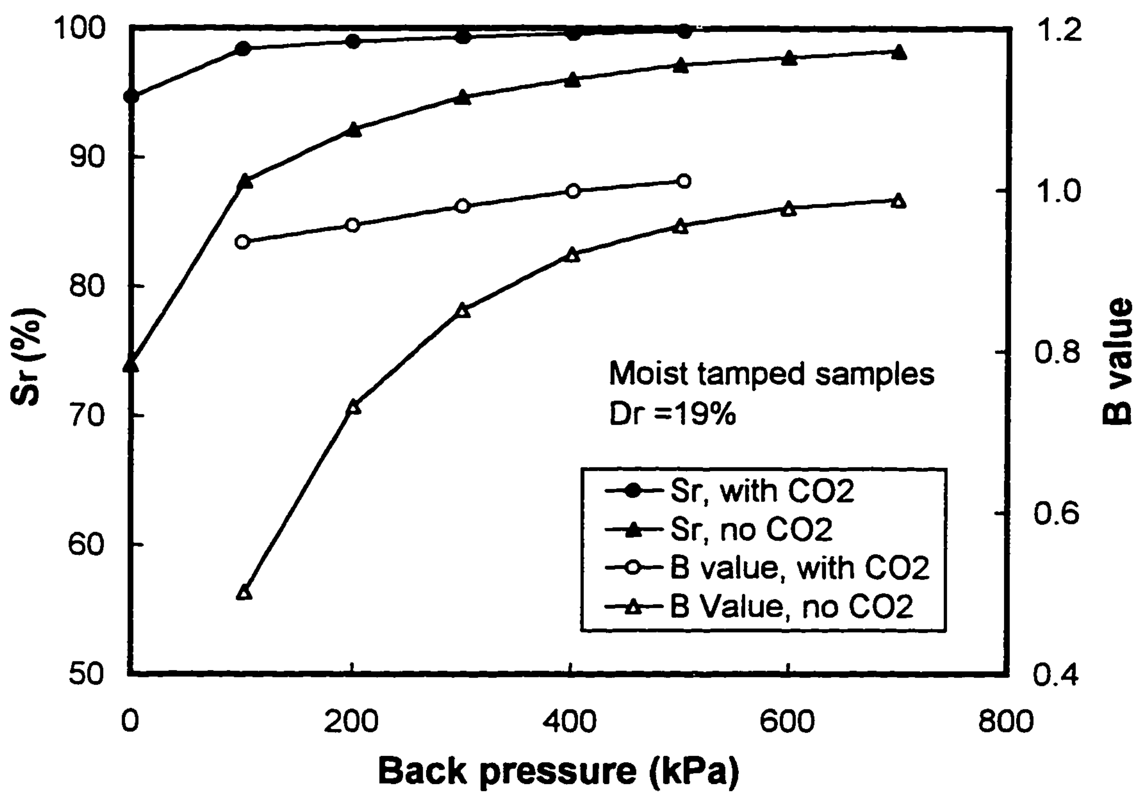

Fig. 4.6 Relationship between BP, B value & Sr (Unimin sand)

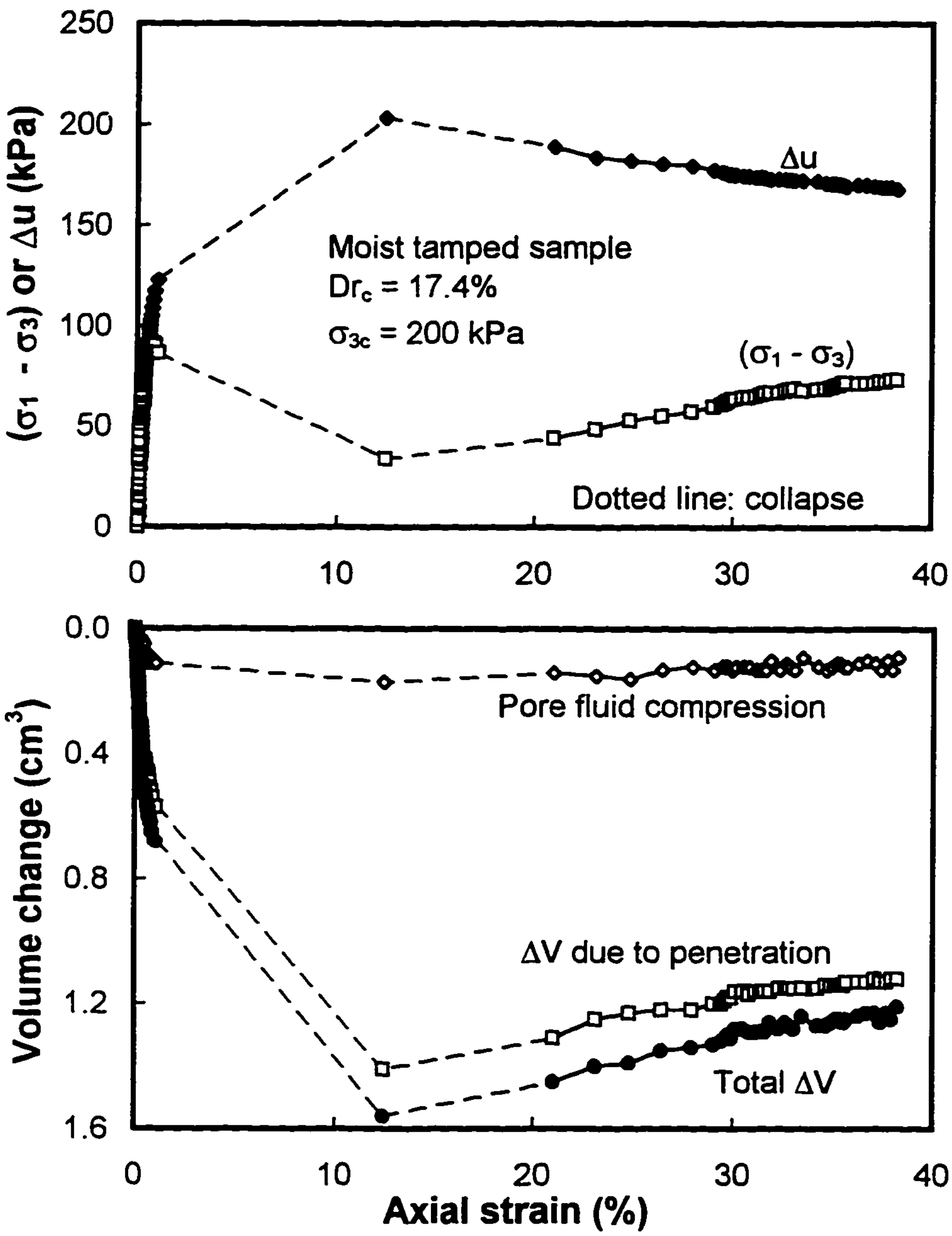

Fig. 4.7 Undrained volume change (loose Unimin sand)

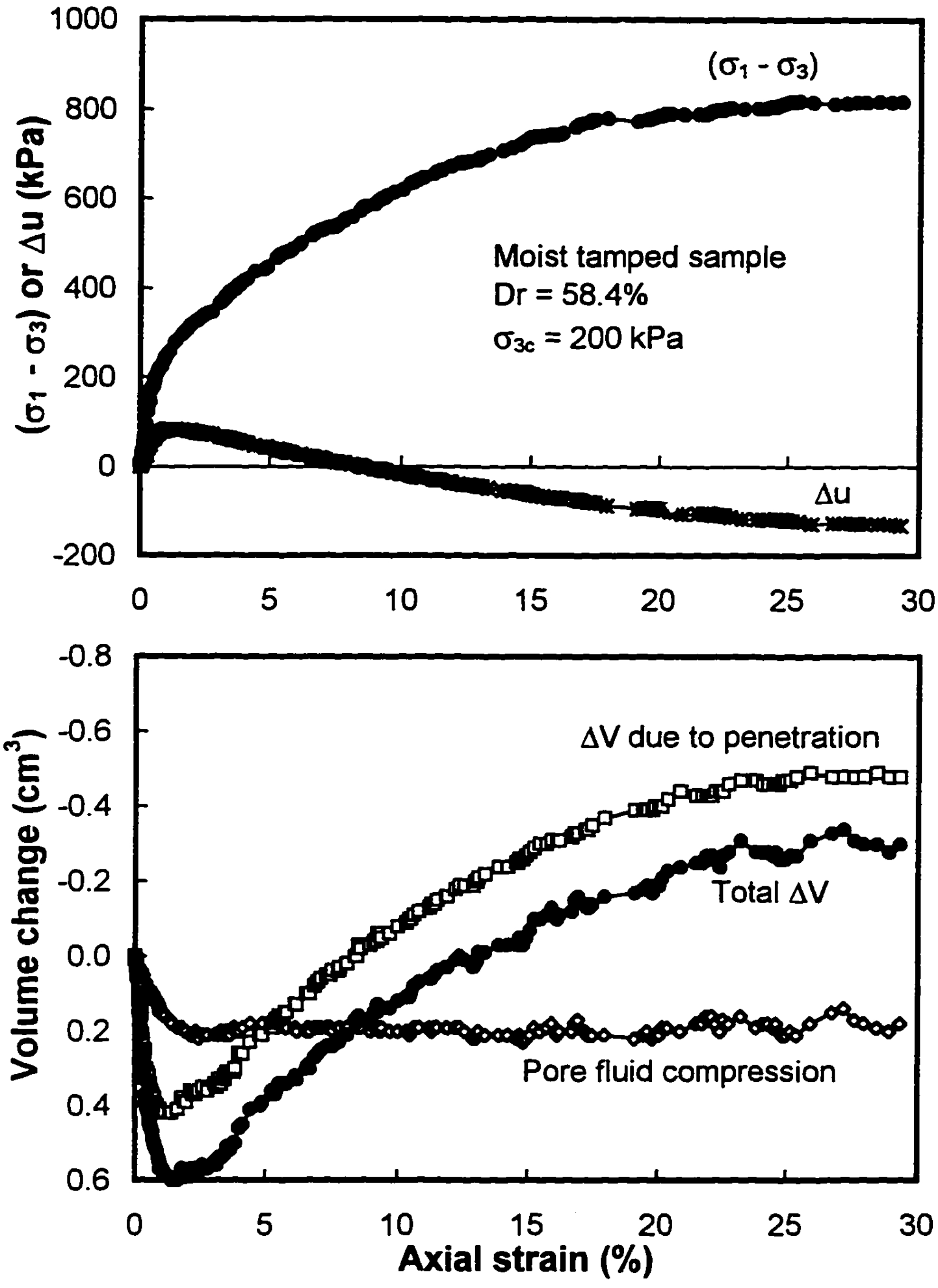

Fig. 4.8 Undrained volume change (medium dense Unimin sand

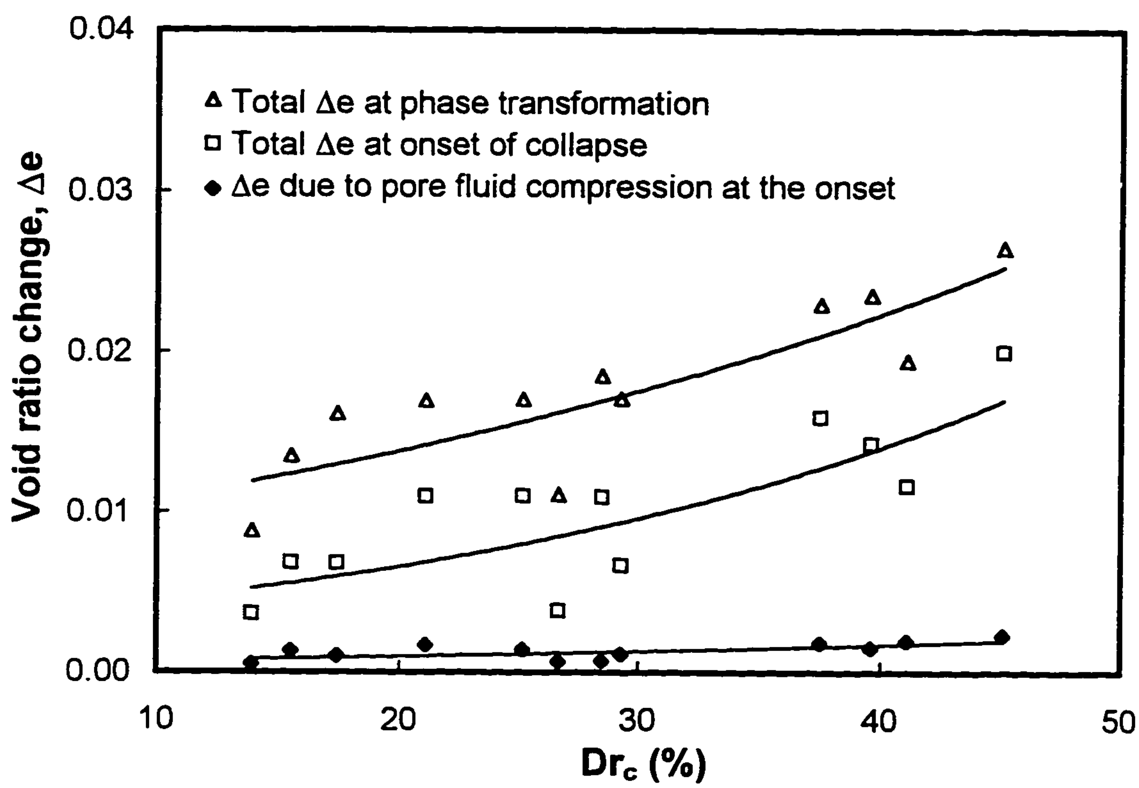

Fig. 4.9 Volume change during undrained loading (Unimin sand

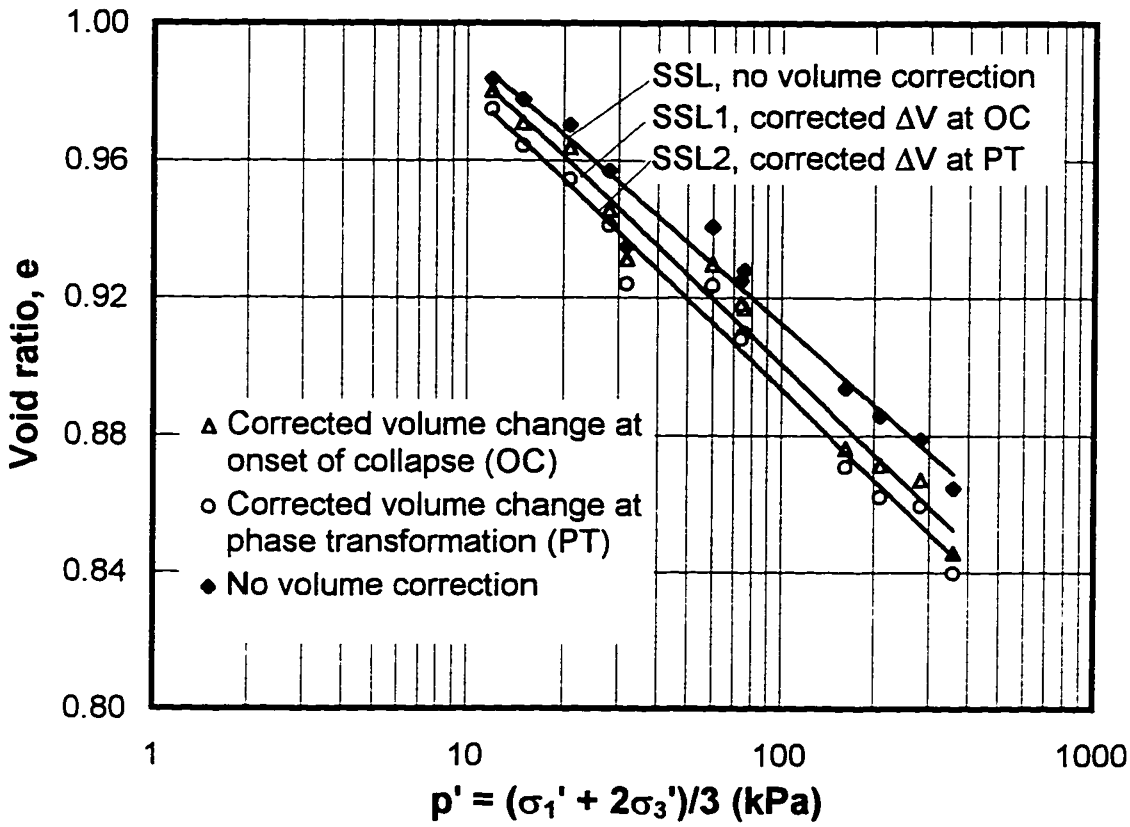

Fig. 4.10 Effect of undrained volume change on steady state line

CHAPTER 5

AREA CORRECTION IN TRIAXIAL TESTS

5.1 Introduction

In order to obtain the steady state strength of sand, it is necessary to shear a sand sample to large axial strain in triaxial tests. A triaxial sample may significantly bulge at large axial strain. This bulging deformation makes the calculation of cross-sectional area difficult, and thus may result in errors in deviator stress.

The bulging deformation results from sample end restraint. In order to reduce the end restraint or the friction between end platens and sample, several types of end platens have been developed, for example, segmented end platens (Taylor, 1941; Tschebotarioff et al, 1956), segmented soil sample (Blight, 1965), shaped end platens (Cooling and Golder, 1940; Larew, 1960), end platen with silicone grease covered by latex membrane (Rowe, 1962). Of these end platens, only the lubricated end platen developed by Rowe (1962) is widely accepted due to its convenience and effectiveness in reducing the end friction. Rowe and Barden (1964) reported that by using the lubricated end platens, triaxial sand samples with 1:1 slenderness could deform uniformly even at large axial strain. Similar results were observed by Bishop and Green (1965). However, the 1:1 samples with lubricated end platens may not provide significantly more accurate results than the 2:1 samples with regular end platens (Bishop and Green, 1965). Also, for samples with slenderness of 2:1, similar central bulging effects are encountered, whether the end platens are lubricated or not (Bishop and Green, 1965, Olson and Campbell, 1964).

The deviator stress of a triaxial sample is equal to applied axial load divided by the cross-sectional area of the sample. Traditionally, the cross-sectional area is calculated by assuming the sample deforming as a right circular cylinder during shear (ASTM, 1993c). In other words, the overall average area of the sample is used to calculate the deviator stress. However, sample bulging due to end restraint leads the cross-sectional area within failure zone always larger than the overall average area, and thus results in the overestimation of shear strength. For example, Bishop and Green (1965) found that the peak effective angle of internal friction of a Ham River sand sample was equal to 37.6°, 37.1° and 36.9° by using the overall average area, the central half average area and the area at mid-height of the sample, respectively. It was noted that the peak deviator stress occurred at an axial strain of 7 %. When a higher axial strain is required, such as in determining the steady state strength of sands, the error due to the area correction may be higher. Therefore, it appears necessary to develop an appropriate method to correct triaxial sample area during shear.

A simple method of correcting the cross-sectional area of a triaxial sample is developed in this Chapter. The error in shear strength of triaxial samples by using the conventional area correction is also evaluated.

5.2 Measurement of sample diameters

Diameter measurement tests were conducted to investigate the deformation profile of a triaxial sand sample at different axial strains. A sand sample was prepared by using moist tamping method, and was saturated by flushing carbon dioxide gas and deaired water and further saturated by using back pressure saturation method. Then, both cell pressure and back pressure were unloaded, cell water was drained off under a suction of 23, 30, or 60 kPa, and the triaxial cell cover was carefully removed. Subsequently, the procedure of measuring the diameters at different axial strains was as follows: (1) the sample was marked at different heights, the diameters at the marked points were measured by using a caliper, and the height of the sample was measured by using the height gauge (Chapter 3); (2) the triaxial cell cover was installed, and a ram lock was fixed on the loading ram at a desired position so that the required axial strain could be reached when the lock touched the top of the triaxial cell cover; (3) the axial load was slowly increased until the desired axial strain was reached; (4) the axial load was unloaded, the triaxial cell cover was removed, and the diameters of the sample at the marked points were measured; (5) the diameters for different axial strains were measured by repeating steps (2) to (4). The suction applied on the sample was maintained constant during the procedure, and the axial loading was thus conducted under drained condition. The samples failed during unloading at large axial strain under suctions of 23 and 30 kPa, so that only the three tests under a suction of 60 kPa were successfully completed. Lubricated end platens (Chapter 3) were used for all samples except the Ottawa sand sample for which end platens covered by latex membrane but no silicon grease was used.

Fig. 5.1 shows the deformation profile for the Ottawa sand sample with unlubricated end platens. It is seen that the sample displayed the maximum diameter at the mid-height and the minimum diameter at the ends, rather than a uniform radial deformation. The maximum diameter was 0.69 mm larger than the minimum one at an axial strain of 5%. The difference between the maximum and the minimum diameters increased to 2.49, 7.54 and 12.79 mm at axial strains of 10, 20 and 30%, respectively. It was also noted that the measured height-diameter curves could be fitted well with parabolas at axial strains of 5 and 10%. At large strains of 20 and 30 %, the measured diameter points were slightly below the fitted parabolas in the lower and upper portions of the sample, and slightly above the fitted curves in the central portion. This appeared to result from the non-uniform rebound deformation during unloading. The axial rebound deformation was over 2.0 mm at large axial strain and mainly occurred in the end portions of a sample. Similar deformation profiles were observed for the two other samples with lubricated ends. Similar results were also found by Roscoe et al (1963b) and Bishop and Green (1965). Therefore, it is reasonable to assume that the deformation profiles at different axial strains are parabolic.

Fig. 5.2 shows the relationship between axial strain and radial strain at the ends of the samples. For the Ottawa sand sample with unlubricated end platens, the radial strain at ends, ε_e, was small, equal to 0.5 and 1.3 % at axial strains of 5 and 20 %, respectively. Under lubricated end condition, the radial strain ε_e was close for both the Ottawa sand and the Unimin sand samples, and was as high as two times that under unlubricated end condition. The above results indicate that lubricated end platens can significantly reduce end restraint. The relationship between axial strain and radial strain at ends for the Unimin sand sample can be obtained by regression analysis from Fig. 5.2 as follows:

$$\varepsilon_e = -0.2712\varepsilon_a + 0.0085\varepsilon_a^{\ 2} - 0.0001\varepsilon_a^{\ 3} \tag{5.1}$$

If a triaxial sample deforms as a circular cylinder, its radial strain should be: $\varepsilon_e = \frac{1}{2}(\varepsilon_v - \varepsilon_a)$, in which ε_v is volume strain and ε_a is axial strain. From a triaxial drained test on a Unimin sand sample which had similar initial condition as the Unimin sand sample shown in Fig. 5.2, the relation between axial strain and volume strain was obtained by regression analysis as: $\varepsilon_v = 0.5278\varepsilon_a - 0.0441\varepsilon_a^2 + 0.0016\varepsilon_a^3$. Then an ε_a- ε_e curve for a right circular cylinder sample could be obtained as the dotted line in Fig. 5.2. It can be seen that the ε_e of the circular cylinder sample was much lower than that of the samples with lubricated ends at large axial strain. Therefore, it appears questionable to assume that a triaxial sample deforms as a right circular cylinder during shear, particularly at large axial strain.

5.3 Derivation of average diameter

Based on the above test results, it can be assumed that in a triaxial test on a sand sample,

(a) the height-diameter curves at different axial strains are parabolas;

(b) the maximum diameter occurs at the middle of the sample;

(c) the diameters at both ends of the sample are the same.

Then, the relationship between diameter and height can be expressed as follows (Fig. 5.3):

$$d = D_m - \frac{1}{\kappa}h^2 \tag{5.2}$$

where, κ = parameter

h = the height at calculated point.

d = the diameter at calculated point.

D_m = the maximum diameter for a given axial strain.

Let H_0 = the initial height of the sample;

D_0 = the initial diameter of the sample;

V_0 = the initial volume of the sample;

H = overall height of the sample for given axial strain;

D_e = the diameter at ends for given axial strain;

$\Delta H = H_0 - H$, the axial deformation of the sample for a given axial strain;

$\Delta D = D_0 - D_e$ the diameter change at sample ends.

When $h = \pm H/2$, $d = D_e$. That is

$$D_e = D_m - \frac{1}{\kappa}\left(\frac{H}{2}\right)^2 \tag{5.3}$$

i.e.

$$\frac{1}{\kappa} = \frac{4(D_m - D_e)}{H^2} \tag{5.4}$$

5.3.1 Sample volume

Sample volume is defined as:

$$V = 2\int_0^{\frac{H}{2}} \frac{\pi}{4} d^2 dh \tag{5.5}$$

Substituting Eqs (5.2) and (5.4) into Eq (5.5) can obtain:

$$V = \frac{\pi}{60} H\left(8D_m^2 + 4D_e D_m + 3D_e^2\right) \tag{5.6}$$

5.3.2 Maximum diameter D_m

From Eq (5.6), the maximum diameter D_m can be expressed as

$$D_m = \frac{1}{4}\sqrt{\frac{120}{\pi}\frac{V}{H} - 5D_e^2} - \frac{1}{4}D_e \tag{5.7}$$

The sample volume is also given as follows:

$$V = V_0(1-\varepsilon_v) = \frac{\pi}{4}D_0^{\,2}H_0(1-\varepsilon_v) \qquad (5.8)$$

Substituting Eq (5.8) into Eq (5.7) can get

$$\boxed{D_m = \frac{D_e}{4}\left(\sqrt{\frac{30(1-\varepsilon_v)(1+\varepsilon_e)^2}{(1-\varepsilon_a)}-5}-1\right)} \qquad (5.9)$$

where, $D_e = D_0(1 - \varepsilon_e)$

$\varepsilon_a = \Delta H / H_0$;

$\varepsilon_v = \Delta V / V_0$, volumetric strain

$\varepsilon_e = \Delta D / D_0$, radial strain at ends.

5.3.3 Average diameter, D_{ave}

The average diameter within the middle portion of a sample is defined as:

$$D_{ave} = \frac{\int_0^{L/2} d\,dh}{\int_0^{L/2} dh} \qquad (5.10)$$

where, L = the length of the central portion (Fig. 5.3).

Substituting Eqs (5.2) and (5.4) into Eq (5.10) can obtain

$$D_{ave} = D_m - \frac{L^2}{3}\frac{(D_m - D_e)}{H^2} \qquad (5.11)$$

Let $$b = \frac{L}{H} = \frac{L}{(H_0 - \Delta H)}$$

where, b is length factor, varying from 0 to 1.

Then Eq (5.11) becomes:

$$\boxed{D_{ave} = D_m - \frac{b^2}{3}(D_m - D_e)} \qquad (5.12)$$

The entire average diameter of the sample can be obtained by substituting b = 1 into Eq (5.12). It can be also obtained, from the assumption that a sample deforms as a right circular cylinder, as follows:

$$D_{b=1} = D_0\sqrt{\frac{(1-\varepsilon_v)}{(1-\varepsilon_a)}} \qquad (5.13)$$

5.4 Determination of the average diameter in failure zone

Eqs (5.9) and (5.12) show that for given strains, the average diameter in the middle portion of a triaxial sample is a function of the length factor, b. The average diameter at b = 0 is equal to the maximum diameter, and the average diameter at b = 1 is the minimum average diameter, i.e. the overall average diameter which is conventionally used in triaxial tests. As an example, Fig. 5.4 shows the average diameters for different b values when a D_0 = 50 mm sample is undrained sheared to an axial strain of 20 %. In the case of fixed ends (ε_e = 0 %), the average diameter is equal to 55.8, 58.0 and 58.8 mm for b = 1, 0.5 and 0, respectively. In other words, the overall average area of the sample, equal to $55.8^2\ \pi / 4 = 24.5$ mm^2, is 10 % less than the maximum area of $58.8^2\ \pi / 4 = 27.2$ mm^2. When the radial expansion strain at end, ε_e increases from 0 % to 4 %, the entire average diameter (b = 1) remains essentially constant, but the maximum average diameter (b = 0) decreases from 58.5 mm to 57.7 mm. These results indicate that the use of the overall average area in calculating deviator stress in triaxial tests may result in large error in the deviator stress at large axial strain, and this error may be reduced if the end restraint is lessened.

It had been realized several decades ago that the shear strength of a triaxial sample may be overestimated if the overall average area is used to calculate deviator stress. It was thus suggested that the deviator stress of a triaxial sample should be calculated by using the diameter at the mid-height of the sample (Roscoe et al., 1959), the central half average diameter of the sample (Bishop and Green, 1965); or the average diameter within the portion containing the failure plane (Duncan and Dunlop, 1968), or the deviator stress is corrected, based on the sample dimensions measured after shear (ASTM, 1993c). It may be noted in Fig. 5.1 that the radial deformation was relatively uniform in the middle third portion of the sample, but varied significantly in the zones near the ends. Similar results were reported by Roscoe et al (1963b). This may imply that the stress in the middle third portion of a triaxial sample is not significantly affected by end restraint, and thus reflects essentially the inherent behaviour of the sample. Therefore, it is suggested that the average diameter in the middle third portion of a triaxial sample should be used in the calculation of deviator stress.

The determination of the middle third average diameter, $D_{1/3}(\varepsilon_e)$ from Eqs (5.9) and (5.12) requires three variables: axial strain, volume strain and radial strain at ends. However, only the axial strain and the volumetric strain can be obtained in conventional triaxial tests, the radial strains at ends are usually unknown. The $D_{1/3}(\varepsilon_e)$ may be replaced approximately by some middle average diameter in which the end radial strain is equal to zero. Fig. 5.5. shows the axial strain - average diameter curves under different conditions. The measured data from Fig. 5.1, which is multiplied by (50 / D_0) (D_0 is the initial diameter of the sample), is also shown in Fig. 5.5. In the case of $\varepsilon_e = 0$, the average diameter increases with axial strain. For a given axial strain, the lower the length factor b, the higher is the average diameter. The average diameter at b = 1/2 is much larger than the overall average diameter (b = 1) at large axial strain. The overall average diameters under different conditions are essentially the same, regardless of the end radial strain ($\varepsilon_e = 0$ or $\varepsilon_e = f(\varepsilon_a)$) and the assumption of deformation profile (parabola or right circular cylinder).

It is also noted in Fig. 5.5 that for a given length factor b, the axial strain - average diameter curve for $\varepsilon_e = f(\varepsilon_a)$ is slightly higher than that for $\varepsilon_e = 0$, and the curve at b = 1/2 for $\varepsilon_e = 0$ is very close to that at b = 1/3 for $\varepsilon_e = f(\varepsilon_a)$ = Eq (5.1). This indicates that for a Unimin sand sample with lubricated end platens, the middle third average diameter is closely approximated to the middle half average diameter under fixed end condition. Therefore, the middle half average diameter with zero end radial strain, $D_{1/2}(0)$ was used in the calculation of deviator stress in this study. $D_{1/2}(0)$ is expressed as follows:

$$D_{1/2}(0) = D_m - \frac{1}{12}(D_m - D_0) \tag{5.14}$$

and

$$D_m = \frac{D_0}{4}\left(\sqrt{\frac{30(1-\varepsilon_v)}{(1-\varepsilon_a)} - 5} - 1\right) \tag{5.15}$$

5.5 Error in strength due to area correction

Using different area correction methods may result in different values of the deviator stress. A comparison of the deviator stresses calculated by using the conventional area correction, $\Delta\sigma_{b=1}$, and by using Eq (5.14), $\Delta\sigma_{b=1/2}$, in an undrained triaxial test on Unimin sand is shown in Fig. 5.6. It is seen that $\Delta\sigma_{b=1/2}$ was the same as $\Delta\sigma_{b=1}$ until an axial strain of 3 %; then $\Delta\sigma_{b=1}$ became larger than $\Delta\sigma_{b=1/2}$, and the difference between $\Delta\sigma_{b=1}$ and $\Delta\sigma_{b=1/2}$ increased with axial strain, equal to 44, 62 and 95 kPa at strains of 15, 20 and 30 %, respectively. This indicates that the conventional area correction may result in large error in deviator stress at large axial strain.

The error in shear strength of a triaxial sample, Er, is defined as follows

$$Er = \frac{\Delta\sigma_{b=1} - \Delta\sigma_{b=1/3}}{\Delta\sigma_{b=1/3}} \tag{5.16}$$

where, $\Delta\sigma_{b=1} = \dfrac{4P}{\pi D_1^{\,2}}$, in which P is applied load, D_1 is the overall average diameter of the sample, calculated by Eq (5.13);

$\Delta\sigma_{b=1/3} = \dfrac{4P}{\pi D_{1/3}^{\,2}}$, in which $D_{1/3}$ is the middle third average diameter, depending on axial strain, volumetric strain and the radial strain at ends, calculated by Eqs (5.9) and (5.12).

So
$$Er = \left(\frac{1-\varepsilon_a}{1-\varepsilon_v}\right)\left(\frac{D_{1/3}}{D_0}\right)^2 - 1 \qquad (5.17)$$

Similarly, the error in deviator stress due to using the middle half average diameter with zero end radial strain, $D_{1/2}(0)$, to replace the middle third average diameter $D_{1/3}$ is as follows:

$$Er = \left(\frac{D_{1/3}}{D_{1/2}(0)}\right)^2 - 1 \qquad (5.18)$$

The error in the deviator stress of an undrained triaxial sample ($\varepsilon_v = 0$) is analyzed, based on Eq (5.17) and the results are shown in Fig. 5.7. It is seen that the error increases with axial strain (Curves 1 and 2). In the case of fixed ends ($\varepsilon_e = 0$), the error is equal to 4.5, 7.0 and 9.5% at axial strains of 10, 15 and 20%, respectively. In the case of lubricated ends ($\varepsilon_e = f(\varepsilon_a)$, calculated by Eq (5.1)), the error is less than that in the case of fixed ends, equal to 2.8, 4.8 and 7.0 % at axial strains of 10, 15 and 20%, respectively. This indicates that lubricated end platens may reduce end restraint, as well as the error in deviator stress by using the conventional area correction. The experimental errors are also shown in Fig. 5.7. The error obtained from data by Bishop and Green (1965) was located on Curve 2. The errors obtained from data in Fig. 5.1 were close or larger than that in the case of fixed ends, even though the end radial strain was not equal to zero (Fig. 5.2). These larger errors appeared to result from the rebound deformation as discussed previously.

Fig. 5.7 also shows the error in deviator stress due to the substitution of $D_{1/2}(0)$ for $D_{1/3}$ (Eq (5.18), Curve 3). It is seen that the error decreases to the minimum value of -1 % at an axial strain of about 12%, then increases to 0% at an axial strain of 30%. This indicates that the deviator stress calculated by using the middle half average diameter $D_{1/2}(0)$ is less than that by using the middle third average diameter $D_{1/3}(\varepsilon_e)$, but the error is lower than 1%. Thus, the substitution of $D_{1/2}(0)$ for $D_{1/3}$ is acceptable for the lubricated end condition, and was used in this study.

The area correction method developed in this Chapter is based on the assumption that the deformation profile of a triaxial sample is parabolic. Thus it can be valid for all cases in which the height-diameter curves of a triaxial sample for different axial strains are parabolas. The accuracy of this method depends on the evaluation of the radial strain at ends. Besides lubricated end condition and axial strain, the end radial strain may be also affected by many other factors including soil type, density of sample, effective confining pressure. Different samples may produce different end radial strains. For more accurate results, an appropriate device should be developed to measure the radial deformation at the ends or at the centre of a sample during shear.

5.6 Conclusions

1. A method of calculating the average diameter in the middle portion of a triaxial sample is developed. The middle average diameter is dependent on axial strain, volumetric strain, the radial strain at the ends of the sample, and the length of the middle portion.

2. The use of middle third average diameter is suggested for calculation of deviator stress in triaxial tests. This middle third average diameter of a triaxial sample with lubricated end platens can be closely approximated by the middle half average diameter with $\varepsilon_e = 0$.

3. The error in deviator stress due to using the conventional sample area correction can be over 10 % at large axial strain under fixed end condition ($\varepsilon_e = 0$). This error can be reduced by approximately 2% by lubricated end platens.

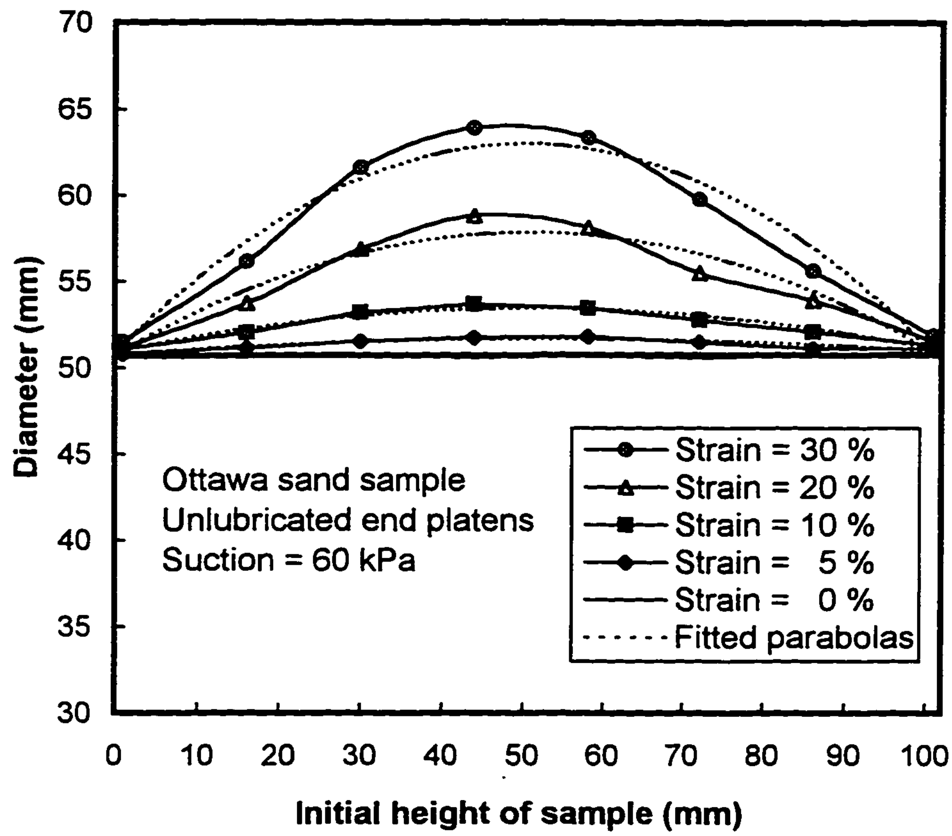

Fig. 5.1 Deformation profiles of triaxial sand sample

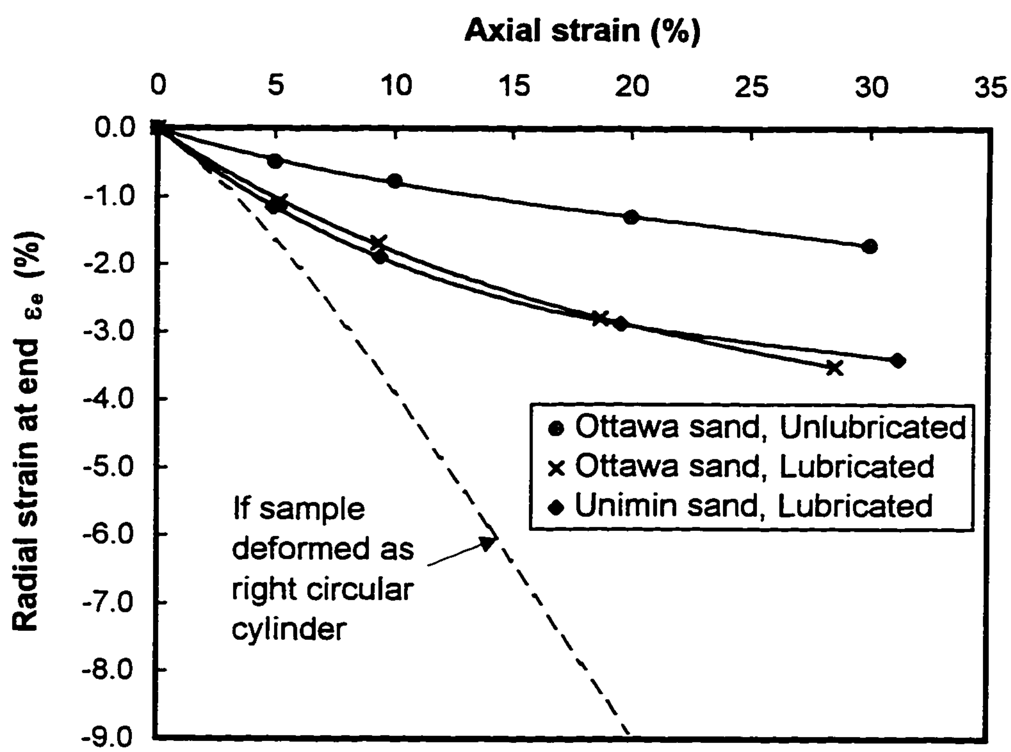

Fig. 5.2 Diameter change at ends in triaxial tests

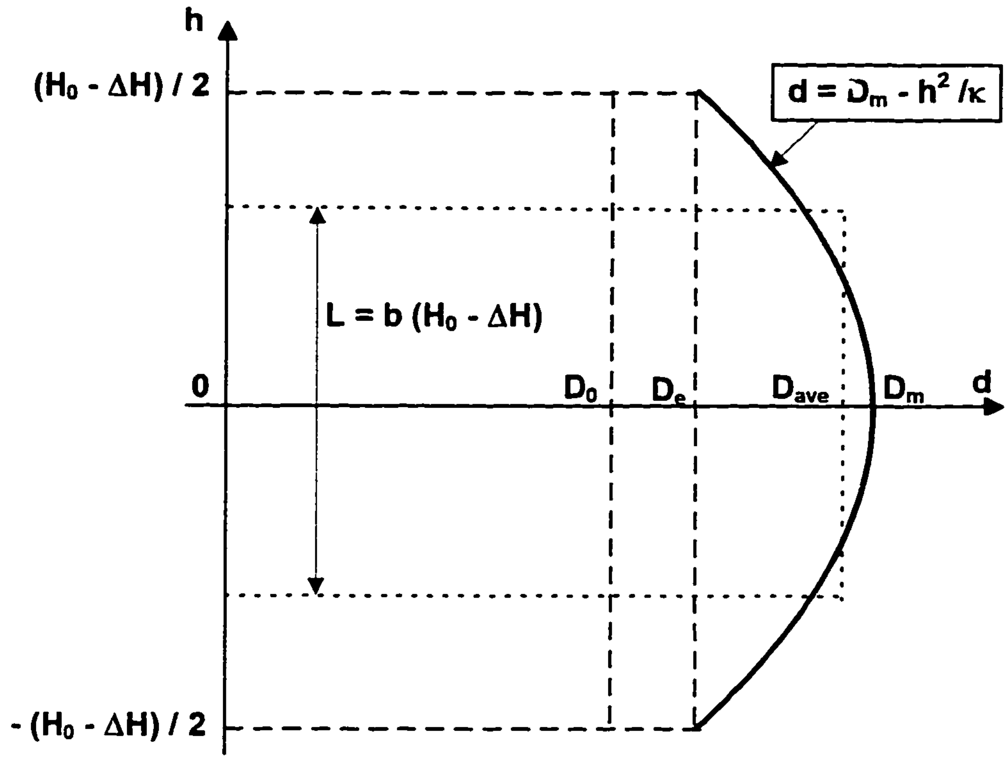

Fig. 5.3 Derivation of average diameter within middle length of a triaxial sample

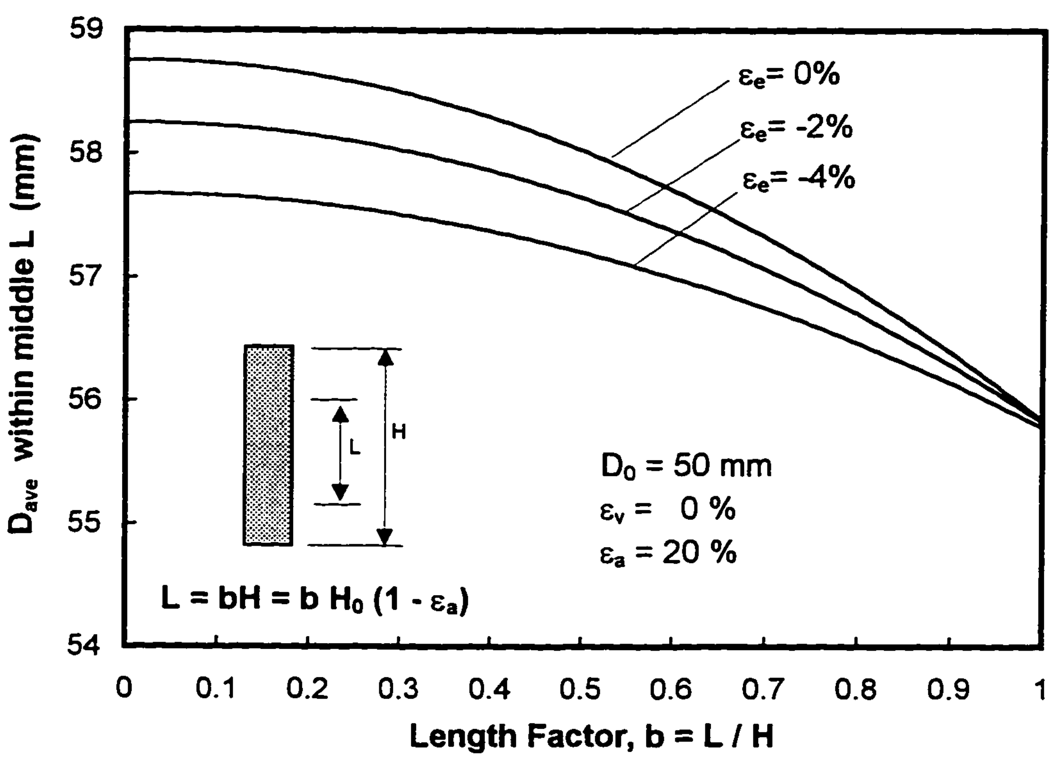

Fig. 5.4 Average diameter within middle length

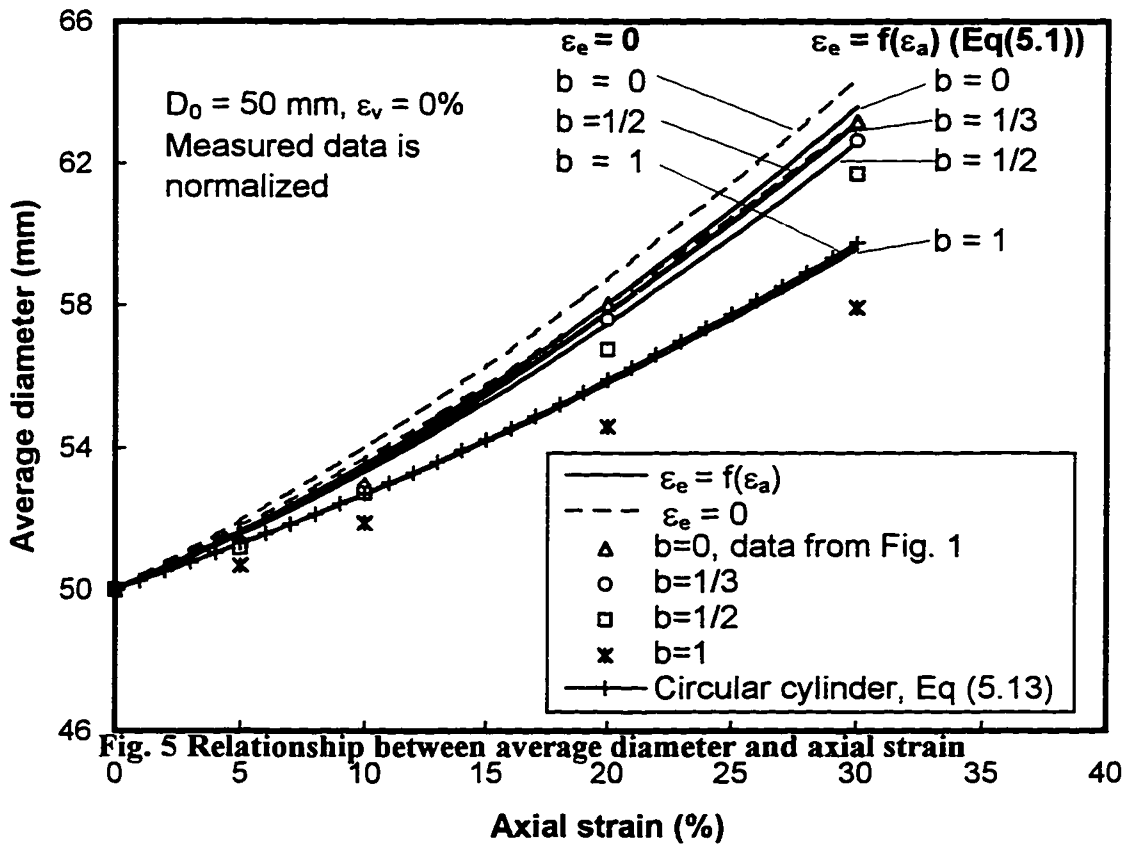

Fig. 5 Relationship between average diameter and axial strain

Fig. 5.5 Relationship between average diameter and axial strain

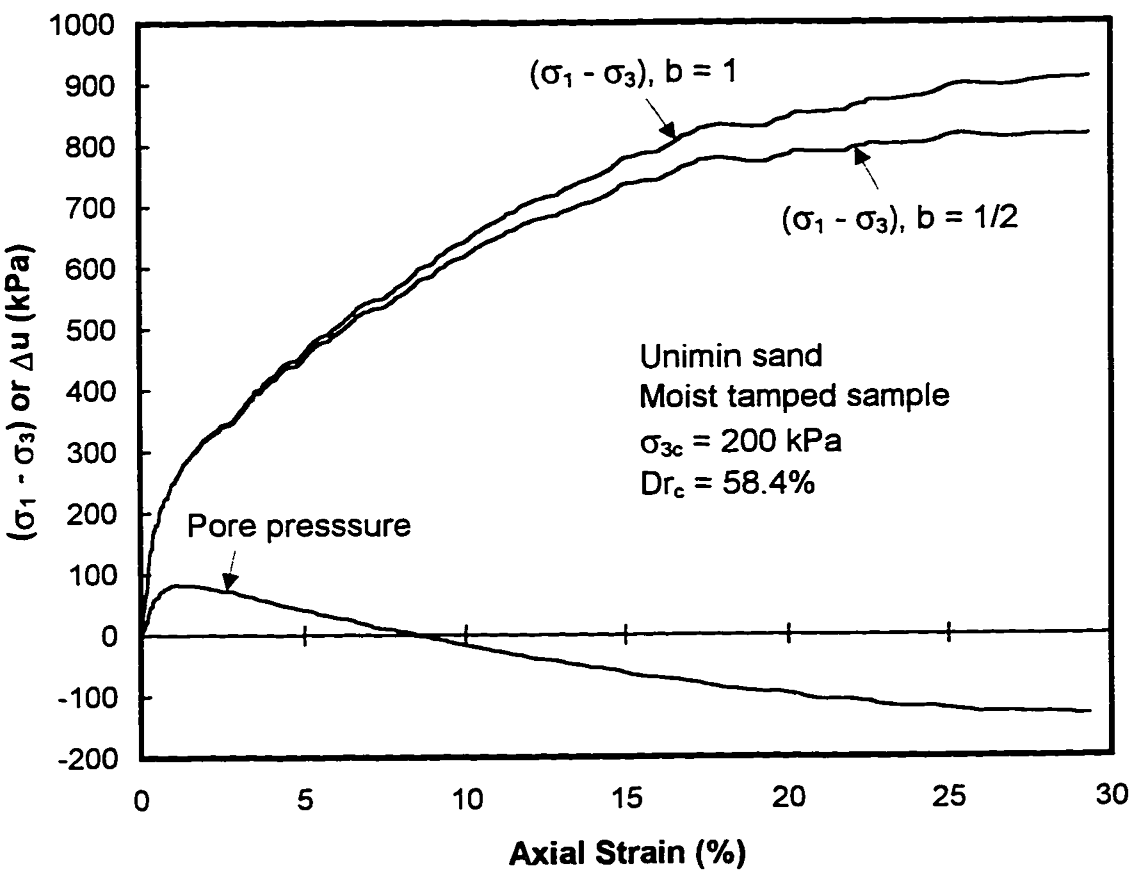

Fig. 5.6 Effect of area correction on deviator stress

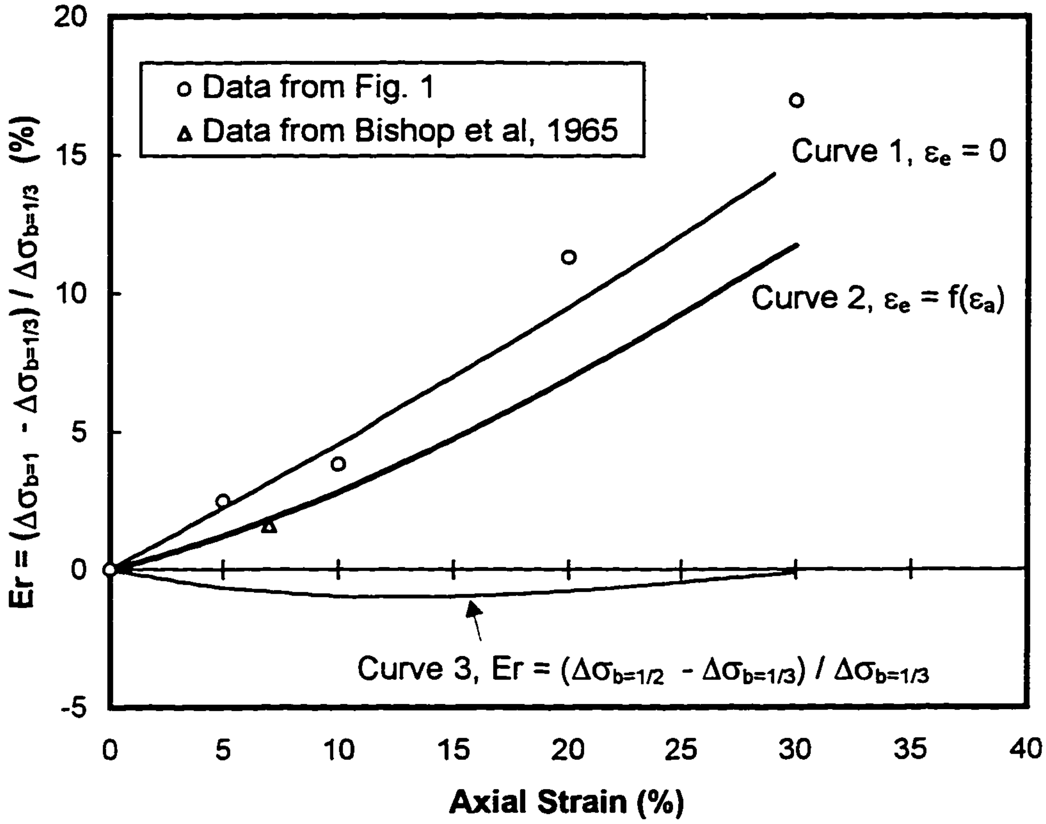

Fig. 5.7 Error in deviator stress due to area correction

CHAPTER 6

INVESTIGATION ON QUASI-STEADY STATE BEHAVIOUR *

6.1 Introduction

There are three types of stress-strain curves in undrained triaxial compression tests on saturated sands: steady state (strain softening) curve, strain hardening curve and the quasi-steady state (partly strain softening) curve (Fig. 6.1) (Castro, 1969). For a sand with strain hardening behaviour, flow liquefaction is not possible, since the resistance of the sand increases continuously during undrained loading. For a sand with steady state behaviour, there is a unique steady state line relating the steady state strength to the void ratio, which is independent of the initial condition of the sand sample, the stress path and loading rate (Castro, 1969; Casagrande, 1975; Castro et al., 1982; Poulos et al., 1985; Sladen et al, 1985; Been et al., 1991; McRoberts, 1992, etc.). Hence, the steady state strength, also referred to as the undrained residual strength, of the sand for a given void ratio can be obtained with the help of the steady state line.

However, in the case of the quasi-steady state behaviour, the sample first collapses and reaches a temporary steady state ("quasi-steady state, QSS"), and on further shearing shows a strain hardening behaviour. Hence, there is no unique ultimate shear resistance in the quasi-steady state behaviour. The quasi-steady state behaviour raises the following questions: (1) why is the collapse with rapid decrease in deviator stress followed by a continuous increase in shear resistance with further strain, and no ultimate shear resistance is reached even at a large

* A version of this chapter has been submitted for publication: Quasi-steady state: a real behaviour? Canadian Geotechnical Journal.

axial strain over 20 %? (2) how should the undrained residual strength of such a sand sample be estimated? (3) what is the field evidence for the quasi-steady state behaviour?

Most sand samples with initial conditions similar to many of natural pluviated sand deposits exhibit the quasi-steady state behaviour in laboratory tests (Vaid et al., 1990; Ishihara, 1993). Therefore, from a practical point of view, a critical examination of the quasi-steady state appears to be necessary. The objective of this chapter is to investigate why the quasi-steady state behaviour occurs and how it is affected by testing procedure. Undrained and drained triaxial tests are used for this purpose.

6.2 Background

Bishop et al. (1965) first found the quasi-steady state behaviour in the undrained triaxial tests on loose Ham River sand. Castro (1969) conducted the comprehensive investigation on the behaviours of Banding sand and a Chilean sand, and presented the three typical undrained behaviour of sands. It can be seen in Fig. 6.1 (curve b) that the induced pore pressure in the sample with the quasi-steady state behaviour increased to a peak at a strain of about 8%, then continuously decreased until the end of the test. Ishihara et al. (1975) called this transition state from increase to decrease in pore pressure as "phase transformation". Alarcon-Guzman et al. (1988) called the transitory steady state in the stress-strain curve as the "quasi-steady state". Unlike the effective stresses at steady state which are only a function of the void ratio, the effective stresses at the quasi-steady state appear also to be affected by some other factors including initial confining pressure and the initial fabric of a sample, etc. (Ishihara, 1993; McRoberts and Sladen, 1992).

6.2.1 Basic concepts and "quasi-steady state"

Casagrande (1936, 1976) defined the critical void ratio as one at which a sandy soil can undergo any amount of deformation without volume change under drained condition. This critical void ratio can be reached from either a loose or a dense state. For undrained condition, dense sands generally develop greater strength when volume changes are prevented during shear, and loose sands show a decrease in strength. The critical void ratio is one at which shearing under zero volume change does not lead to a change in shear strength (Taylor, 1948). Following the concept of the critical void ratio, Poulos (1981) developed the concept of steady state: The steady state of deformation for a soil mass is that state in which the mass is continuously deforming at constant volume, constant normal effective stress, constant shear stress, and constant velocity. The steady state of deformation is achieved after all particle orientation has reached a statistically steady state condition and after all particle breakage, if any, is complete, so that the shear stress needed to continue deformations and the velocity of deformation remain constant.

Based on the concept of the critical void ratio, in conventional drained triaxial tests on a dense sand sample (void ratio less than the critical void ratio), the increase in void ratio commences only once the peak deviator stress is reached. The dilation accompanies with the decrease in deviator stress until both the deviator stress and the void ratio reach ultimate values. In a loose sand sample with void ratio larger than critical, the deviator stress increases monotonicaly with the decrease in void ratio until an ultimate state of the sample is attained. In other words, the void ratio increases in a dense sample and decreases in a loose sand sample during drained loading. This has been verified by using computed tomography to directly measure the local void ratio of triaxial sand samples (Desrues et al., 1996). Correspondingly, since the volume change during shear is prevented in conventional undrained triaxial tests, the dilation potential in a dense sand sample produces a monotonic increase in deviator stress (Fig. 6.1, Curve c), while the compression potential in a loose sand sample results in a collapse deformation and a steady state of deformation is reached (Fig. 6.1, Curve a).

However, what is the drained behaviour of a sand sample which may exhibit the quasi-steady state behaviour under undrained loading? The sample might display dilation after some strain, even though large compression may have occurred prior to that strain. Lee and Seed (1967) conducted a series drained triaxial tests on loose and dense Sacramental River sand samples under different effective confining stresses, but did not observe such a drained behaviour in this sand. From the concept of the steady state, ultimate state should be reached after all particle orientation has reached a statistically constant condition and after all particle breakage is compiete. In contrast, the deviator stress in the quasi-steady state behaviour continuously increases at large strain after a temporary steady state (Fig. 6.1, Curve b). Therefore, the quasi-steady state behaviour is not in agreement with the concepts of the critical void ratio and the steady state of deformation.

6.2.2 Field behaviour, steady state and quasi-steady state behaviour

The quasi-steady state has led some researchers to suggest the terms of "limited liquefaction" or "flow with limited deformation" (Ishihara, 1993). These terms imply that the flow deformation, if any, can be prevented by increase in shear resistance of a sand deposit with further straining. However, it is difficult to understand how once the rapid collapse of a sand mass with the quasi-steady state behaviour as shown in Fig. 6.1 (Curve b) is initiated, the collapse or significant failure can be prevented. Furthermore, for most sands, even the loosest samples exhibit the quasi-steady state behaviour (Alarcon et al., 1988 and Ishihara, 1993). It is of interest to note that even though the initial void ratio of an undrained Toyoura sand sample was larger than the maximum void ratio (as determined by Japanese standard test), the sample could still display a quasi-steady state behaviour (Fig. 6.2) (Ishihara, 1993). The application of the terms "limited liquefaction" or "flow with limited deformation" for cases where a sudden collapse occurs appears questionable.

Except for the increase in deviator stress at large axial strain in the quasi-steady state behaviour, there is no other significant difference between the steady state and the quasi-steady state behaviours. Thus, it has been suggested (Ishihara, 1994) that the flow behaviour (steady state behaviour) and the flow with limited deformation behaviour (quasi-steady state behaviour) should be placed in one category (Ishihara, 1994). Finno et al. (1996) compared the steady state behaviour and the quasi-steady state behaviour under plane strain condition and triaxial shear condition. Their test results indicate that the steady state points of masonry sand samples with the steady state or the quasi-steady state behaviour were located essentially on straight lines in an e-logp' plot, even though the steady state line from the undrained plane strain tests appeared slightly higher than that from the undrained triaxial tests. Also, under the undrained plane strain shear condition, the development of shear band and the volume changes inside the shear bands were similar for both behaviours, except for the problematic volume change at low strain in the quasi-steady state behaviour. Therefore, for practical purpose, a close examination of the quasi-steady state behaviour appears to be necessary.

6.2.3 End restraint

A triaxial sand sample would deform as a right circular cylinder during shear without end restraint. The friction between end platens and a sample restricts its radial deformation near the ends, and the sample bulges at its middle portion under deviator stress. This end restraint causes strain and stress non-uniformities in triaxial samples, and affects their stress-strain characteristics, pore pressure or volume change, and strength characteristics (Duncan and Dunlop, 1968).

Various methods have been attempted to reduce the end restraint (Taylor, 1941, Larew, 1960, Rowe, 1962, Blight, 1965, Goto and Tastsuoka, 1988). Only the lubricated end platens developed by Rowe (1962), which are covered by a rubber membrane over a smear of lubricant, are effective and practicable to reduce the end restraint. Nevertheless, there have been some conflicting results about the effect of the lubricated end platens in triaxial tests in literature. Some investigators observed that the lubricated end platens could prevent a triaxial sample from bulging (Rowe and Barden, 1964, Barden and McDermott, 1965, Lee and Seed, 1964, etc.), while others found that the lubricated technique was virtually ineffective (Olson and Campbell, 1964, Casagrande and Poulos, 1964). Bishop and Green (1965) discovered that the 4 inch × 4 inch sand samples with lubricated ends could deformed uniformly during drained loading, but the 4 inch × 8 inch samples with the lubricated ends displayed bulging similar to the samples with regular ends. Compared with drained tests on sands with regular end platens, the samples with lubricated ends exhibited lower shear strength (Rowe and Barden, 1964, Olson and Campbell, 1964, Lee and Seed, 1964, Ueng et al., 1988), or the same shear strength (Bishop and Green, 1965); and displayed larger expansive volume change (Lee, 1978) or less expansive volume change (Raju at al., 1972, Ueng et al., 1988). For undrained tests on sands, lubricated end platens result in larger shear strength or less induced pore pressure (Lee, 1978), or similar shear strength and pore pressure as the regular end platens (Castro, et al., 1982).

These results indicate that the lubricated end platens may reduce, but not eliminate the friction between the platens and the soil, and their effect may depend on many factors including the characteristics of the lubricated end platens, stress level, slenderness ratio of a sample, and physical characteristics of sands.

An experimental investigation was therefore carried out to investigate the influence of end restraint on the quasi-steady state behaviour. These results were also used to investigate the effect of area correction on the QSS behaviour.

6.3 Experimental program

Unimin sand from St-Canut, Quebec was mainly used in this study. Unimin sand is an angular medium crushed quartz sand. The mean grain diameter D_{50} is 0.87 mm and the coefficient of uniformity ($Cu = D_{60} / D_{10}$) is 2.00. The specific gravity Gs is 2.665. The minimum void ratio of 0.646 and the maximum void ratio of 1.027 were determined according to the ASTM test methods D 4253-93 (Method 1A) and D 4254-91 (Method A), respectively.

A computerized triaxial apparatus was used to conduct conventional undrained and drained triaxial tests on the tested material under stress controlled conditions. A Hall Effect radial displacement transducer (HRDT) was used to measure the radial deformation of samples during saturation and consolidation. The volume change of moist tamped samples during saturation and the membrane penetration during consolidation were determined for each sample by measuring the axial and radial deformations.

The samples were prepared by using moist tamping method. Shearing was conducted under stress-controlled mode with stress rate of 10 kPa/min. Lubricated end platens were used in all tests except those where the effect of regular (unlubricated) end platens was investigated. The details of the lubricated and regular end platens are presented in Fig. 3.6.

6.4 Effect of area correction on QSS

The steady state strength or the quasi-steady state strength is usually obtained at large axial strain in undrained triaxial tests. This large strain can cause a sample to bulge significantly at its middle portion due to the effect of end restraint. The deviator stress of a sample is equal to the applied axial load divided by its cross-sectional area. Conventionally, the cross-sectional area is calculated by assuming a sample deforming as a right circular cylinder during shear (ASTM, 1993). In other words, the total average area is used to calculate the deviator stress. However, the average area at the failure zone is larger than the total average area. Fig. 6.3 shows the measured deformation profile at axial strain varying from zero to 31 %. The measurements were taken successively as the axial strain was increased in a drained sample under a constant suction of 54 kPa. No cell pressure was applied; the effective confining stress was therefore equal to the suction pressure. Clearly, the larger the axial strain, the more the sample bulges, and the difference between the two average areas increases with axial strain. Thus, the continuous increase in deviator stress after the phase transformation (PT) in the quasi-steady state behaviour (Fig. 6.1, curve b) may be affected by the conventionally corrected area.

Based on the observed deformed shape of the sample, a correction of the average area within the failure zone of a triaxial sand sample can be developed (Chapter 5). It is reasonable, from Fig. 6.3, to assume that the deformed profile is a parabola. Similar observation has also been made by Bishop and Green (1965). The diameter at any height of the sample can then be expressed as:

$$d = D_m - \frac{4(D_m - D_e)}{H^2} h^2 \qquad (6\text{-}1)$$

where, d = the diameter at height, h, of the sample;

H = the total height of the sample;

D_m = the maximum diameter for a given strain;

D_e = the diameter at the ends of the sample for a given strain.

Thus, the average diameter within the middle portion of the sample can be determined from both the diameters at the middle (D_{max}) and at the ends (D_e) of the sample for given axial strain and volumetric strain. The average diameter within the middle third portion is used as the average diameter to calculate the deviator stress of the sample. The diameter at ends is usually unknown during shear. However, it is found that the average diameter within the middle third portion under lubricated end condition is close to that within the middle half portion under fixed end condition ($D_e = D_0$) at different axial strains (Chapter 5). Therefore, the average diameter can be expressed as follows:

$$D_{ave} = D_{max} - \frac{1}{12}(D_{max} - D_0) \tag{6-2}$$

where D_{ave} = the corrected average diameter used in the calculation of the deviator stress;

D_0 = the pre-shear diameter.

The total volume of the sample calculated by using Eq (6.1) is equal to the initial volume minus the volume change. So the maximum diameter D_{max} at given axial strain ε_a and volumetric strain ε_v can be derived as follows:

$$D_{max} = \frac{D_0}{4}\left(\sqrt{\left(\frac{30(1-\varepsilon_v)}{(1-\varepsilon_a)} - 5\right)} - 1\right) \tag{6-3}$$

The quasi-steady state curve by Castro (1969) as modified by Eq (6.2) is shown in Fig. 6.1. It can be seen that the modified stress-strain curve is below the conventional curve from a strain of about 5%, and this difference larger with further axial strain. Thus, the quasi-steady state behaviour or the increase in deviator stress after the PT is in small measure due to the use of the conventional area correction. In the present study, the deviator stress in triaxial tests was calculated by using Eq (6.2).

6.5 Source of post-PT increase in deviator stress

The shear resistance of a sand sample depends on its effective friction angle and the effective stress in the sample: $\tau = \sigma'\tan\phi' = (\sigma - u)\tan\phi'$. So the increase in deviator stress after the PT in the QSS behaviour must be due to either the increase in the effective stress σ' or due to the decrease in the pore pressure u, or also due to the increase in the effective friction angle ϕ' with further strain.

Undrained tests on Unimin sand were conducted to investigate the post-PT behaviour. The test results are shown in Fig. 6.4. All samples prepared at different initial densities were consolidated under an effective confining pressure of 200 kPa. Their consolidated relative densities ranged from 17.4 to 35.4 %. It can be seen in Fig. 6.4(a) that the loose samples (relative densities after consolidation, Dr_c = 17.4 and 26.7%) exhibited the quasi-steady state behaviour. On reaching the critical stress ratio line (Vaid and Chern, 1985) or the collapse surface (Sladen et al., 1985), the samples suddenly collapsed, deforming from a strain of less than 1% to a strain of over 20% in less than two seconds. During collapse, the pore pressure rapidly increased close to the cell pressure and reached phase transformation at a strain of approximate 15%. The pore pressure subsequently decreased with increase in deviator stress. No collapse occurred for the Dr_c = 35.4 % sample. After the phase transformation was reached at a strain of 4%, its deviator stress or pore pressure respectively increased or decreased with further axial strain.

The stress paths of these samples are shown in Fig. 6.4(c). It is seen that for the loose samples, once collapse was initiated, the deviator stresses rapidly dropped to low values at the phase transformation, then increased along a straight line in the p-q plot. No decrease in deviator stresses occurred for the Drc = 35.4 % sample, and its post-PT stress path also lies on a straight line. It is noted that all the post-PT stress paths of the samples essentially lie on a unique straight line, despite their different densities. This is consistent with the results of triaxial tests on Fraser River sand by Vaid and Thomas (1995). They also found that the friction angle of the sand at phase transformation is independent of density, initial stress state (isotropic and anisotropic consolidation), type of response (contractive and dilative), and mode of loading (compression and extension). These results indicate that the post-PT stress path or the "Critical Stress Path" which is defined as the locus of the stress states when the friction resistance of a sand mass is fully mobilized for a given effective stress (Fig. 6.4(c)), is unique for a given sand. When the effective stress path of a sand sample reaches the critical stress path, the sample will attain a critical state, irrespective of whether it collapses or not. Therefore, the post-PT effective friction angle does not vary with further axial strain, but is constant for a given sand. This indicates that the effective stress or the induced pore pressure is the only factor which can affect the deviator stress after the phase transformation.

In conventional triaxial undrained tests, the variation of the induced pore pressure in a sample depends on the volume change of the soil skeleton of the sample. If the skeleton volume decreases, some of the effective stress on the skeleton will be transferred to the pore fluid, thus increasing the pore pressure. As discussed in chapter 4, the volume of a saturated sand sample is not constant under undrained loading condition, but decreases at the initial stage of the loading, and then increases with axial strain after the phase transformation. Thus, the post-PT increase in deviator stress results from the dilation potential of the sample.

The dilation potential reflects the global volume change of a triaxial sample. It can originate from the failure zone (the middle portion of the sample), or from the end zones near sample ends. If the post-PT dilation potential was mainly due to the dilation of the failure zone, the quasi-steady state behaviour shown in Fig. 6.1 (curve b) and Fig. 6.4 would be the inherent behaviour of the sands. From the concept of the steady state, the strain-stress curves should then tend to an ultimate state at large strain, because the dilation of the failure zone cannot be unlimited. However, no ultimate state appears even at an axial strain of over 30% in the quasi-steady state behaviour and in the strain hardening behaviour (Fig. 6.4).

Fig. 6.5 shows typical results of drained triaxial test on loose Unimin sand samples under low effective confining stress. It is seen that the deviator stress increased with axial strain until an ultimate value was reached at a strain of 13%; and remained essentially constant with further strain. However, the corresponding volume strain of the sample reached a peak at approximately 12 % strain, and remained constant only until a strain of about 15%. It then continuously decreased with further strain. Based on the concept of the critical void ratio, the constant deviator stress and the constant effective confining stress should be related to a constant void ratio within the failure zone. Since the post-peak patterns of deviator stress and volumetric strain are different, it is suggested that they reflect responses within *different* zones of the sample at large strain. The deviator stress results from the *failure zone* of the sample. Hence, once the failure zone reaches an ultimate state, the deviator stress remains at the ultimate value with further strain. The volume strain however results from the *global* volume change of the sample. If the end zones of the sample exhibit dilation potential at large strain due to end restraint, the volume strain will also display a corresponding dilation tendency, even though the failure zone itself may have reached an ultimate state.

Based on the results in Figures 6.4 and 6.5, it is concluded that if a sand sample exhibits quasi-steady state behaviour under undrained loading, its angle of internal friction will remain constant after phase transformation, and the post-PT increase in deviator stress will result from the dilation potential of the sample. This dilation potential does not develop from the failure zone, since the steady state may have been reached in the zone at very large strain. Once the failure zone of a drained sand sample reaches an ultimate state, the deviator stress will reach a peak and remain constant; but its global volume may continuously increase with further shearing. This global dilation results from the end zones of the sample due to end restraint. This end restraint also exists in undrained triaxial tests and causes the post-PT increase in deviator stress.

It is of interest to note that in constant volume simple shear tests on loose Fraser River sand samples, no large drop in shear stress occurs and the post-PT increase in shear stress is much less than that in undrained triaxial tests (Vaid and Sivathayalan, 1996). The end restraint is significantly minimized in simple shear tests. Uthayakumar (1996) conducted a series of hollow cylinder torsional tests on Fraser River sand samples with Dr_c = 30 %, in which the total mean normal stress $\sigma_m = (\sigma_1 + \sigma_2 + \sigma_3)/3$ was maintained constant; the parameter $b = (\sigma_2 - \sigma_3)/(\sigma_1 - \sigma_3)$ = 0; and the angle between major principal stress σ_1 and vertical direction, α_σ also remained constant. It was found that both the magnitude of the deviator stress, and its tendency to increase with shear strain increased with decrease in angle α_σ after phase transformation (Fig. 6.6). The end restraint or the end friction may be an important factor to cause the difference in the deviator stress with varying α_σ. When the major principal stress is applied vertically ($\alpha_\sigma = 0°$), the end friction force $F = f\sigma_1$ (f is the friction parameter between end platens and sand samples) is large and results in a higher increase of the deviator stress after phase transformation. As the direction of the major principal stress varies from vertical ($\alpha_\sigma = 0°$) to horizontal ($\alpha_\sigma = 90°$), the end friction force decreases from $F = f\sigma_1$ to $F = f\sigma_3$; consequently, the deviator stress shows lesser increase after phase transformation. The results in the simple shear tests and the hollow cylinder torsional tests provide further evidence to confirm that the behaviour of sands in undrained triaxial compression tests is affected by end restraint.

6.6 Effect of lubricated end platens

6.6.1 Test results

Four pairs of undrained triaxial tests on Unimin sand samples with regular end platens (RE) and lubricated end platens (LE) were conducted to study the effect of the end restraint. The lubricated end platens were similar to those used by Castro et al. (1982). The test results are shown in Fig. 6.7 and Table 6.1. There was little difference in pore pressure and deviator stress for the very loose samples (Dr_c = 17.4%, Fig. 6.7(a)) between with the regular ends and with the lubricated ends. The two stress-strain curves essentially coincided, as did the pore pressure curves. However, for the denser samples (Dr_c = 26.7, 35.4 and 70.0%, Fig 6.7(b), (c), (d)), the samples with lubricated ends exhibited significantly higher induced pore pressures and lower deviator stresses than the samples with regular ends. The denser the samples, the larger the differences, particularly at large axial strain. For example, the difference in deviator stress at a strain of 25% increased from 27 kPa for the Dr_c = 26.7% samples, to 66 kPa for the Dr_c = 35.4% samples and 360 kPa for the Dr_c = 70.0% samples (Table 6.1). These results indicate that the end restraint effect on undrained behaviour of sands increases significantly with the densities of sand samples. The lubricated ends can significantly reduce the end restraint on dense samples, while the lubrication effect becomes small in loose samples.

The lubrication effect also depends on the axial strain. It can be seen in Figs 6.7(c) and 6.7(d) that the deviator stress curves and pore pressure curves for lubricated ends coincided with those for regular ends at very low axial strain. The differences in deviator stress and pore pressure between the two types of end platens appeared at a strain of about 0.8 % and increased with axial strain until a strain of 16%, after which the differences remained essentially constant.

As shown in Fig. 6.7(a), for very loose samples, the effect of the end lubrication is negligible. Hence, if sand samples with regular ends are prepared at very loose state, their steady state points will be close to those of samples with lubricated ends. This is in agreement with the test results provided by Castro et al. (1982). However, the effect of lubricated ends on deviator stress and pore pressure obtained above is in conflict with the results published by Lee (1978), where the lubricated ends increased the undrained shear resistance of sand. It is known that the lesser the restraint on a sample, the lower is the shear resistance. Thus the shear resistance with lubricated ends should not be larger than that with regular ends under similar other conditions. Lee's result might be subject to an error in void ratio due to the extrusion of high vacuum grease in the lubricated ends. Castro et al. discovered that much of high vacuum grease in the lubricated ends, which consisted of about 0.25 mm of high vacuum grease covered with a 0.25 mm thick rubber membrane, was extruded into drainage ports during consolidation and caused significant errors in the calculated void ratios of the samples. This problem becomes particularly acute at high stresses (Castro et al., 1982). Lee's lubricated end platens consisted of two alternating layers of 0.38 mm thick rubber membranes separated by a "generous" smear of high vacuum grease. Thus, the void ratios of the samples with such lubricated ends might be significantly underestimated.

Fig. 6.8 summarizes the stress paths for the four pairs of the tests comparing the behaviour of lubricated and regular end platens. Clearly, after phase transformation, the stress states of all the samples were located on a straight line - the critical stress path, regardless of the type of end platens and the densities of the samples. These results provide further evidence to prove that the critical stress path is unique for a given sand.

6.6.2 Factors affecting efficiency of lubricated end platens

The lubricated end platens can significantly reduce the end restraint; however, some evidence indicates that the end restraint is not entirely eliminated. It is noted in Fig. 6.3 that even though the lubricated end platens were used in the diameter measurement tests, the Unimin sand sample displayed obvious bulging at different axial strains; the larger the axial strain, the more the sample bulged. Similar bulging phenomena were observed in all the undrained triaxial tests on the Unimin sand. It may be also noted in Fig. 6.5 that a sand sample with lubricated ends could display large dilation potential during drained loading after its failure zone had reached the ultimate state.

One major factor affecting the efficiency of the lubricated end platens is the thickness of the grease layer on the platens. Duncan and Dunlop (1968) found that the friction angle between a sliding metal block and a rubber membrane was over 20 degrees for 0.0008 mm thick grease, but decreased to about one degree for 0.3 mm thick grease. Because of its viscous nature, the grease between two solid blocks is very easily extruded under pressure. The thickness of the grease layer in the lubricated end platens depends on the amplitude and duration of axial stress, the size of the platens, the viscosity of the grease and the initial thickness of the grease layer (Duncan and Dunlop, 1968). For a triaxial test on a given sample with selected grease, the size of the platens and the viscosity of the grease are constant; the thickness of grease layer is influenced mainly by the initial grease thickness and the amplitude of the axial stress. The larger the axial stress and the thicker the initial grease layer, the more the grease is extruded. The extrusion may result in increase in the end friction and an error in void ratio of the sample. Generous use of grease in the lubricated end platens may show an apparent decrease in void ratio of a sand sample, and result in an error in the position of the steady state line. However, a thin smear of grease may not be enough to eliminate the end friction or the end restraint.

The mean grain size of a sand may also affect the efficiency of the lubricated end platens. Lee (1978) found that increasing the grain size of soils significantly increases the amount of the sliding friction force between sample and lubricated platens, for any constant normal stress and constant rubber membrane and grease thickness. The coarse particles of soil can penetrate through the rubber membrane and bear directly on the solid end platens. Lee's results also indicate that the friction due to the penetration of coarse particles can be reduced by increasing the thickness of the rubber membrane. However, the use of thick rubber membrane may result in error in void ratio of the samples. For example, the modulus of rubber is 1,400 kPa (ASTM, 1993c, p1079). Under a pressure of 100 kPa, the deformation of two 0.7 mm thick rubber membranes in end platens is equal to $\frac{100}{1400} \times (2 \times 0.7) = 0.10$ mm. This deformation can result in an error of about 0.002 in terms of void ratio for a 50 × 100 mm sand sample.

6.7 Conclusions

1. The quasi-steady state behaviour is not an inherent, but a test induced behaviour of loose sands. The post-PT increase in deviator stress in the quasi-steady state behaviour is caused mainly by the decrease in pore pressure due to end restraint. The deviator stress in the strain-hardening behaviour may be also significantly affected by the end restraint.

2. In drained tests on a loose sand sample, the post-peak patterns of deviator stress and volumetric strain are different, Available data suggests that they reflect the responses within different zones of the sample at large strain.

3. Compared with the regular end platens, the lubricated end platens can lessen the post-PT decrease in the pore pressure of a sand sample and thus result in lower deviator stress at large axial strain. For very loose sand samples, there is no significant difference between the results of the triaxial tests with the lubricated end platens or with the regular end platens.

Table 6.1. Effect of end type on undrained behaviour of Unimin sand

Sample		At onset of Collapse		At Phase Transformation			At ε_a = 25%	
Dr (%)	End Type	Δu (kPa)	(σ1 - σ3) (kPa)	Δu (kPa)	(σ_1 - σ_3) (kPa)	E (kPa)	Δu (kPa)	(σ_1 - σ_3) (kPa)
17.4	L	123	87	203	34	165	184	53
	R	123	91	197	36	187	183	55
26.7	L	106	114	199	50	234	159	100
	R	96	146	192	82	265	149	127
35.4	L			135	156	362*	67	309
	R			128	185	416*	47	375
70.0	L			86	260	875*	-153	858
	R			81	272	13465*	-297	1218

* Modulus between ε_a(PT) and ε_a(PT) + 0.3%

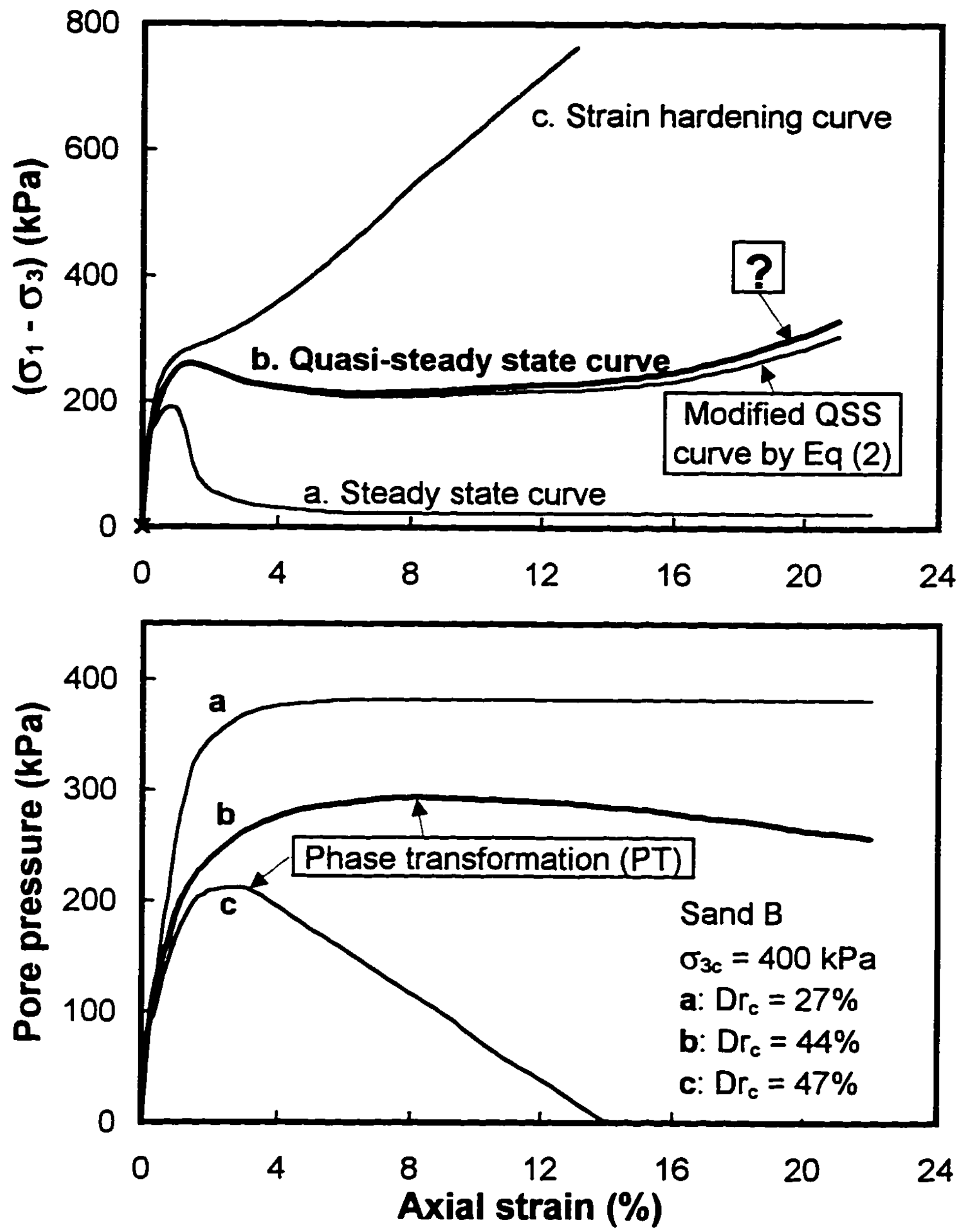

Fig. 6.1 Typical undrained stress-strain curves (modified from Castro, 1969)

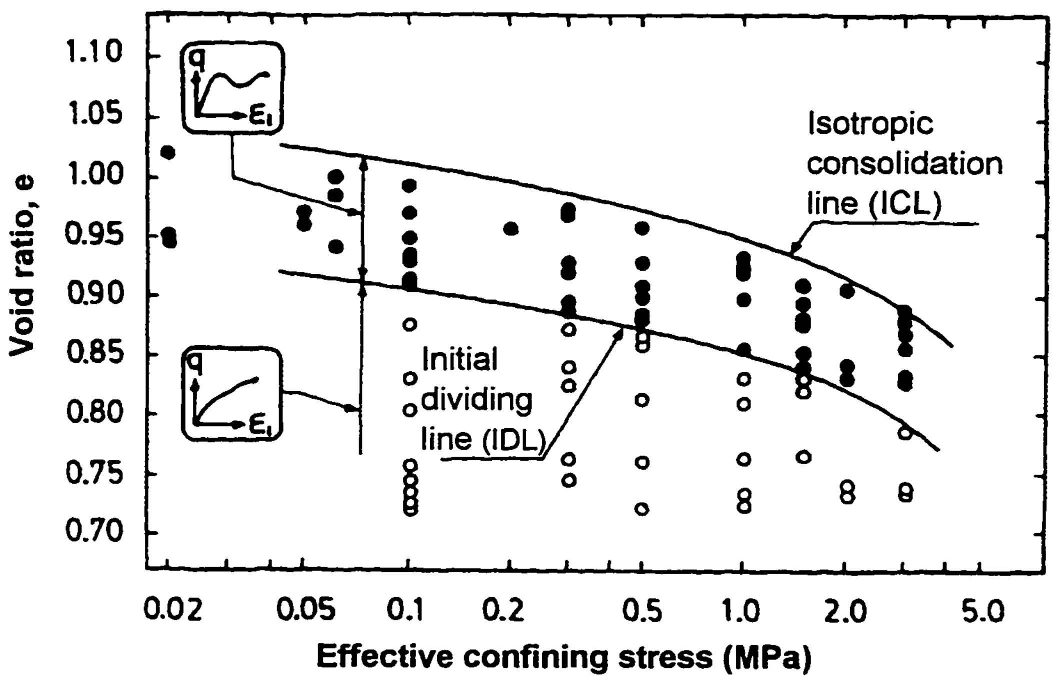

Fig. 6.2 Initial condition for Toyoura sand to exhibit QSS behaviour (after Ishihara, 1993)

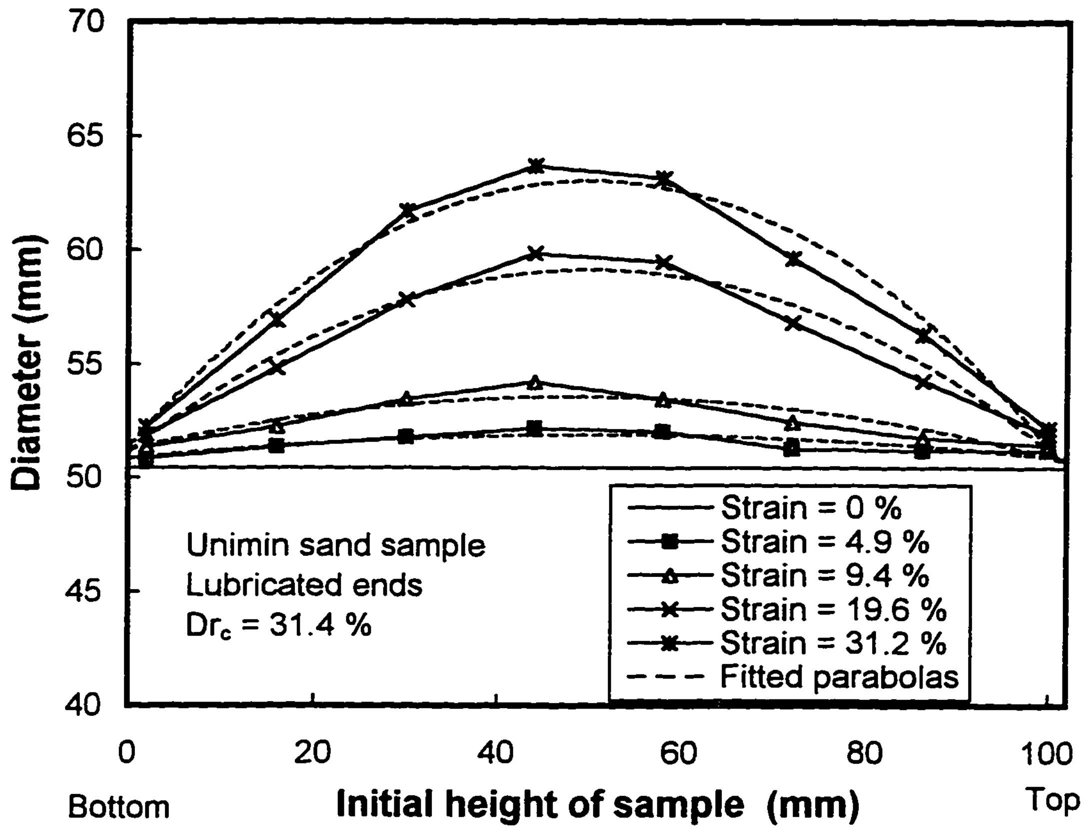

Fig. 6.3 Deformation profile at different axial strains

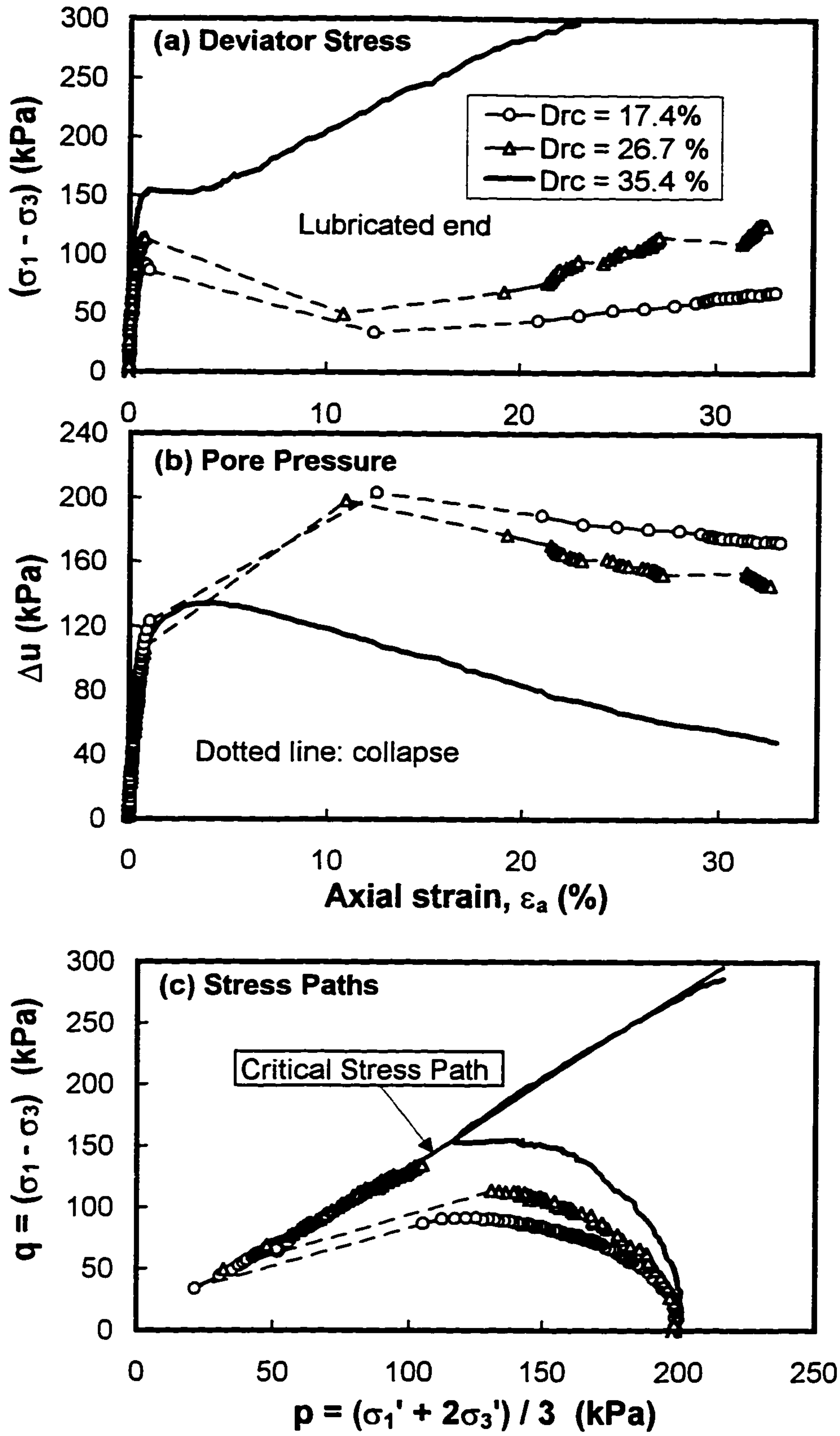

Fig. 6.4 Typical results of undrained triaxial tests on Unimin san

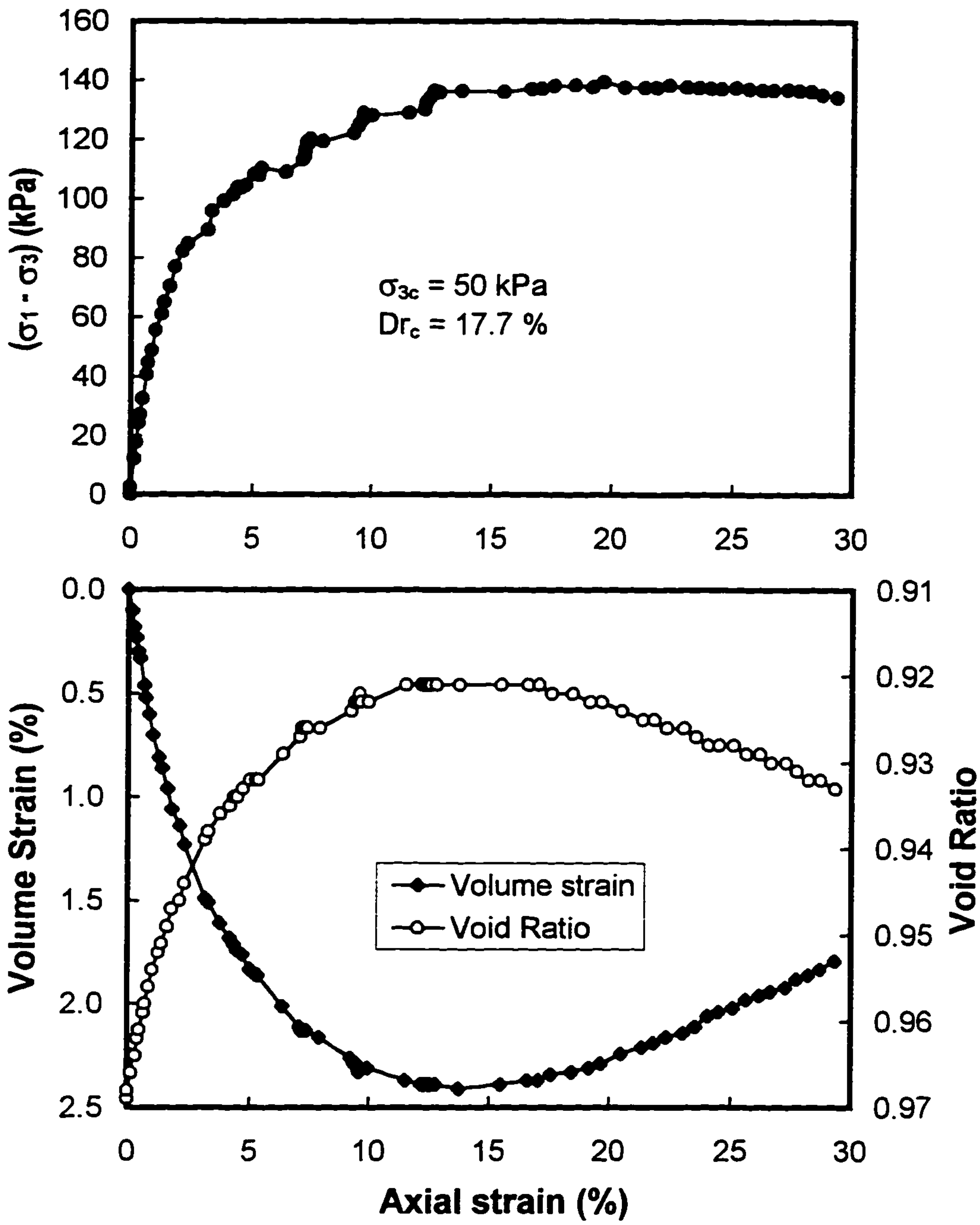

Fig. 6.5 Typical results of drained test on loose Unimin sand

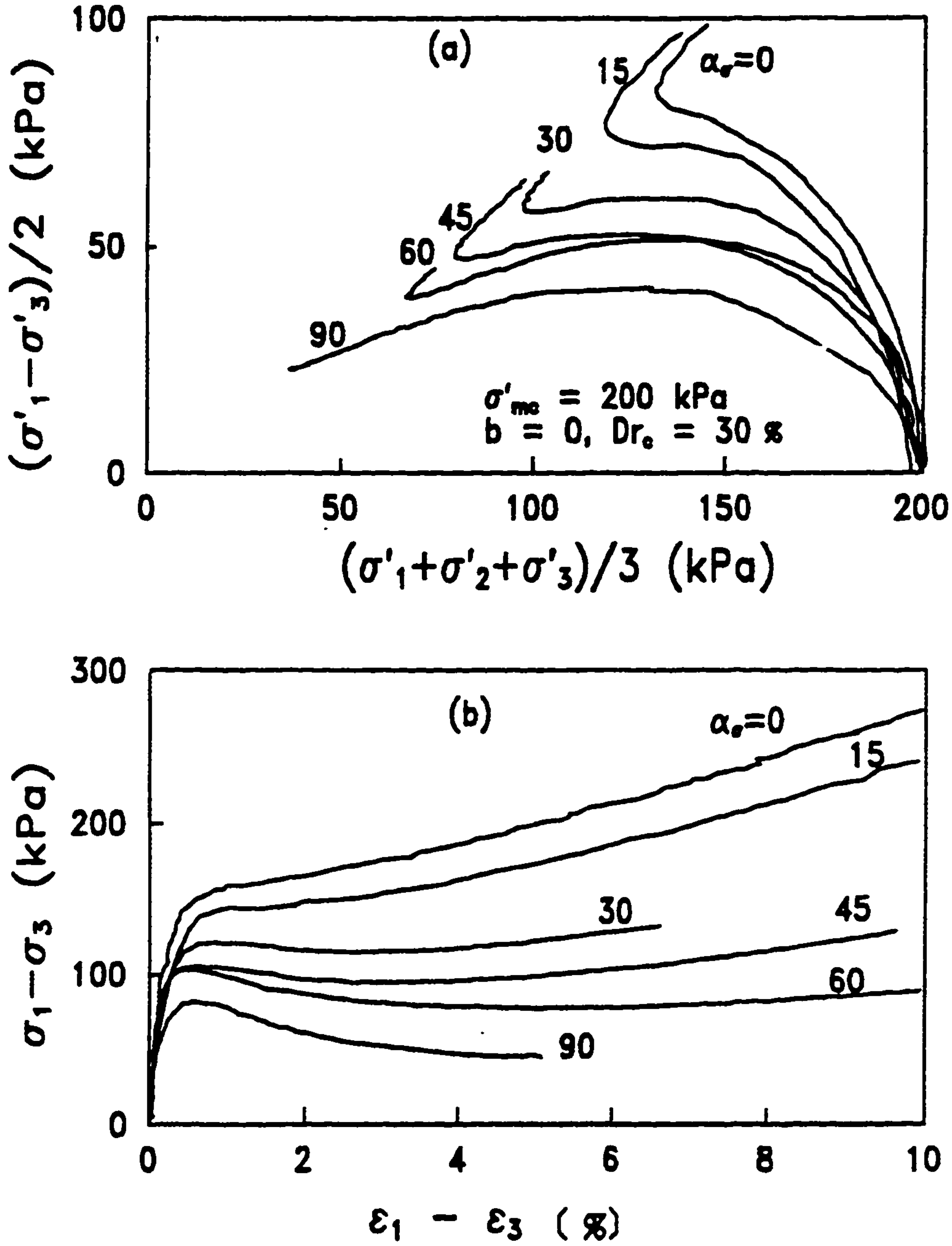

Fig. 6.6 Results of hollow cylinder torsional tests with various major directions (after Uthayakumar, 1996)

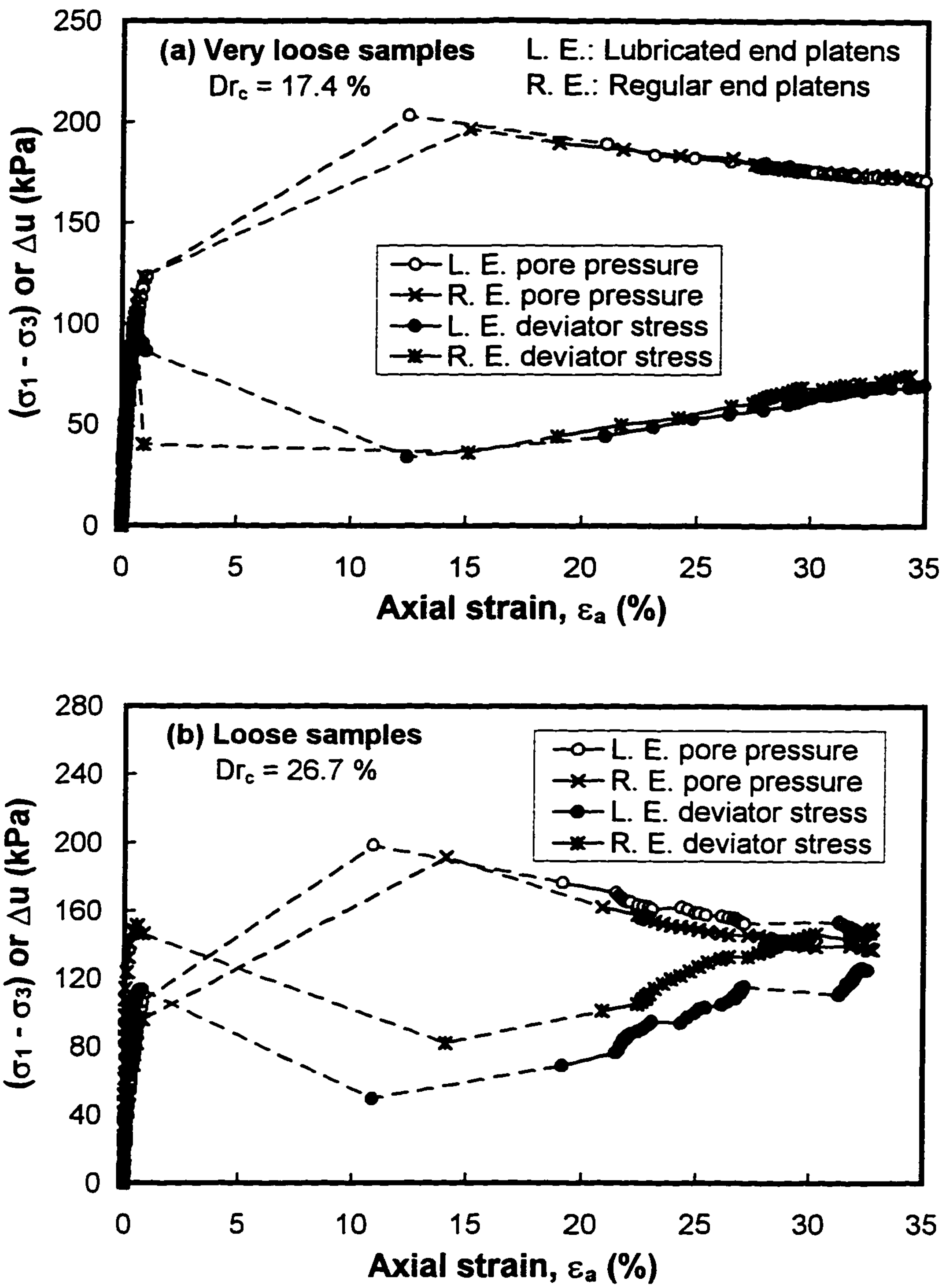

Fig. 6.7(a, b) Effect of end restraint on behaviour of Unimin sand

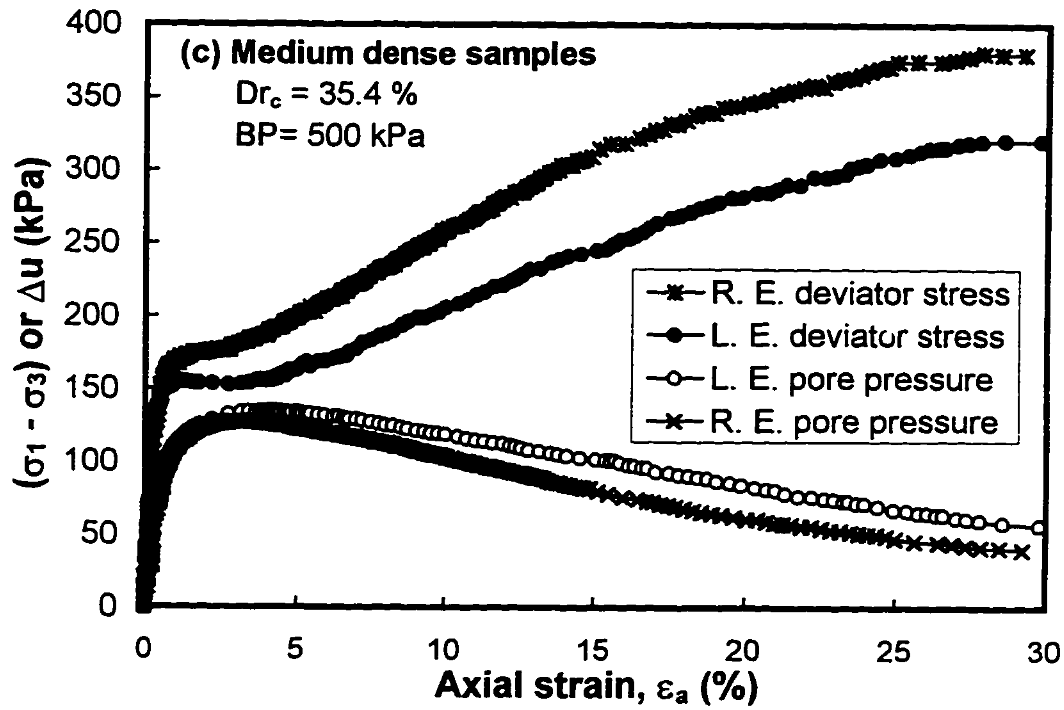

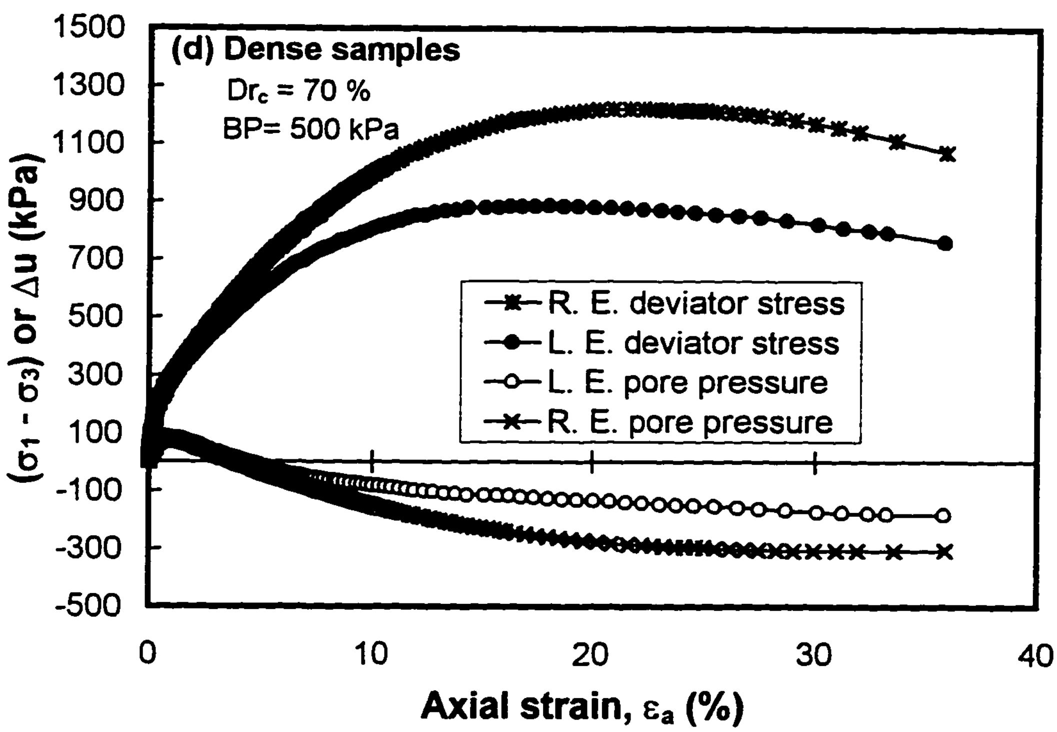

Fig. 6.7(c, d) Effect of end restraint on behaviour of Unimin sand

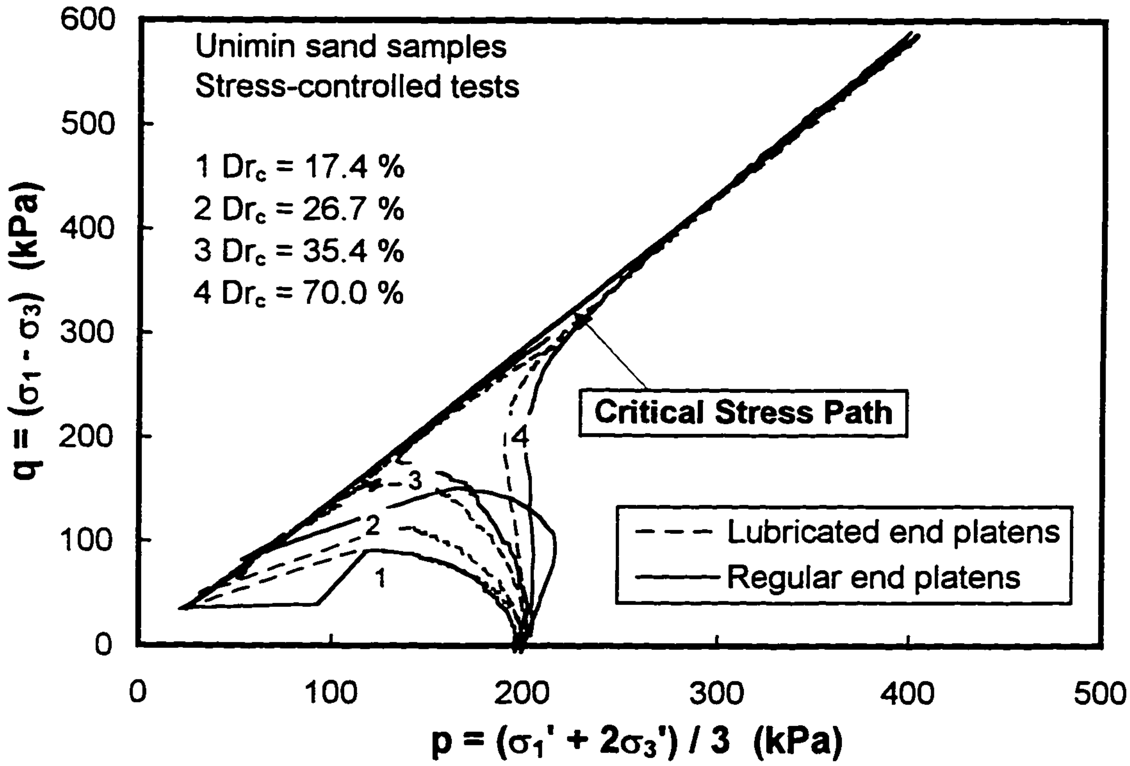

Fig. 6.8 Effect of end restraint on stress path

CHAPTER 7

DETERMINATION OF STEADY STATE STRENGTH

7.1 Introduction

Based on the concepts of the critical void ratio and the steady state of deformation, Poulos et al. (1985) developed a steady state approach to estimate the undrained residual strength of a sand deposit, and suggested that highly contractive samples should be used in order to obtain a reliable steady state line. They also pointed out that for most sands, a quasi-steady state behaviour is shown even in the triaxial tests on very loose samples (Poulos et al., 1988). Thus, it is of interest to know what is the undrained residual strength for the above sands. By definition, the steady state is reached only after a sample has undergone a large axial strain which is sufficient to erase the original structure of the sample. This has led investigators to regard that the state at large axial strain as the steady state of the sample. In fact, test results may be affected by many factors and diverge from the definition of the basic concepts.

This Chapter will discuss the distinction between some basic concepts and test behaviour, and recommend an approach of determining the steady state strength of a sample with QSS behaviour.

7.2 Basic concepts and laboratory behaviour

7.2.1 Critical void ratio, steady state and critical state

Casagrande (1936) defined that the critical void ratio is one at which a cohessionless soil can undergo any amount of deformation or actual flow without volume change under drained condition. Taylor (1948) supplemented that under undrained condition, the critical void ratio is one at which shearing leads to no strength change. The critical void ratio is a function of effective stress, and can be reached from either a loose or dense state in drained tests (Casagrande, 1975). Many observations support this concept. Desrues et al. (1996) discovered, by using computed tomography technique to measure the local void ratio of triaxial sand samples, that under the same effective confining stress, the global void ratio in dense samples was much less than that in loose samples, but the local void ratio within the shear band of the dense samples was the same as the global and local void ratio of the loose samples (Fig. 7.1). This evidence directly proves the concept of the critical void ratio.

Two further concepts, the steady state of deformation and the critical state were developed, from the concept of the critical void ratio, by Roscoe et al (1958) and Poulos (1981), respectively. Roscoe et al. (1958) stated that the critical state is an **ultimate** state at which any arbitrary further increment of shear distortion will not result in any change of void ratio under drained condition, or any change of effective stress under undrained condition. The critical state points so defined can be expected to be located on or near a line on a yield surface. Poulos (1981) stated that the steady state of deformation for any mass of particles is that state in which the mass is continuously deforming at constant volume, constant normal effective stress, constant shear stress, and ***constant velocity***. The steady state of deformation is achieved **only after** all particle orientation has reached a statistically steady state condition and after all particle breakage, if any, is complete, so that the shear stress needed to continue deformations and the velocity of deformation remain constant.

It is observed that the definition of the critical state combines Casagrande's and Taylor's definitions and implies that the critical state points are located on a unique line. The definition of the steady state emphasizes that it is a continuous deformation state with constant parameters. Many investigators consider that despite the difference in the definitions, there is no clear distinction between the critical state and the steady state. Both concepts in fact describe the same failure phenomenon that a soil mass is continuously deforming at constant volume and constant stresses (Sladen et al., 1985, Been et al., 1991, Poorooshasb and Consoli, 1991, Chu, 1995, etc.). In order to avoid confusion with the post-PT critical stress state, in which the shear resistance has been fully mobilized for a given effective confining stress, only the term "steady state" is used in the rest of this chapter.

The concept of the steady state and the uniqueness of the steady state line in triaxial compression tests on a given sand have been verified by many investigators (Been et al., 1985, 1991; Castro, 1969, Castro et al., 1982, 1992; Poulos et al, 1985, 1988; McRoberts and Sladen, 1992; Negussey and Islam, 1994; Sladen et al., 1985; Vaid and Chern, 1985; etc.). However, the concept of the steady state seems invalid in the case of quasi-steady state behaviour, since after the phase transformation, the deviator stress increases with further strain. Also, by definition, the steady state is an **ultimate** state, and can be achieved **only after** all particle orientation in a sample has reached a statistically steady state condition. Thus, it seems that the steady state must occur at large strain, and in triaxial tests, there might not be sufficient strain to reach the steady state for most soils (Poulos et al., 1988). These statements in the definitions have led some investigators to assume that in the quasi-steady state behaviour, the state at large axial strain is the actual steady state (for example, Ishihara, 1993, Verdugo et al., 1996).

7.2.2 Steady state in QSS behaviour

Computer activated stress-controlled triaxial tests on sand samples with lubricated end platens were used in this investigation. Typical undrained results for loose Unimin sand are shown in Figs. 7.2 and 7.3. The sample shown in Fig. 7.2 had a relative density of 45.1% after consolidation under an effective confining pressure of 1092 kPa (Figs. 7.2). It is clear that the sample exhibited a "quasi-steady state behaviour" (Fig. 7.2 (a)). The deviator stress reached a peak value of 584 kPa at an axial strain of 1.6 % after 36 minutes of axial loading. Then, the sample suddenly collapsed and within 2 seconds deformed to 15.6 % strain with a deviator stress drop of 106 kPa. After that, the deviator stress continuously increased to 591 kPa at an axial strain of 25 % and remained essentially constant with further strain. It may be noted that during the rapid collapse, the cell pressure increased by 58 kPa since the servo-actuated constant pressure system could not respond fast enough to immediately compensate the induced cell pressure. After the collapse, the cell pressure decreased within 55 seconds to the initial value at a strain of 17% and then remained constant. Correspondingly, the excess pore pressure decreased from 954 kPa to 877 kPa at the same time and then decreased slowly with further strain. However, the effective cell pressure did *not* display similar change as the cell pressure and the excess pore pressure. Therefore, the induced cell pressure, which may occur during rapid collapse, does not affect the effective stress and the shear resistance significantly, although it can affect excess pore pressure and the measured pore fluid compression (Fig. 7.2 (d)).

Fig. 7.2 (b) shows the detail of strain and pore pressure changes during collapse of this sample. Before collapse, the sample strained slowly, at a strain rate of about 1.8 %/min. Once the collapse was initiated, its strain rate suddenly increased to about 900 %/min, and essentially remained constant during collapse. After the collapse, the strain rate decreased to about 3.6 %/min. The pore pressure increased very rapidly, from 752 kPa to 950 kPa, in the first half of the collapse, and then remained constant until the end of the collapse. A steady state was achieved by the end of the collapse, between axial strains of 9 % and 15 %. Further straining resulted in a decrease in pore pressure and a increase in deviator stress.

The sample in Fig. 7.3 had a relative density of 25.2 % at the start of axial loading. Fig. 7.3 (a) and (b) show that it developed a peak strength of 187 kPa at a strain of 1.1 %, then liquefied and strained to 26.3 % in 3 seconds. The pore pressure increased from 236 kPa at the onset of the collapse to 390 kPa at a strain of 11.1 %, then decreased to 367 kPa at a strain of 26.3 %; correspondingly, the deviator stress decreased from 187 kPa to 80 kPa, and then increased to 100 kPa. It is also noted that since a high air pressure supply was used to activate the servo actuator, rather than the high water pressure supply used in the test shown in Fig. 7.2, the induced cell pressure was low, equal to 20 kPa at a strain of 11.1 %, and was compensated at a strain of 28%. The detail of pore pressure and vertical deformation during collapse of this sample are shown in Fig. 7.3 (b). The sample deformed similarly to the sample in Fig. 7.2, its strain rate was equal to 2.4 %/min before collapse; remained at about 760 %/min during collapse; and thereafter reduced to 5.4 %/min. Its pore pressure increased very rapidly during collapse to an ultimate value of 390 kPa, and remained at this ultimate value until a strain of 16%. The pore pressure subsequently decreased even though the collapse deformation continued to a strain of 26.3 %. In this test, a steady state was developed within a strain range of 9% to 16 %, because the pore pressure, the deviator stress and the strain rate remained constant. The deviator stress increased with further strain even though the collapse induced a strain of over 26 %.

7.2.3 Steady state in drained test

Fig. 7.4 shows the typical results of drained triaxial tests on loose Unimin sand. The sample had a relative density of 17.7 % under effective confining stress of 50 kPa. It can be seen in Fig. 7.4 (a) that the deviator stress increased with axial strain, accompanied by several small rapid jumps (strain rate from 7.8 to 10.8 %/min), then reached an ultimate value of 138 kPa at a strain of 12.5 %, and essentially remained constant thereafter. The deformation increased from a strain rate of 0.35 %/min at the initial stage of loading, to an average strain rate of 1.2 %/min between strains of 5 % to 12.5 %, and subsequently suddenly went up to about 16.8 %/min and remained constant (Fig. 7.4 (b)). The void ratio of the sample decreased from 0.969 at the start of axial loading to 0.921 at a axial strain of 11.5 %, and remained at 0.921 until axial strain was 17 %, and then continuously increased to 0.933 at the end of the test. It is clear that by definition, a steady state of deformation was achieved when the void ratio, the deviator stress and the strain rate of the sample stayed constant between strains of 12.5 and 17 %.

It is noted that beyond a strain of 17 %, the void ratio of the sample continuously increased, even though the deviator stress and the strain rate remained constant. This result corresponds to the quasi-steady state behaviour in undrained tests, when after phase transformation, the deviator stress increases with further axial strain. Based on the concept of the critical void ratio, a constant shear stress must be accompanied by constant void ratio. Therefore, the only reason for the increase of void ratio at large strain in a drained test is that the void ratio within shear zone of the sample remains constant, and the increase in the measured void ratio results from the dilation of the end zones of the sample (Chapter 6). All drained and undrained tests on loose sand samples in this study showed similar **threshold strain** (i.e., the strain at which the sample dilates or pore pressure decreases) of about 15 %, which is in agreement with Ishihara's (1994) observation that quasi-steady state often occurs below a strain of 15 %.

7.2.4 Different deformation stages during shear

Figures 7.5 to 7.7 show the results of the undrained or drained triaxial tests on the samples for which steady states could not be readily distinguished by the definition of steady state. The results of the three tests and other triaxial tests are also shown in an e - logp' plot (Fig. 7.8), designated as (1), (2) and (3), respectively. It is seen in Fig. 7.8 that in the undrained test (1), the sample had an initial state near the steady state line of the Unimin sand, and both its states at peak shear stress and at phase transformation (PT) were close to the steady state line as well. In undrained test (2), the state points at consolidation state, at phase transformation and at peak state appear to be much lower than the steady state line. In drained test (3), the initial state of the sample was located above the steady state line, but its final state was far below the steady state.

Undrained tests

The results of test (1) are presented in detail in Figs. 7.5. The deviator stress increased to a value of 156 kPa at a strain of 0.9 %, and remained constant until the pore pressure reached peak value of 135 kPa (the phase transformation) at a strain of 4.2 %. Then the deviator stress increased to 322 kPa at a strain of 28 % and remained constant again with further strain; while the pore pressure decreased essentially along a straight line until the end of the test (Fig. 7.5 (a)). Clearly, by definition, there was no obvious steady state in this test.

It may be noted in Fig. 7.5 that there were four distinct deformation stages with constant strain rates during shear: **initial stage, collapse stage, critical stress stage** and **post failure stage** (Fig. 7.5 (c)). In the initial stage, both the deviator stress and the pore pressure increased with strain, and the strain rate was low, equal to about 0.08 %/min. By the end of the initial stage, the sample suddenly collapsed and entered to the collapse stage at which it deformed from a strain of 0.9 % to a strain of 4 % at a fast and constant strain rate of 7.6 %/min. Correspondingly, the deviator stress remained constant, and the pore pressure increased to peak and then essentially remained constant by the end of this stage (Fig. 7.5 (a)). In the critical stress stage, the sample deformed to an axial strain of 28 % at a low strain rate of 1.7 %/min, accompanied by continuous increase in deviator stress and continuous decrease in pore pressure. The stress state followed the critical stress path in this stage (Fig. 7.5 (b)). In the post failure stage which started at a strain of 28 %, both the deviator stress and the strain rate remained constant, but the pore pressure continuously decreased so that the effective stress state moved away from the critical stress path. The steady state of this sample seemed to appear very shortly by the end of the collapse stage, when the deviator stress, pore pressure and strain rate were constant.

It is interesting that the collapse of the sample did not cause any decrease in deviator stress, even though the pore pressure increased rapidly during collapse. As a result, once the collapse was initiated, the stress path of the sample followed a horizontal line until reaching the critical stress path (Fig. 7.5(b)). This proves that in a p'-q plot, the collapse surface (Sladen et al, 1985) is a straight line segment followed by a horizontal line through a steady state point (Vaid and Chern, 1985; Kramer, 1996), rather than a straight line through the steady state point.

The results of test (2) on the sample with consolidated relative density of 70 % are shown in Fig. 7.6. The sample deformed in three distinct deformation stages in which the strain rates remained constant, equal to 0.06, 0.4 and 4.7 %/min, respectively (Fig. 7.6(c)). Compared with test (1), no collapse stage deformation occurred in this case. In the critical stress stage, the deviator stress increased to a peak value of 887 kPa at a strain of 15 %, accompanied by a decrease in pore pressure from 86 to -114 kPa (Fig. 7.6(a)); and the stress path followed the critical stress path of the sand. In the post failure stage, the deviator stress slightly decreased with further straining, while the pore pressure continuously decreased. No steady state appeared in this test.

Drained tests

There are three deformation stages in a drained test: **initial stage, pre-peak stage** and **post peak stage**. The drained sample (3) had an initial state (Dr_c = 37.9 %, σ_{3c} = 696 kPa) above the steady state line (Fig. 7.8), and the test results are shown in Fig. 7.7. In the initial stage, the sample deformed at a low strain rate of 0.07 %/min, accompanied by an increase in deviator stress and a decrease in void ratio. The change from initial stage to pre-peak stage was not so clear as the change from initial stage to collapse stage or critical stress stage in undrained tests. The deviator stress continuously increased until reaching a peak value of 1655 kPa (Fig. 7.7(a)), at which the stress path of this sample arrived the critical stress path of the sand (Fig. 7.7(b)). Subsequently, the sample entered into the post peak stage and deformed at a constant strain rate of 2.8 %/min (Fig. 7.7(c)), accompanied by a slight decrease in deviator stress (Fig. 7.7(a, b)). The void ratio displayed a continuous decrease and maintained this tendency at the end of the test. No steady state was reached in this test, even though the sample exhibited high contractive response.

The sample shown in Fig. 7.4 also had an initial state (Dr_c = 17.7 %, σ_{3c} = 50 kPa) above the steady state line (test (4) in Fig. 7.8). Its behaviour was different from that of the sample shown in Fig. 7.7 mainly in the post peak stage, at which the deviator stress of this sample essentially remained constant, the void ratio remained constant until an axial strain of 17 % and subsequently increased with further strain. The steady state was reached between strains of 13 to 17 %.

7.2.5 Modified definition of the steady state

It may also be noted in Figs. 7.2 and 7.3 that the deviator stress, the pore pressure and the effective confining stress remained essentially constant after strains of 25 % to 27 %. The corresponding strain rate was also constant, equal to 4.2 %/min for the sample shown in Fig. 7.2 and 8.4 %/min for the sample shown in Fig. 7.3, respectively. This indicates that the state at large strain may also satisfy the definition of the steady state of deformation. Therefore, in the quasi-steady state behaviour of sands, there appear to be two steady states: the quasi-steady state which occurs before phase transformation, and the steady state at large axial strain (Verdugo and Ishihara, 1996).

However, it should be mentioned that the results of triaxial tests on sands may be affected by non-uniform deformation which may occur during shear (Chapter 6). Non-uniform deformation in triaxial tests on sand samples may develop due to the formation of shear band or due to the effect of end restraint. Shear band in a triaxial sample may develop in relatively dense state after some axial strain; as a result, the void ratio in the shear zone is larger than the global void ratio of the sample (Desrues et al., 1996). In this case, the shear resistance for a given void ratio is underestimated since it is significantly affected by the void ratio change in the shear band. This may be the reason why a continuous decrease in pore pressure at large strain can be accompanied by a decrease in deviator stress in an undrained test (Fig. 7.6); or a decrease in global void ratio can be also accompanied by a decrease in deviator stress in a drained test (Fig. 7.7); and the steady state points from drained tests on dense sample are always lower than that from the tests on loose samples (Verdugo and Ishihara, 1996). Shear band may not be a serious problem for loose sand samples (Zhang and Garga, 1997).

End restraint is an important factor affecting the results of triaxial tests on sand samples. It affects triaxial tests on sands by decreasing the pore pressure of undrained samples and increasing the global void ratio of drained samples, which may become significant in the critical stress stage of a shear. In this case, the steady state strength of sands for a given void ratio is overestimated (Chapter 6). Therefore, the second "steady state" at large strain shown in Figures 7.2 and 7.3, as well as in the tests by Verdugo and Ishihara (1996), should be the state at which both the behaviour of a sand sample and the effects of non-uniform deformation have reached ultimate states.

As stated by Poulos et al. (1988), the steady state strength is the fundamental strength of a sand for a given void ratio, which cannot be lost as a peak strength does, and also cannot be increased after all particle orientation or/and all particle breakage is complete. However, the steady state strength measured in triaxial tests may be underestimated due to the formation of shear band, or overestimated due to the effect of end restraint. Therefore, in order to avoid confusion which may result from above definition of the steady state, following definition is recommended:

The steady state of deformation for any mass of particles is that state in which the mass is continuously deforming at constant volume, constant normal effective stress, constant shear stress, and constant velocity. **The constant shear stress is the minimum strength of the mass, which is dependent on the local void ratio within the shear zone.**

7.3 Steady state strength in QSS behaviour

7.3.1 Determination of steady state strength

When determining the steady state strength of sand by using triaxial tests, following considerations are pertinent:

(1) The triaxial samples must exhibit a collapse stage of shear deformation, i.e. their initial states are located above the steady state line of the sand. A sample with relatively dense initial state (below the steady state line) will undergo initial stage deformation, and then critical stress stage deformation at which the measured behaviour of the sample may be significantly affected by end restrain or/and the formation of shear band.

(2) Steady state occurs in collapse stage of shear deformation, rather than in critical stress stage and post failure stage. The shear resistance at very large axial strain may be affected by non-uniform deformation of the samples.

(3) Lubricated end platens are necessary to reduce the effect of end restraint on the behaviour of the sand samples. The deformation of the latex membranes in the lubricated end platens should be considered when calculating the void ratio of the samples.

(4) Lateral deformations should be measured by adequate devices such as the HRDT used in this study during saturation and consolidation, to improve the accuracy of void ratio determination.

(5) Stress-controlled triaxial tests are recommended unless further investigations can prove that for a given void ratio, stress-controlled and strain-controlled triaxial tests could provide the same steady state strength of a sand.

Limited data indicates that there is no significant difference between the steady state lines from stress-controlled and strain-controlled triaxial tests (Been et al., 1991, Sladen et al., 1985, Poulos et al., 1988). However, as Casagrande (1975) mentioned, collapse deformation of sands is an important behaviour related to flow liquefaction in nature, and cannot be observed in strain-controlled tests. The main difference between the two loading modes is that strain rate remains constant in strain-controlled loading, but varies at different deformation stages of a test and for samples with different initial conditions in stress-controlled loading (Figures 7.2 to 7.7). Some evidences indicate that in strain-controlled tests, the induced pore pressures depend on the particular strain rate applied: the faster the strain rate, the greater the induced pore pressure until a limiting strain rate is reached irrespective of how fast it is increased (Alarcon and Leonards, 1988). Thus, steady state strength may be also affected by strain rate.

(6) The steady state strength of a sand sample should be determined by considering the test information including shear stress, pore pressure, strain rate, and effective stress path under undrained loading condition or volume change under drained loading condition.

In undrained tests, the lowest stress during collapse may not be the steady state strength in some cases. It can be seen in Fig. 7.9 that in the CAU test on a sample with Dr = 38.2 % (curve b), the stress state dropped from peak point (480, 467) to point (254, 372) during collapse, then went to the steady state point (272, 364). The mean effective stress at the point (254, 372) was equal to 254 kPa, less than that (272 kPa) at the steady state. However, in the CIU test on a sample with Dr = 37.5 %, the stress state dropped to point (280, 206), then went to the steady state point (171, 242) during collapse. The deviator stress at point (280, 206) was 36 kPa less than that at the steady state point. The lower stresses during collapse appear to be caused by the effect of rapid collapse on the measured pore pressure and axial load; and were not the stresses at steady state. The stress state point at which the stress path of a sample first contacts the critical stress path in undrained triaxial tests defines the steady state.

The test results may be also affected by the data acquisition system. The vertical deformation can be very fast during collapse in undrained tests, equal to 96 %/min for loose Unimin sand samples in this study and 8100 %/min for loose Banding sand samples (Castro, 1969). A DC amplification recorder (Model 1243, Buchan Instruments Inc.) was attempted to be used in this study, but it was found that the response of the writing pens in the recorder was too slow to record the rapid changes in axial load, pore pressure and vertical deformation during collapse. The data shown in Fig. 7.9 was recorded by a computerized triaxial test system. A control cycle of the system, including to record, handle and save test data, and to adjust pressure and axial load, takes about one second. If the steady state of a sample is reached at the end of collapse, the test system can provide the appropriate steady state information of the sample, such as in the test shown in Fig. 7.2 and curve (a) in Fig. 7.9. However, if during rapid collapse, the steady state is followed by an increase in deviator stress, such as shown in Fig. 7.3, the data acquisition system may miss the data at steady state and then provide an overestimated steady state strength. For example, in the CIU test on a sample with Dr = 25.2 % (Fig. 7.9, curve d), the stress state dropped from the peak point to point (60, 80) which was determined from Fig. 7.3 as the steady state point of the sample. The stress state then rapidly increased to point (75, 100) in one second. If the data point (60, 80) were not to be recorded, the steady state strength would be overestimated by (100 - 80) = 20 kPa. Therefore, a fast data acquisition system is essential.

In drained triaxial tests on loose sand, the steady state strength can be determined when both the deviator stress and the volumetric strain remain constant, even temporarily, with axial strain. However, it seems more difficult to determine steady state strength in drained triaxial tests than in undrained triaxial tests, since a sample with an initial state even above the steady state line can be densified during drained loading so that non-uniform deformation may develop. A drained sand sample thus should be prepared at loose density and consolidated under low consolidation pressure; but such a sample may be accompanied by serious sample heterogeneity and large error in void ratio and then may result in large error in estimation of steady state strength.

7.3.2 Steady state behaviour of Unimin sand

All undrained triaxial tests on loose Unimin sand samples in this study, among which the lowest relative density at consolidation stage was equal to 14 %, showed the quasi-steady state behaviour (Figures 7.2 and 7.3). Corresponding to the undrained quasi-steady state behaviour, the drained tests on very loose Unimin sand samples displayed a temporary steady state in which both deviator stress and void ratio remained constant, thereafter the void ratio continuously increased with further strain, accompanied by constant deviator stress and constant axial strain rate (Fig. 7.4). It can be seen in Fig. 7.8 that the steady states of the undrained tests on Unimin sand samples are located on or near a straight line in e - log p' plot, except the two points from dense samples (Fig. 7.8 (a)). In a p' - q plot, all steady state points from drained or undrained tests on loose samples, and the peak points from tests on dense samples lie on a straight line (Fig. 7.8 (b)).

The steady states from drained tests also reside on or near the steady state line obtained from the undrained tests (Fig. 7.8(a)). This indicates that the steady states strength for a given void ratio from drained and undrained tests are the same for the Unimin sand. Similar results were observed for Syncrude tailings (Poulos et al., 1988), Erksak sand (Been et al., 1991) and Toyoura sand (Verdugo et al., 1996). Conversely, based on the test data from Castro (1969), Alarcon et al. (1988) found a significant difference between the steady state lines from drained and undrained triaxial tests. However, among the three sands used by Castro, only in sand B did six drained steady state points locate above the undrained steady state line, accompanied by two drained points on the undrained line (Fig. 70 in Castro, 1969). For the two other sands, the undrained and drained steady state points lie on the same line (Figs. 90 and 111 in Castro, 1969). Therefore, it may be a common conclusion for most sands that steady state line is independent of shear drainage conditions.

It is seen in Fig. 7.10 that the steady state points from the consolidated isotropically undrained (CIU) tests and from the consolidated anisotropically undrained (CAU) tests are also located on or near the same straight line in an e-logp' plot. In other words, for a given void ratio, the CIU test and the CAU test will give the same steady state strength, regardless of the consolidation stress ratio, Kc = $\sigma_{1c}'/\sigma_{3c}'$. Similar results were provided by Castro (1969), Poulos et al. (1988) and Castro et al. (1992). Conversely, Baziar and Dobry (1995) indicated that the consolidation stress ratio affects the steady state strength. The strength ratio, S_{us} / σ_{1c} (S_{us} = $(\sigma_1 - \sigma_3)_{us}$ / 2 cos ϕ_{us}' is a steady state strength on failure plane, suffix us denotes undrained steady state) was approximately constant for a given Kc, and increases as Kc increases. However, it may be seen in Fig. 7.11 that there is no unique relation between Kc and strength ratio for Unimin sand; for a given Kc, the strength ratio could vary from 0.05 to 0.4. The higher strength ratio for Kc = 2.0 than for Kc = 1.0 in Baziar and Dobry's tests may result from the higher densities in the Kc = 2.0 samples, rather than the different Kc values.

7.3.3 Shear strength at large strain

Fig. 7.12 shows the difference between the steady states and the states at large strain (ε_a = 30 %) in the drained and undrained tests on loose Unimin sand samples. Clearly, all state points at large strain were above or at the right side of the steady state points (Fig. 7.12 (a)). In the drained tests, the steady states occurred at strains of 13% to 19%; when the samples deformed from an axial strain at steady state to an axial strain of 30 %. The mean effective stress p' showed little change, but the global void ratio could be increased by about 0.01. In the undrained tests, the mean effective stress p' was 11 to 105 kPa lower at steady states (ε_a = 12 - 20 %) than at a strain of 30 %. In a p' - q plot, almost all steady state points and the state points at large strain were located on a unique line, except for several points at large strain which were within the post failure stage (Fig. 7.12 (b)). Therefore, for a given void ratio, the use of the state at large axial strain for loose sand samples is likely overestimate the steady state.

7.4 Sensitivity of steady state strength of sand

The steady states of all drained and undrained triaxial tests are shown in Fig. 7.13. This figure presents data in three groups as follows: Group 1, CIU and CD tests on fresh Unimin sand; Group 2, CAU, CIU and CD tests on previously used or unused Unimin sand from Group 1 tests; Group 3, CAU, CIU and CD confirmatory tests on fresh Unimin sand.

Clearly, all steady state points of the CAU tests in Group 2 were significantly below the steady state line determined from Group 1 CIU tests. For a given void ratio, the mean effective stress in Group 2 CAU tests was 40 to 150 kPa less than that in Group 1 CIU tests (Fig. 7.13 (a)). Thus, it appeared that for the Unimin sand, the steady state strength might be dependent on consolidation stress ratio K_c. In order to confirm this conclusion, two CIU tests and one CD test were conducted on the same material as in the Group 2 CAU tests. These test results indicate that the steady state points from the two CIU tests and the CD test were also below the steady state line from the tests in Group 1, and were located within the range of the steady state points from the Group 2 CAU tests (Fig. 7.13 (a)). This indicated that the smaller steady state strength in the second group may result from the variation of the material properties, rather than the different consolidation conditions. It was also observed during sample preparation that the number of tampings for a given density was less in group 2 than in group 1. It was thus expected that the maximum void ratio of the material in group 2 should be smaller than that in group 1. Regrettably, further information could not be obtained since the material used in the second group was disposed of.

The tests in Group 3, ten CAU tests, two CIU tests and one CD test, were carried out on fresh Unimin sand. In order to ensure the material to be the same for each sample, a large container was filled with fresh Unimin sand and was well shaken before each sample preparation. The results of these tests are also shown in Fig. 7.13. It can be seen that in an e - log p' plot, the steady state points from the tests in Group 3 are located in the same range as that in Group 1 (Fig. 7.13 (a)). In a p'-q plot, the steady state points from all the tests are located essentially on a straight line (Fig. 7.13(b)). These results indicate that the angle of internal friction of a sand is independent of small change in grain physical properties and consolidation stress ratio; while the steady state strength is very sensitive to the characteristics of sand grains.

Similar sensitivity of shear strength on material properties was observed from drained triaxial tests on dense Ham River sand thirty years ago by Bishop and Green (1965). They found that the peak internal friction angle decreased linearly with initial void ratio (note: under drained condition, the peak friction angle of a dense sand sample is larger than its residual friction angle; for a loose sand sample, both the peak and the residual friction angles are the same and is constant for a sand, Mohamad and Dobry, 1986). However, for a given initial void ratio, the peak friction angle of a sample which was prepared from the used material or from the fresh material remaining on the bottom of a container was about 1° lower than that of a sample prepared from fresh material.

The scatter in the shear strength of a sand appears to depend on its coefficient of uniformity. Table 7.1 and Fig. 7.14 summarize the overall scatters in void ratio for a given mean effective stress at steady state for different sands. It may be noted that for the sands with low coefficient of uniformity (Cu = 1.4 - 1.8), the overall scatters in void ratio at steady state were about 0.02, corresponding to the void ratio error due to the measurement of sample dimensions (Vaid and Sivathayalan, 1996). However, for sands with high coefficient of uniformity (Cu = 2.0 - 2.7), the overall scatters in void ratio could exceed 0.05. This indicates that besides the error in void ratio, small change in grain size distribution, which may occur mainly in the sands with high coefficient of uniformity, may also significantly affect the steady state strength. For the Unimin sand (Cu = 2.0), the overall scatter in void ratio at steady state was only equal to 0.02, if the samples were prepared from the fresh and well mixed material. Thus, the effect of the small change in grain size distribution on steady state strength may be reduced by preparing a sample after mixing the test material well.

7.5 Conclusions

1. A steady state in the quasi-steady state behaviour can occur prior to phase transformation. In some cases, a state at large strain also satisfies the requirements stipulated in the definition of the steady state of deformation. In order to avoid this confusion, a modified definition of the steady state is suggested as follows:

> The steady state of deformation for any mass of particles is that state in which the mass is continuously deforming at constant volume, constant normal effective stress, constant shear stress, and constant velocity. **The constant shear stress is the minimum strength of the mass, which is dependent on the local void ratio within shear zone.**

2. Four deformation stages may occur in undrained triaxial tests on a sand: initial stage, collapse stage, critical stress stage and post failure stage. Within each stage, the strain rate is essentially constant. The undrained steady state usually exists in the collapse stage. Three deformation stages may occur in drained triaxial tests on sand: initial stage, pre-peak stage and post-peak stage. The drained steady state may exist in post-peak stage.

3. The steady state strength should be determined by considering all test information including shear stress, pore pressure, strain rate, and effective stress path under undrained loading condition or volume change under drained loading condition.

4. The steady state strength is very sensitive to small change in grain size distribution of a sand with high coefficient of uniformity.

Table 7.1 Scatter of void ratio at steady state for different sands

Sands	Uniformity Coefficient $Cu = D_{60}/D_{10}$	Overall Scatter in Void Ratio at Steady State (1)	Reference
Ham River sand	2.3	Large scatter in ϕ_{peak}	Bishop et al., 1965
Banding sand #6	1.7	0.02	Castro et al., 1982
Mine tailings	2.7	0.05 (2)	Castro et al., 1982
Syncrude tailings	2.4	0.11	Sladen et al., 1987
WA sand	1.4	0.02	Konrad, 1990
DS sand	2.1	0.06	Konrad, 1990
Ottawa sand C109	1.5	0.014	Vaid et al., 1990
Erksak 330/0.7	1.8	0.02	Been et al., 1991
Toyoura sand	1.7	0.02	Ishihara, 1993
Unimin sand	2.0	0.06	This study
Unimin sand (3)	2.0	0.02	This study

(1) All data was obtained from triaxial compression tests.

(2) The SS line was not straight. The scatter was 0.05 at σ_3' = 200 kPa and 0.08 at σ_3' = 600 kPa

(3) Fresh Unimin sand was well shaken before each sample preparation.

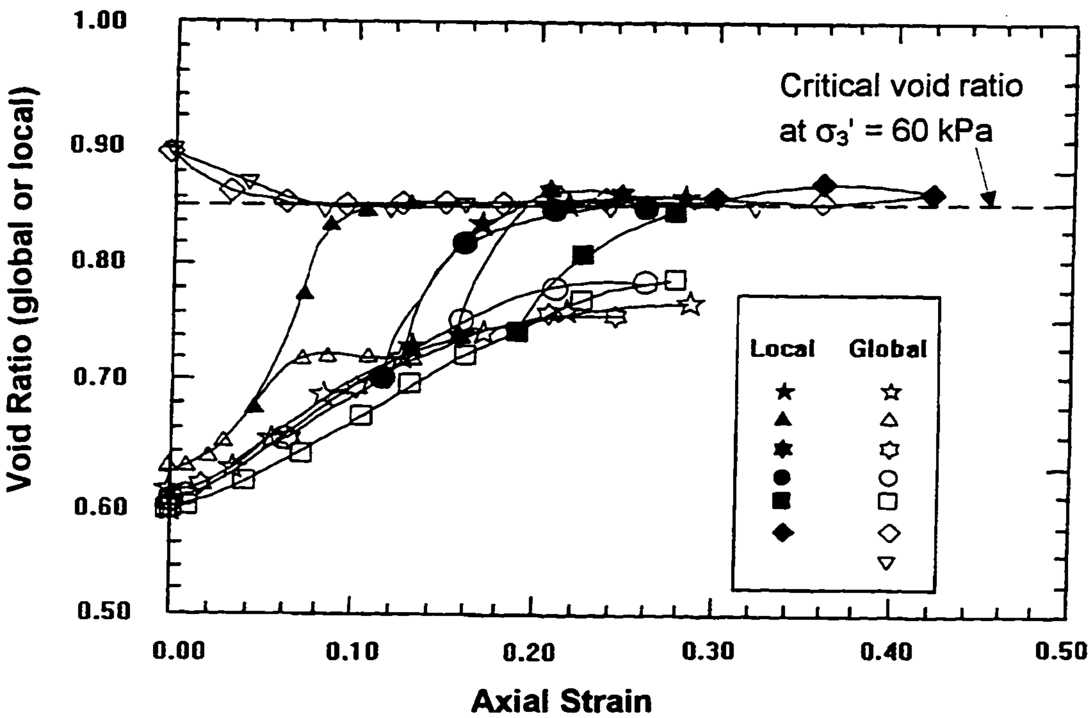

Fig. 7.1 Results of triaxial tests on Hostun RF sand (after Desrues et al, 1996)

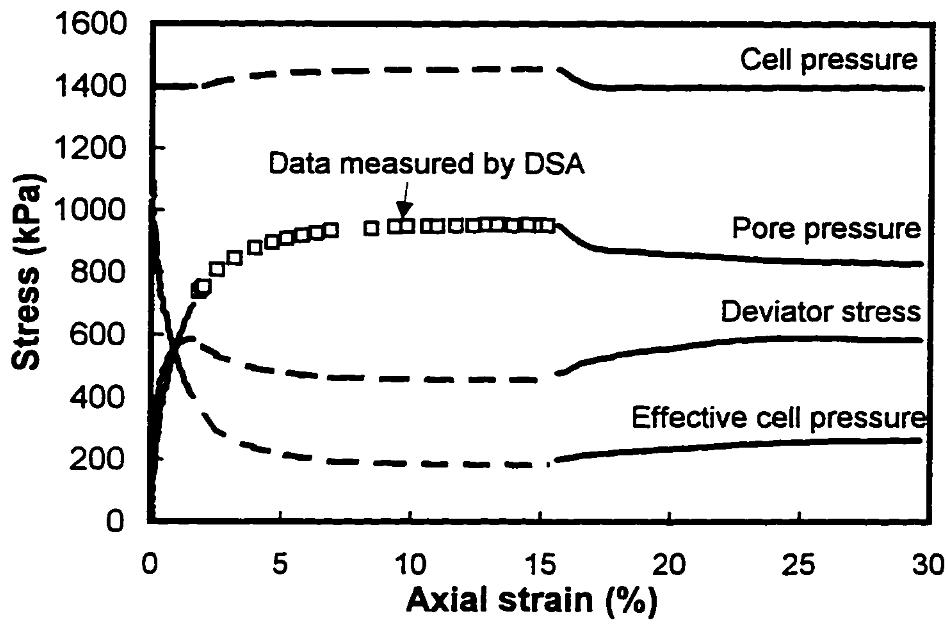

Fig. 7.2(a) Stress - strain curves

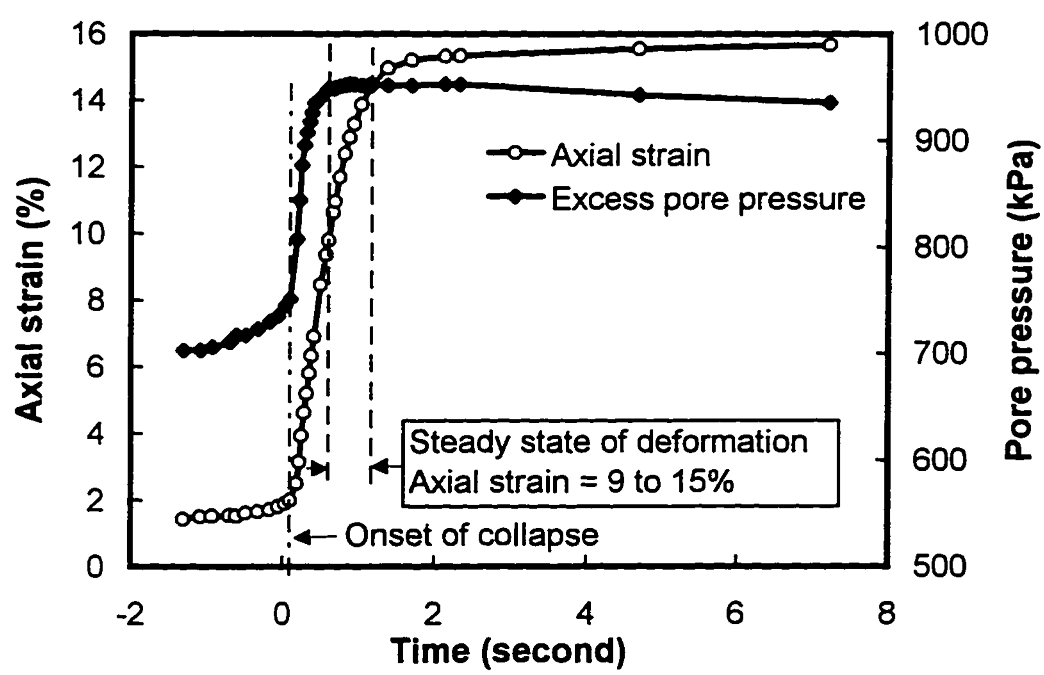

Fig. 7.2(b) Axial strain and pore pressure during collapse

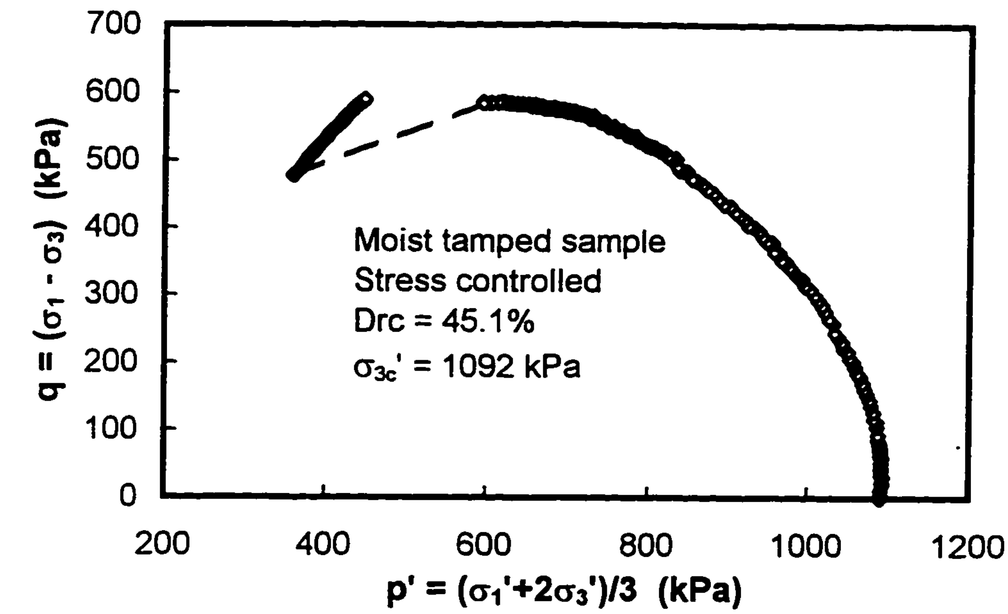

Fig. 7.2(c) Effective stress path

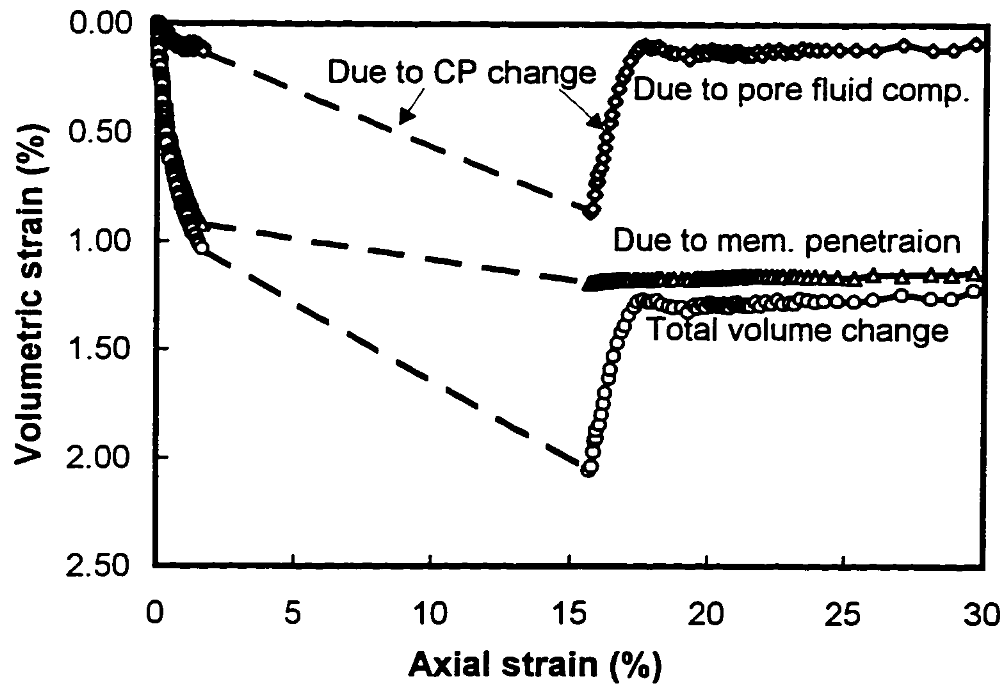

Fig. 7.2(d) Volume change during undrained shear

Fig. 7.2 Results of undrained triaxial test (Dr = 45.1%)

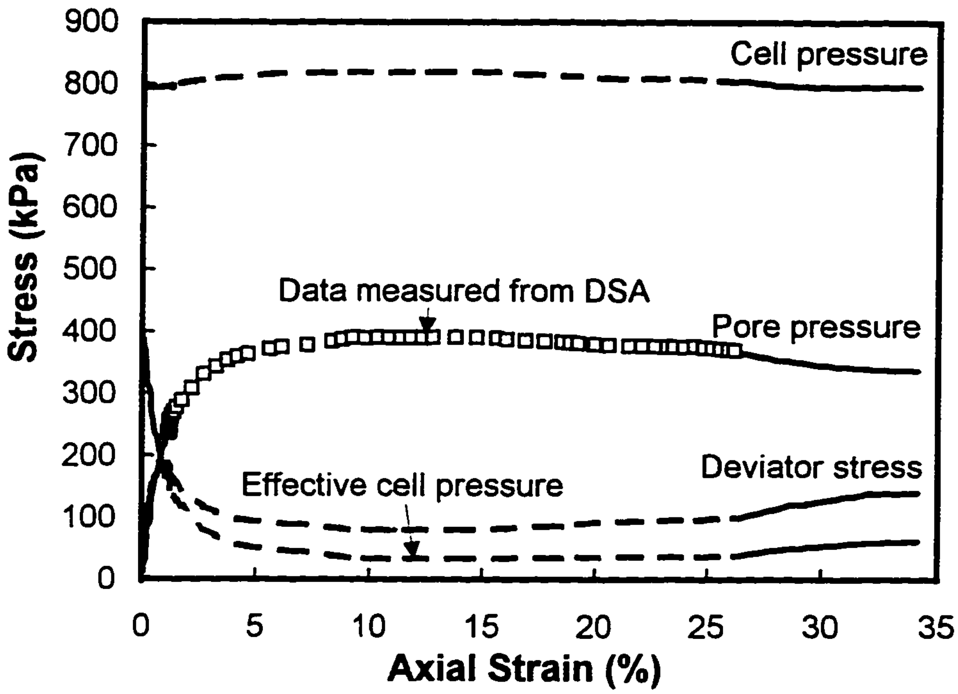

Fig. 7.3(a) Stress strain curves

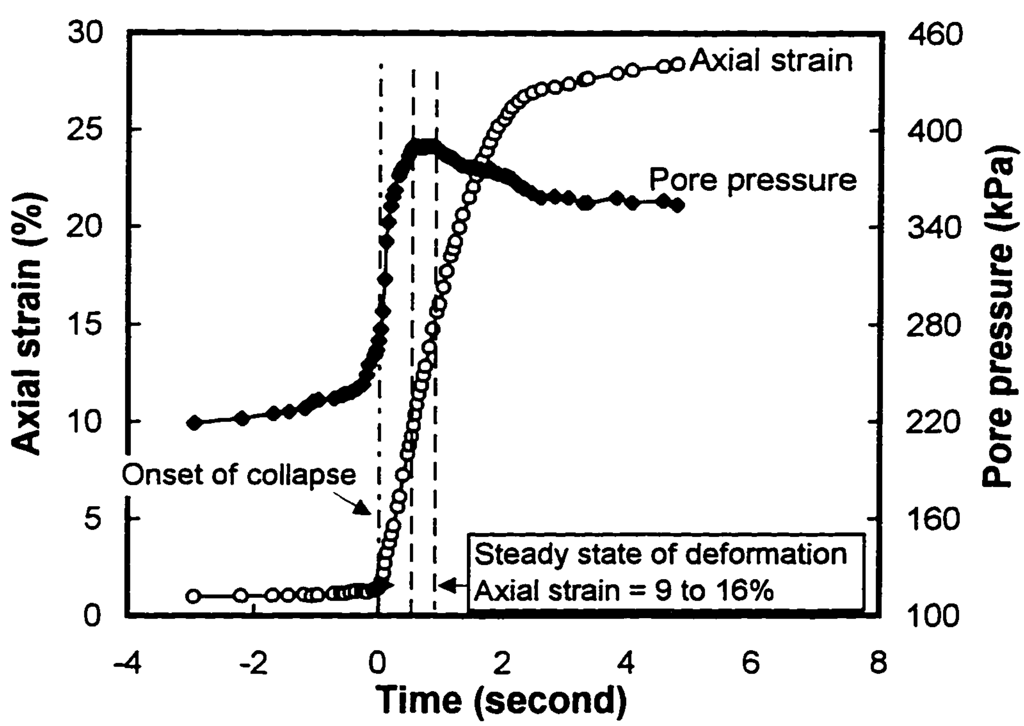

Fig. 7.3(b) Strain and pore pressure during collapse

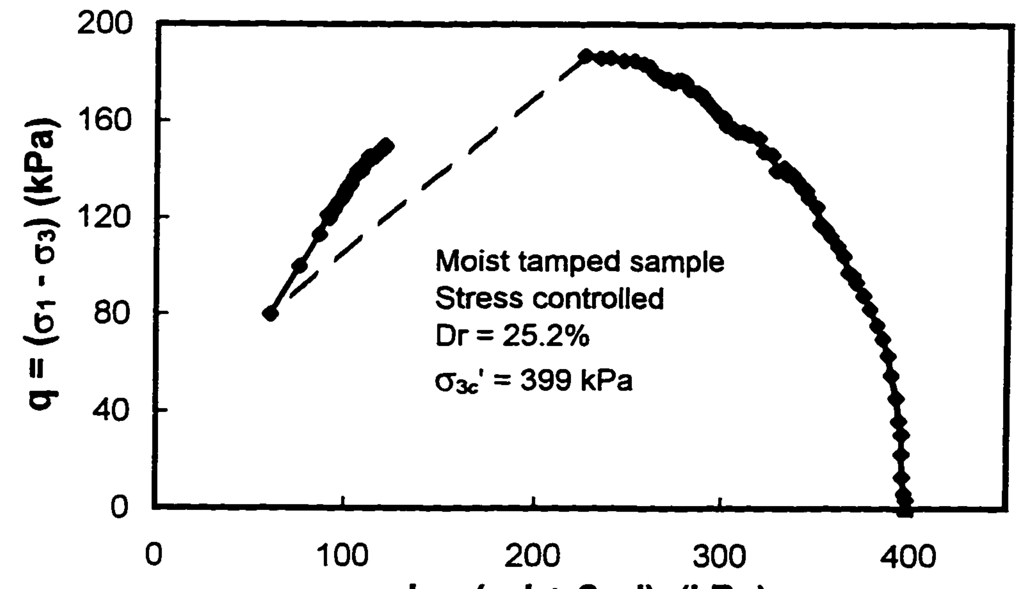

Fig. 7.3(c) Effective stress path

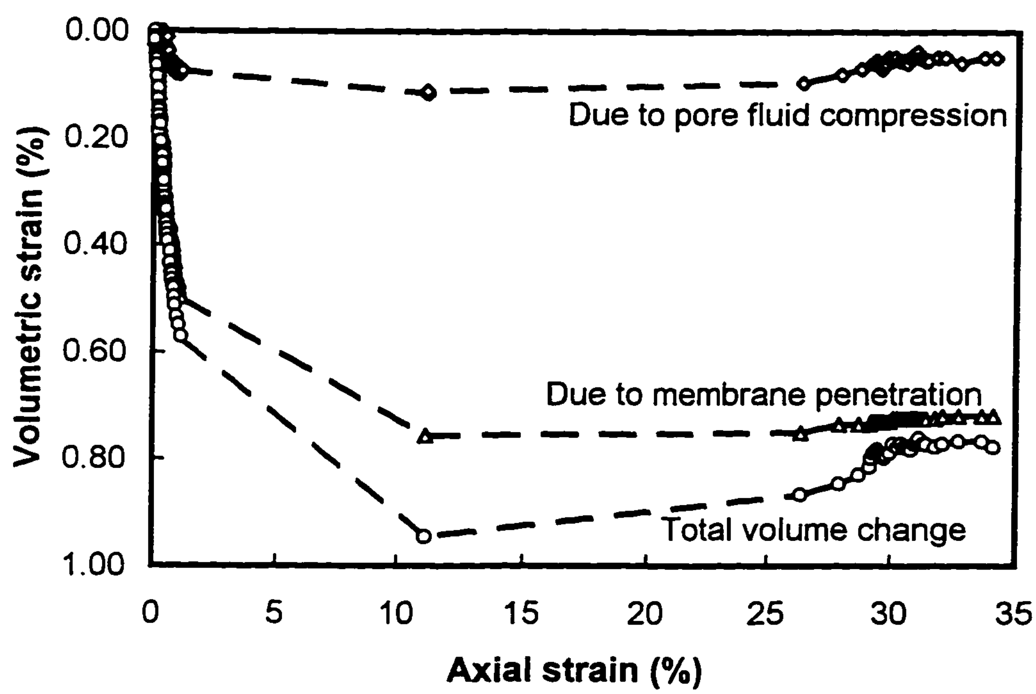

Fig. 7.3(d) Volume change during undrained loading

Fig. 7.3 Results of undrained triaxial tests (Dr = 25.2%)

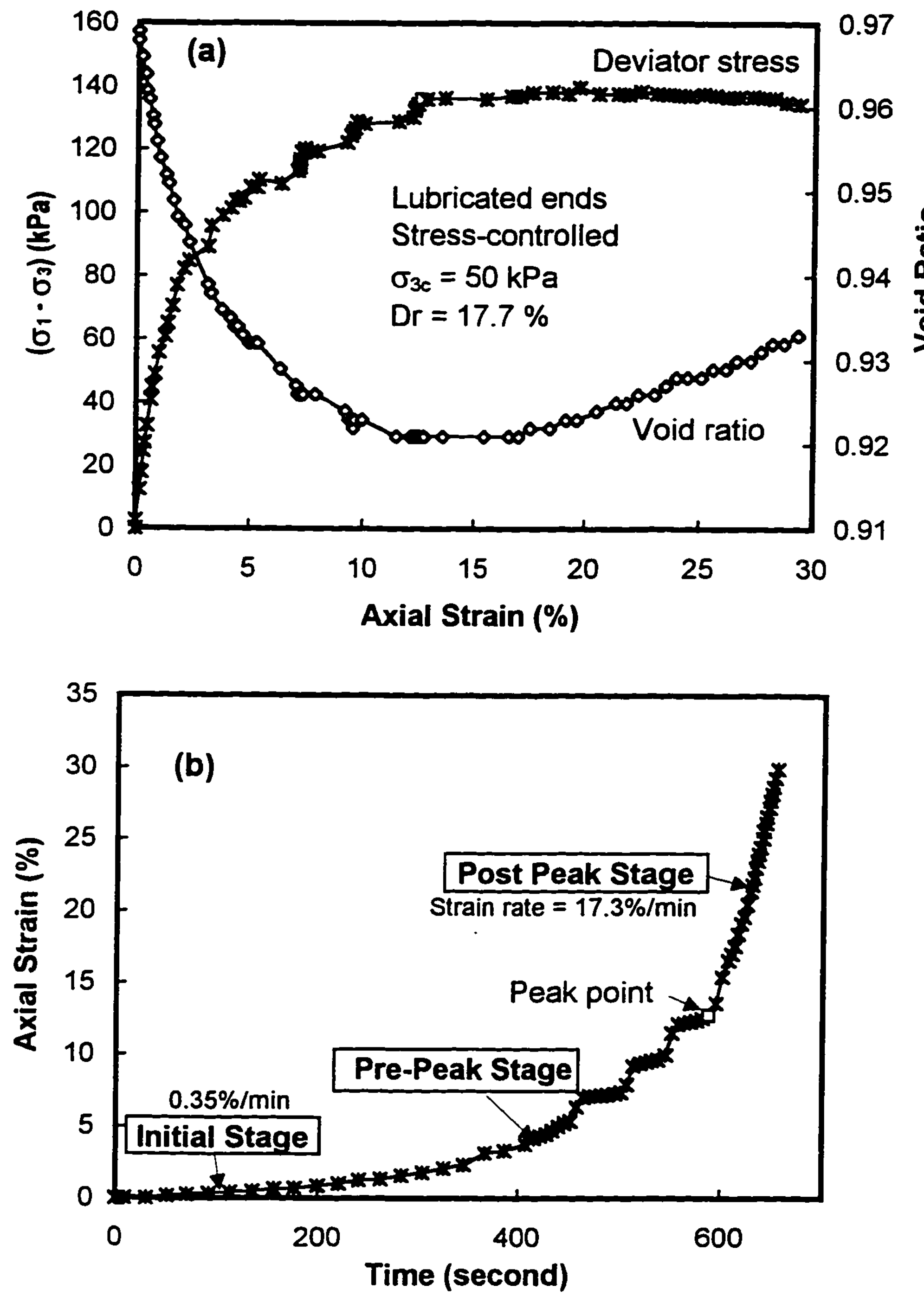

Fig. 7.4 Typical results of drained triaxial tests on loose sand

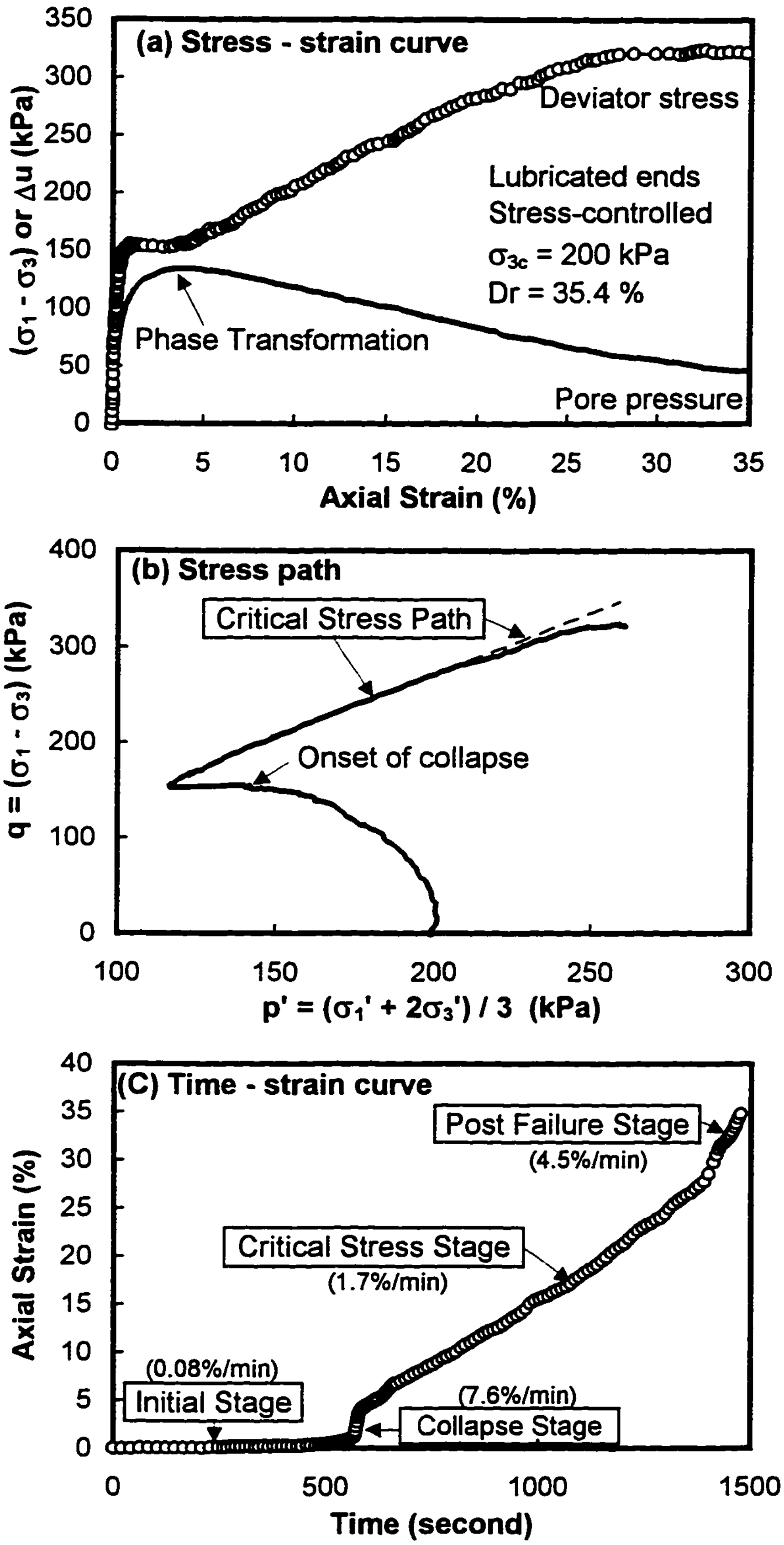

Fig. 7.5 Results of undrained triaxial test (Dr = 35.4%)

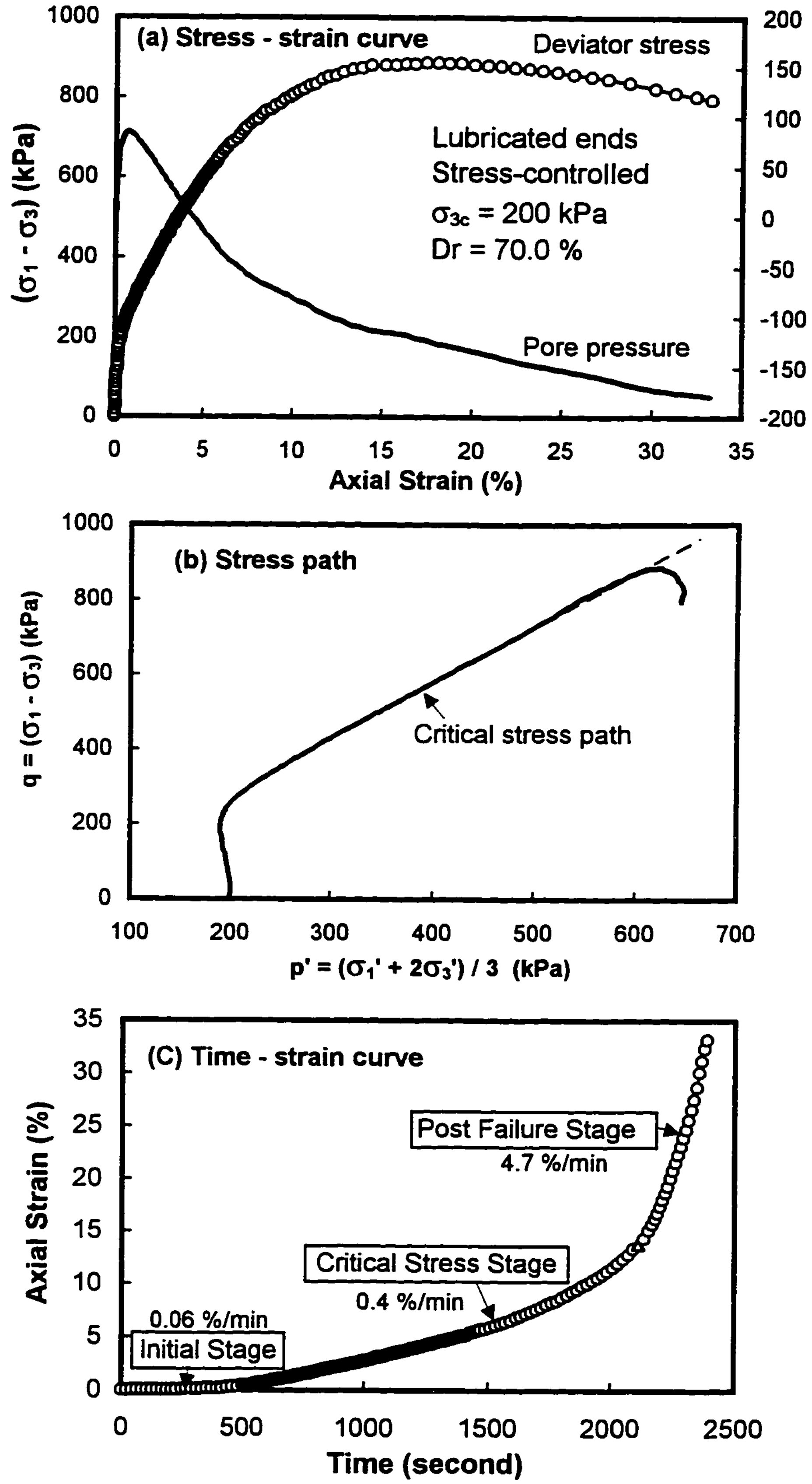

Fig. 7.6 Results of undrained triaxial test on dense Sample

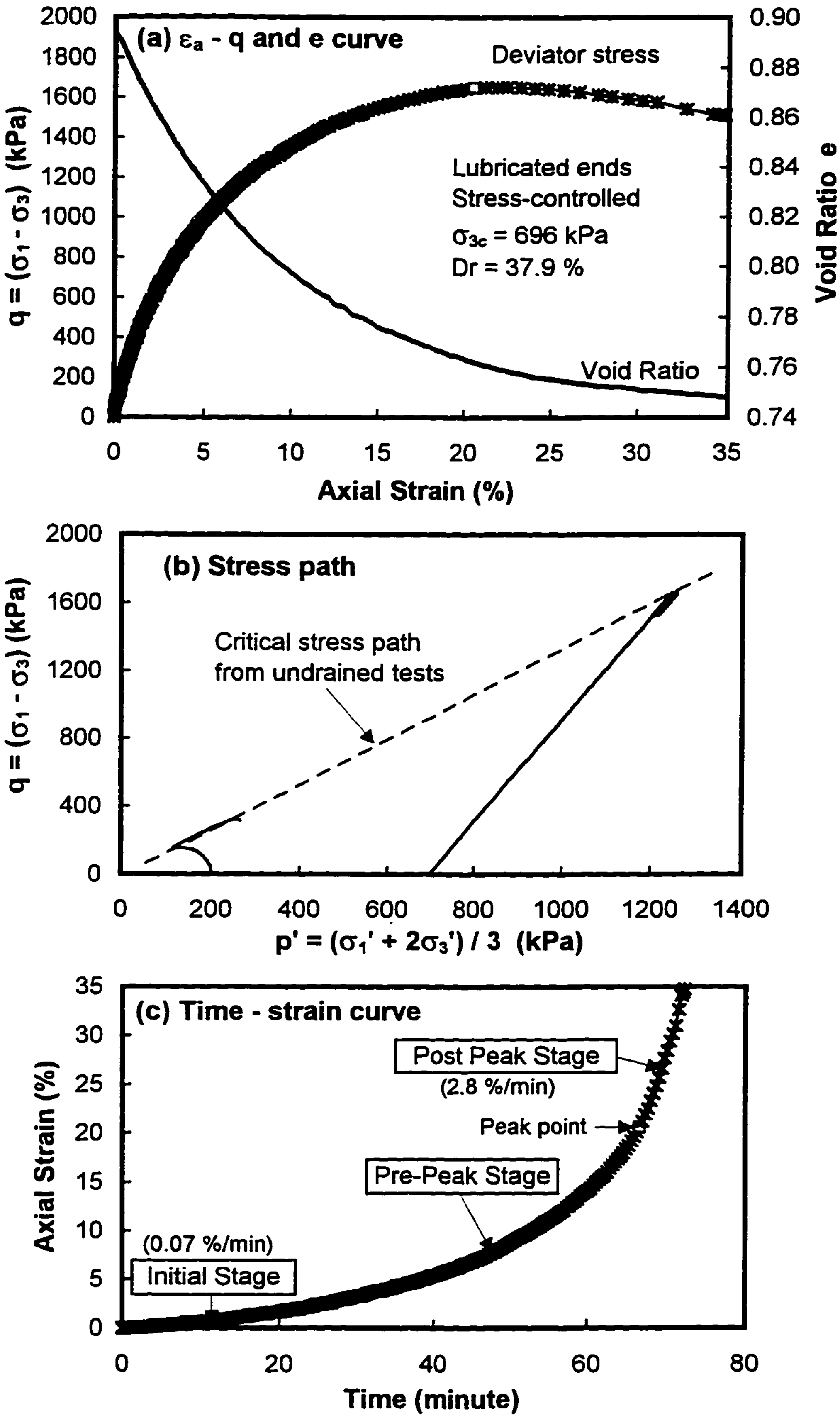

Fig. 7.7 Results of drained triaxial tests (Dr_c = 37.9%)

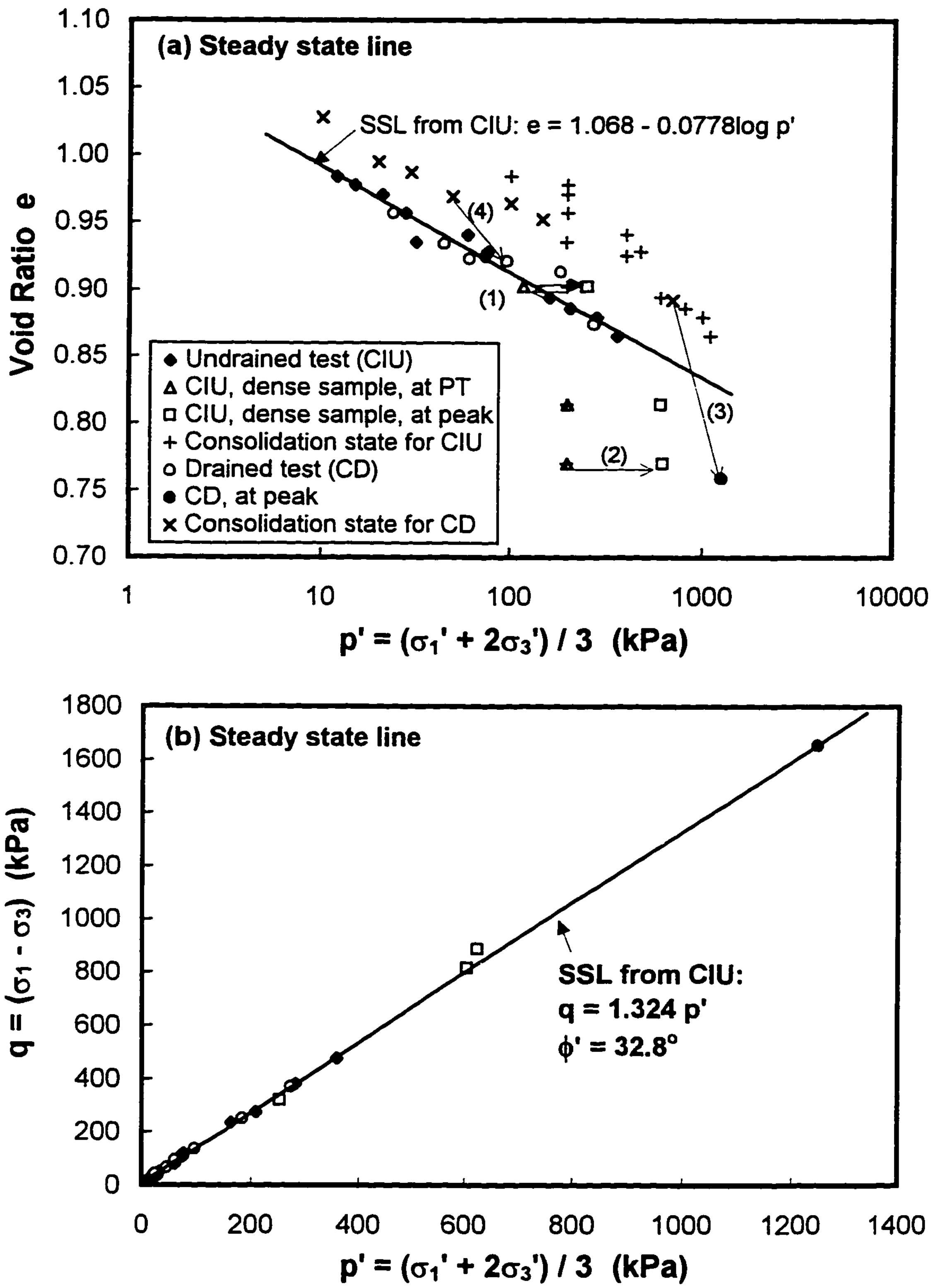

Fig. 7.8 Steady state line of Unimin sand

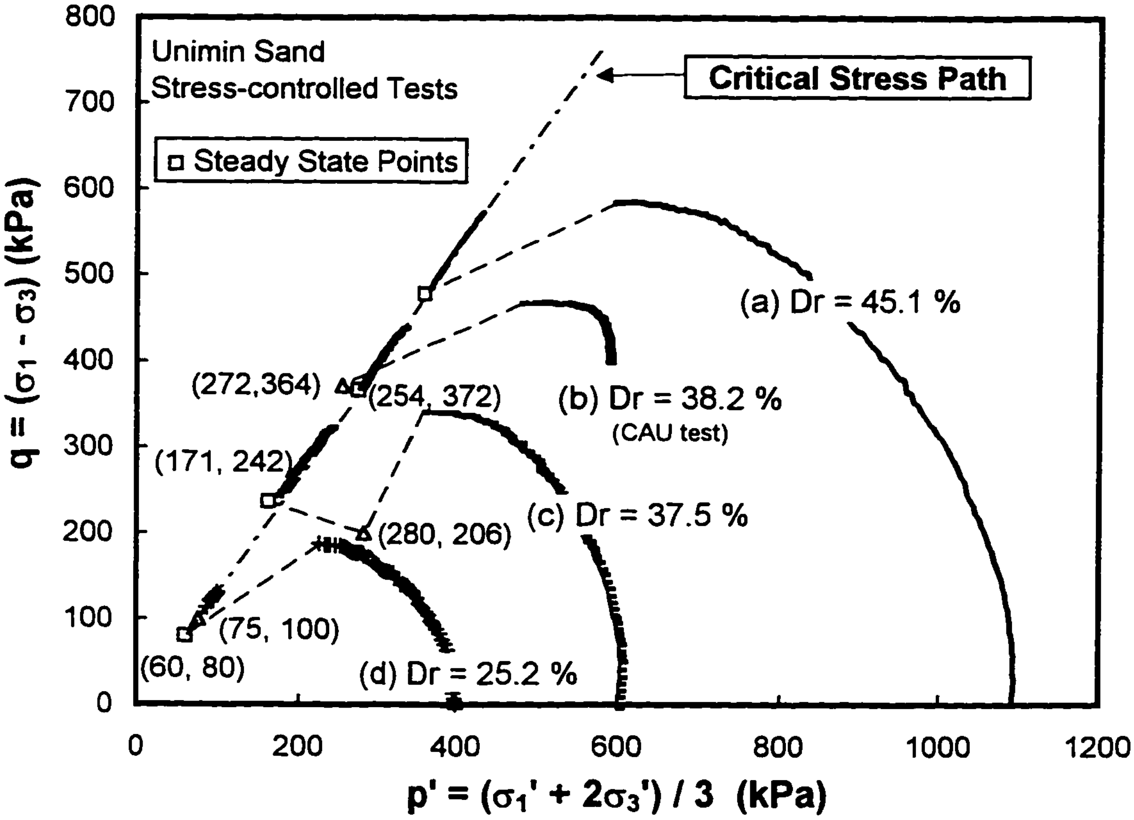

Fig. 7.9 Typical stress paths in undrained tests on loose sand

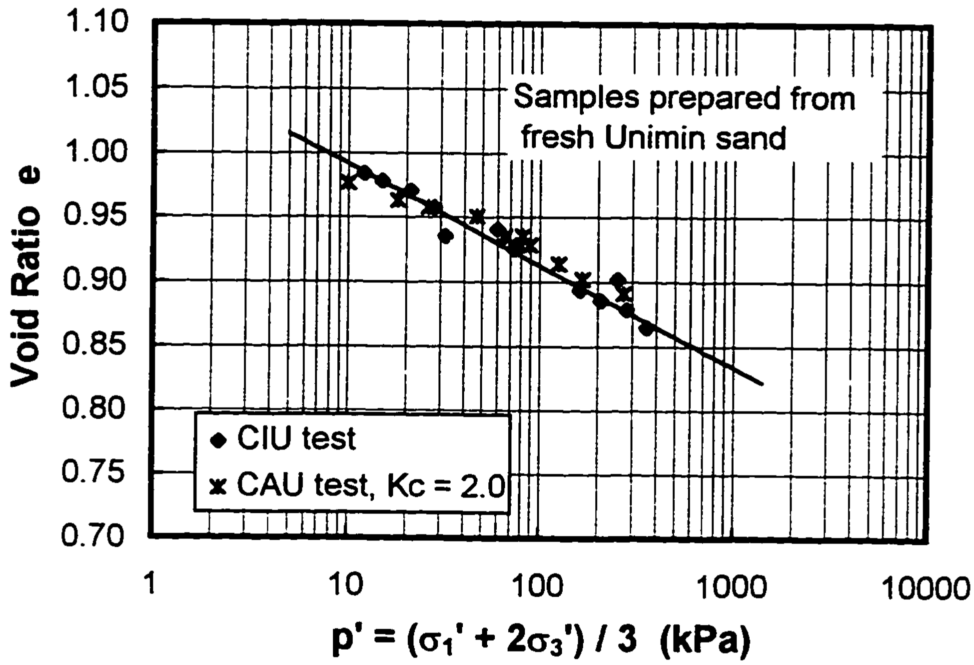

Fig. 7.10 Steady state from CIU and CAU tests

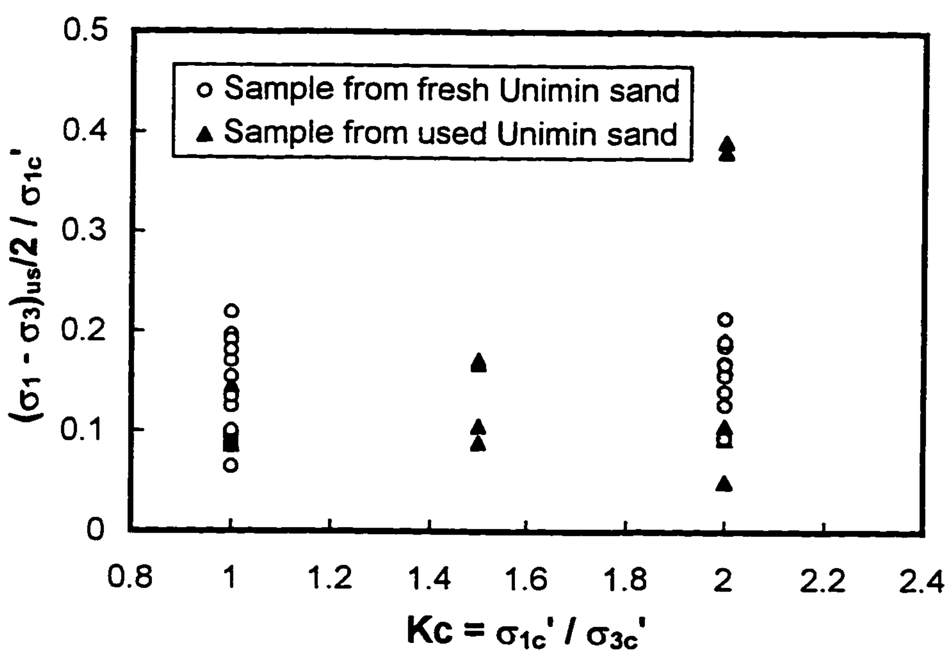

Fig. 7.11 Effect of consolidation stress ratio on steady state strength ratio

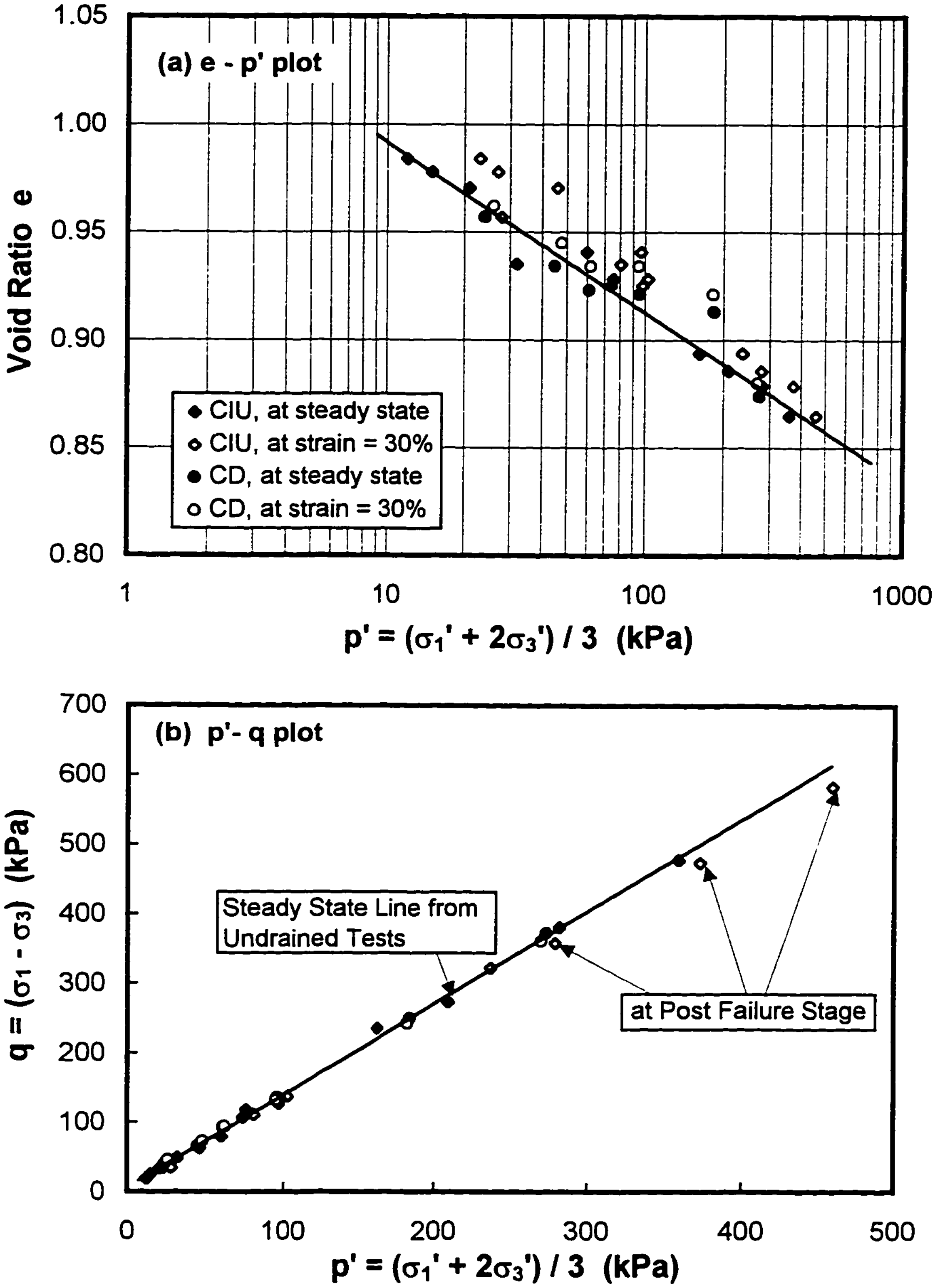

Fig. 7.12 Steady states and states at large strain

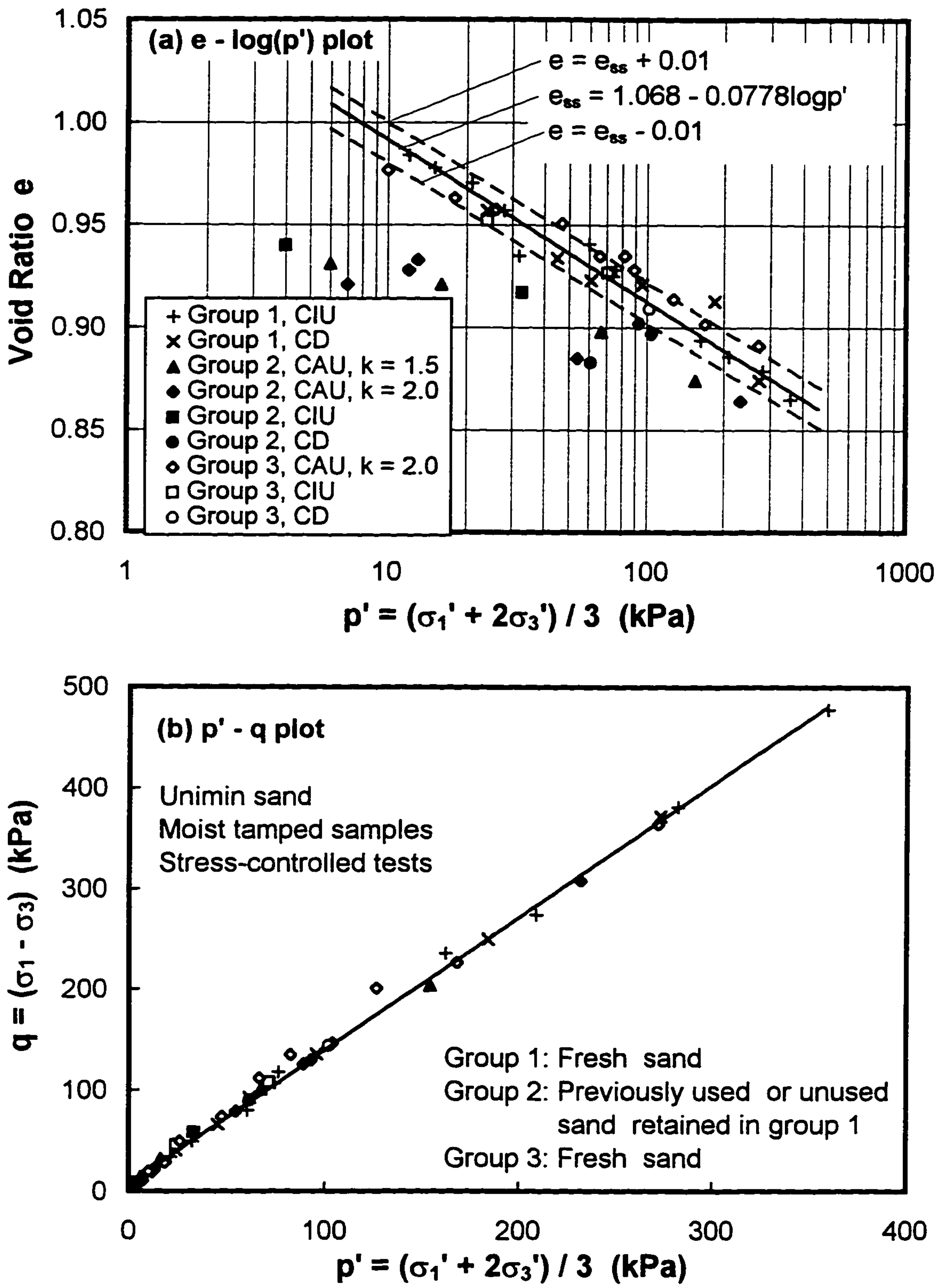

Fig. 7.13 Sensibility of steady state strength

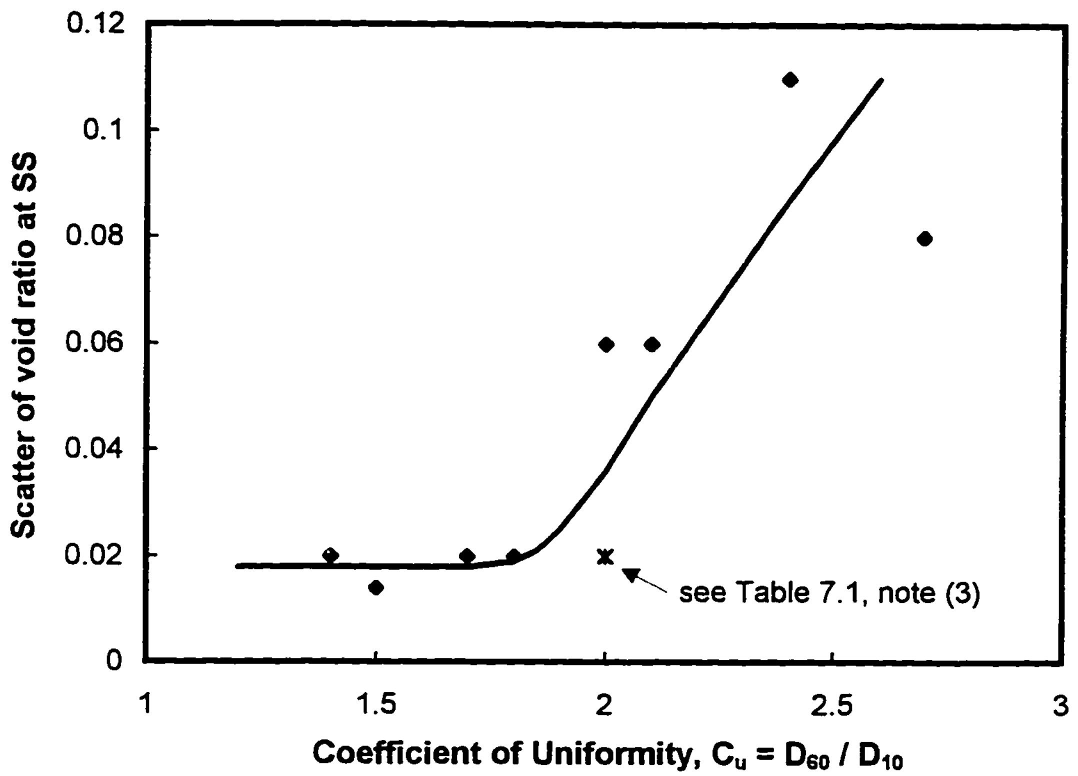

Fig. 7.14 Overall scatter of void ratio at steady state for different sands

CHAPTER 8

LIMITATIONS OF THE TRIAXIAL TESTS

8.1 Introduction

Triaxial tests have been greatly improved and are widely used to determine the strength characteristics of soils since the triaxial apparatus was developed by Casagrande in 1930s (as noted in Nagaraj, 1993). The basic principles and the limitations underlying the tests have been admirably described by Bishop and Henkel (1962), and reevaluated in several state-of-the-art papers (Baldi et al., 1988, Lacasse and Berre, 1988, Saada and Townsend,1981). The purpose of this chapter is to present some of the limitations of conventional triaxial tests in determining the steady state strength of sands.

The steady state strength of a sand is very sensitive to the density and the grain characteristics of the sand. It is often obtained at large axial strain in a triaxial test, while non-uniform deformation may become significant at large axial strain and then affect the behaviour of the sand. As a result, the steady state strength of a sand may be influenced by some factors including sample preparation, dimension measurement, volume change during undrained loading, test apparatus, loading modes, end restraint, and the correction of sample cross-sectional area. Therefore, the uncertainty of the steady state strength should be attended in determining the undrained residual strength of a sand.

8.2 Dimension measurement

The accuracy of void ratio prior to shear depends on dimension measurement, volume change during saturation, and membrane penetration during consolidation. The volume change during saturation and consolidation can be directly measured by using the LVDT and the HRDT.

Thus, the error in void ratio of a sand sample before shear may be caused mainly by the dimension measurement.

The void ratio error due to dimension measurement depends on the resolutions of measurement devices, the size of a sample, observer's skill, etc.. The resolutions of the height gauge and the caliper used in this study are 0.01 mm. So the maximum void ratio error due to the resolution is about 0.001 for a 50 × 100 mm sand sample (Table 8.1). The error in height in dimension measurements is within 0.03 mm by using the height gauge (Chapter 4). The height error may be also affected by installing triaxial cell cover. A comparison of the measured heights of a sand sample before the installation and after the removal of the triaxial cell cover indicates that the height of the sample did not change during the installation under a suction of 25 kPa. Thus, the height error of a triaxial sample by using the height gauge may be less than 0.04 mm, resulting in an error in void ratio less than 0.001. The diameter error in dimension measurement may be over 0.1 mm by using a caliper to directly measure the diameter. This error can result in an overall error in void ratio of 0.02 for a 50 × 100 mm sand sample, and then may cause a significant error in steady state strength. A main difficulty in diameter measurement by using a caliper is how to contact the caliper on the surface of a sample accurately. A small push of the caliper on a loose sand sample may produce a significant error in void ratio, and this error may be different for different observers.

8.3 Volume change during undrained loading

The membrane penetration of a triaxial granular sample depends on the effective confining stress (Newland and Allely, 1957), so the variation of pore pressure during undrained loading may change the membrane penetration and thus the volume of the sample as well (Newland and Allely, 1959). However, it is not clear how to determine the volume change during undrained loading and how the undrained volume change affects the undrained behaviour of sands.

Some questions on the determination of undrained volume change are: (1) besides the effective confining stress and the surface area, the bulging deformation which develops with axial strain may also affect the membrane penetration; (2) which volume change should be corrected in the determination of steady state line? The undrained volume changes of the Unimin sand samples in this study were 0.40 ~ 1.00 cm^3 (0.004 ~ 0.010 in void ratio) larger at phase transformation than at the onset of collapse (Table 4.5). Different volume corrections may result in significant change in the position of the steady state line (Fig. 4.14). It seems logical to correct the volume change at phase transformation, for the steady state of a loose sand sample often occurs close to the phase transformation. However, the in-situ undrained residual strength is usually determined from the "initial" in-situ void ratio before loading, rather than the void ratio at failure state (steady state). The void ratio at the onset of collapse may be closer to this "initial" void ratio than that at phase transformation.

The data directly relating undrained volume change to the steady state strength is limited. Seed et al. (1989) and Nicholson et al. (1993b) compared the results of conventional undrained triaxial tests, constant volume triaxial tests and large undrained triaxial tests on Monterey 16 sand. They found that for a given void ratio, the steady state strengths from the undrained triaxial tests on large samples and the constant volume triaxial tests were same, and smaller than those from the conventional undrained triaxial tests, if the initial states of the samples were above the steady state line. In the conventional undrained tests, the steady state points with the correction of membrane penetration volume change were also located on the steady state line determined from the constant volume tests and the undrained tests on large samples. Thus, it was concluded that the real steady state strength could be obtained from the constant volume tests or from the conventional undrained tests with the correction of membrane penetration volume change which occurs during undrained loading.

Seed et al. (1989) and Nicholson et al. (1993b) assumed that the effect of the membrane penetration volume change is negligible for large samples; the higher steady state strength exhibited in a small sample results from its lower void ratio due to membrane penetration, even though the initial void ratios of both the large and the small samples are the same. However, the steady state strength of a large sand sample seems not always smaller than that of a small sample. Castro et al. (1982) found that for Sand #19, the steady state line from large samples (73 × 107 mm) was much lower than that from small samples (36 × 53 mm); while for Banding

Sands #1 and #6, the steady state points from 71 mm diameter samples tended to plot on or above the steady state line determined from the comparable tests on 36 mm diameter samples. It is noted that both Banding Sand #1 and #6 have low coefficient of uniformity, equal to 1.53 and 1.70, respectively; while the coefficients of uniformity of Sand #19 and Monterey 16 sand are high, equal to 2.98 and about 2.2, respectively. Thus, it appears that the lower steady state strength in large sand samples may occur only in the sands which have high coefficients of uniformity. Also, the constant volume system used by Seed and coworkers may not be able to maintain the sample volume constant during rapid collapse (Chapter 4). Therefore, further evidence is necessary to verify the effect of undrained volume change on the steady state strength of sands.

8.4 Strain rate and axial loading system

Casagrande (1975) found that for a given void ratio, the steady state strength of a Banding sand sample was much higher under strain-controlled loading than under stress-controlled loading. He attributed this large difference in the steady state strength to the different strain rates under different loading modes (the strain rate in the stress-controlled tests during collapse was about 20000 times faster than that in the strain-controlled tests on the sand). He considered that the rapid collapse deformation in stress-controlled tests on loose sand samples develops a **flow structure**, in which the sample develops its minimum friction resistance; while the relatively slow strain rate in the strain-controlled tests causes locally groups of sand grains to lose temporarily their flow structure and so results in higher shear resistance. Dennis (1988) provided the same results for the Banding sand.

However, the same steady state lines from stress-controlled and strain-controlled tests were observed for Syncrude tailings (Poulos et al., 1988) and for Erksak 330/0.7 sand (Been et al., 1991). Poulos et al. (1988) considered that the effect of strain rate may be dependent on soil types. Nevertheless, this may not be the only reason why the results of stress-controlled and strain-controlled tests are so different for the Banding sand, but are the same for the Syncrude tailings and Erksak 330/0.7 sand. The results of the undrained strain-controlled triaxial tests on loose sand samples may be also affected by loading systems.

There are usually three types of axial loading systems in triaxial apparatus: motorized loading system, dead weight loading system, and servo (or pneumatic) loading system (Head, 1986). The motorized loading system is used to apply axial load to a sample in strain-controlled tests, in which the motor speed provides a predetermined constant strain rate and the resulting axial load is measured at selected intervals. The dead weight loading system is used to conduct stress-controlled tests. In this system, the axial stress is applied in increments by increasing small increments of dead load, and the deformation resulting from each increment is observed. In the servo loading system, an electric-pneumatic regulator, which is activated by feedback signals from a control computer, is used to control the axial stress. Strain-controlled tests or stress-controlled tests can be conducted by using a vertical displacement transducer or a load transducer as the feedback transducer, respectively.

In the motorized loading system, the motor controls the strain rate during shear and no collapse deformation can occur. In the dead weight loading system, the vertical deformation of a sample is unlimited and depends on the axial load and the characteristics of the sample; so a loose sand sample can develop a steady state of deformation when its stress state reaches collapse surface of the sand. Both stress-controlled and strain-controlled tests can be carried out using the servo loading system. However, once the collapse of a loose sand sample is initiated, the axial deformation is so fast that it cannot be prevented by a servo loading system even though the strain-controlled loading mode is setup. In other words, it is impossible in such a servo loading system to control the strain rate during collapse if the predetermined strain rate is less than the collapse strain rate. Therefore, the undrained triaxial tests on loose sand samples under servo loading condition will provide the same steady state strength for a given void ratio, regardless of the loading modes. No detailed information about the strain-controlled tests on the Syncrude tailings and Erksak 330/0.7 sand was provided. Hence it is not certain that the above discussion can be used to explain why the steady state lines from strain- and stress-controlled tests are the same for both of those materials.

Other investigations on the effect of strain rate on the undrained behaviour of sands have also provided some contradictory results. With the increase in strain rate, the undrained shear strength of a sand could increase (Lee et al. 1969, Yamamura et al., 1993), decrease (Nash et al, 1961), or did not change (Whitman et al., 1962). The effect of strain rate seems to depend on some factors including drainage conditions, density of a sample, confining pressure, etc.. Anyway, before further evidence confirms that the steady state strength from the strain- and stress-controlled triaxial tests are the same, undrained stress-controlled tests should be used in the determination of the steady state strength. The collapse behaviour of sands which can only occur in stress-controlled tests is close to flow liquefaction in nature (Casagrande, 1975), and the collapse failures are induced through stress-controlled loading over a much broader range in void ratios than through strain-controlled loading (Dennis, 1988).

A major disadvantage of the stress-controlled loading is how to record test information during rapid collapse. The strain rate during collapse in undrained stress-controlled triaxial tests on loose sand samples is usually very fast; it could be over 8000 %/min for Banding sand samples under dead weight loading (Castro, 1969), or 900 %/min for Unimin sand samples under servo loading (this study). It is necessary to use electronic instrumentation to acquire tested data during the rapid collapse deformation. There are usually two types of data acquisition systems: analogue system such as strip chart recorder, and digital system such as dynamic signal analyzer and computerized data-acquisition device. A strip chart recorder can record continuous changes in axial load, axial deformation, pore pressure and cell pressure, but processing the plotted results requires time and may introduce some error. Also, the writing pens in some strip chart recorders may not respond fast enough to record the real changes of the measured parameters during the rapid collapse deformation (for example, the strip chart recorder, Model Soltec 1243, failed to record the rapid collapse deformation and was replaced with a dynamic signal analyzer in this study). A computer in a triaxial test system is usually used to record and handle test data and to control test procedure. The maximum frequency of acquiring data in such a system may not be able to record enough data points during rapid collapse. For example, in the 486 4DX 100 computerized system used in this study, the minimum interval between two data acquisitions is about one second, while a collapse of a loose sample may occur within 2 seconds. In this case, an additional data acquisition system should be used.

Another disadvantage in stress-controlled loading may be the impact effect of rapid collapse on the measured load and pore pressure in a triaxial sample. At the onset of a collapse, the deformation of a sample varies suddenly from low strain rate to very high strain rate. This rapid variation in strain rate may cause the measured load to be lower than the real load in the sample (see, for example, Fig. 7.5, curve D), if the load transducer is installed above a sample as shown in Fig. 3.7. Also, it is well known that force F is equal to mass, m, times acceleration, a. The huge acceleration at the onset of collapse may produce an additional force on the pore pressure transducer in the test system at that time and then result in an overestimated pore pressure (Fig. 7.9, Curve b). The rapid invasion of the loading piston into the triaxial cell during collapse may temporally increase the cell pressure due to the relatively slow drainage of the cell water (Fig. 7.2 (a)). This increase in cell pressure does not affect the effective confining stress since the same increase in pore pressure also occurs (Fig. 7.2 (a)), but may cause significant change in the measured cell water volume change (Fig. 7.2(d)). Therefore, the rapid collapse in a loose sand sample may result in some measurement error in pore pressure and axial stress in some cases, particularly when the collapse strain rate is very hige, such as in the undrained tests on Banding sand conducted by Castro (Castro, 1969, strain rate over 8000 %/min).

8.5 Non-uniform deformation

The effect of non-uniform deformation on test results has been widely mentioned in literature. The non-uniform deformation can develop due to the formation of shear band (for example, Desrues et al., 1996 and Finno et al., 1996) or due to the effect of end restraint (for example, Rowe and Barden, 1964, Bishop and Green, 1965). The formation of shear band depends on sample density and test types. In triaxial tests, shear band usually occurs in a dense sample, and the global void ratio of the sample is smaller than the void ratio within the shear band (Desrues et al., 1996). For loose sand samples, no obvious shear band appears during drained and undrained shear (Desrues et al., 1996 and this study). So the effect of shear band may not be significant on the undrained behaviour of loose sands.

The effect of end restraint may be an important source of the error in the test results in triaxial tests on sands. Various methods have been tried in attempts to reduce the effects of end restraint, such as use of height : diameter ratio of 2 : 1 or higher (Taylor, 1941), segmented end platens (Tschebotarioff et al., 1956), segmented soil sample (Blight, 1965), shaped end platens (Larew, 1960), and lubricated end platens (Rowe, 1962). However, only the lubricated end platens have been proved to be effective and practical in reducing the friction between end platens and a sample, and are widely accepted in the triaxial tests to determine the steady state strength of sands. Nevertheless, the lubricated end platens are not a perfect technique to eliminate the end restraint. If the end platens are smeared with generous amount of high vacuum grease, much of the grease may be extruded and then cause significant error in calculated void ratios. This problem becomes particularly acute at high stresses (Castro et al., 1982). While a thin smear of high vacuum grease may not be enough to eliminate the effect of end restraint, and the central bulging of a triaxial sample with such lubricated end platens may still occur (Olson and Campbell, 1964, Casagrande and Poulos, 1964, Bishop and Green, 1965, and this study).

Dilation potential within the end zones of a sand sample may develop with axial strain due to end restraint, and then causes the increase in sample global volume under drained loading or causes the pore pressure of the sample to decrease under undrained loading (Chapter 5). Some factors, including the thicknesses of the rubber membrane and the vacuum grease on lubricated platens, the characteristics of the sample, axial strain and stress level, may affect the effect of dilation potential on the behaviour of the sample. For the loose Unimin sand samples with lubricated end platens in this study, the steady state of deformation could be reached and remained until an axial strain of about 15 %; then deviator stress or global volume increased with further strain under undrained loading condition or drained loading condition, respectively (Figs. 7.2 ~ 7.3). Similar results are also provided by Ishihara (1994). Therefore, it may be concluded that for most sand samples with lubricated end platens, the deviator stress may be overestimated after some threshold strain due to end restraint. The threshold strain is about 15 ~ 20 % for loose samples, and may be very small for dense samples.

8.6 Triaxial extension tests

It is usually considered that the steady state line is unique in undrained triaxial **compression** tests, regardless of consolidation stress, sample preparation method, and stress path. The unique steady state line of Toyoura sand from triaxial compression and **extension** tests was also observed by Been et al. (1991). However, Vaid et al. (1990) found that for Ottawa sand C-109, the steady state lines in extension always lie below that in compression, with amount of shift increasing with increase in initial void ratio, while the slopes of the steady state lines are the same for both compression and extension. Thus, it appears that triaxial extension tests may be affected by some other factors.

The results of conventional triaxial extension tests on sands have been questioned by some investigators (Roscoe et al., 1963, Proctor and Barden, 1969, Lade, 1982, Wu and Kolymbas, 1991 and Yamamuro and Lade, 1995). The effects of membrane strength, gravity and piston friction may have significant influence on the results of the extension tests on sands at low pressure (Wu and Kolymbas, 1991). The extension test results are subject to five times greater error from experimental measurement than for the corresponding compression test (Proctor and Barden, 1969).

The major problem in conventional extension tests may be that they have substantially more strain localization than triaxial compression tests (Roscoe et al., 1963b). The strain localization in an extension sample appears to begin very early during shear (Yamamuro and Lade, 1995). Once strain localization occurs, virtually all of the shearing occurs in the localization zone, which may be a very small part of the sample (Fig. 8.1). This strain localization makes the volumetric strain in the localization zone substantially different from the global volumetric strain of the sample (Roscoe et al., 1963, Lade, 1982). Thus, a lower shear strength in extension than in compression may result from the void ratio change within the strain localization zone (shear zone).

Based on the test results shown in Fig. 8.1, a model is developed to conceptually explain why for a given void ratio, the extension strength of a sand is lower than the compression strength

(Fig. 8.2). It is assumed that the sample deforms uniformly until strain localization appears, then all axial and radial strains occur evenly within the shear zone (b). If there is no movement of soil grains from the end zones (a and c) to the shear zone (b), the solid volume of the shear zone will remain same before and after strain localization. That is

$$A_i \lambda \frac{1}{1+e_i} = A(\lambda + \Delta)\frac{1}{1+e} \tag{8.1}$$

where, A_i, e_i and λ are the cross-sectional area and the void ratio of the sample, and the length of zone (b) before locally straining, respectively;

A, e and Δ are the cross-sectional area and void ratio of the shear zone, and the vertical deformation of the sample after locally straining, respectively.

Thus, the difference between the void ratios in the shear zone (b) before and after strain localization is as follows:

$$e - e_i = (1+e_i)\left(\frac{A}{A_i}\frac{\lambda+\Delta}{\lambda} - 1\right) \tag{8.2}$$

If no pore water migrates into or out of the shear zone, the total volume of zone (b) remains constant during strain localizing:

$$A(\lambda + \Delta) = A_i H_i - A_i(H_i - \lambda) \tag{8.3}$$

where, H_i is the height of the sample before strain localization.

i.e.
$$A = \frac{\lambda}{\lambda + \Delta} A_i \tag{8.4}$$

Substituting Eq (8.4) into Eq (8.2) can obtain that $e - e_i = 0$. This indicates that without water migration between the shear zone (b) and zones (a) and (c), the void ratio of the shear zone in the sample would not vary during undrained triaxial extension loading. However, since most axial strain and radial strain occur within the shear zone (b), the necking deformation of the sample may be accompanied by the migration of water into the shear zone. The water migration may cause the cross-sectional area of the shear zone larger than the value calculated from Eq (8.4): $A > \frac{\lambda}{\lambda + \Delta} A_t$, and thus increase the void ratio of the shear zone (Eq (8.2)). In other words, the void ratio in the shear zone is larger than the global void ratio of the sample. This may be one of the reasons why the undrained extension strength is less than the undrained compression strength. Another reason for the lower extension strength may be that the average area used in calculation of deviator stress in a triaxial extension test is greater than the average area in shear zone, and thus results in an underestimation of shear strength.

It is also noted in Eq (8.2) that the void ratio increase in the shear zone of an undrained triaxial extension sample is affected by the void ratio before strain localization or the initial void ratio of the sample. The higher the initial void ratio, the larger the void ratio change becomes. This may explain why the steady state lines in extension always lie below that in compression, with amount of shift increasing with increase in initial void ratio.

Table 8.1 Void ratio change due to dimension changes

ΔD (mm) / ΔH (mm)	0	0.01	0.05	0.1	0.15	0.2
0	0	0.001	0.004	0.008	0.012	0.015
0.01	0.000	0.001	0.004	0.008	0.012	0.016
0.05	0.001	0.002	0.005	0.009	0.013	0.016
0.1	0.002	0.003	0.006	0.010	0.013	0.017
Note: 50 mm × 100 mm Unimin sand sample, Dr = 30 %.						

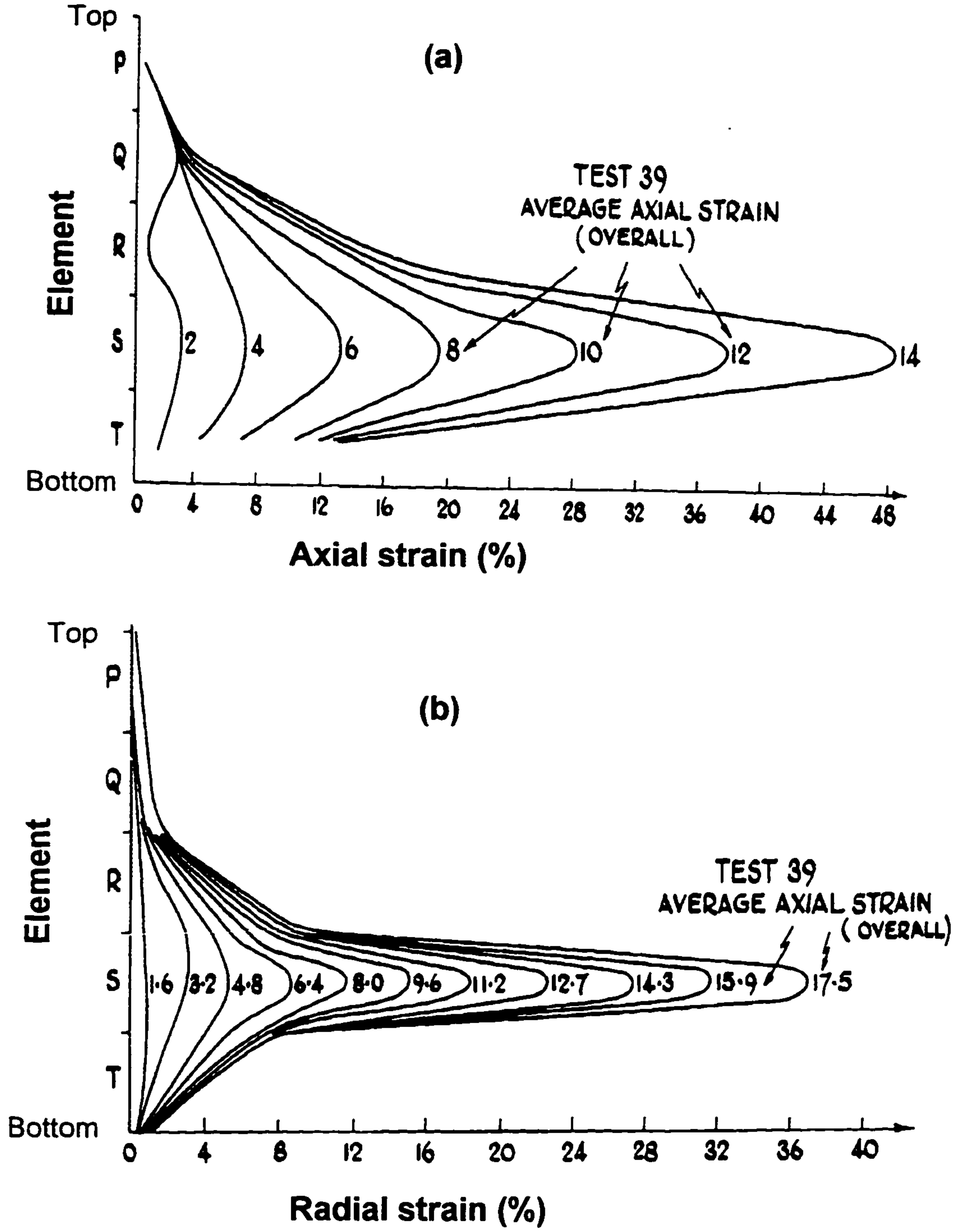

Fig. 8.1 Non-uniform deformation in triaxial extension test on sand (after Roscoe et al., 1963)

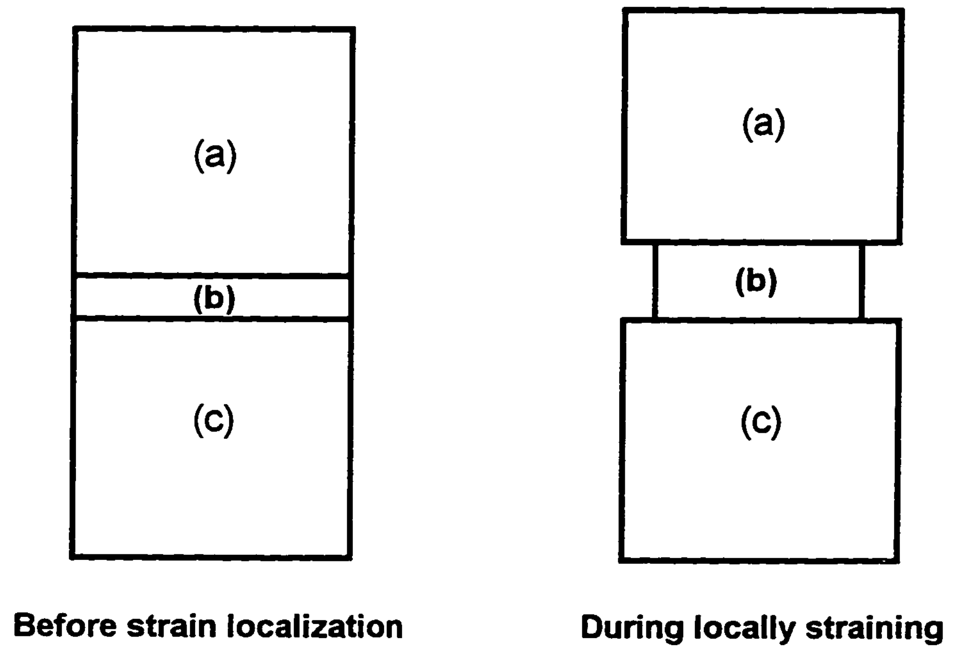

Fig. 8.2 Schematic diagram of strain localization in extension tests

CHAPTER 9

CONCLUSIONS AND RECOMMENDATIONS

9.1 Summary: determination of SS strength

The main objective of this study was to develop an approach to determine the steady state strength of sands with "quasi-steady state behaviour" in triaxial tests.

There is no distinct difference between steady state behaviour and "quasi-steady state behaviour". An important response in the so called "quasi-steady state behaviour" is the post-PT increase in shear resistance under triaxial undrained loading condition. However, this post-PT increase in shear stress is not an inherent behaviour of sands, but is caused mainly by end restraint. Most loose sands exhibit such a behaviour in conventional undrained triaxial tests.

Experimental evidence from literature and from this study shows that the steady state line of a sand is independent of the methods of sample preparation, drainage conditions, consolidation stress ratio. Some investigations showed that different effective consolidation stresses or different stress paths can provide different steady state strengths for a given void ratio. However, it should be noted that different shear conditions may result in different effects of end restraint and non-uniform deformation, which can also affect steady state strength. It is suggested that there are four deformation stages in an undrained triaxial test on loose sand: initial state, collapse stage, critical stress stage and post failure stage. The strain rate in the test remains constant in a deformation stage, but is different in various deformation stages. Sand samples with different densities may exhibit different strain rates in their collapse stages. This may explain why strain rate can affect the steady state strength in some cases, but not in other cases. If the constant strain rate in a strain-controlled test is close to the collapse strain rate in a stress-controlled test, both the strain- and stress-controlled tests will provide similar steady state strength. If the collapse strain rate is much larger than the constant strain rate, the steady state strength from the strain-controlled test may be larger than that from the stress-controlled test.

Another important steady state behaviour is that a steady state strength is significantly affected by the local void ratio and is sensitive to the local grain characteristics in a shear zone. Small changes in density or grain distribution, which may occur due to sample preparation, saturation, consolidation, loading conditions and some other factors, can cause large changes in steady state strength.

The main limitation of triaxial tests on sands is the non-uniform deformation due to end restraint, the formation of shear band, and necking. Necking deformation often occurs in a triaxial extension tests. The extension strength of a sand sample depends on the shear resistance of its narrow necking zone. Extension steady state strength is often determined at low axial strain before large necking deformation develops. However, the void ratio in the necking zone may have changed before visible necking deformation develops, and thus an underestimated steady state strength is provided for the global void ratio of the sample. Furthermore, the necking failure mode in the extension tests may not be similar to the field extension failure mode. Therefore, the steady state strength from triaxial extension tests is not reliable.

Shear band often occurs in triaxial compression test on a dense sand sample, and its shear strength depends mainly on the local void ratio in the shear band. Once the shear band develops, its local void ratio may become larger than the global void ratio and thus result in an underestimated strength for the sample. The effect of shear band is insignificant in undrained triaxial tests on loose sands. However, under drained loading condition, a loose sample may become dense during loading and a shear band may develop at large strain.

End restraint or friction between sample and end platens plays an important role in the "quasi-steady state" behaviour. Some effects of end restraint are the dilation potential in end zones and bulging deformation. The end zone dilation potential can result in the decrease in pore pressure under undrained loading condition or expansion volume change under drained loading condition. The bulging deformation can result in an overestimated deviator stress due to the conventional area correction. The effects of end restraint are mainly affected by the density of a sample, the characteristics of end platens, axial effective stress and axial strain. The use of loose samples and lubricated end platens can reduce the end restraint effects.

Based on the above discussion on steady state behaviour and the limitations of triaxial tests, care should be taken on the following test details in order to obtain more reliable steady state strength from triaxial tests:

Sample preparation: Sand samples should be prepared at loose state to reduce the effects of end restraint and shear band on steady state strength. It is difficult to prepare a loose and uniform sand sample. Moist tamping method is usually used to prepare a loose sand sample; but such a sample may not be uniform, since the compaction of each succeeding layer can further densify the material in the layer below it, and the upper portion of a layer may be denser that its lower portion. An **undercompaction** tamping method (Ladd, 1978) is usually employed to correct the over-densification of the lower layers, while a sample prepared by such a method may not be very uniform. A "zero drop tamping method" was used to reduce the over-densification in this study. The variation in density in a layer can be reduced by decreasing the thickness of each layer (Riemer, 1992).

End platen: Lubricated end platens, consisting of a **thin** smear of grease and a latex membrane, should be used to reduce the effect of end restraint. The use of **generous** amount of grease in the lubricated end platens can cause significant error in estimation of void ratio due to the extrusion of the grease under pressure. The deformation of the latex membranes in the lubricated end platens should be deducted from the total vertical deformation when evaluating void ratios.

Void ratio evaluation The error in the void ratio of a sand sample may result from dimension measurements, the volume changes during saturation, consolidation and loading. The height of a sample can be measured accurately by using the height gauge developed in this study. Until a better measuring device is developed, the conventional caliper, rather than a perimeter tape, should be used to carefully measure the diameter of a sample. The axial and radial deformations during saturation and consolidation should be directly measured by using a LVDT and a HRDT. The volume change during undrained loading results mainly from the variation of membrane penetration, but its effect on undrained steady state strength is not clear. The undrained volume change due to the build up of pore pressure should decrease the volume of sand sample; and the smaller the sample, the larger the change of its void ratio. This implies that the steady state line from large samples should be lower than that from small samples. However, it was observed that the steady state line from large samples could be located on or above that from small samples (Castro et al., 1982). Thus, the undrained volume correction on the steady state line appears not to be necessary unless further evidence can prove the effect of the undrained volume change to be significant.

Calculation of deviator stress: A steady state strength often occurs at large axial strain, accompanied by bulging deformation. This bulging deformation results in the entire average area of a sample being smaller than the average area in its shear zone. Thus, the steady state strength is overestimated. An appropriate area correction method, such as developed in this study, should be used in the calculation of deviator stress.

Loading mode and data acquisition: It is unknown how strain rate affects the steady state strength. Thus, stress-controlled loading should be used in the triaxial tests to determine the steady state strength. In order to record enough data points during rapid collapse, a fast data acquisition system such as a dynamic signal analyzer should be used.

Selection of steady state point: The steady state point of a loose sand sample should be determined, based on the modified definition of the steady state of deformation, from the test data including stress-strain curve, effective stress path, strain rate, and induced pore pressure under undrained loading or volume change under drained loading.

9.2 Conclusions

1. The volume changes of a moist, tamped, loose sand sample (nominally 50 mm in diameter and 100 mm in height) during saturation due to flushing water and due to applying back pressure can reach 1.78 and 0.92 cm^3, respectively; and the total volume change during the entire saturation procedure can be 2.79 cm^3 for the Unimin sand.

2. Volume change of a moist tamped sand sample during saturation and membrane penetration during consolidation can be easily determined by directly measuring axial and radial dimensional changes of a sample.

3. Air can dissolve in deaired water rapidly. The compressibility of pore water in a saturated sand sample is much larger than that of pure water. For water pluviated sand samples, the average compressibility of pore water was about 20×10^{-6} (1 / kPa) in the pressures range of 0 to 500 kPa. The compressibility of the pore water in moist tamped samples varied from 3 ~ 14 $\times 10^{-6}$ (1/kPa) during undrained loading.

4. The volume change of a sand sample during undrained loading consists of two components: the compression of pore fluid and penetration volume change. The pore fluid volume change varied from 0.08 to 0.39 cm^3 at the phase transformation, mainly depending on pore pressure and the densities of samples. The penetration volume change varied from 0.30 to 1.73 cm^3 at the onset of collapse and from 0.77 to 2.20 cm^3 at the phase transformation, depending on the induced pore pressure.

5. Different steady state lines were obtained from volume corrections applied at the onset of collapse and at phase transformation. The difference between the uncorrected and "corrected" steady state lines becomes important as the mean effective stress increases.

6. A new method of area correction in triaxial tests was developed. The average diameter in the middle portion of a sample is dependent on axial strain, volumetric strain, end radial strain, and the length of the middle portion. A middle third average diameter is suggested to be used

in the calculation of deviator stress in triaxial tests. This middle third average diameter of a triaxial sample with lubricated end platens can be closely approximated by the middle half average diameter with $\varepsilon_e = 0$.

7. The error in deviator stress due to using the conventional sample area correction can be over 10 % at large axial strain under fixed end condition ($\varepsilon_e = 0$). This error can be reduced by lubricated end platens.

8. The quasi-steady state behaviour is not an inherent one, but a test induced behaviour of loose sands, which mainly occurs in triaxial tests. The post-PT increase in deviator stress in the quasi-steady state behaviour is caused mainly by the decrease in pore pressure due to end restraint. The deviator stress in the strain-hardening behaviour may be also significantly affected by the end restraint.

9. In drained tests on a loose sand sample, the post-peak patterns of deviator stress and volumetric strain are different. Available data suggests that they reflect the responses within different zones of the sample at large strain.

10. Compared with regular end platens, the lubricated end platens can lessen the post-PT decrease in the pore pressure of a sand sample and thus result in lower deviator stress at large axial strain. For very loose sand samples, there is no significant difference between the results of the triaxial tests with the lubricated end platens or with the regular end platens.

11. Four deformation stages may occur in undrained triaxial tests on a sand: initial stage, collapse stage, critical stress stage and post failure stage. Within each stage, the strain rate is essentially constant. The undrained steady state usually exists in the collapse stage. Three deformation stages may occur in drained triaxial tests on sand: initial stage, pre-peak stage and post-peak stage. The drained steady state may exist in post-peak stage.

12. A steady state in quasi-steady state behaviour can occur prior to phase transformation. In some cases, a state at large strain also satisfies the requirements stipulated in the definition of

the steady state of deformation. In order to avoid this confusion, a modified definition of the steady state is suggested as follows:

> The steady state of deformation for any mass of particles is that state in which the mass is continuously deforming at constant volume, constant normal effective stress, constant shear stress, and constant velocity. **The constant shear stress is the minimum strength of the mass, which is dependent on the local void ratio within shear zone.**

13. The steady state strength should be determined by considering all test information including shear stress, pore pressure, strain rate, and effective stress path under undrained loading condition or volume change under drained loading condition.

14. The steady state strength is very sensitive to small change in grain size distribution of a sand with high coefficient of uniformity.

15. The steady state strength is independent of the consolidation stress ratio, $Kc = \sigma_{1c}' / \sigma_{3c}'$.

9.3 Recommendations for further research

Further research on the following related to undrained residual strength of sands is suggested:

1. The development of a diameter measurement device, which could be easily placed at the surface of a loose sand sample.

2. The effect of undrained volume change in undrained triaxial tests on the behaviour of sands.

3. The determination of the undrained residual strength of the sands which have high coefficient of uniformity.

4. The accuracy of constant volume shear tests on sands. Constant volume simple shear tests and constant volume triaxial tests have be developed to determine the steady state strength

of sand. Probably, the volume of a sand sample may not remain constant during shear in such a constant volume test due to the accuracy of a volume control system, and may result in large error in steady state strength.

5. Quantify the effect of end restraint on the undrained behaviour of sand samples with lubricated end platens. The use of lubricated end platens can significantly reduce the effect of end restraint. However, end restraint may exist even under lubricated end condition and result in an overestimation of steady state strength.

6. The development of field tests to directly determine the undrained residual strength of sands. The difficulties and cost in determining the in-situ void ratio of sands have limited the application of the steady state approach based on laboratory tests in liquefaction evaluation. Field vane tests may be a possible approach for this purpose, since the steady state strength from drained and undrained tests are the same for a given void ratio. The key question in the field vane tests should be the changes in void ratios, which may occur during the installation the vane to a desired depth and during shear.

REFERENCES

1. Alarcon-Guzman, A. and Leonards, G. A. (1988), Discussion of " Liquefaction evaluation procedure," by S.J. Poulos, G. Castro and J.W. France. J. Geotechnical Engineering, ASCE, **114**(2): 232-236.

2. Alarcon-Guzman, A., Leonards, G. A. and Chameau, J. L. (1988), Undrained Monotonic and cyclic strength of sand. J. Geotechnical Engineering, ASCE, **114**(10): 1089-1109.

3. Andrus, R. D. and Youd, T. L. (1987), Subsurface investigation of a liquefaction induced lateral spread Thousands Springs Valley, Idaho. Miscellaneous Paper GL-87-8, US Army Engineer Waterways Experiments Station.

4. Ansal, A. M and Erken, A. (1996), Posttesting correction procedure for membrane compliance effects on pore pressure. J. Geotechnical Engineering, ASCE, **122**(1): 27-38.

5. Arthur, J. R. F. and Phillips, A. B. (1975), Homogeneous and layered sand in triaxial compression. Geotechnique, **25**(4): 799-815.

6. ASTM (1993a), D 4253-93, Standard test method for maximum index density and unit weight of soils using a vibratory table. ASTM Standards, Vol. 04.08, Soil and rock; dimension stone; geosynthetics, pp: 661-673.

7. ASTM (1993b), D 4254-91, Standard test method for minimum index density and unit weight of soils calculation of relative density. ASTM Standards, Vol. 04.08, Soil and rock; dimension stone; geosynthetics, pp: 674-681.

8. ASTM (1993c), D 4767-88, Standard test method for consolidated-undrained triaxial compression test on cohesive soils. ASTM Standards, Vol. 04.08, Soil and rock; dimension stone; geosynthetics, 1071 - 1080.

9. Baldi, G. and Nova, R. (1984), Membrane penetration effects in triaxial testing. J. Geotechnical Engineering, ASCE, **110**(3): 403-419.

10. Baldi, G., Hight, D. W. and Thomas, G. E. (1988), A reevaluation of conventional triaxial test methods. Advanced Triaxial Testing of Soil and Rock, ASTM STP 977, pp. 219 - 263.

11. Barden, L. and McDermott, J. W. (1965), The use of free ends in triaxial testing of clays. J. Soil Mechanics and Foundations Division, ASCE, **91**(6): 1-24.

12. Barden, L. and Proctor, D. C. (1971), The drained strength of granular material. Canadian Geotechnical J., **8**(8): 372-383.

13. Baziar, M. H., Dobry, R. and Elgamal, A. W. (1992), Engineering evaluation of permanent ground deformations due to seismically-induced liquefaction. Technical Report NCEER-92-0007, National Center for Earthquake Engineering Research, SUNY-Buffalo, Buffalo, NY, 1992.

14. Baziar, M. H. and Dobry, R. (1995), Residual strength and large deformation potential of loose silty sands. J. Geotechnical Engineering, ASCE, **121**(12): 896-906.

15. Been, K. and Jefferies, M. G. (1985), A state parameter for sands. Geotechnique, **35**(2): 99-112.

16. Been, K., Jefferies, M. G. and Hachey, J. (1991), The critical state of sands. Geotechnique, **41**(3): 365-381.

17. Begemann, H. K. S., Koning, H. L. and Lindenberg, J. (1977), Critical density of sand. Proc. 9th ICSMFE, Tokyo, Vol. 1: 43-46.

18. Bezuijen, A. (1989), Liquefaction of a sand body constructed by means of hydraulic fill. Proc. 12th ICSMFE, Vol. 2: 891-894, Rio De Janeiro, August 13-18, 1989.

19. Bishop, A. W. and Eldin, A. K. G.(1950), Undrained triaxial tests on saturated sands and their significance in the general theory of shear strength. Geotechnique, **2**: 13-32.

20. Bishop, A. W. and Eldin, A. K. G. (1953), The effect of stress history on the relation between and porosity of sand, Proc. 3rd ICSMFE, Vol. 1: 100-105, Zurich, Switzerland.

21. Bishop, A. W. and Green, E. G. (1965), The influence of end restraint on the compression strength of a cohesionless soil. Geotechnique, **15**(3): 243-266.

22. Bishop, A. W., Webb, D. and Skinner, A. E. (1965), Triaxial tests on soils at elevated cell pressure. Proc. 6th ICSMFE, Vol. 1: 170-174, Montreal.

23. Bishop, A. W. (1966), The strength of soils as engineering materials. Geotechnique, **16**(2).

24. Bishop, A. W. (1967), Progressive failure -- with special reference to mechanism causing it. Proc. The Geotechnical Conference, Oslo, Norway, Vol. 2: 142-150.

25. Bishop, A. W. and Henkel, D. F. (1969), The measurement of soil properties in the triaxial test. Edward Arnold (Publishers) Ltd, London, England.

26. Bishop, A. W. (1971), Shear strength parameters for undisturbed and remolded soil specimens. Stress-strain Behaviour of Soils, Roscoe Memorial Symposium, Cambridge University, 3-58.

27. Bjerrum, L., Kringstad, S. and Kummeneje, O. (1961), The shear strength of a fine sand. Proc. 5th ICSMFE, Vol. 1: 29-37.

28. Blight, G. E. (1965), Shear stress and pore pressures in triaxial testing. J. Soil Mechanics and Foundations Division, ASCE, **91**(6): 25-39.

29. Blight, G. E. (1967), Observations on the shear testing of indurated fissured clays. Proc. Geotech. Conf., Oslo, Vol. 1, pp 97-102.

30. Bolton, J. M., Durnford, D. S. and Charlie, W. A. (1994), One-dimensional shock and quasi-static liquefaction of silt and sand. J. Geotechnical Engineering, ASCE, **120**(10): 1874-1889.

31. Bolton, M.D. (1986). The strength and dilatancy of sands. Geotechnique **36**(1): 65-78.

32. Casagrande, A. 1936. Characteristics of cohesionless soils affecting the stability of earth fills. Contributions to Soil Mechanics, 1925 - 1940. pp 257-276, Boston Society of Civil Engineers, 1940 (originally published in the Journal of Boston Society of Civil Engineers, 1936).

33. Casagrande, A. (1938), The shearing resistance of soils and its relation to the stability of the earth dams. Proc. Soils and Foundation Conference of the U.S. Engineer Department.

34. Casagrande, A. (1975), Liquefaction and cyclic deformation of sands: a critical review. Harvard Soil Mechanics Series No. 88, Harvard University, Cambridge, Mass., 1976 (originally presented at Fifth Pan-American Conference on Soil Mechanics and Foundation Engineering, 1975, Buenos Aires, Argentina)..

35. Casagrande, A. (1975), Liquefaction and cyclic deformation of sands: a critical review. Presented at Fifth Pan-American Conference on Soil Mechanics and Foundation Engineering, November 1975, Buenos Aires, Argentina.

36. Castro, A. (1969), Liquefaction of sands. Ph.D. thesis, Harvard University, Cambridge, Mass., USA.

37. Castro, G. (1977), Liquefaction and cyclic mobility of saturated sands. J. Geotechnical Engineering, ASCE, **101**(6): 551-569.

38. Castro, G. and Poulos, S. J. (1977), Factors affecting liquefaction and cyclic mobility. J. Geotechnical Engineering, ASCE, **103**(6): 501-516.

39. Castro, G., Poulos, S. J., France, J. W. and Enos, J. L. (1982), Liquefaction induced by cyclic loading. Report to National Science Foundation, Washington, D.C..

40. Castro, G. and Troncoso, J. (1989), Effects of 1985 Chilean Earthquake on three tailing dams. Proc. 5th chilean congress on Seismicity and Earthquake Engineering, Santiago, Chile, 1989, pp. 35-59.

41. Castro, G., Seed, R. B., Keller, T. O. and Seed, H. B. (1992), Steady-state strength analysis of Lower San Fernando Dam slide. J. Geotechnical Engineering, ASCE, **118**(3): 406-427.

42. Chameau, J. L. and Sutterer, K. (1994), Influence of fines in liquefaction potential and steady state considerations. 13th ICSMFE, New Delhi, India.

43. Chang, C. T. and Hwang, J. H. (1995), Study on cyclic shear strength of soils from different methods. Proc. Third international conference on recent advances in geotechnical earthquake engineering and soil dynamics, Vol. 1: 27-30, April 2-7, 1995, St. Louis, Missouri.

44. Charlie, W. A., Scott, C. E. , Soller, T. J., Butler, L. W. and Doehring, D.O. (1995), Estimating liquefaction potential of sand using the Piezovane. Geotechnique **45**(1): 55-67.

45. Chen, L. S. (1948), An investigation of stress-strain and strength characteristics of cohesionless soils by triaixal compression tests. Proc. 2nd ICSMFE, Vol. 5, pp 35-43, Rotterdam

46. Christian, H. A., Woeller, D. J., Weemees, I. and Robertson, P. K. (1994), Use of SASW and SCPT to evaluate liquefaction potential of the Fraser delta foreslope, Vancouver, British Columbia. Proc. 47th Canadian Geotechnical Conference, 166-175, Sep. 21-23, 1994, Halifax, Nova Scota.

47. Chu, J. (1995), An experimental examination of the critical state and other similar concepts for granular soils. Canadian Geotechnical. J., **32**: 1065-1075.

48. Clayton, C. R. I., Khatrush, S. A., Bica, A. V. D. and Siddique, A. (1989), The use of Hall effect semiconductors in geotechnical instrumentation. ASTM, Geotechnical Testing J., 12(1): 69-76.

49. Cole, E. R. (1967), The behavior of soils in the simple shear apparatus. Ph.D. thesis, University of Cambridge, Cambridge, England.

50. Cooling, L. F. and Golder, H. Q. (1940), Portable apparatus for compression test of clay soil. Engineering 147.

51. Committee on Earthquake Engineering, NRC (1985), Liquefaction of sands during earthquakes. National Academy Press, Washington, D.C..

52. Cornforth, D. H. (1964), Some experiments on the influnce of strain conditions on the strength of sand. Geotechnique, **14**(2): 143-167.

53. Coulter, H. W. and Migliaccio, R. R. (1966), Effects of the earthquake of March 27, 1964, at Valdez, Alaska. Geotechnical Survey Professional Paper 542-c, US Department of the Interior.

54. Cunning, J. C., Robertson, P. K. and Sego, D. C. (1994), Shear wave velocity to evaluate in situ state of sands. Proc. 47th Canadian Geotechnical Conference, pp 297-306, Sep. 21-23, 1994, Halifax, Nova Scota.

55. Datir, U. D. and Ingreji, N. K. (1994), Effect of different parameters on liquefaction potential of soils under cyclic loading. Proc. The 13th ICSMFE, New Delhi, India.

56. De Alba, P. A., Seed, H. B. and C. K. Chan (1976), Sand liquefaction in large-scale simple shear tests. J. Geotechnical Engineering, ASCE, 102(9): 909-927.

57. De Alba, P. A., Seed, H. B., Retamal, E. and Seed R. B. (1988), Analyses of dam failures in 1985 chilean earthquake. J. Geotechnical Engineering, ASCE, 114(12): 1414-1434.

58. Davies, M. P. and Campanella, R. G. (1994), Selecting design values of undrained strength for cohesionless soils. Proc. 47th Canadian Geotechnical Conference, pp 176-186, Sep. 21-23, 1994, Halifax, Nova Scota.

59. Dennis, N. D. (1988), Influence of specimen prparation techniques and testing procedures on undraiend steady state shear strength. Advanced Triaxial Testing of Soil and Rock, ASTM 977, pp. 642-654.

60. Desrues, J., Chambon, R., Mokni, M. and Mazerolle, F. (1996), Void ratio evolution inside shear bands in triaxial sand specimens studied by computed tomography. Geotechnique, 46(3): 529-546.

61. Duncan, J. M. and Dunlop, P. (1968), The significance of cap and base restraint. J. Soil Mechanics and Foundations Division, ASCE, **94**(1): 271-290.

62. Dobry, R. (1995), State of the art: Liquefaction and deformation of soils and foundations under seismic conditions. Proc. Third international conference on recent advances in geotechnical earthquake engineering and soil dynamics, Vol. 3: 231-276, April 2-7, 1995, St. Louis, Missouri.

63. Eckersley, D. (1990), Instrumented laboratory flowslides. Geotechnique **40**(3): 489-502.

64. El-Sohby, M. A. and Andrawes, K. Z. (1973), Experimental examination of sand anisotropy. Proc. 8th ICSMFE, Moscow, Vol. 1: 103-109.

65. Endo, K., Tohno,I., Chiba, T., Shamoto, Y. and Sangawa, A. (1988), Liquefaction phenomoena discovered at archeological excavation site at Lake Biwa. Proc. Annual Meeting, Japanese Society of SMFE.

66. Erten, D. and Maher, M. H. (1995), Effect of fines content on cyclic undrained behavior of sand. Proc. 3rd international conference on recent advances in geotechnical earthquake engineering and soil dynamics, Vol. 3: 11-21, April 2-7, 1995, St. Louis, Missouri.

67. Evans, M. D., Seed, H. B. and Seed, R. B. (1992), Membrane compliance and liquefaction of sluiced gravel specimens. J. Geotechnical Engineeriang, ASCE, 118(6): 856-872.

68. Evans, M. D. and Harder, L. F. (1993), Evaluating liquefaction potential of gravelly soil in dams. Proc. Geotechnical Practice in Dam Rehabilitation Conf., ASCE, New York, 467-481.

69. Evans, M. D. and Zhou, Shengping (1995), Liquefaction behavior of sand-gravel composites. J. Geotechnical Engineering, ASCE, **121**(3): 287-298.

70. Fear, C. E. and Robertson, P. K. (1994), Estimating undrained shear strength of sand using shear wave velocity. Proc. 47th Canadian Geotechnical Conference, pp 307-316, Sep. 21-23, 1994, Halifax, Nova Scota.

71. Fear, C. E. and Robertson, P. K. (1995), Estmating the undrained strength of sand: a theoretical framework. Canadian Geotechnical. J. **32**: 859-870.

72. Finn, W. D. L., Pickering, D. J. and Bransby, P. L. (1971), Sand liquefaction in triaxial and simple shear tests. J. Geotechnical Engineering, ASCE, **97**(4): 639-659.

73. Finn, W. D. L. (1990), Analysis of post-liquefaction deformations in soil structures. H.Bolton Seed, Vol.2, Memorial Symposium Proceedings, May 1990, Editor J.Michael Duncan, Vancouver, B.C., Canada.

74. Finn, W. D. L. (1991), State of the art: Assessment of liquefaction potential and post liquefaction behavior of earth structures: Developments 1981-1991. Proc. 2nd Int. Conf. on Recent Advances in Geotechnical Earthquake Engineering and Soil Dynamics, St. Louis, MO, March 11-15, 1991, Vol. 2: 1833-1850.

75. Finn, W. D. L., Ledbetter, R. H. and Marcuson III, W. F. (1995), State of the Art Paper: The evolution of geotechnical earthquake engineering practice in North America: 1954-1994. Third international conference on recent advances in geotechnical earthquake engineering and soil dynamics, Vol. 2: 881-909, April 2-7, 1995, St. Louis, Missouri.

76. Finno, R.J ., Harris, W. W., Mooney, M. A. and Viggiani, G. (1996), Strain localization and undrained steady state of sand. J. Geotechnical Engineering, ASCE, **122**(6): 462-473.

77. Fredlund, D. G. and Rahardjo, H. (1993), Soil mechanics for unsaturated soils. John Wiley & Sons, Inc..

78. Frydman, S., Zeithlen, J. D. and Alpan, I. (1973), The membrane effect in triaxial testing of granular soils. J. Testing and Evaluation, **1**(1): 37-41.

79. Gens, A. (1982), Stress-strain and strength characteristics of a low plasticity clay. Ph.D. thesis, Imperial College of Science and Technology, University of London.

80. Garga, V. K. and Khan, M. A.(1991), Laboratory evaluation of K_0 for overconsolidated clays. Canadian Geotechnical Journal, **28**: 650-659.

81. Garga, V. K. and Zhang, H. (1997), Volume changes in undrained triaxial tests on sands. Accepted for publication in Canadian Geotechnical Journal.

82. Georgiannou, V. N., Burland, J. B. and Hight, D. W. (1990), The undrained behavior of clayey sands in triaxial compression and extension. Geotechnique **40**(3): 431-449.

83. Georgiannou, V. N., Hight, D. W. and Burland. J. B. (1991a), Undrained behavior of natural and model clayey sands. Soils and Foundations, **31**(3): 17-29.

84. Georgiannou, V. N., Hight, D. W. and Burland, J. B. (1991b), Behavior of clayey sands under undrained cyclic triaxial loading. Geotechnique, **41**(3): 383-393.

85. Germanov, T. and Kostov, V. (1994), Liquefaction potential evaluation of sands from NPP sites. Proc. The 13th ICSMFE, New Delhi, India.

86. Goto, S. and Tastsuoka, F. (1988), Effect of end conditions on triaxial compressive strength for cohesionless soil. Advanced Triaxial Testing of Soil and Rock, ASTM STP 977, pp. 692-705.

87. Hanzawa, H. (1980), Undrained strength and stability analysis for a quick sand. Soils and Foundations, **20**(2): 17-29.

88. Hazen, A. (1920), Hydraulic fill dams. ASCE Transaction, Vol. 83: 1713-17745.

89. Hofmenn, B. A., Sego, D. C. and Robertson, P. K. (1994), Undisturbed sampling of a deep loose sand deposit using ground freezing. Proc. 47th Canadian Geotechnical Conference, pp 287-296, Sep. 21-23, 1994, Halifax, Nova Scota.

90. Hvorslev, M. J. (1937), On the physical properties of remoulded cohesive soils. Ingenioervidenskabelige Skrifter, Series A, No. 45.

Hvorslev, M. J. (1950),Triaxial tests on sands, Reid Bedford Bend, Mississippi River. Potamology Investigation Report, 5-3. Waterways Experiment Station, Vicksburg, Miss.

91. Hyodo, M., Tanimizu, H., Yasufuku, N. and Murata, H. (1994), Undrained cyclic and monotonic triaxial behavior of saturated loose sand. Soils and Foundations, **34**(1): 19-32.

92. Ibrahim, A. A. and Kagawa, T. (1991), Microscopic measurement of sand fabric from cyclic tests causing liquefaction. Geotechnical Testing J., **14**(4): 371-382.

93. Ishihara, K. (1974), Liquefaction of subsurface soil during earthquakes. Technicrat Vol. 7, Fuji Marketing Research Co., Ltd. No. 5.

94. Ishihara, K., Tatsuoka, F. and Yasuda, S. (1975), Undrained deformation and liquefaction of sand under cyclic stresses. Soils and Foundations, **15**(1): 29-44.

95. Ishihara, K., Sodekawa, M. and Tanaka, Y. (1978), Effects of overconsolidation on liquefaction characteristics of sands containing fines. Dynamic Geotechnical Testing, ASCE, SPT 654, pp 246-264.

96. Ishihara, K. and Takatsu, H. (1979), Effects of overconsolidation and Ko-conditions on the liquefaction characteristics of sands. Soils and Foundations, **19**(4): 59-68.

97. Ishihara, K. (1985), Stability of natural deposits during earthquakes. Proc. 11th ICSMFE, San Francisco, Vol.1: 321-376.

98. Ishihara, K., Kokusho,T . and Silver, M.L. (1989), State-of-the-art report: Recent developments in evaluating liquefaction characteristics of local soils. Proc. 12th ICSMFE, Vol. 4: 2719-2734, Rio De Janeiro, August 13-18, 1989.``

99. Ishihara, K. and Koseki, J. (1989), Cyclic shear strength of fines containing sands. Special Volume on Influence of Local Soils on Seismic Response. 12th ICSMFE, Rio de Janeiro.

100. Ishihara, K., Verduga, R. and Acacio, A. A. (1991), Characterization of cyclic behavior of sand and post-seismic stability analysis. Proc. the Asian Regional Conference on Soil Mechanics and Foundation Engineering, Bangkok, Thailand, Vol. 2: 45-68.

101. Ishihara, K. (1993), Liquefaction and flow failure during earthquake. Geotechnique **43**(3): 351-415.

102. Ishihara, K. (1994), Evaluation of residual strength of sandy soils. 13TH ICSMFE, New Delhi, India. Vol. 5: 175-181.

103. Khan, M. A. (1993), Strength-deformation behaviour of a weathered clay crust. Ph.D. thesis, University of Ottawa, Ottawa, Canada.

104. Khan, M. A. (1993), Manual of operation of automatic stress-path control system. University of Ottawa, Ottawa, Canada.

105. Kiekbusch, M. and Schuppener, B. (1977), Membrane penetration and its effect in pore pressure. J. Geotechnical Engineering, ASCE, **103**(11): 1267-1279.

106. Konrad, J. M. (1990a), Minimum undrained strength of two sands. J. Geotechnical Engineering, ASCE, **116**(6): 932-947.

107. Konrad, J. M. (1990b), Minimum undrained strength versus steady-state strength of sands. J. Geotechnical Engineering, ASCE, **116**(6): 948-963.

108. Konrad, J. M. (1993), Undrained response of loosely compacted sands during monotonic and cyclic compression tests. Geotechnique, **43**(1): 69-89.

109. Kramer, S. L. and Sivaneswaran, N. (1989), A non-destructive specimen-specific method for measurement of membrane penetration in the triaxial test. Geotechnical Testing Journal, **12**(1): 50-59.

110. Kramer, S. L. (1996), Geotechnical earthquake engineering. Prentice-Hall, Inc., Upper Saddle River, NJ 07458, USA.

111.Kuerbis, R. and Vaid, Y. P. (1988), Sand sample preparation - the slurry deposition method. Soils and Foundations, **28**(4): 107-118.

112.Kuerbis, R. and Vaid, Y. P. (1989), Static and cyclic undrained behavior of silty sands. Special Volume for Discussion Session on Influence of Local Soils on Seismic Response, 12th ICSMFE, Rio de Janeiro.

113.Lacasse, S. and Berre, T. (1988), Triaxial testing methods for soils. Advanced Triaxial Testing of Soil and Rock, ASTM STP 977, pp. 264 - 289.

114.Ladd, C., Foott, R, Ishihara, K., Schlosser, F. and Poulos, H. G. (1977), Stress-deformation and strength characteristics. Proc. 9th ICSMFE, Vol. 2, Tokyo.

115.Ladd, R. S. (1974), Specimen preparation and liquefaction of sands. J. Geotechnical Engineering, ASCE, **100**(10): 1180-1184.

116.Ladd, R. S. (1978), Preparing test specimens using udercompaction. Geotechnical Testing J., 1(1): 16-23.

117.Lade, P. V. and Duncan, J. M. (1975), Elastro-plastic stress-strain theory for cohesionless soil. J. Geotechnical Engineering, ASCE, **101**(10): 1037-1053.

118.Lade, P. V. (1977), Membrane penetration effects in undrained tests. J. Geotechnical Engineering, ASCE, **103**(2): 109-125.

119.Lade, P. V., Yamamuro, J. A. and Skeyers, B. D. (1996), Effects of shear band formation in triaxial extenstion tests. Geotechnical Testing J., ASTM, **19**(4):398-410.

120.Lam, W. K. and Tatsuoka, F. (1988), Triaxial compressive and extension strength of sand affected by strength anisotropy and sample slenderness. Advanced Triaxial Testing of Soil and Rock, ASTM SPT 977, 655-666.

121.Lambe, T. W. (1951), Soil Testing for Engineers, John Wiley & Sons, Inc., New York.

122.Larew, H. G. (1960), Discussion on non-uniform conditions in triaxial test specimens (Woodland, Shockley and Ahlrin). ASCE Research Conference on Shear Strength of Cohesive Soils, Session 2, p. 1013, University of Colorado, Boulder.

123.La Rochelle, P. (1967), Membrane, drain and area correction in triaxial test on soil samples failing along a single shear plane. Proc. 3rd Pan-American Conference on Soil Mechanics & Foundation Engineering, Vol. 1, pp 273-292, Caracas, Venezuela.

124.Lee, C. J. (1995), Static shear and liquefaction potential of sand, Proc. Third international conference on recent advances in geotechnical earthquake engineering and soil dynamics, Vol. 3: 115-118, April 2-7, 1995, St. Louis, Missouri.

125.Lee, I. K. and Seed, H.B. (1964), Discussion on "Importance of free ends in triaxial testing" by Rowe, P.W. and Barden, L., J. Sol Mechanics and Foundations Division, ASCE, **90**(6): 173-175.

126.Lee, I. K. (1966), Stress dilatancy performance of feldspar. J. Sol Mechanics and Foundations Division, ASCE, **92**(2): 79-103.

127.Lee, I. K., White, W. and Ingles, O. G. (1983), Geotechnical engineering, Chapter 3, Pitman Publishing Inc., Marshfield.

128.Lee, K. L. and Seed, H. B. (1967), Drained strength characteristics of sands. J. Sol Mechanics and Foundations Division, ASCE, **93**(6).

129.Lee, K. L., Seed, H. B. and Dunlop, P. (1969), Effect of transient loading on the strength of sand. Proceedings, 7th ICSMFE, Mexico, Vol. 1, pp. 239-247.

130.Lee, K. L. (1978a), End restraint effects on undrained static triaxial strength of sand. J. Geotechnical Engineering, ASCE, **104**(6): 687-704.

131.Lee, K.L. (1978b), End restraint effects on cyclic triaxial strength of sand. J. Geotechnical Engineering, ASCE, **104**(6): 704-719.

132.Lindenberg, J. and Koning, H. L. (1981), Critical density of sand. Geotechnique, **31**(2): 231-245.

133.Marcuson III, W. F., Hynes, M. E. and Franklin, A. G. (1990), Evaluation and use of residual strength in seismic safety analysis of embankments. Earthquake Spectra, **6**(3): 529-572.

134.Marsal, R. J. (1977), Research on granular materials. Universidal National Autonoma De Mexico.

135.Martin, G. R., Finn, W. D. L. and Seed, H. B. (1978), Effects of system compliance on liquefaction tests. J. Geotechnical Engineering, ASCE, **104**(4): 463-479.

136.McRoberts, E. C. and Sladen, J. A. (1992), Observations on static and cyclic sand-liquefaction methodologies, Canadian Geotechnical. J., **29**: 650-665.

137.Mitchell, J. K. (1976), Fundamentals of soil behaviour. New York, Wiley.

138.Miura, S. and Shosuke, T. (1982), A sample preparation method and its effect on static and cyclic deformation- strength properties on sand. Soils and Foundations, **22**(1): 61-77.

139.Mohamad, R. (1984), Evaluation of seismically-induced liquefaction flow failure of earth dams. Ph.D. thesis, Rensselaser Polytechnic Institute, at Troy, New York.

140.Mohamad, R. and Dobry, R. (1986), Undrained monotonic and cyclic triaxial strength of sand. J. Geotechnical Engineering, ASCE, **112**(10): 941-958.

141.Mogami, T. and Kubo, K. (1953), The behavior of soil during vibration. Proc. 3rd ICSMFE, Vol. 1: 152-153.

142.Molenkamp, F. and Luger, H. J. (1981), Modelling and minimization of membrane penetration effects in tests on granular soils. Geotechnique, **31**(4): 471-486.

143.Morris, D. V. (1983), A note on earthquake - induced liquefaction. Geotechnique, **33**(4): 451-454.

144.Mulilis, J. P., Seed, H.B., Chan, C. K., Mitchell, J. K. and Arulanandan, k. (1977), Effects of sample preparation on sand liquefaction. J. Geotechnical Engineering, ASCE, **103**(2): 91-108.

145.Mulilis, J. P., Townsend, F. C. and Horz, R. C. (1978), Triaxial testing techniques and sand liquefaction. Dynamic Geotechnical Testing, ASTM STP 654, 265-279.

146.Nagaraj, T. T. (1993), Principles of testing soils, rocks and concrete. Elsevier Science Publishers B.V..

147.Nash, K. L. (1953), The shearing resistance of a fine closely graded sand. Proc. 3rd ICSMFE, Zurish, Switzland, Vol. 1: 160-164.

148.Nash, K. L. and Dixon, R. K. (1961), The measurement of pore pressure in sand under rapid triaxial tests. Proceedings, Conference on the Pore Pressure and Suction in Soils, Butterworths, London, pp. 21-25.

149.Negussey, D., Wijewickreme, W. K. D. and Vaid, Y. P. (1988), Constant-volume friction angle of granular materials. Canadian Geotechnical J., **25**: 50-55.

150.Negussey, D. and Islam, M. S. (1994), Uniqueness of steady state and liquefaction potential. Canadian Geotechnical J., **31**: 132- 139.

151.Newland, P. L. and Allely, B. H. (1957). Volume changes during drained triaxial tests on granular materials. Geotechnique, **7**: 17-34.

152.Newland, P. L. and Allely, B. H. (1959), Volume changes during undrained triaxial tests on saturated dilatant granular materials. Geotechnique, **9**: 174-182.

153.Nicholson, P. G., Seed, R. B. and Anwar, H. A. (1993a), Elimination of membrane compliance in undrained triaxial testing. I. Measurement and evaluation. Canadian Geotechnical J., **30**(5): 727-738

154.Nicholson, P. G., Seed, R. B. and Anwar, H. A. (1993b), Elimination of membrane compliance in undrained triaxial testing. II. Mitigation by injection compensation. Canadian Geotechnical J., **30** (5): 739-746

155.Norris, G. M. (1981), Effect of end membrane thickness on the strength of "frictionless" cap and base tests. Laboratory Shear Strength of Soil, ASTM STP 740, 303-314.

156.Norris, G., Siddharthan, R., Zafir, Z. and Madhu, R. (1997), Liquefaction and residual strength of sands from drained triaxial tests. J. Geotechnical and Geoenviroment Engineering, ASCE, **123**(3): 220-228.

157.Oda, M., Koishikawa, I. and Higuchi, T. (1978), Experimental study of anisotropic shear strength of sand by plane strain test. Soils and Foundations, **18**(1): 25-38.

158.Ohara, S. and Yamamoto, T. (1991), A practical method for obtaining correction factor of liquefaction resistance for membrane penetration. Soils and Foundations, **31**(2): 188-196.

159.Olson, R. R. and Campbell, L. M. (1964), Discussion on "Importance of free ends in triaxial testing". J. Soil Mechanics and Foundations Division, ASCE, **90**(6): 167-173.

160.Palmeira, E. M. and Milligan, G. W. E. (1989), Scale effects in direct shear tests on sand. Proc. The 12th ICSMFE, Vol. 1: 739-742.

161.Park, C. S. and Tatsuoka, F. (1994), Anisotropic strength and deformation of sands in plane strain compression. Proc. 13th ICSMFE, 1994, New Delhi, India.

162.Penman, A. D. M. (1953), Shear characteristics of a saturated silt, measured in triaxial compression. Geotechnique, **3**(8): 312-328.

163.Pickering, J. (1973), Drained liquefaction testing in simple shear. J. Soil Mechanics and Foundations Division, ASCE, **99**(12): 1179-1183.

164.Pillai, V. S. and Salgado, F. M. (1994), Post-liquefaction stability and deformation analysis of Duncan Dam. Can. Geotech. J., **31**: 967-978.

165.Pillai, V. S. and Stewart, R. A. (1994), Evaluation of liquefaction potential of foundation soils at Duncan Dan. Canadian Geotechnical J., **31**: 951-966.

166.Pitman, T. D., Robertson, P. K. and Sego, D. C. (1994), Influence of fines on the collapse of loose sands. Canadian Geotechnical J., **31**: 718-739.

167.Poorooshasb, H. B. and Consoli, N. C. (1991), The ultimate state. Panamerican Conference on Soil Mechanics and Foundation Eng., **9**(3): 1083-1090.

168.Poulos, S. J. (1971), The stress-strain curves of soils, Geotechnical Engineers Inc., Winchester, Mass. 1-80.

169.Poulos, S. J. (1981), The steady state of deformation. J. Geotechnical Engineering. ASCE, **107**(5): 553-562.

170.Poulos, S. J., Castro, G. and France, J. W. (1985), Liquefaction evaluation procedure. J. Geotechnical Engineering, ASCE, **111**(6): 772-792.

171.Poulos, S. J., Castro, G. and France, J. W. (1988), Liquefaction evaluation procedure: Reply. J. Geotechnical Engineering, ASCE, **114**: 232-256.

172.Pradel, D. and Lade, P.V. (1989), Instability of sand under applied shear stresses. Proc. The 12th ICSMFE, Vol. 1: 743-748.

173.Ramana, K. V, and Raju, V. S. (1981), Constant-volume triaxial tests to study the effects of membrane penetration. Geotechnical Testing J., **4**(3): 117-122.

174.Raju, V. S. and Sadasivan, S. K. and Venkataraman, M. (1972), Use of lubricated and conventional end platens in triaxial tests on sands. Soils and Foundations, **12**(4): 35-43.

175.Raju, V. S. and Sadasivan, S.K. (1974), Membrane penetration in triaxial tests on sands. J. Geotechnical Engineering, ASCE, **100**(4): 482-489.

176.Reades, D. W. and Green, G. E. (1976), Independent stress control and triaxial extension tests on sand. Geotechnique, **26**(4): 551-576.

177.Riemer, M. F., Seed, R. B., Nicholson, P. G. and Jong, H. L. (1990), Steady state testing of loose sands: limiting minimum density. J. Geotechnical Engineering, ASCE, **116**(2): 332- 337.

178.Riemer, M. F. (1992), The effects of testing conditions on the constitutive behaviour of loose, saturated sands under monotonic loading. PhD Thesis, University of California at Berkeley, California, USA.

179.Riemer, M. F., Seed, R. B. (1997), Factors affecting apparent position of steady state line. J. Geotechnical and Geoenviroment Engineering, ASCE, **123**(3): 281-288.

180.Robertson, P. K. (1994), Design considerations for liquefaction. 13TH ICSMFE, New Delhi, India.

181.Robertson, P. K. (1994), Suggested terminology for liquefaction. Proc. 47th Canadian Geotechnical Conference, pp 277-286, Sep. 21-23, 1994, Halifax, Nova Scota.

182.Robertson, P. K., Hofmenn, B. A. and List, B. R. (1995), CANLEX (Canadian Liquefaction Experiment): A one year update. Third international conference on recent advances in geotechnical earthquake engineering and soil dynamics, Vol. 2: 815-823, April 2-7, 1995, St. Louis, Missouri.

183.Robertson, P. K., Sasitharan, S., Cunning, J. C. and Sego, D. C. (1995), Shear-wave velocity to evaluate in-situ state of Ottawa sand. J. Geotechnical Engineering, ASCE, **121**(3): 262-273.

184.Roscoe, K. H., Schofield, A. N. and Wroth, C. P. (1958), On the yielding of soils. Geotechnique, **8**(1): 22-53.

185.Roscoe, K. H., Schofield, A. N. and Wroth, C. P. (1959), Correspondence on "On the yielding of soils," Geotechnique, **9**(2): 72.

186.Roscoe, K. H. and Poorooshasb, H. B. (1963a), A fundamental principle of similarity in model tests for earth pressure problems. Proc. 2nd Asian Conference on Soil Mechanics, Vol. 1: 134-140.

187.Roscoe, K. H., Schofield, A. N., and Thurairajah, A. (1963b), An evaluation of test data for selecting a yield criterion for soils. Proc. the Symposium on Laboratory Shear Testing of Soils, American Society for Testing and Materials, Special Technical Publication No. 361, pp. 111-128.

188.Roscoe, K. H., Schofield, A. N. and Wroth, T. A. (1963c), Yielding of clays in states wetter than critical. Geotechnique, **13**(3): 211-240.

189.Roscoe, K. H. and Burland, J. B. (1968), On the generalized stress-strain behaviour of wet clay. Proc. Conference on Engineering Plasticity, Cambridge.

190.Rowe, P. W. (1962), The stress dilatancy relation for static equilibrium of an assembly of particles in contact, Proc., Royal Society, London, Series A, Vol. 269: 500-527.

191.Rowe, P. W. and Barden, L. (1964), Importance of free ends in triaxial testing. J. Soil Mechanics and Foundations Division, ASCE, **90**(1): 1-27.

192.Rowe, P. W., Barden, L. and Lee, I. K. (1964), Energy component during the triaxial cell and direct shear tests. Geotechnique, **14**(3).

193.Rowe, P. W. (1969), The relation between the shear strength of sands in triaxial compression, plane strain and direct shear. Geotechnique, **19**(1): 75-86.

194.Saada, A. S. and Townsend, F. C. (1981), Laboratory strength testing of soils. Laboratory Shear Strength of Soil. ASTM STP 740, pp. 7 - 77.

195.Sasitharan, S., Robertson, P. K., Sego, D. C. and Morgenstern, N.R. (1993), Collapse behavior of sand. Canadian Geotechnical J., **30**: 569-577.

196.Sasitharan, S., Robertson, P. K., Sego, D. C. and Morgenstern, N.R. (1994), State-boundary surface for very loose sand and its practical implications. Canadian Geotechnical J., **31**: 321-334.

197.Sasitharan, S. (1994), Collapse behavior of very loose sand. Ph. D. thesis, University of Alberta, Edmonton, Alberta.

198.Seed, H. B. and Lee, K. L. (1966), Liquefaction of saturated sands during cyclic loading. J. Soil Mechanics and Foundations Division, ASCE, **92**(6).

199.Seed, H. B. and Lee, K. L. (1967), Undrained strength characteristic of cohesionless soils. J. Soil Mechanics and Foundations Division, ASCE, **93**(6): 333-360.

200.Seed, H. B., Lee, K. L., Idriss, I. M. and Makdisi, F. (1973), Analysis of the slides in the San Fernando dams during the earthquake of February 9, 1971. Report No. EERC 73-2, Earthquake Engineering Research Centre, University of California, Berkely, California.

201.Seed, H. B., Lee, K. L., Idriss, I. M. and Makdisi, F. (1975), The slides in the San Fernando dams during the earthquake of February 9, 1971. J. Geotechnical Engineering, ASCE, **101**(7): 651-689.

202.Seed, H. B., Makdisi, F. I. and De Alba, P. (1978), Performance of earth dams during earthquakes. J. Geotechnical Engineering, ASCE, **104**(7): 967-994.

203.Seed, H. B. (1979a), Soil liquefaction and cyclic mobility evaluation for level ground during earthquake. J. Geotechnical Engineering,. ASCE, **105**(2): 201-255.

204.Seed, H. B. (1979b), Consideration in the earthquake resistance design of earth and rockfill dams. Geotechnique, **29**: 215-263.

205.Seed, H. B., Idriss, I. M. and Arango, I. (1983), Evaluation of liquefaction potential using field perfomance data. J. Geotechnical Engineering, ASCE, **109**(3): 458-482.

206.Seed, H. B. (1987), Design problems in soil liquefaction. J. Geotechnical Engineering, ASCE, **113**(8): 827-8454.

207.Seed, R. B. and Anwar, H. A. (1989), Development of a laboratory technique for correcting results of undrained triaxial shear tests on effects of membrane compliance. Geotechnical Research Report, No. SU/GT/86-02, Stanford University.

208.Seed, R. B., Anwar, H. A. and Nicholson, P. G. (1989), Elimination of membrane compliance effects in undrained testing. Proc. The 12th ICSMFE, Vol. 1: 111-114. Rio De Janeiro, August 13-18, 1989.

209.Shockley, W. G. and Ahlvin, R. G. (1960), Nonuniform conditions in triaxial test specimens. Research Conference on Shear Strength of Cohesive Soils, ASCE. Boulder, Colorado, pp. 341-357.

210.Siddiqi, F. H. (1984), Strength evaluation of cohesionless soils with oversized particles. Ph. D. thesis, University of California, Davis.

211.Silver, M. L., Chan, C. K., Ladd, R. S., Lee, K. L., Tiedemann, D. A., Townsend, F. C., Valera, J. E. and Wilson, J. H. (1976), Cyclic triaxial strength of standard test sand. J. Geotechnical Engineering, ASCE, 102(5): 511-523.

212.Skempton, A. W (1954), The pore-pressure coefficients A and B. Geotechnique, **5**(4): 143-147.

213.Sladen, J. A., D'Hollander, R. D. and Krahn, J.(1985), The liquefaction of sands, a collapse surface approach. Canadian Geotechnical J., **22**: 564-578.

214.Sladen, J. A. and Handford, G. (1987), A potential systematic error in laboratory testing if very loose sands. Canadian Geotechnical J., **24**: 462-466.

215.Sladen, J. A. and Oswell, J. M. (1989), The behavior of very loose sand in the triaxial compression test. Canadian Geotechnical J., **26**: 103-113.

216.Stark, T. D. and Contreras, I. A. (1996), Constant volume ring shear apparatus. Geotchnical Testing J., **19**(1): 3-11.

217.Steensen-Bach, J. O. (1989), Strength evaluation of a natural sand. Proc. The 12th ICSMFE, Vol. 1: 757-762.

218.Suchida, H. (1970), Prediction and countermeasure against the liquefaction in sand deposits. Abstract of the Seminar, Port and Harbor Research Institute.

219.Symes, M. J. P. R., Gens, A. and Hight, D. W. (1984), Undrained anisotropy and principal stress rotation in saturated sand. Geotechnique, **34**(1): 11-27.

220.Tanaka, Y., Kokusho, T., Yoshida and Kudo, K. (1991), A method for evaluating membrane compliance and system compliance in undrained cyclic shear tests. Soils and Foundations, **31**(3): 30-42.

221.Tanaka, Y. and Shirakawa, K. (1995), Changes of yield stress of sand during undrained cyclic loading. Proc. Third international conference on recent advances in geotechnical earthquake engineering and soil dynamics, Vol. 1: 95-102, April 2-7, 1995, St. Louis, Missouri.

222.Tatsuoka, F, Ochi, K., Fujii, S. and Okamoto, M. (1986), Cyclic undrained triaxial and torsional shear strength of sands for different sample prepararion methids. Soils and Foundations, **26**(3): 23-41.

223.Tatsuoka, F., Sakamoto, M., Kawamura, T. and Fukushima, S. (1986), Strength and deformation characteristics of sand in plane stain compression at extremely low pressures. Soils and Foundations, **26**(1): 65-84.

224.Taylor, D. W. (1939), A comparison of results of direct shear and cylindrical compression tests. Am. Soc. Test Mat. **39**: 1058-1070.

225.Taylor, D. W. (1941), Seventh progress report on shear strength, Research Report, Massachusetts Institute of Technology, Cambridge, Mass. 1941.

226.Taylor, D. W. (1948), Fundamentals of Soil Mechanics, Chapter 14. John Wiley and Sons, Inc., New York.

227.Terzaghi, K. and Peck, R. B. (1948), Soil Mechanics in Engineering Practice. 2nd edition, P 108, Chichester: Wiley.

228.Terzaghi, K., Peck, R. B. and Mesri, G. (1996), Soil Mechanics in Engineering Practice. 3rd edition, Chapter 3, John Wiley and Sons, Inc., New York.

229.Timoshenko, S. P. (1953), History of strength of materials. McGraw-Hill Book Co., Inc., New York, N.Y., p361.

230.Toki, S., Tatsuoke, F., Miura, S., Yoshimi, Y., Yasuda, S., and Makihara, Y. (1986), Cyclic undrained triaxial strength of sand by a cooperative test program. Soils and Foundations, **26**(3): 117-128.

231.Tokimatdsu, K. and Nakamura, K. (1986), A liquefaction test without membrane penetration effects. Soils and Foundations, **26**(4): 127-138.]

232.Tokimatdsu, K. and Nakamura, K. (1987), A simplified correction for membrane compliance in liquefaction tests. Soils and Foundations, **27**(4): 111-122.

233.Troncoso, J. H. and Verdugo, R. (1985), Silt content and dynamic behavior of tailing sands. Proc. 11th ICSMFE, San Francisco, Vol. II: 1311-1314.

234.Troncoso, J. H., Ishihara, K. and Verdugo, R. (1988), Aging effects on cyclic shear strength of tailings materials. Proc. 9th World Conference on Earthquake Engineering, Tokyo and Kyoto.

235.Uchida, K. and Vaid. Y. P. (1994), Sand behavior under strain path control. Proc. 13TH ICSMFE, 1994, New Delhi, India.

236.Ueng, T., Tzou, Y. and Lee, C. (1988), The effect of end restraint on volume change and partical breakage of sands in triaxial tests. Advanced Triaxial Testing of Soil and Rock, ASTM STP 977, pp. 679-691.

237.Uthayakumar, M. (1996), Liquefaction of sands under multi-axial loading. Ph.D. thesis, University of British Columbia, Canada.

238.Vaid, Y. P. and Finn, W. D. L. (1979), Static shear and liquefaction potential. J. Geotechnical Engineering, ASCE, **105**(10): 1233-1246.

239.Vaid, Y. P. and Chern, J. C. (1983), Effect of static shear on resistance to liquefaction. Soils and Foundations, **23**(1): 47-60.

240.Vaid, Y. P. and Negussey, D. (1984), A critical assessment of membrane penetration in the triaxial test. Geotechnical Testing J., ASCM, 7(2): 70-76.

241.Vaid, Y. P. and Negussey, D. (1984), Relative density of pluviated sand samples. Soils and Foundations, **24**(2): 101-105.

242.Vaid, Y. P. and Chern, J.C. (1985), Cyclic and monotonic undrained response of saturated sands. Advances in the art of testing soils under cyclic conditions, ASCE Annual Convention, Detroit, Mich., 120-147.

243.Vaid, Y. P. and Negussey, D. (1988), Preparation of reconstituted sand specimens. Advanced Triaxial Testing of Soil and Rock, ASTM STP 977, 405-417.

244.Vaid, Y. P., Chung, E. K. F. and Kuerbis, R. H. (1990), Stress path and steady state. Canadian Geotechnical J., **27**: 1-7.

245.Vaid, Y. P., Kuerbis, R. H. and Chern, J. C. (1990), Static liquefaction of sands and -silty sands. Proc. 43rd Canadian Geotechnical Conference, Vol. 1, pp. 247-256. Quebec.

246.Vaid, Y. P. and Thomas, J. (1994), Post-liquefaction behavior of sand. 13th ICSMFE, New Delhi, India.

247.Vaid, Y. P. and Thomas, J. (1995), Liquefaction and postliquefaction behavior of sand. J. Geotechnical Engineering, ASCE, **121**(2): 163-173.

248. Vaid, Y. P. and Sivathayalan, S. (1996a), Static and cyclic liquefaction potential of Fraser Delta sand in simple shear and triaxial tests. Canadian Geotechnical J. **33**: 281-189.

249. Vaid, Y. P. and Sivathayalan, S. (1996b), Errors in estimates of void ratio of laboratory sand specimens. Canadian Geotechnical J. **33**(6): 1017-1020.

250. Verdugo, R. and Ishihara, K. (1996). The steady state of sandy soils. Soils and Foundations, **36**(2): 81-91.

251. Vesic, A. S. and Clough, G. W. (1968), Behavior of granular materials under high stress. J. Soil Mechanics and Foundations Division, ASCE, **94**(6).

252. Wang, W. (1984), Earthquake damage to earth and levees in relation to soil liquefaction. Proc. Int. Conf. on Case Histories on Geotech. Engrg., University of Missouri-Rolla, Vol. 1: 551-521.

253. Webb, D. L. (1969), Residual strength in conventional triaxial tests, Proc. of 7th ICSMFE, Vol. 1.

254. Wesley, L. D. (1975), Influence of stress path and anisotropy on the behaviour of a soft alluvial clay. Ph.D. thesis, Imperial College of Science and Technology, University of London.

255. Whitman, R. V. and Healy, K. A. (1962), Shear strength of sands during rapid loadings. J. Soil Mechanics and Foundations Division, ASCE, **88**(2): 99-132.

256. Wong, R. K. S. and Arthur, J.R.F. (1985), Determinations and uses of strain distributions in sand samples. Geotechnical Testing J., ASTM, **8**(3): 101-110.

257. Wong, R. T., Seed, H. B. and Chan, C. K. (1975), Cyclic loading liquefaction of Gravely soils. J. Geotechnical Engineering, ASCE, **101**(6): 571-583.

258. Wood, D. M. (1990), Soil behavior and critical state soil mechanics. Cambridge University Press, First published 1990, reprinted 1992,1994.

259. Wroth, C. P. and Houdsby, G. T. (1985), Soil mechanics - property characterization and analysis produces. Proc. 11th ICSMFE, Vol. 1, San Francisco.

260. Wu, W. and Kolymbas, D. (1991), On some issues in triaxial extension tests. Geotechnical Testing J., ASTM, 14(3): 276-287.

261. Yamamuro, J. A. and Lade, P. V. (1993), Effects of strain rate on instability of granular soils. Geotechnical Testing Journal, ASTM, **16**(3): 304-313.

262. Yamamuro, J. A. and Lade, P. V. (1995), Strain localization in extension tests on granular materials. J. Engineering Mechanics, ASCE, **121**(7): 828-836.

263. Yoshimi, Y. and Oh-oka, H. (1975), Influence of degree of shear stress reversal on the liquefaction potential of saturated sand. Soils and Foundations, **15**(3): 27-40.

264. Yoshimi, Y. and Tokimatsu, K. (1978), Two-dimensional pore pressure changes in and deposits during earthquakes. Proc. 2nd Inter. Conf. on Microzonation for Safer Construction, Vol. 2: 853-863.

265. Zhang, H. and Garga, V. K. (1997), Discussion of "Strain localization and undrained steady state of sand". J. Geotechnical Engineering, ASCE (in press).

APPENDIX A: PLOTS OF TRIAXIAL TESTS

Note: Lubricated end platens were used for all tests, except four where the effect of regular end platens (RE) was investigated.
Group 1: CIU and CD tests on fresh sand.
Group 2: CAU, CIU and CD tests on previously used or unused sand from Group 1.
Group 3: CAU, CIU and CD confirmatory tests on fresh sand.

Table A.1 Summary of triaxial tests on Unimin sand (Group 1)

Figure Number	Test Type	Consolidation State				Steady State			Platen
		Dr (%)	e	σ_3' (kPa)	Kc	e	p' (kPa)	q (kPa)	
A.01	CIU	13.9	0.984	100	1.0	0.984	12	19	
A.02	CIU	15.5	0.978	200	1.0	0.978	15	26	
4.7	CIU	17.4	0.971	200	1.0	0.971	21	34	
A.04	CIU	17.7	0.969	201	1.0	0.969	23	36	RE
7.3	CIU	25.2	0.941	399	1.0	0.941	60	80	
A.06	CIU	26.7	0.935	198	1.0	0.935	32	49.5	
A.07	CIU	26.7	0.935	201	1.0	0.935	53	82	RE
A.08	CIU	28.5	0.928	471	1.0	0.928	76	118	
A.09	CIU	29.3	0.925	398	1.0	0.925	74	107	
A.10	CIU	37.5	0.894	601	1.0	0.894	162	236	
A.11	CIU	39.6	0.886	806	1.0	0.886	209	274	
A.12	CIU	41.4	0.879	997	1.0	0.879	282	381	
7.2	CIU	45.1	0.865	1092	1.0	0.865	359	478	
A.14	CIU	21.1	0.957	200	1.0	0.957	28	35	
7.5	CIU	35.4	0.902	200	1.0	0.902	117	156	
A.16	CIU	35.4	0.902	201	1.0	0.902	136	185	RE
4.8	CIU	58.4	0.814	200	1.0				
7.6	CIU	70.0	0.770	200	1.0				
A.19	CIU	69.8	0.771	201	1.0				RE
A.20	CD	2.4	1.028	10	1.0	0.957	24	41	
A.21	CD	11.2	0.995	20	1.0	0.934	45	66	
A.22	CD	13.1	0.987	30	1.0	0.923	61	93	
7.4	CD	17.7	0.969	50	1.0	0.921	96	136	
A.24	CD	19.3	0.964	100	1.0	0.913	184	250	
A.25	CD	22.3	0.952	148	1.0	0.874	273	372	
7.7	CD	37.9	0.892	696	1.0				

Table A.2 Summary of triaxial tests on Unimin sand (Group 2)

Figure Number	Test Type	Consolidation State				Steady State		
		Dr (%)	e	σ_3' (kPa)	Kc	e	p' (kPa)	q (kPa)
A.27	CAU	27.8	0.931	52	1.5	0.931	6	14
A.28	CAU	30.4	0.921	101	1.5	0.921	16	32
A.29	CAU	36.5	0.898	200	1.5	0.898	67	101
A.30	CAU	42.7	0.874	400	1.5	0.874	154	204
A.31	CAU	27.4	0.933	53	2.0	0.933	13	22
A.32	CAU	28.5	0.928	53	2.0	0.928	12	20
A.33	CAU	30.4	0.921	53	2.0	0.921	7	11
A.34	CAU	35.4	0.902	198	2.0	0.902	93	130
A.35	CAU	36.8	0.897	100	2.0	0.897	104	147
A.36	CAU	40	0.885	53	2.0	0.885	54	79
A.37	CAU	45.5	0.864	399	2.0	0.864	232	308
A.38	CIU	25.6	0.94	52	1.0	0.94	4	9
A.39	CIU	31.5	0.917	200	1.0	0.917	33	58
A.40	CD	25.6	0.940	30	1.0	0.883	61	90

Table A.3 Summary of triaxial tests on Unimin sand (Group 3)

Figure Number	Test Type	Consolidation State				Steady State		
		Dr (%)	e	σ_3' (kPa)	Kc	e	p' (kPa)	q (kPa)
A.41	CAU	15.8	0.977	52	2.0	0.977	10	20
A.42	CAU	19.3	0.964	76	2.0	0.963	18	29
A.43	CAU	22.6	0.951	100	2.0	0.951	47	74
A.44	CAU	26.7	0.935	199	2.0	0.935	82	135
A.45	CAU	28.5	0.928	202	2.0	0.928	89	126
A.46	CAU	26.7	0.935	202	2.0	0.935	66	112
A.47	CAU	20.8	0.958	98	2.0	0.958	26	50
A.48	CAU	32.2	0.915	298	2.0	0.914	127	201
A.49	CAU	35.4	0.902	300	2.0	0.902	168	227
A.50	CAU	38.2	0.891	455	2.0	0.891	272	364
A.51	CIU	22.3	0.952	149	1.0	0.952	24	46
A.52	CIU	28.9	0.927	299	1.0	0.927	71	108
A.53	CD	10	0.999	52	1.0	0.909	102	144

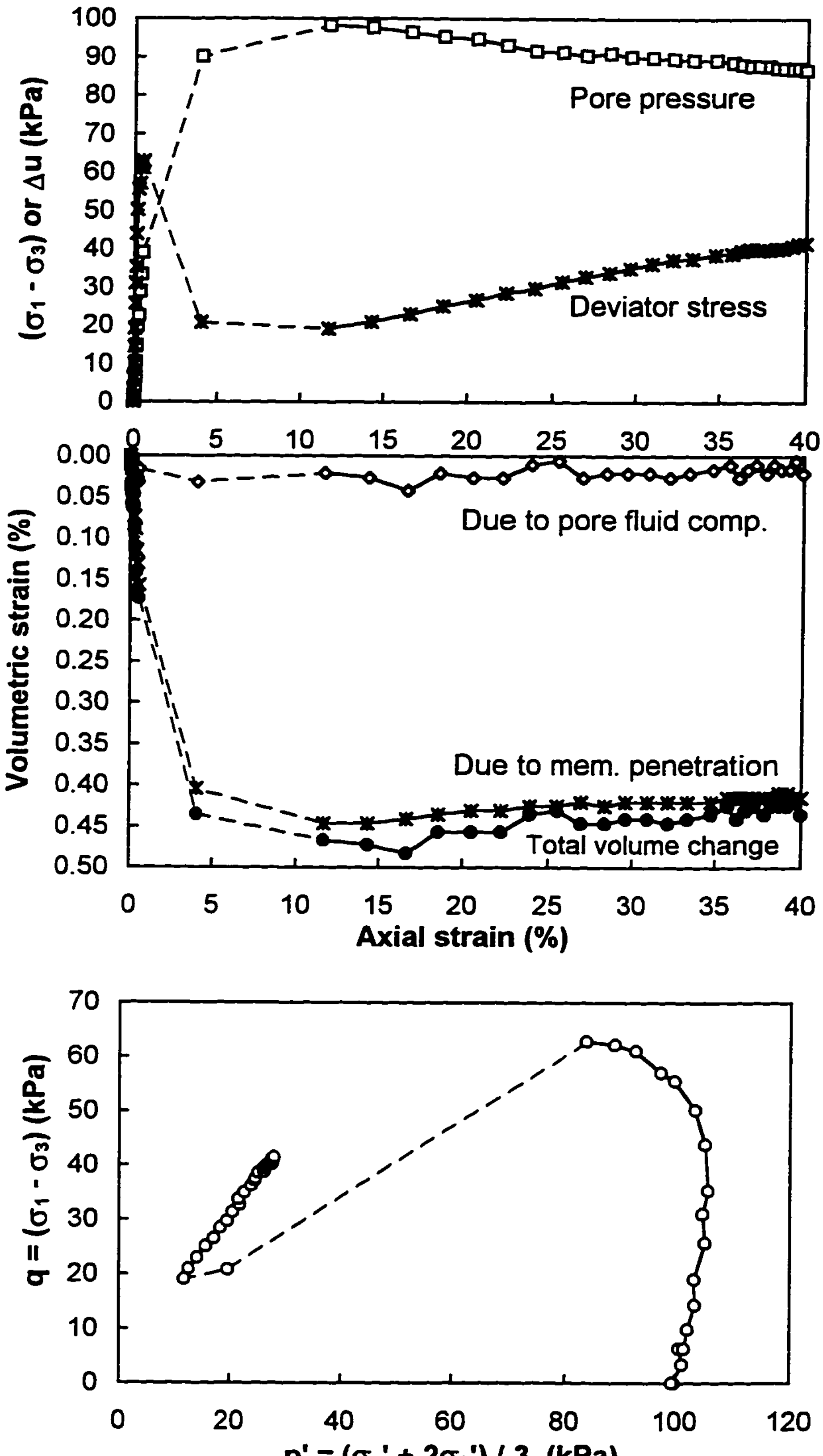

Fig. A.01 Group 1, CIU test, Dr_c = 13.9%, σ_{3c}' = 100 kPa

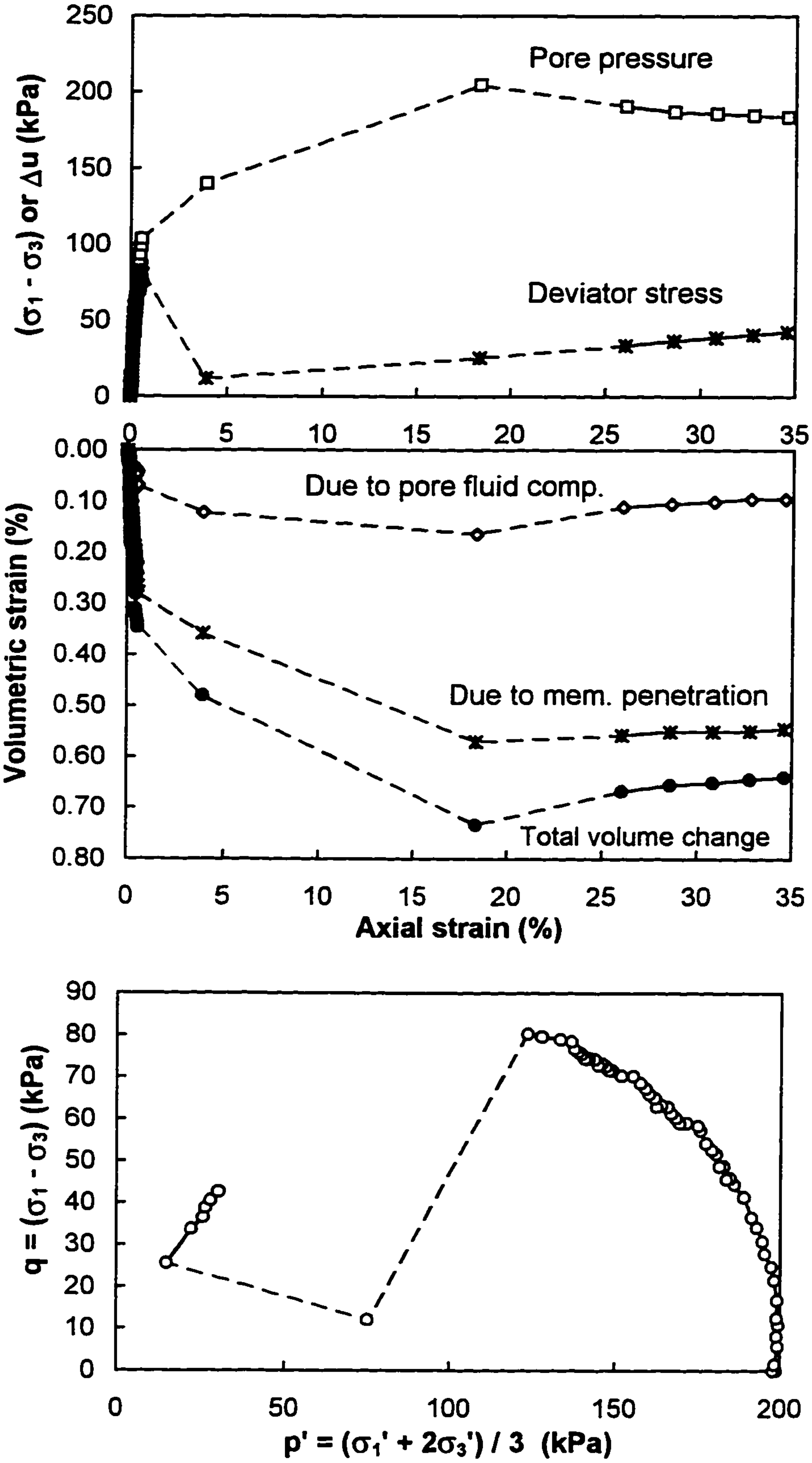

Fig. A.02 Group 1, CIU test, Dr_c = 15.5%, σ_{3c}' = 200 kPa

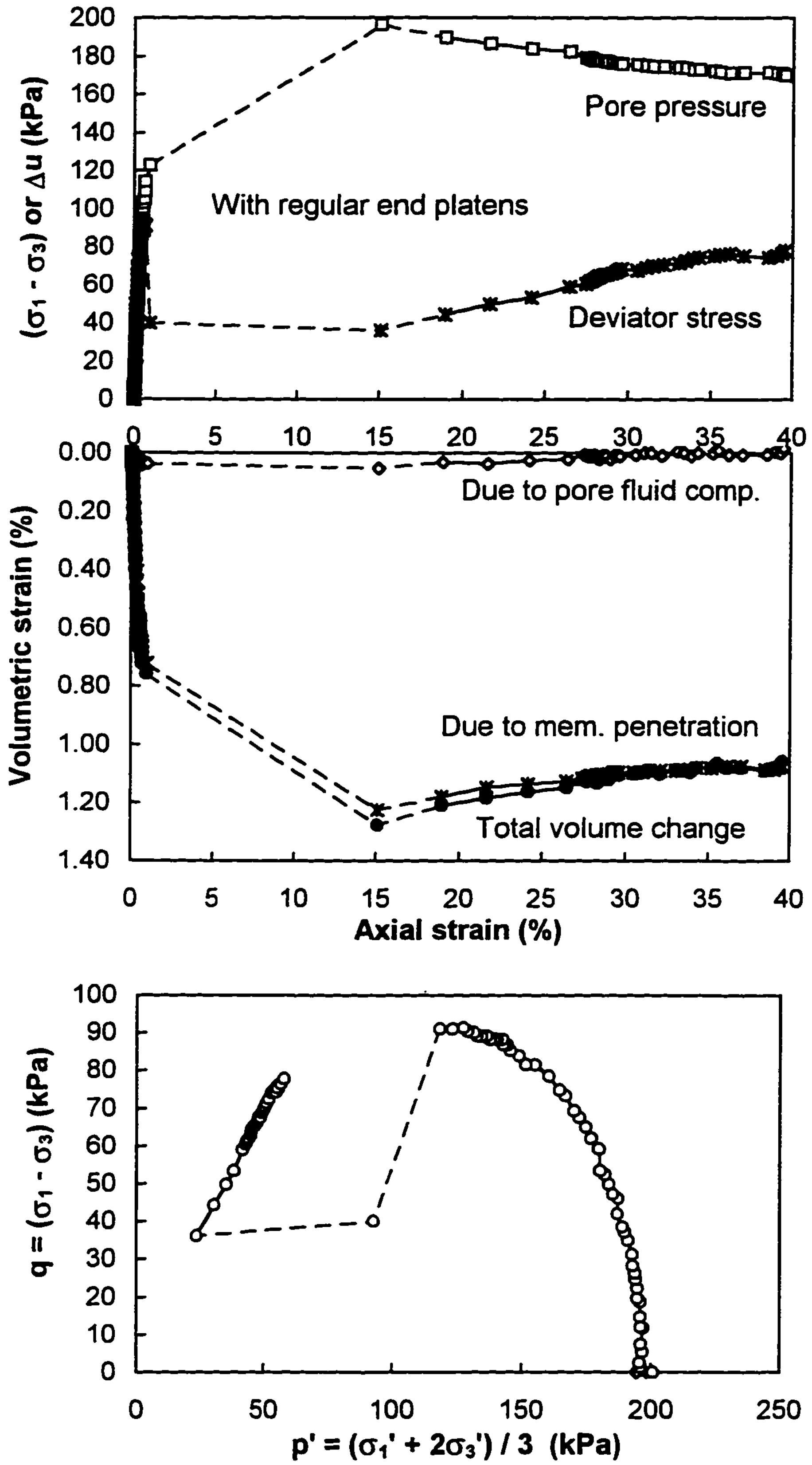

Fig. A.04 Group 1, CIU test, Dr_c = 17.7%, σ_{3c}' = 201kPa

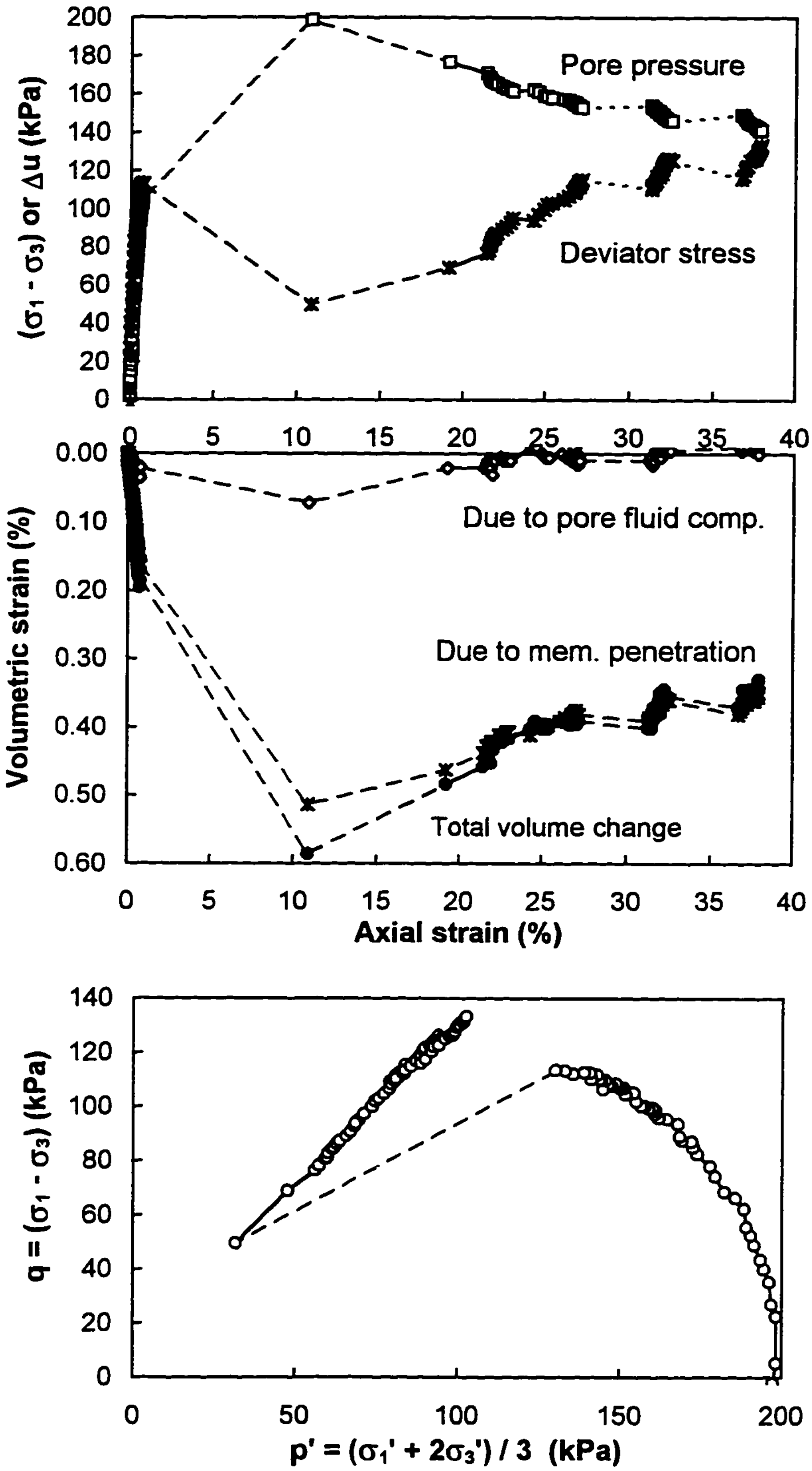

Fig. A.06 Group 1, CIU test, Dr_c = 26.7%, σ_{3c}' = 198 kPa

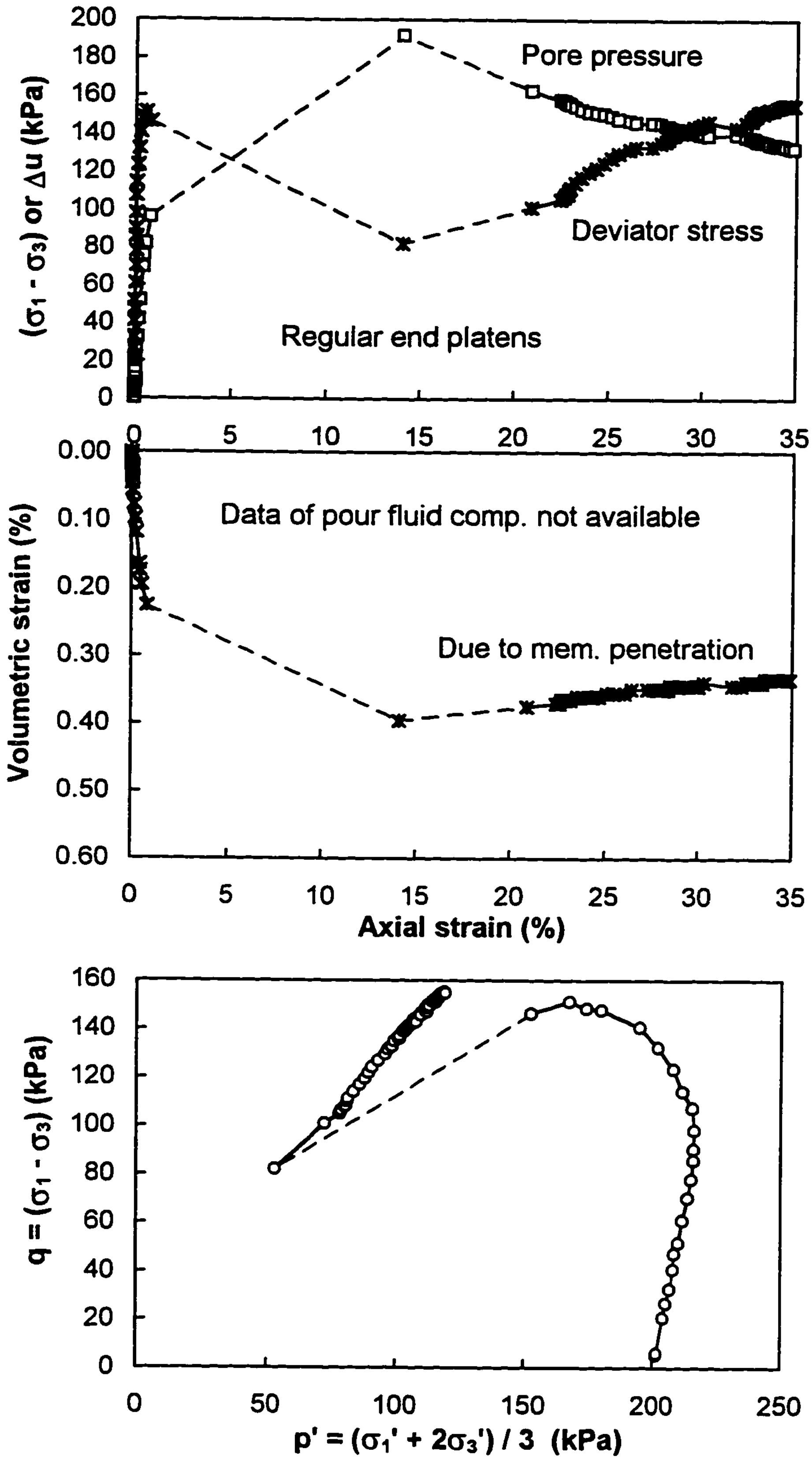

Fig. A.07 Group 1, CIU test, Dr_c = 26.7%, σ_{3c}' = 201 kPa

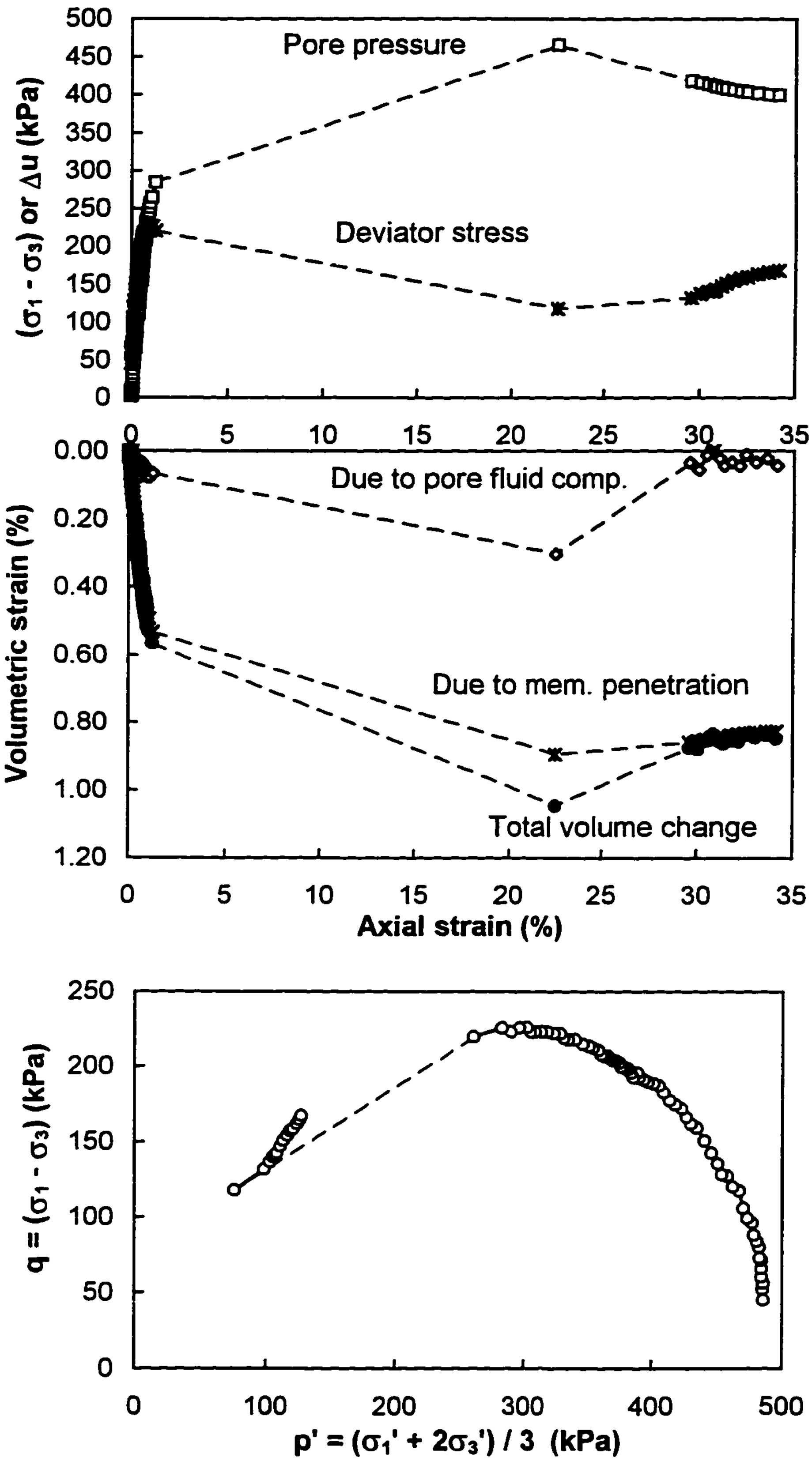

Fig. A.08 Group 1, CIU test, Dr_c = 28.5%, σ_{3c}' = 471 kPa

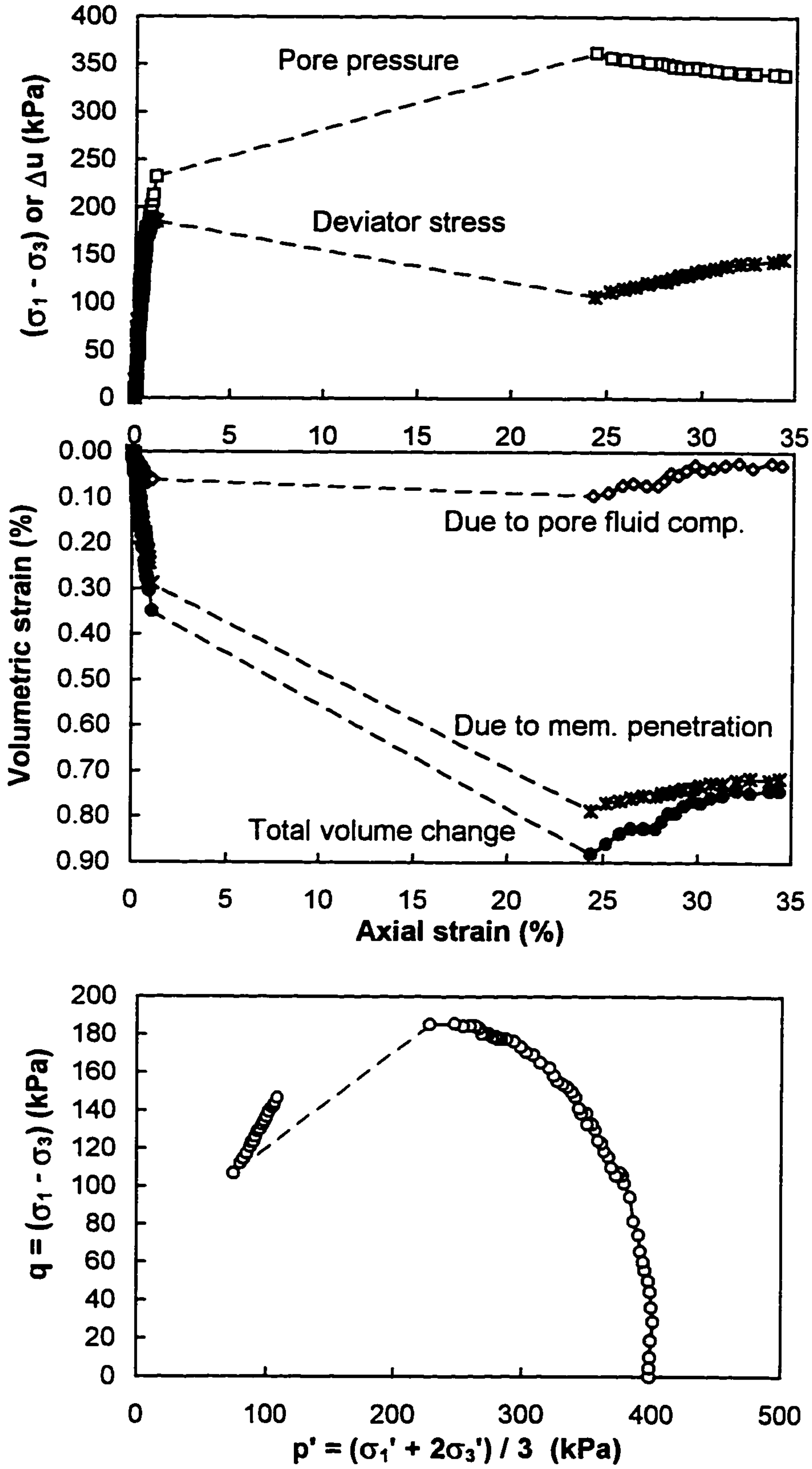

Fig. A.09 Group 1, CIU test, Dr_c = 29.3%, σ_{3c}' = 398 kPa

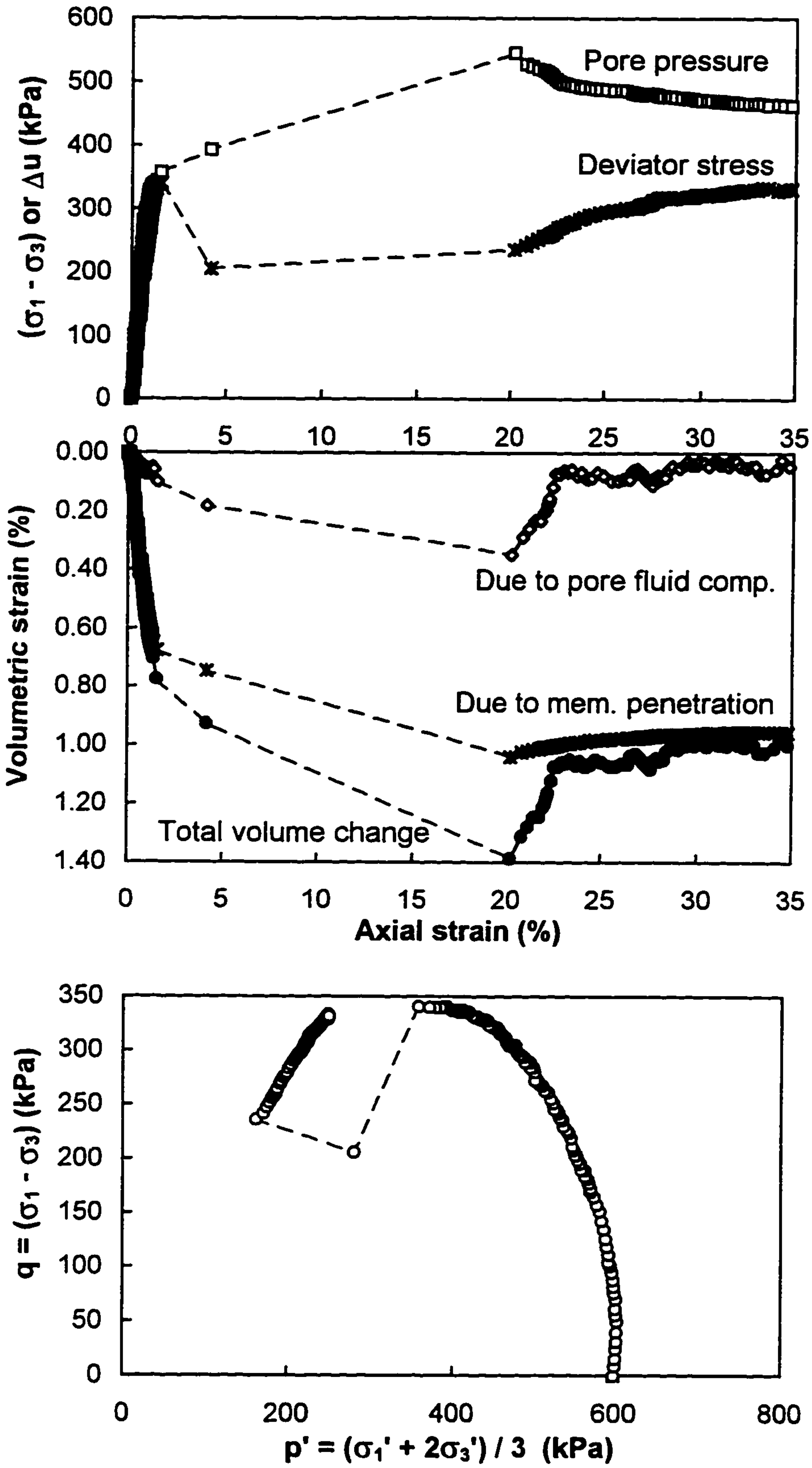

Fig. A.10 Group 1, CIU test, Dr_c = 37.5%, σ_{3c}' = 601 kPa

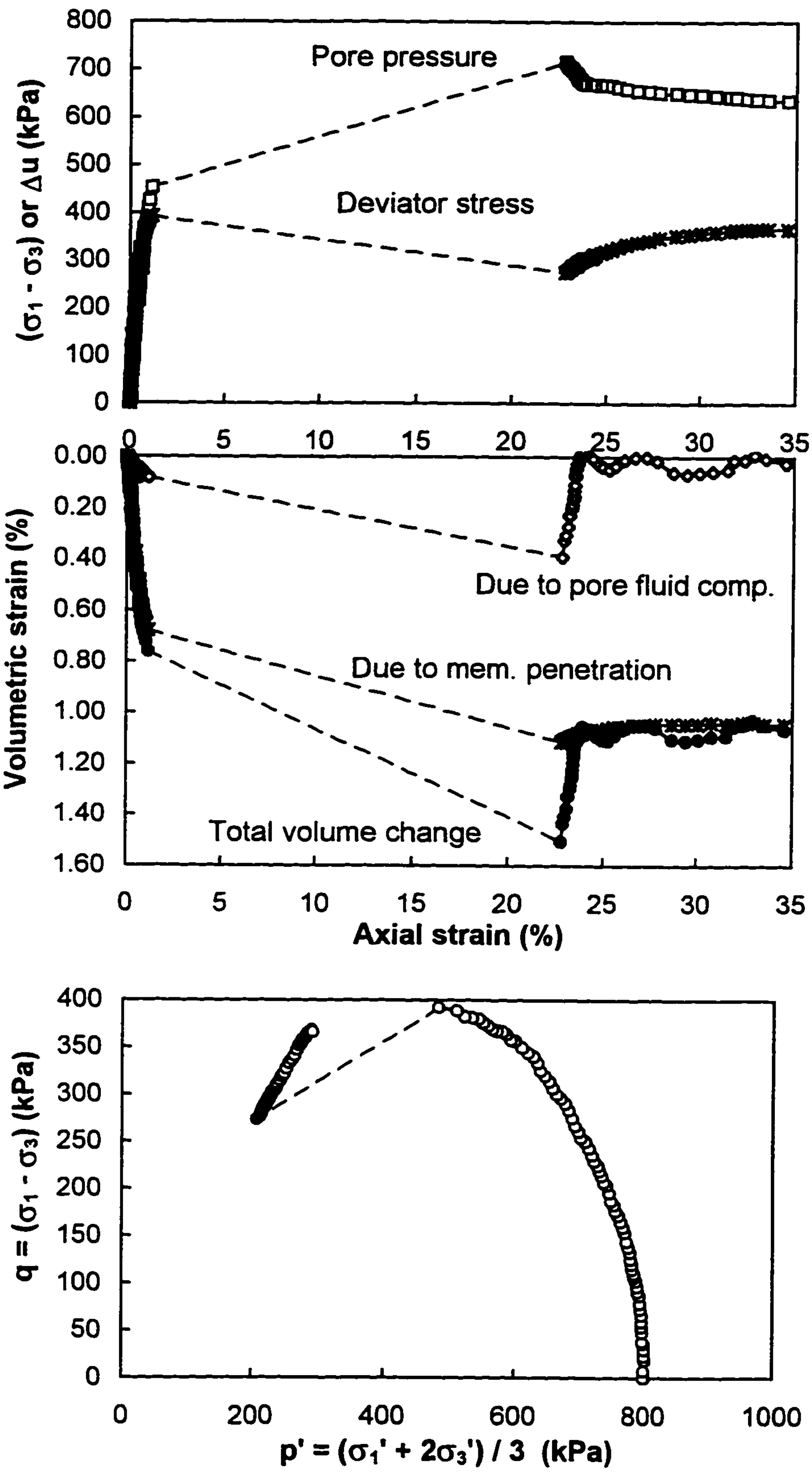

Fig. A.11 Group 1, CIU test, Dr_c = 39.6%, σ_{3c}' = 806 kPa

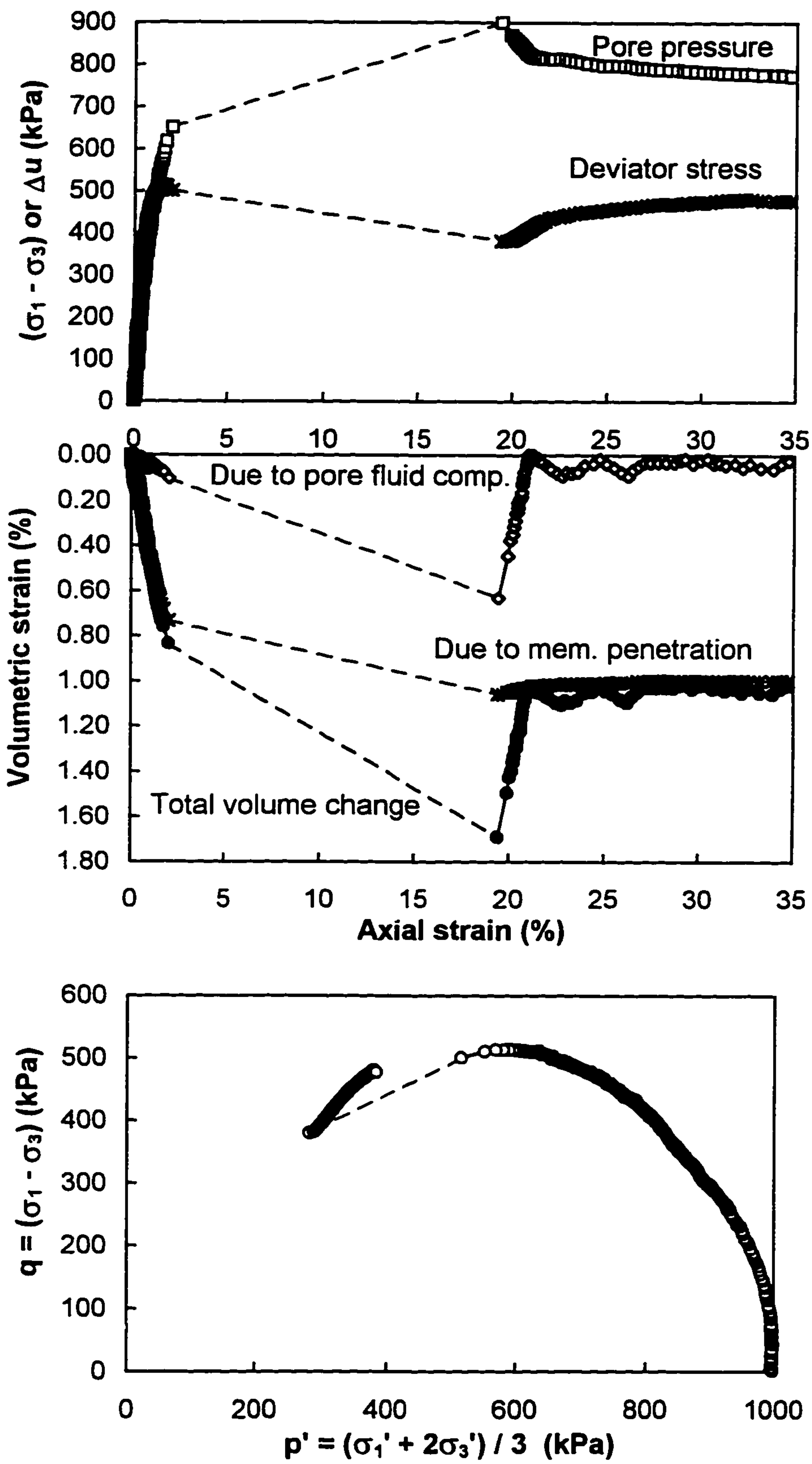

Fig. A.12 Group 1, CIU test, Dr_c = 41.4%, σ_{3c}' = 997 kPa

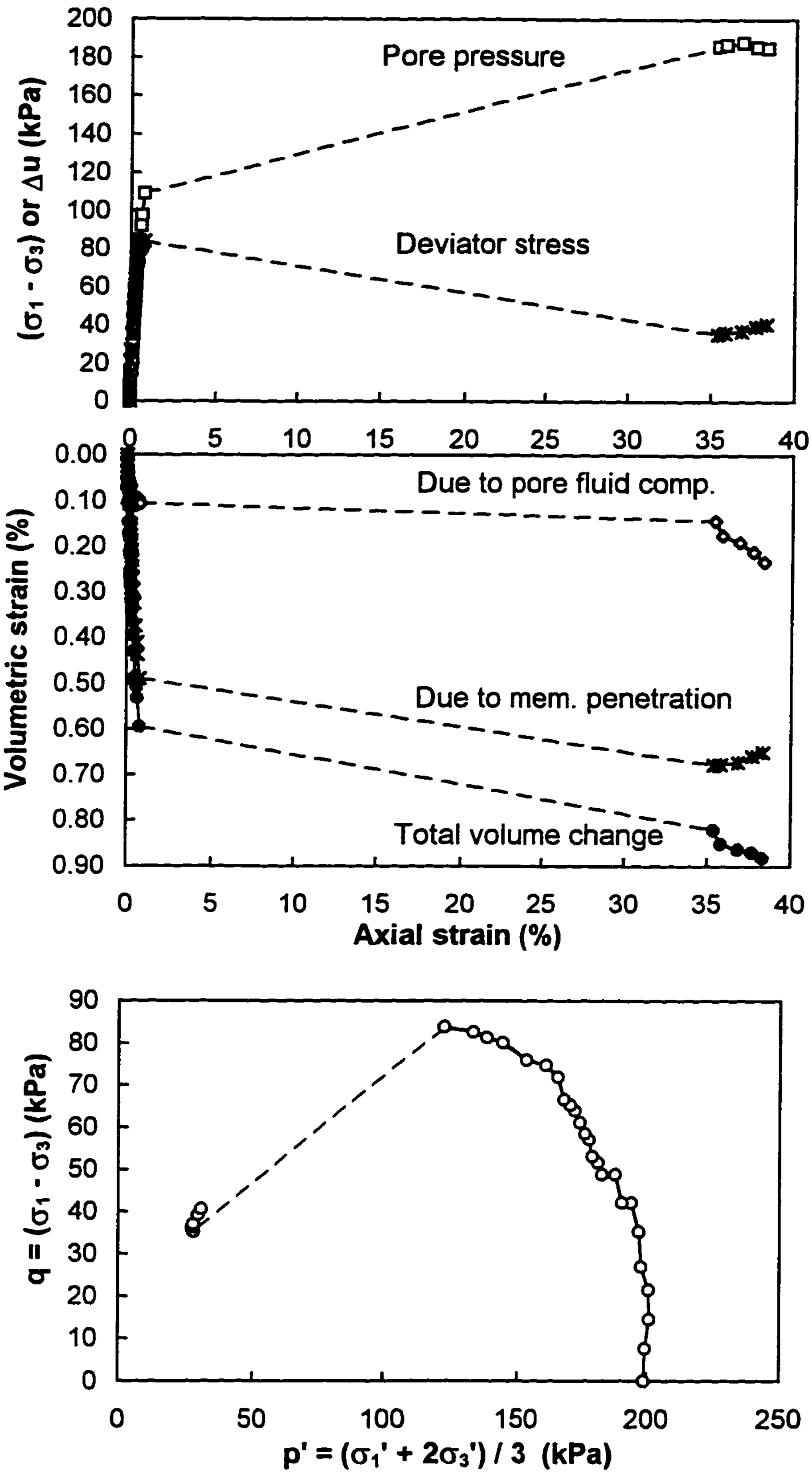

Fig. A.14 Group 1, CIU test, $Dr_c = 21.1\%$, $\sigma_{3c}' = 200$ kPa

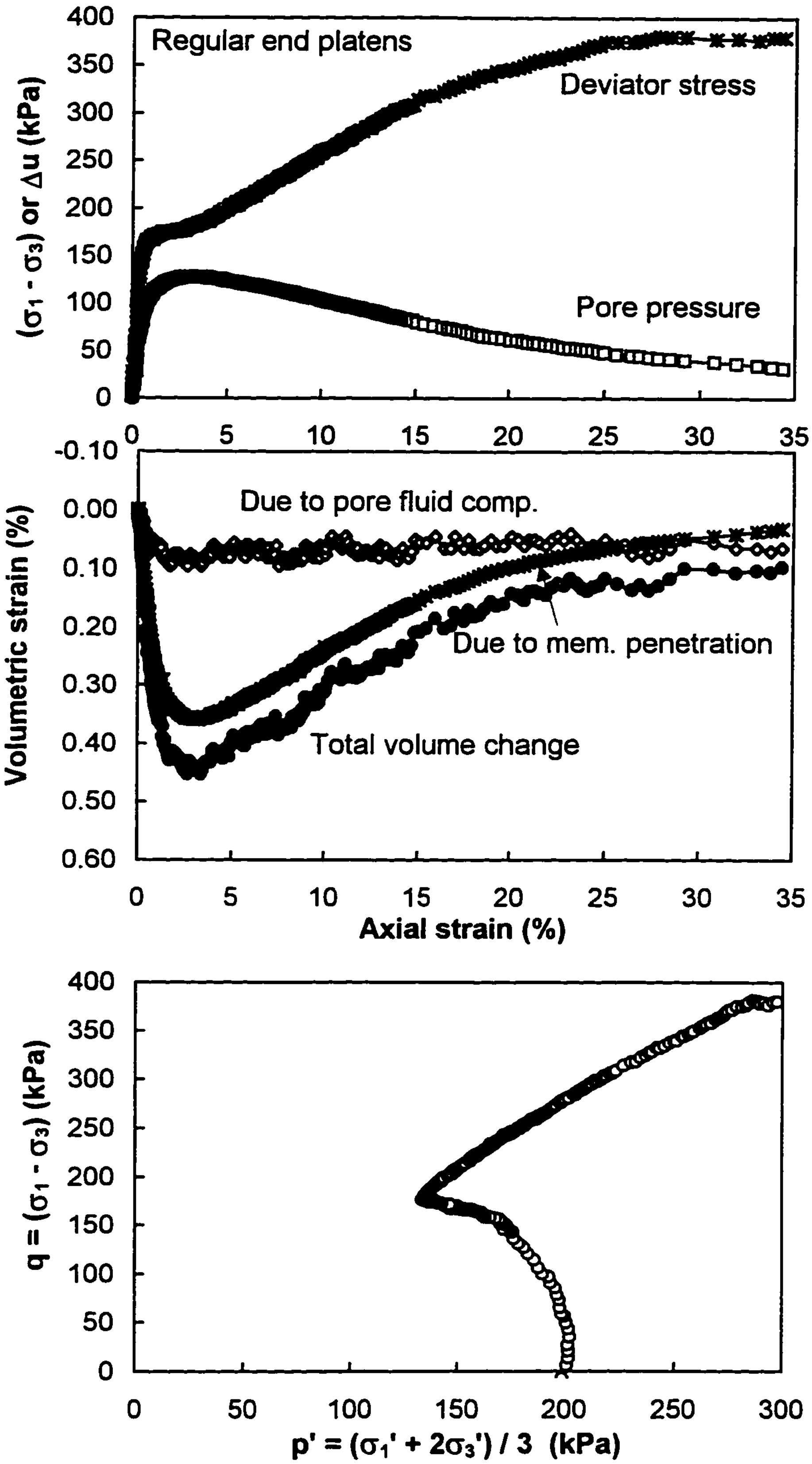

Fig. A.16 Group 1, CIU test, Dr_c = 35.4%, σ_{3c}' = 201 kPa

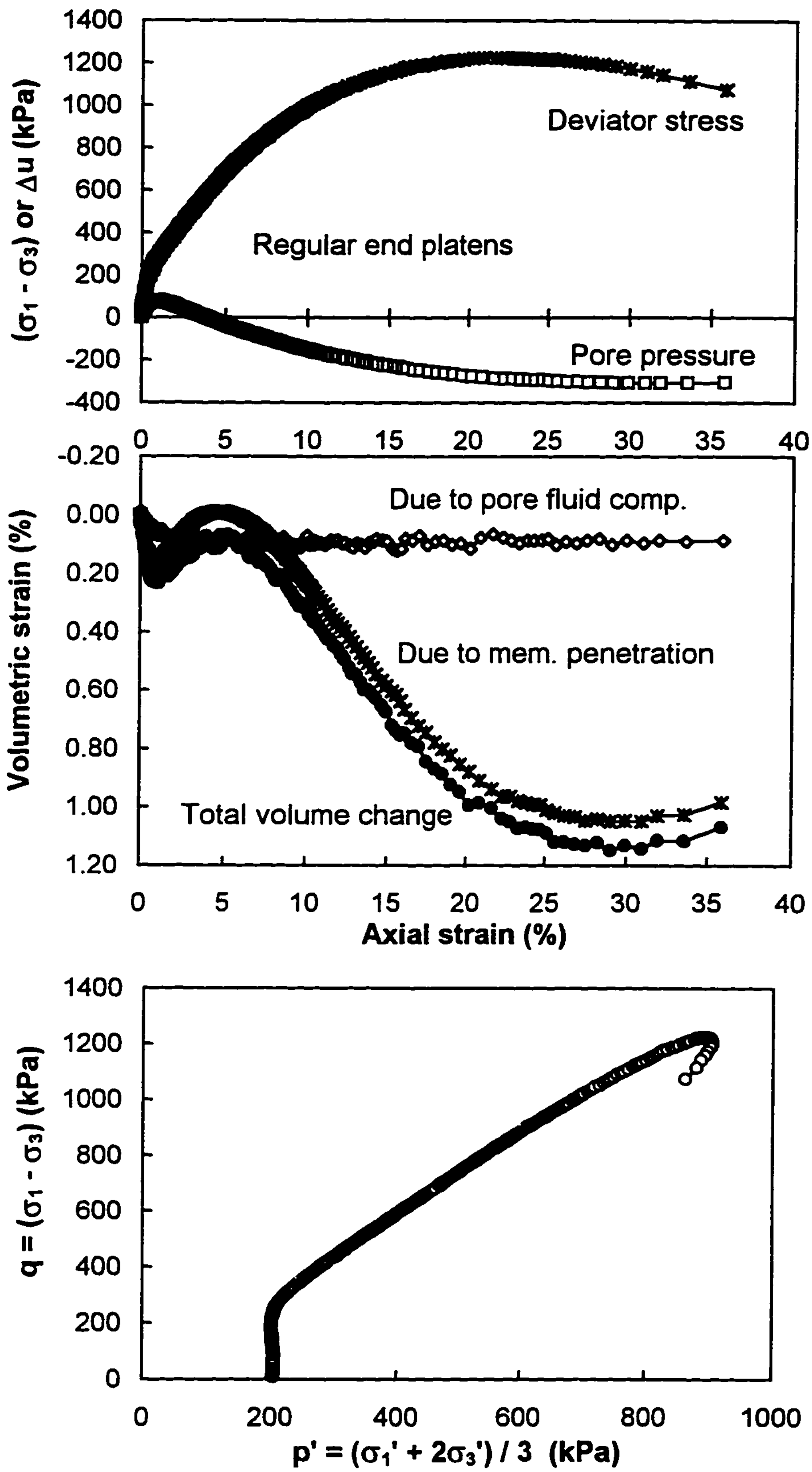

Fig. A.19 Group 1, CIU test, Dr_c = 69.8%, σ_{3c}' = 201 kPa

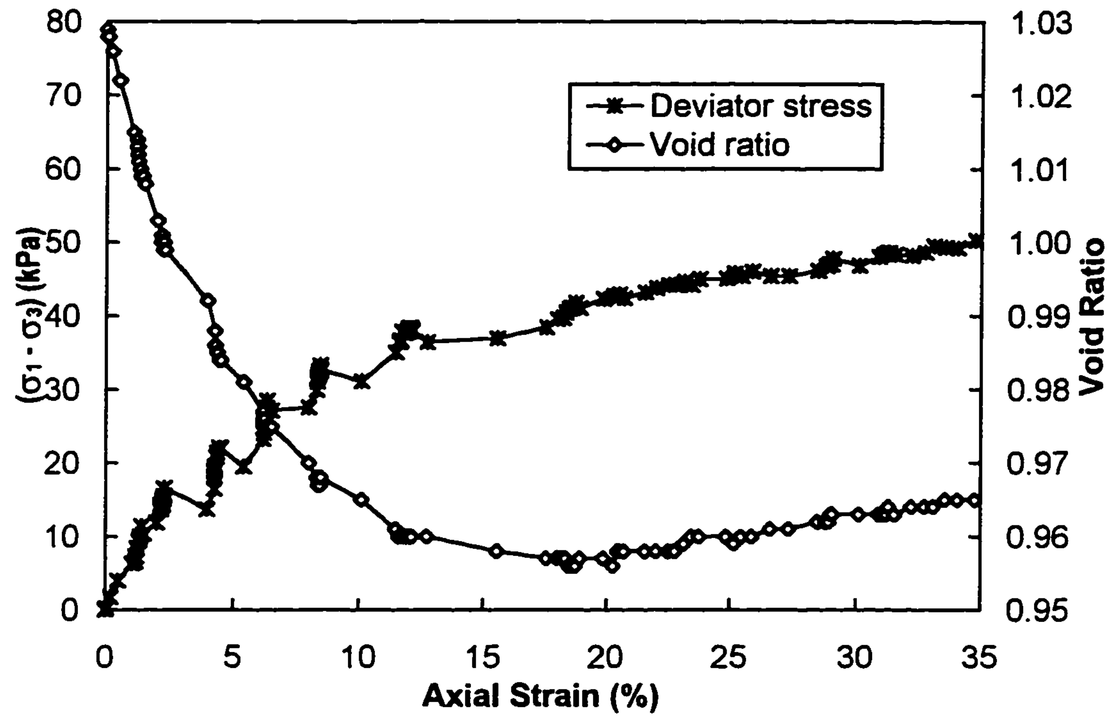

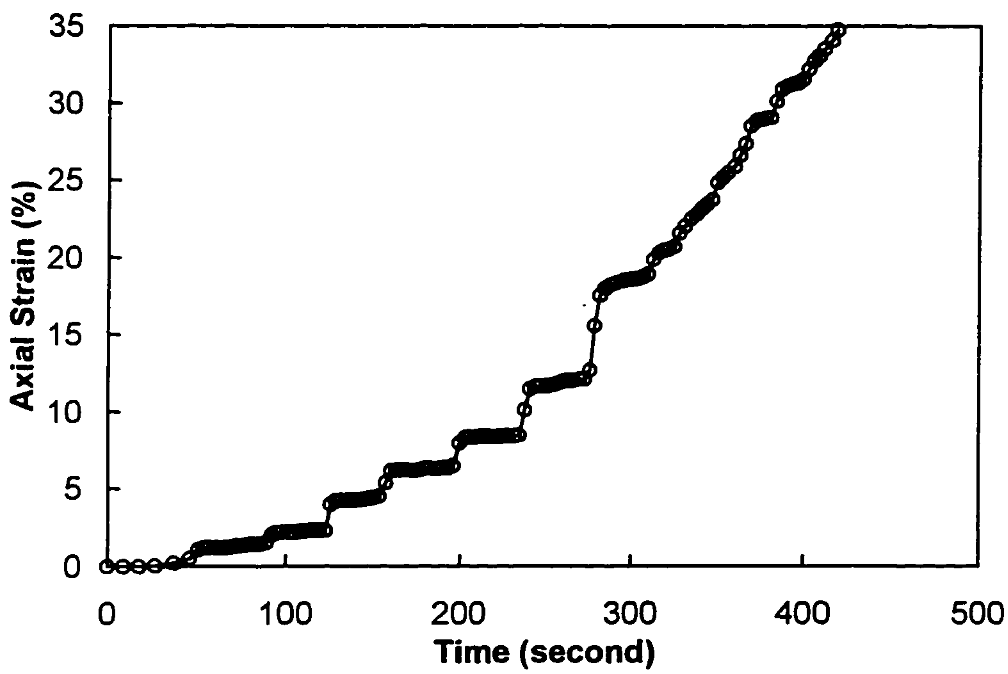

Fig. A.20 Group 1, CD test, Dr_c = 2.4%, σ_{3c}' = 10 kPa

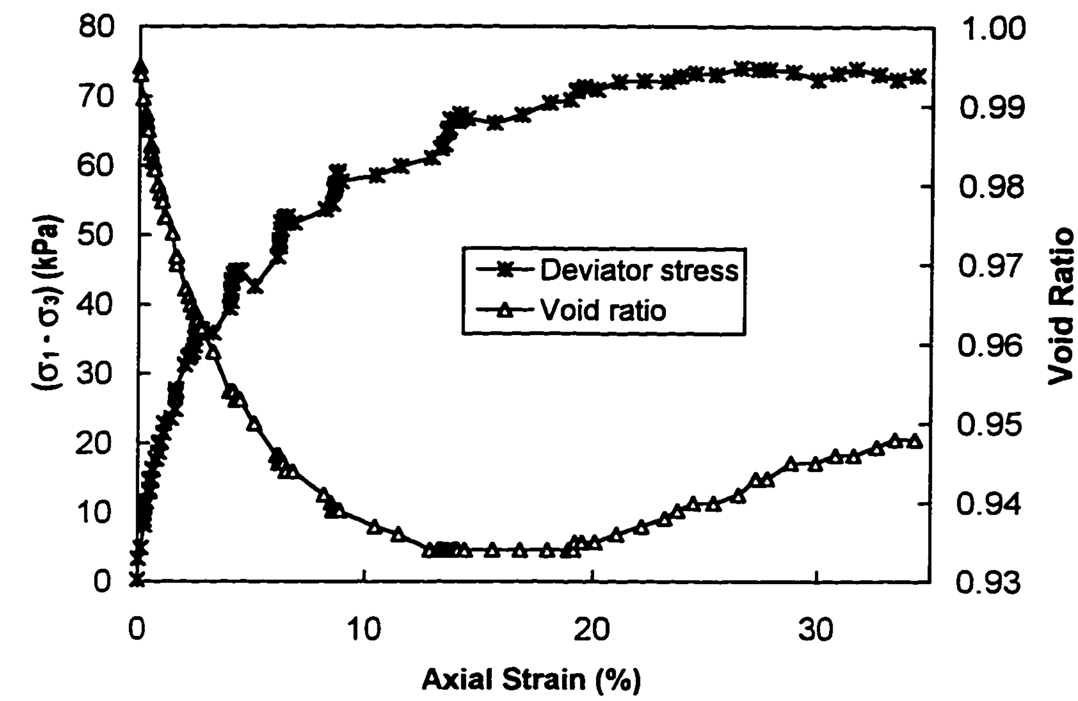

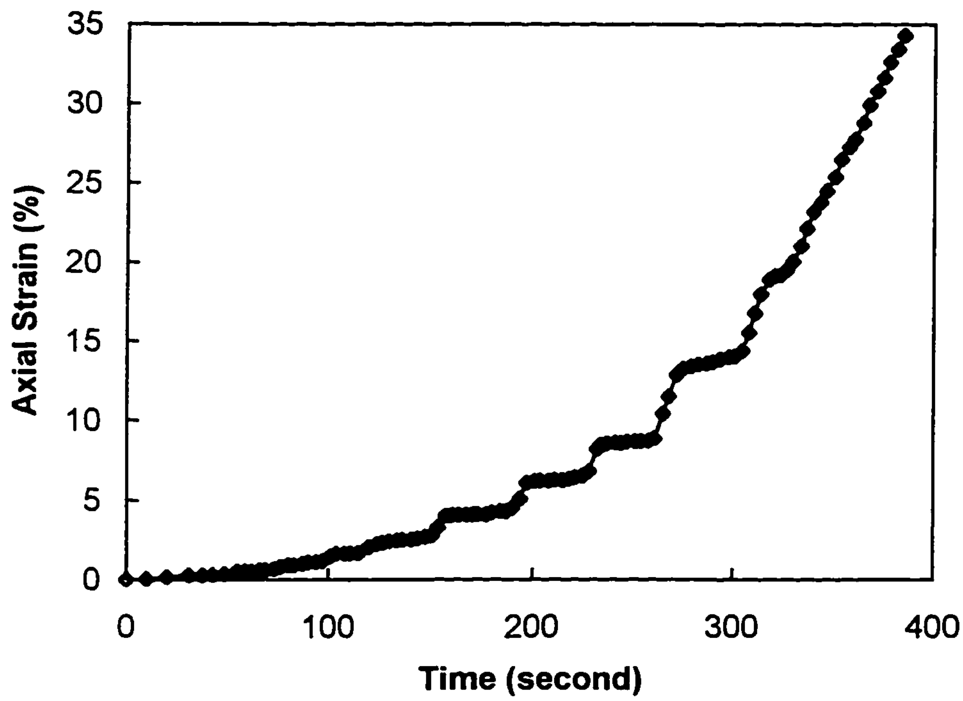

Fig. A.21 Group 1, CD test, Drc = 11.2%, σ_{3c}' = 20 kPa

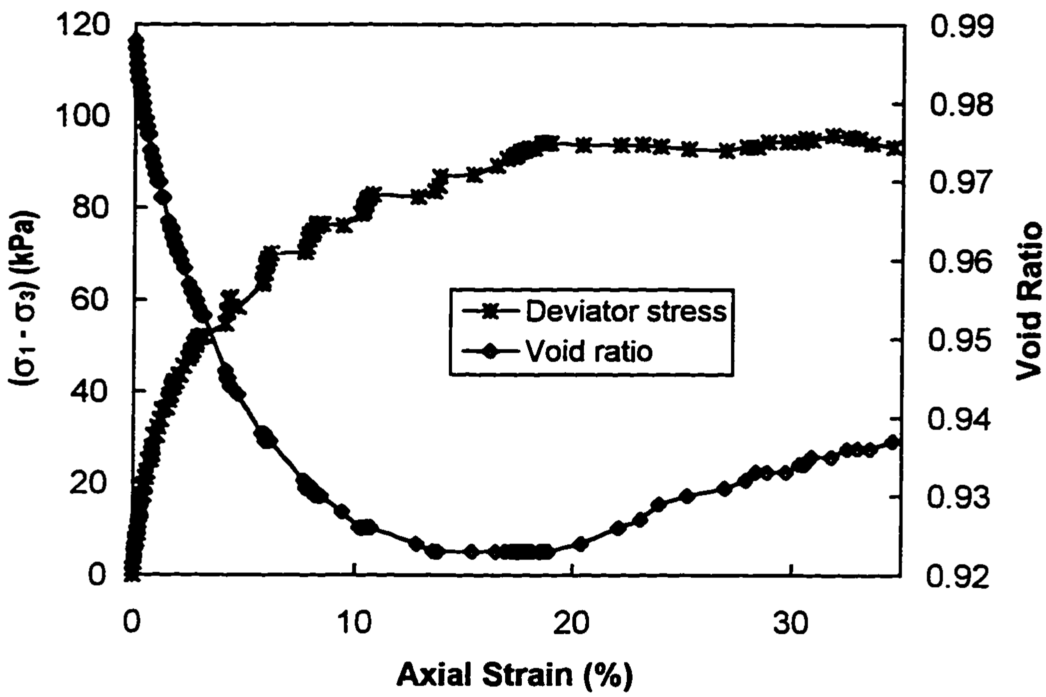

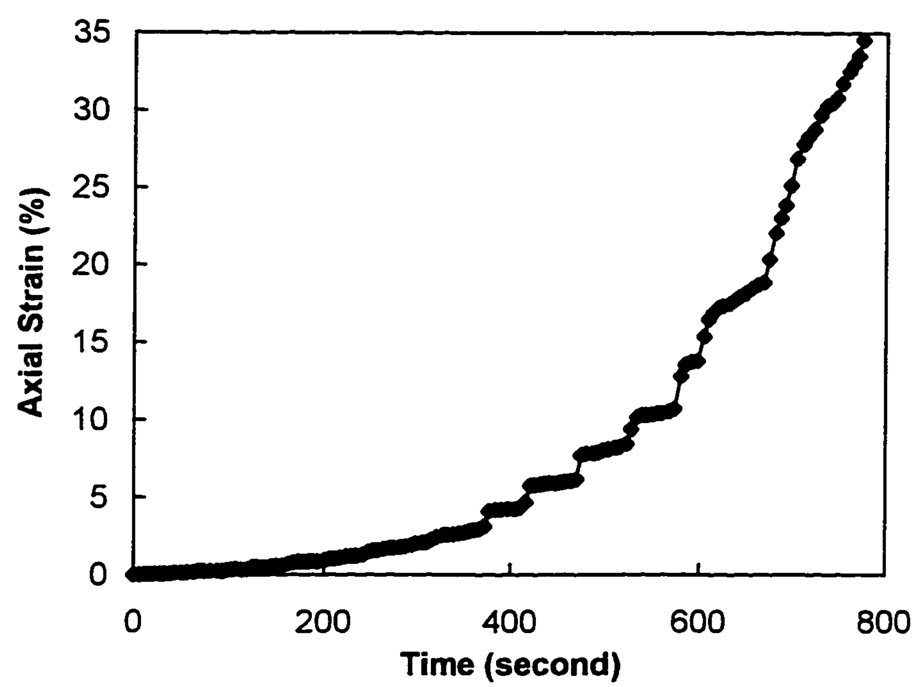

Fig. A.22 Group 1, CD test, Drc = 13.1%, σ_{3c}' = 30 kPa

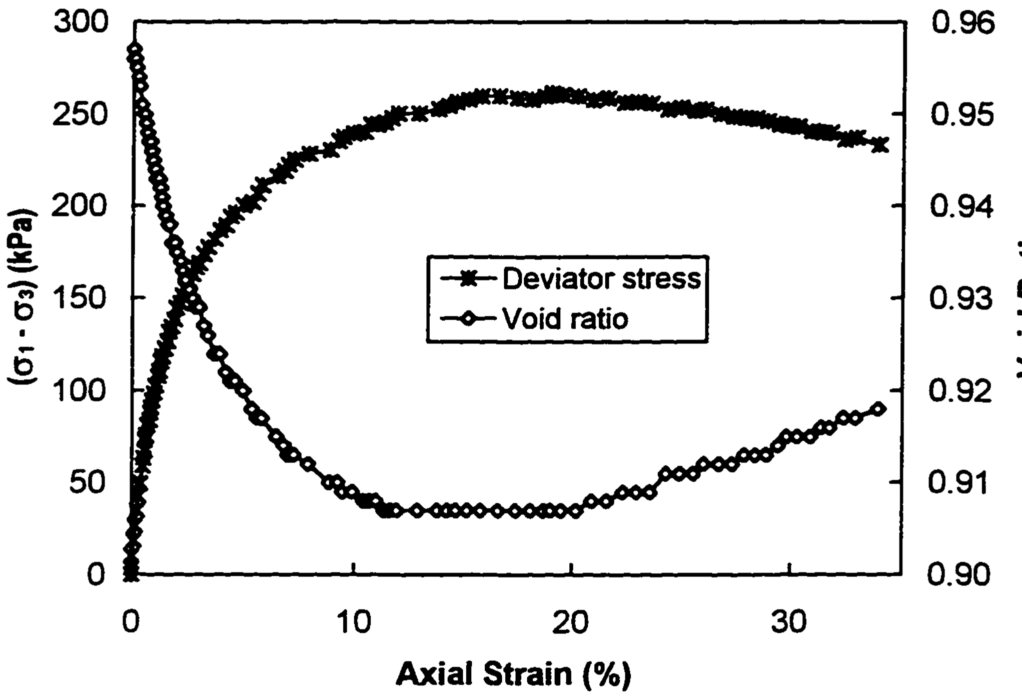

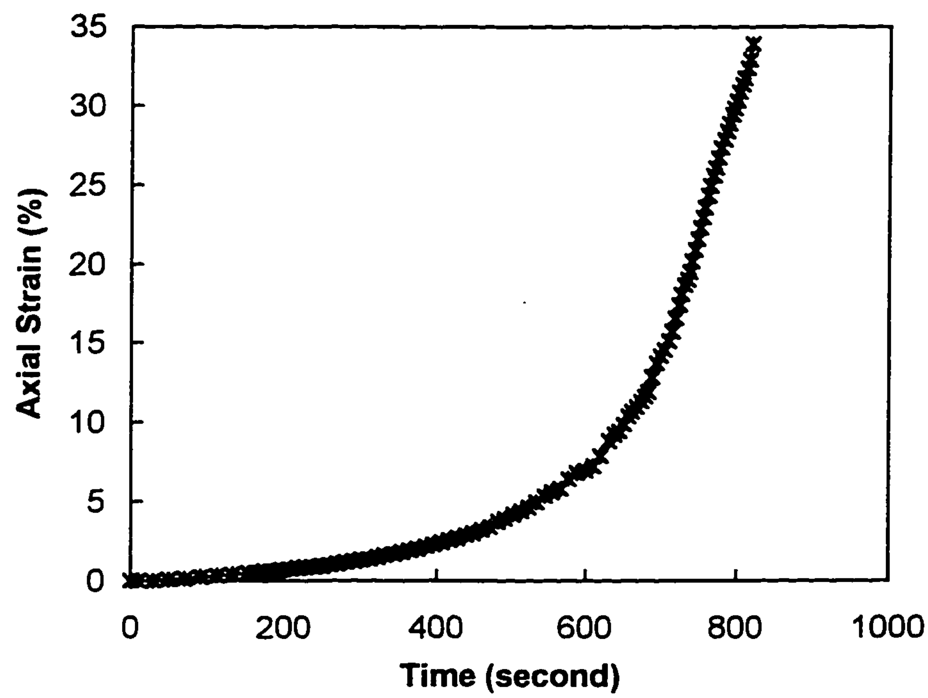

Fig. A.24 Group 1, CD test, Dr_c = 19.3%, σ_{3c}' = 100 kPa

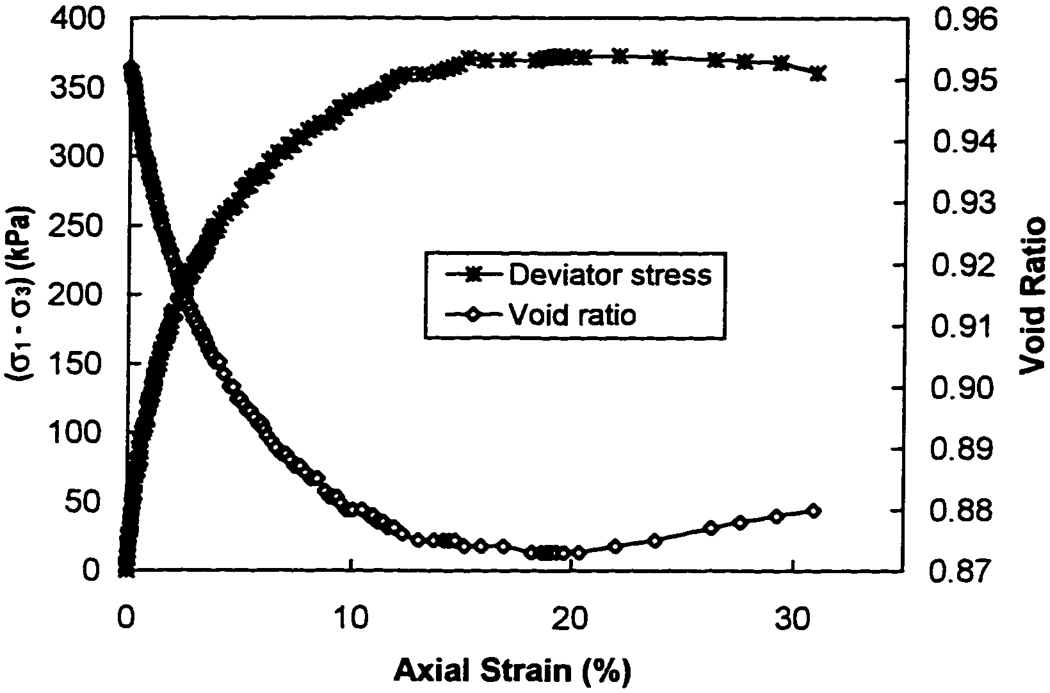

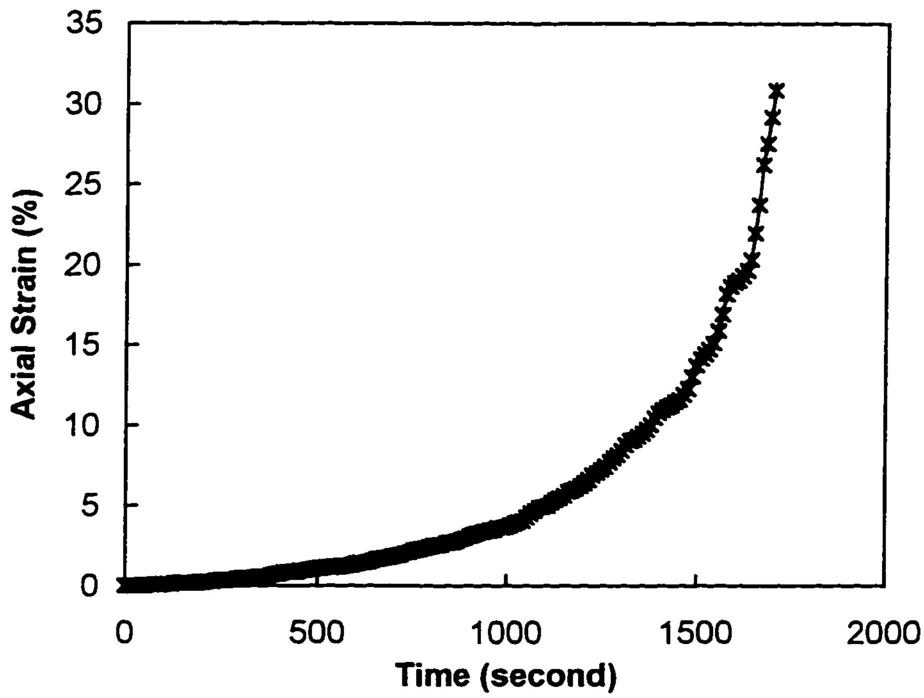

Fig. A.25 Group 1, CD test, Dr_c = 22.3%, σ_{3c}' = 10 kPa

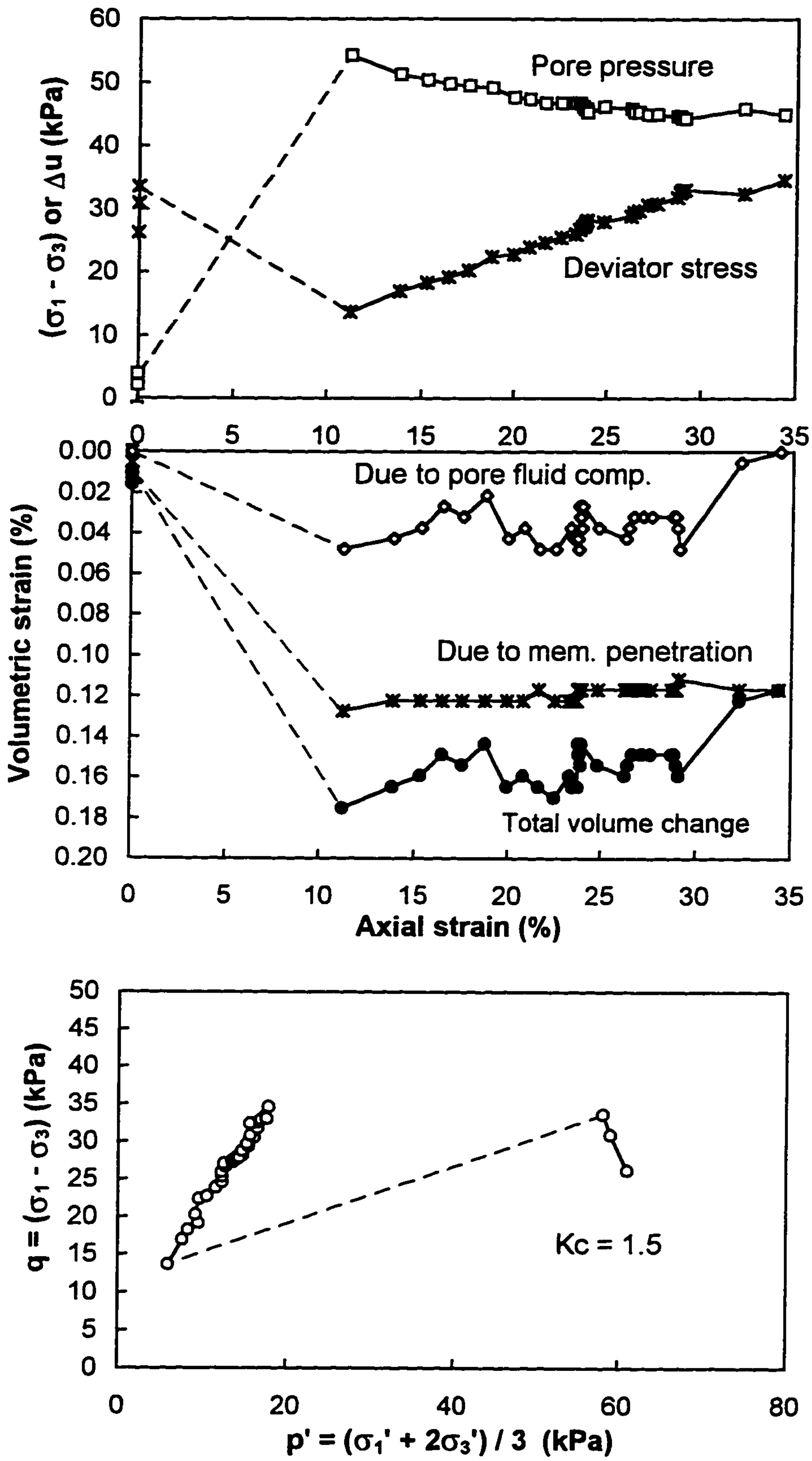

Fig. A.27 Group 2, CAU test, Dr_c = 27.8%, σ_{3c}' = 52 kPa

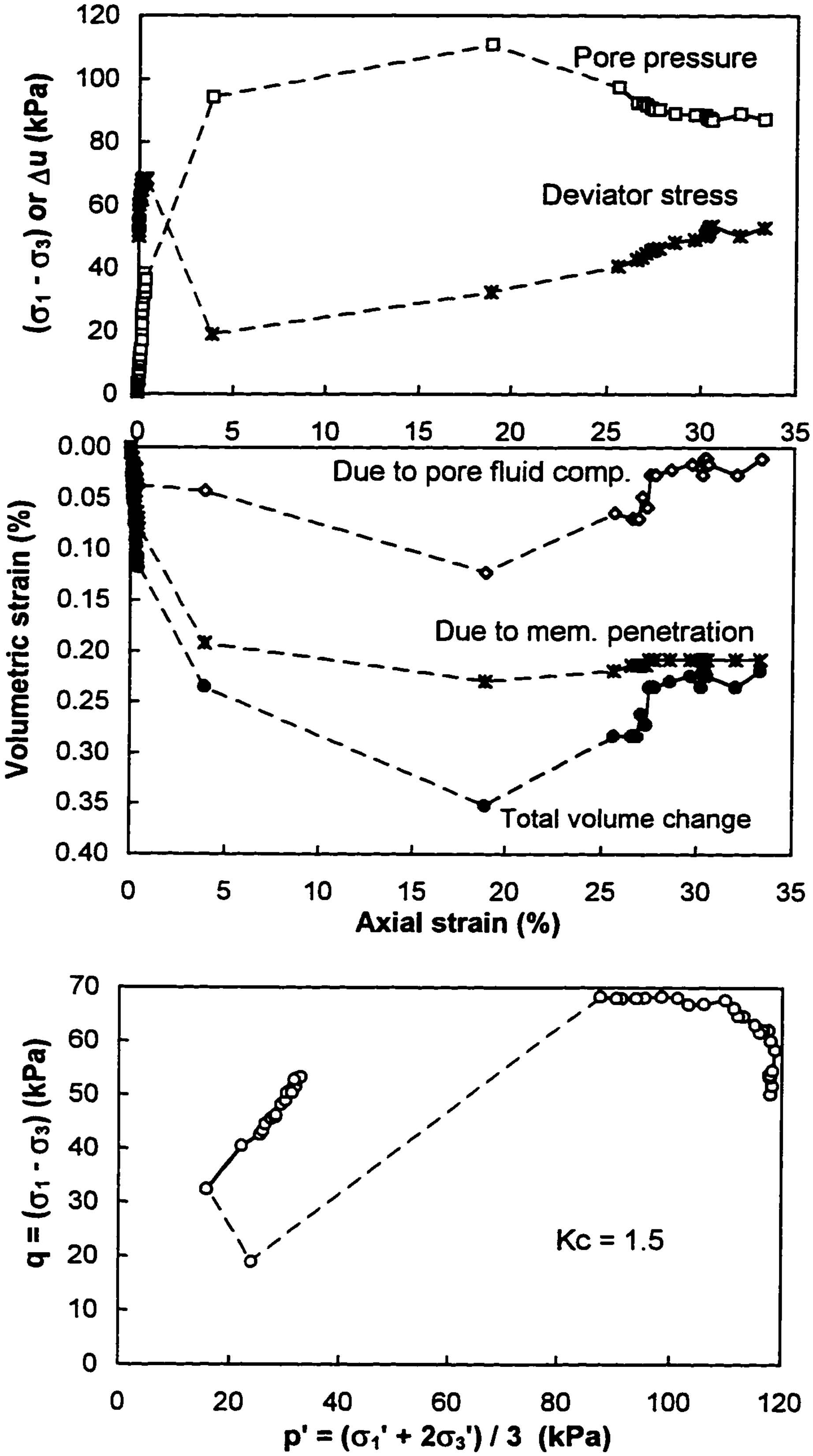

Fig. A.28 Group 2, CAU test, Dr_c = 30.4%, σ_{3c}' = 101 kPa

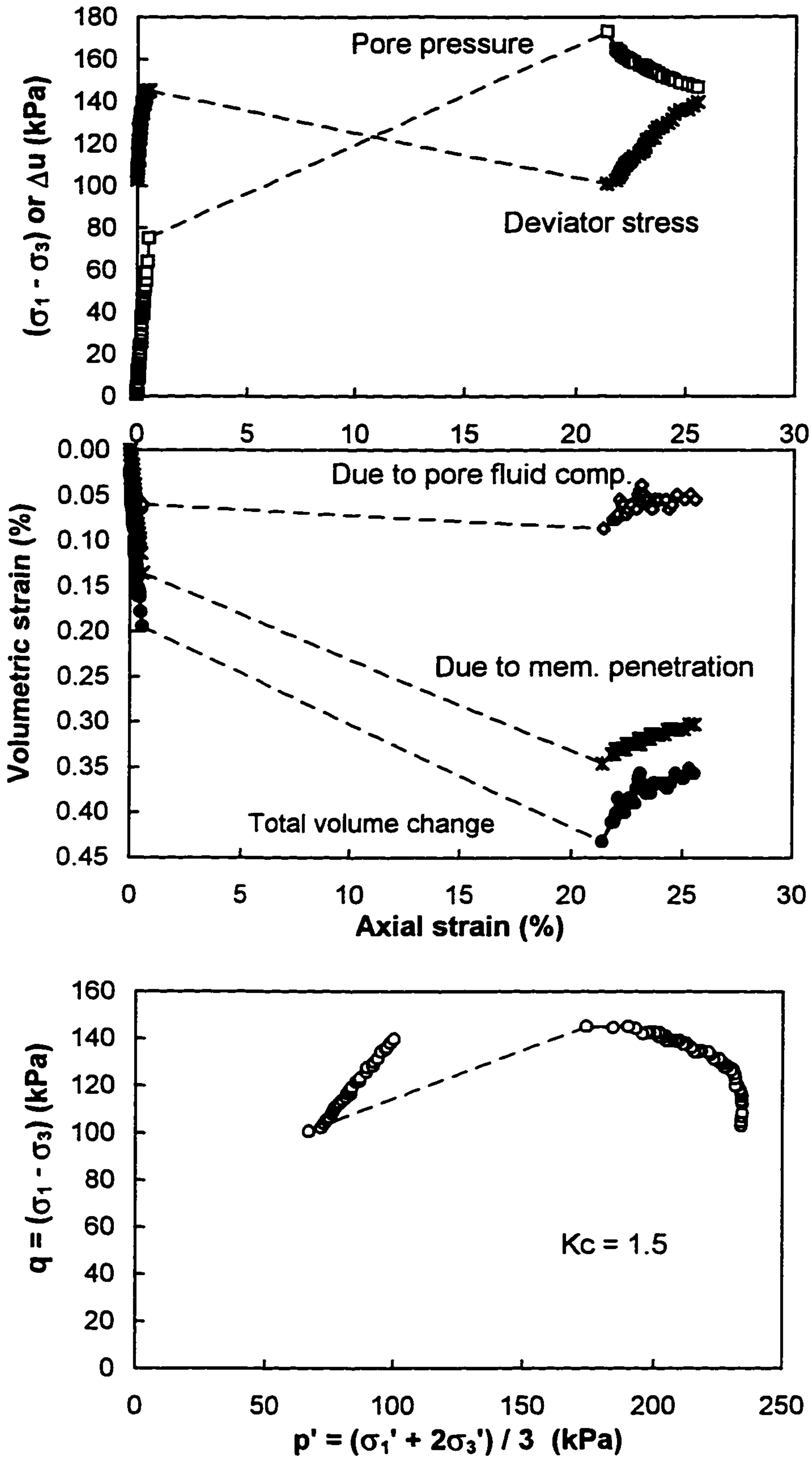

Fig. A.29 Group 2, CAU test, Dr_c = 36.5%, σ_{3c}' = 200 kPa

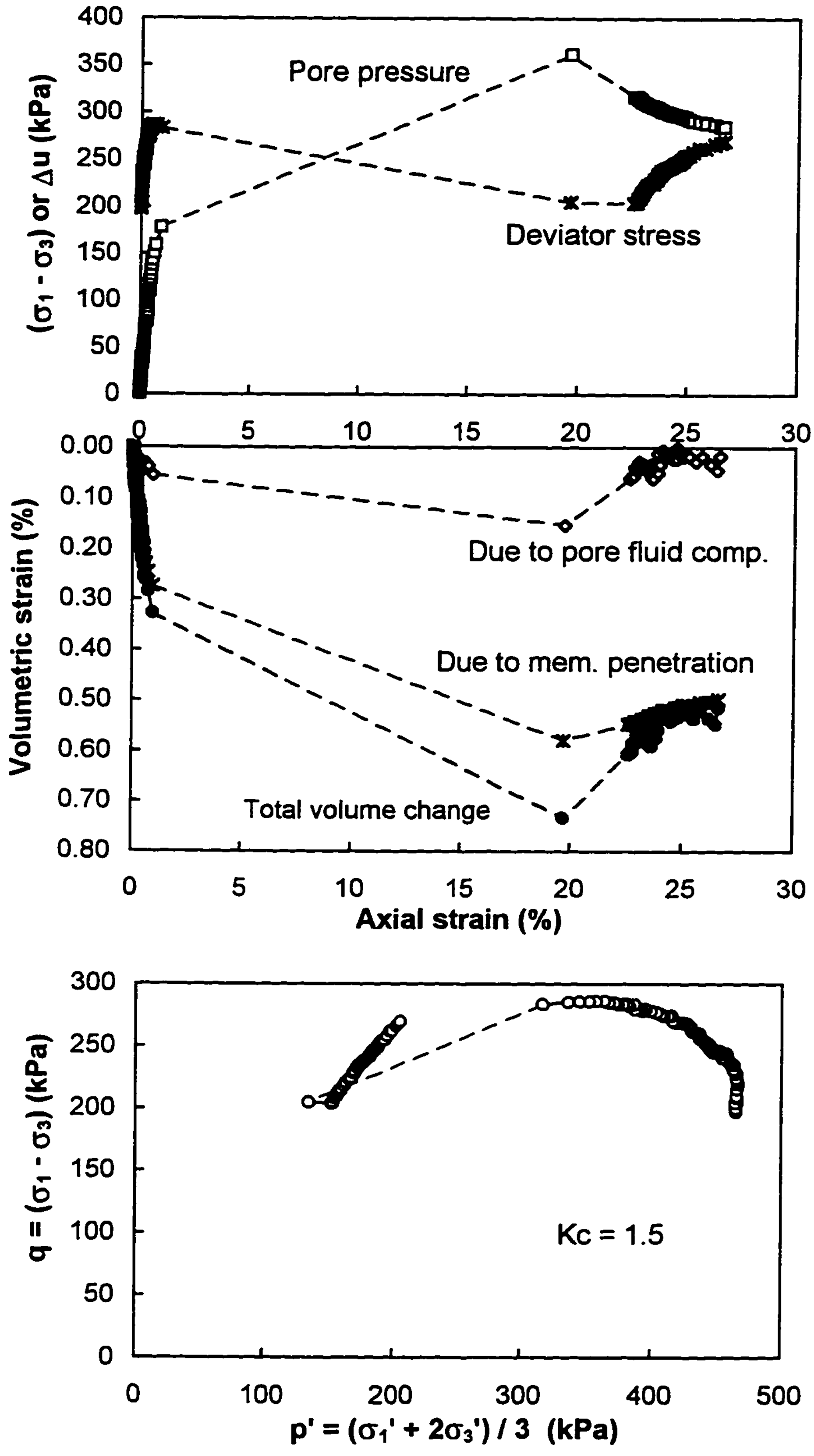

Fig. A.30 Group 2, CAU test, Dr_c = 42.7%, σ_{3c}' = 400 kPa

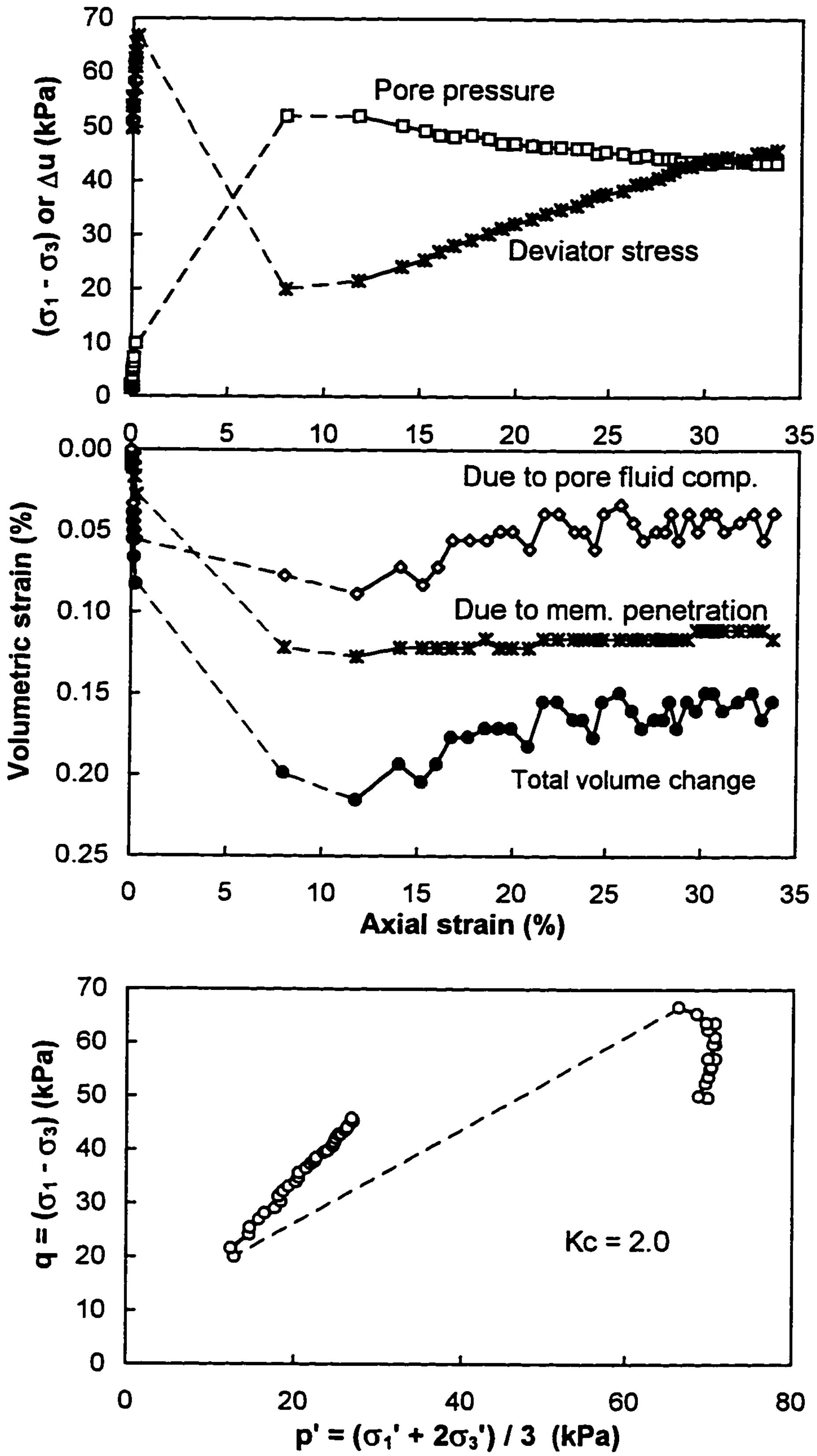

Fig. A.31 Group 2, CAU test, Dr_c = 27.4%, σ_{3c}' = 53 kPa

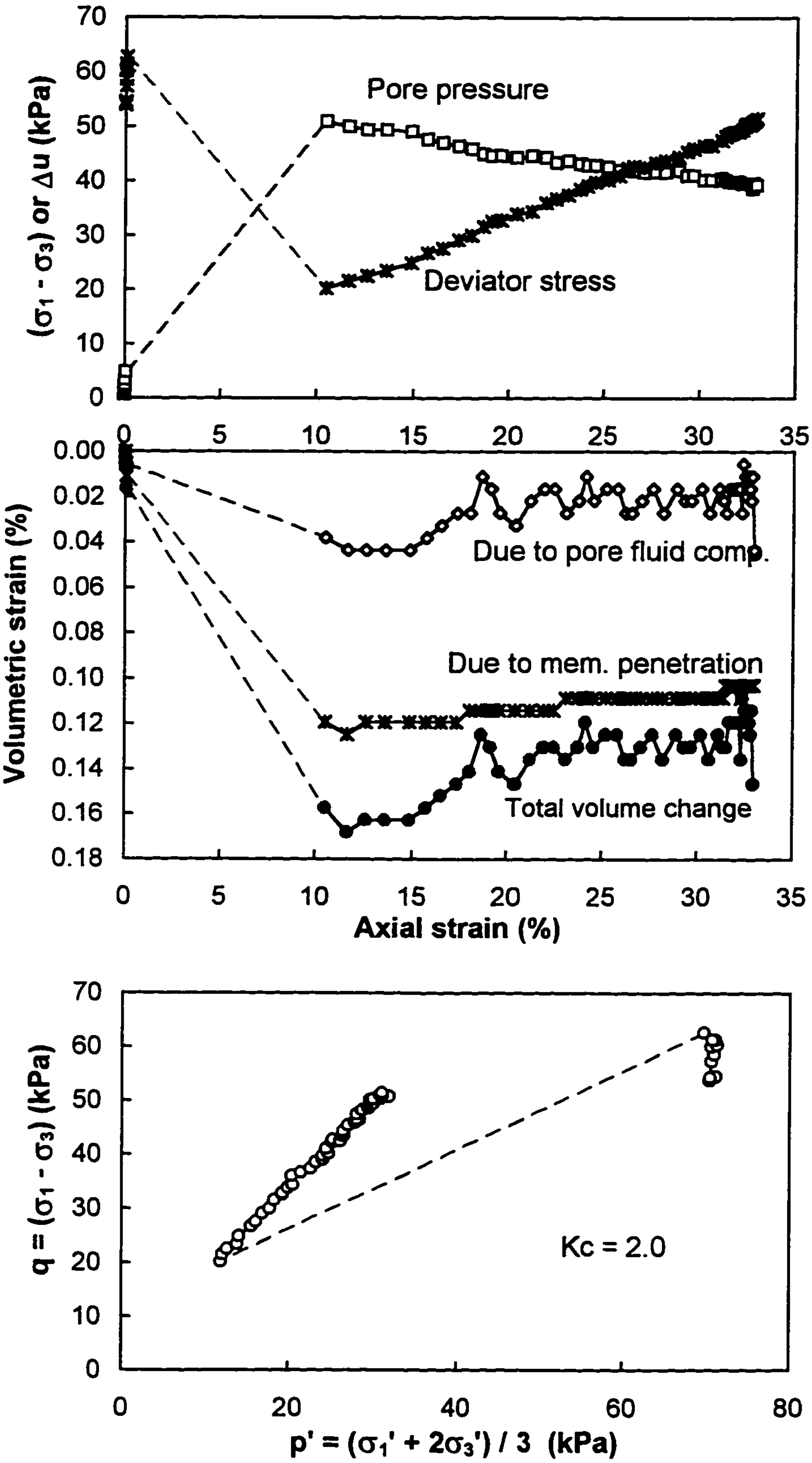

Fig. A.32 Group 2, CAU test, Dr_c = 28.5%, σ_{3c}' = 53 kPa

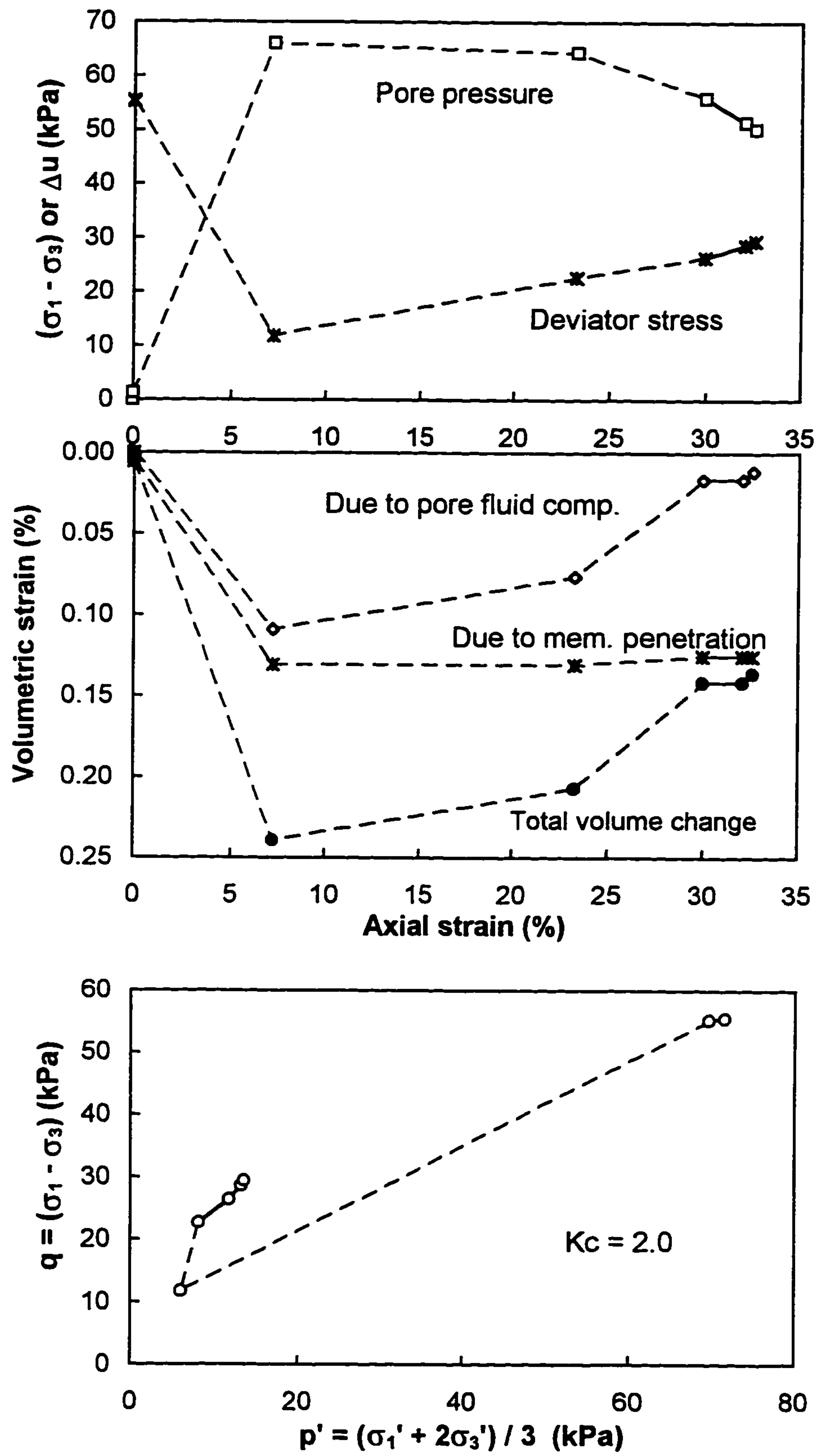

Fig. A.33 Group 2, CAU test, Dr_c = 30.4%, σ_{3c}' = 53 kPa

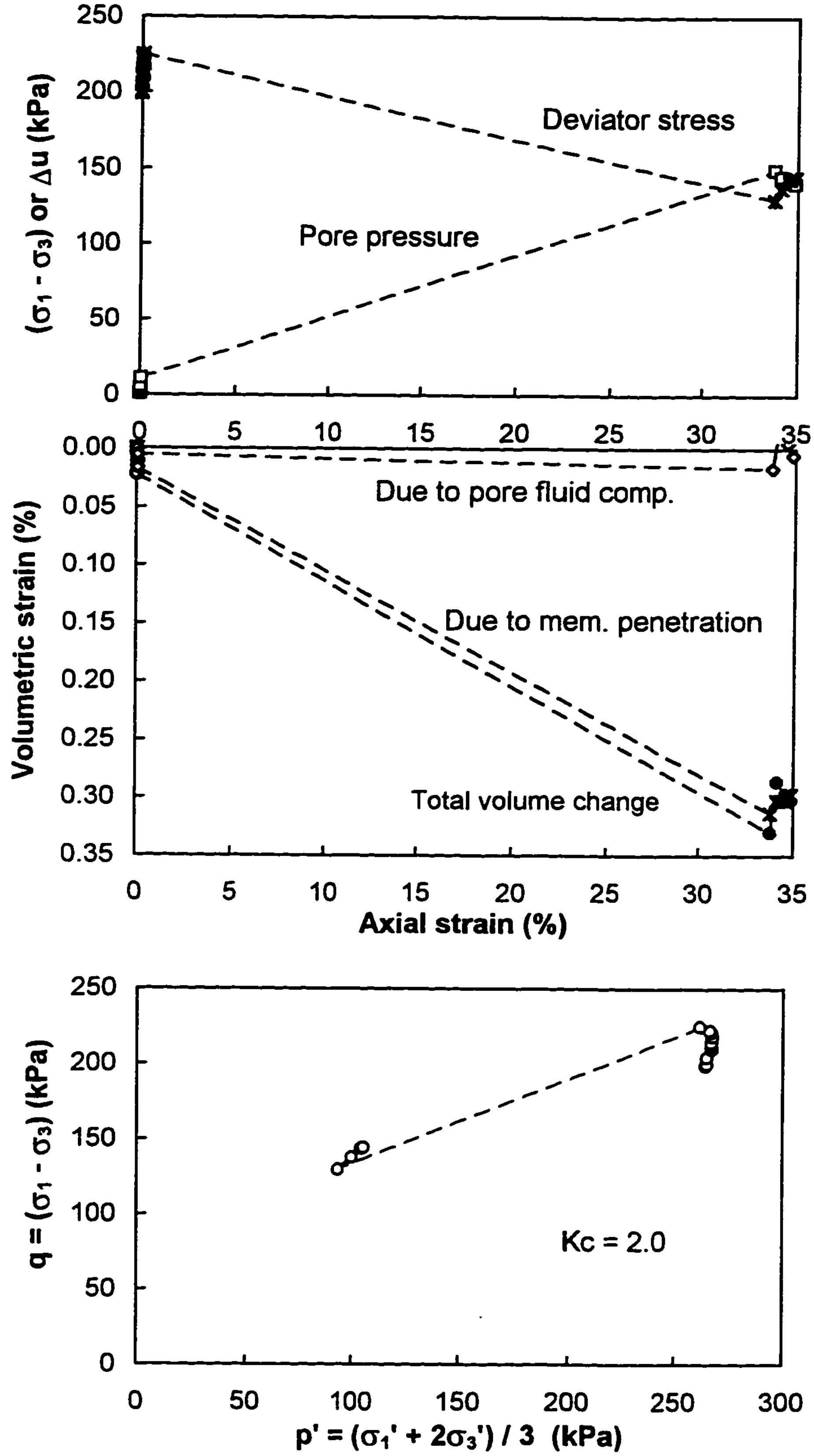

Fig. A.34 Group 2, CAU test, Dr_c = 35.4%, σ_{3c}' = 198 kPa

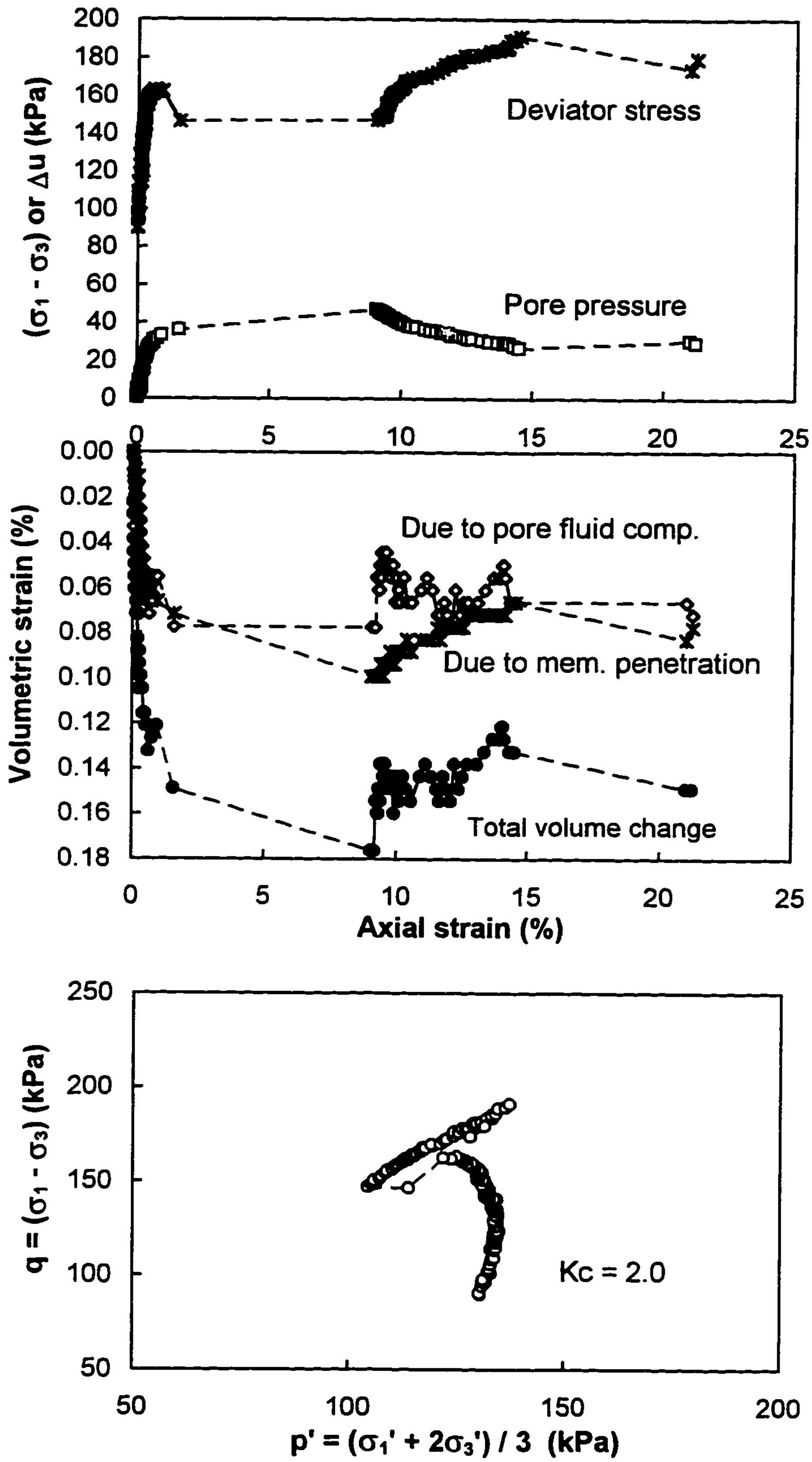

Fig. A.35 Group 2, CAU test, Dr_c = 36.8%, σ_{3c}' = 100 kPa

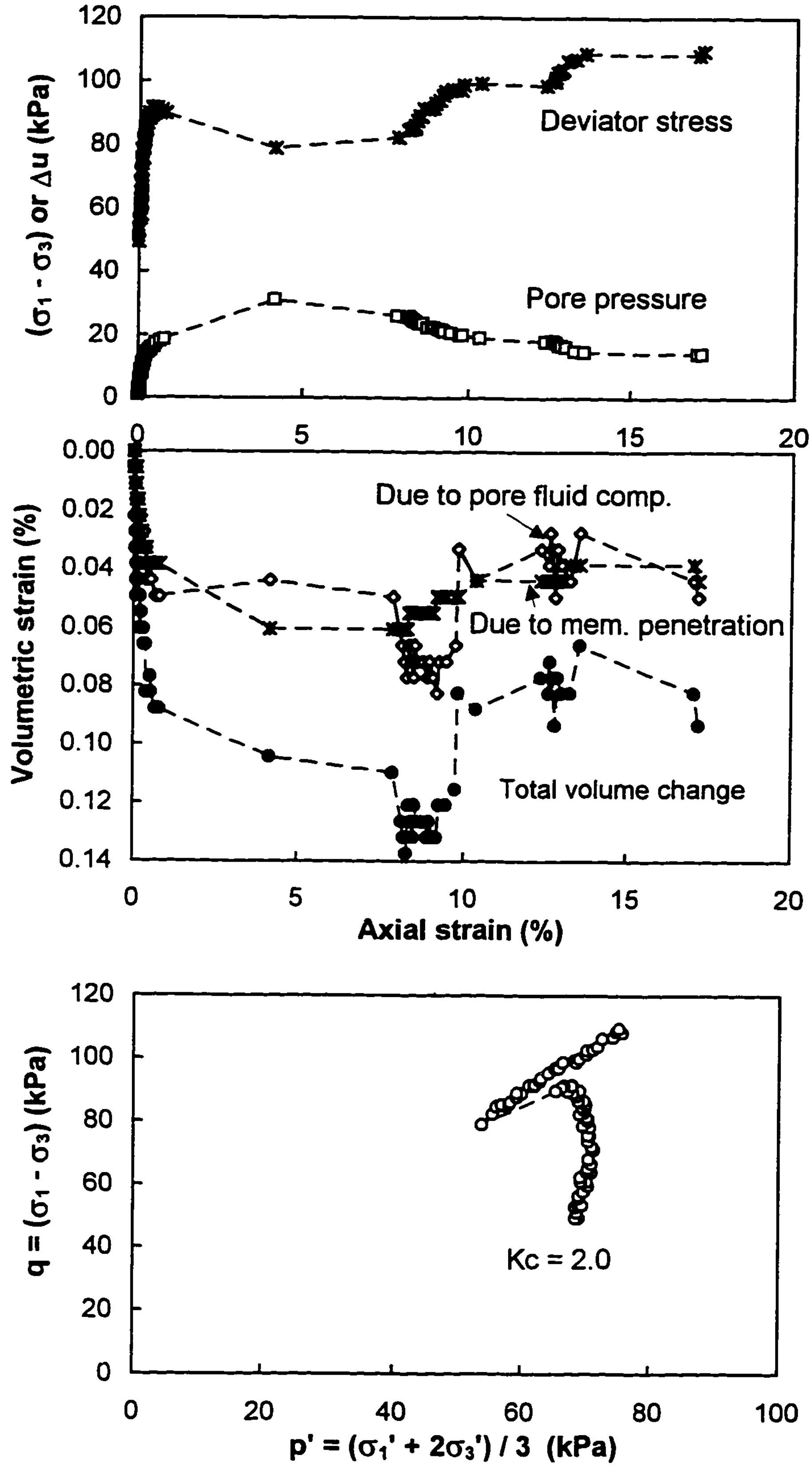

Fig. A.36 Group 2, CAU test, Dr_c = 40.0%, σ_{3c}' = 53 kPa

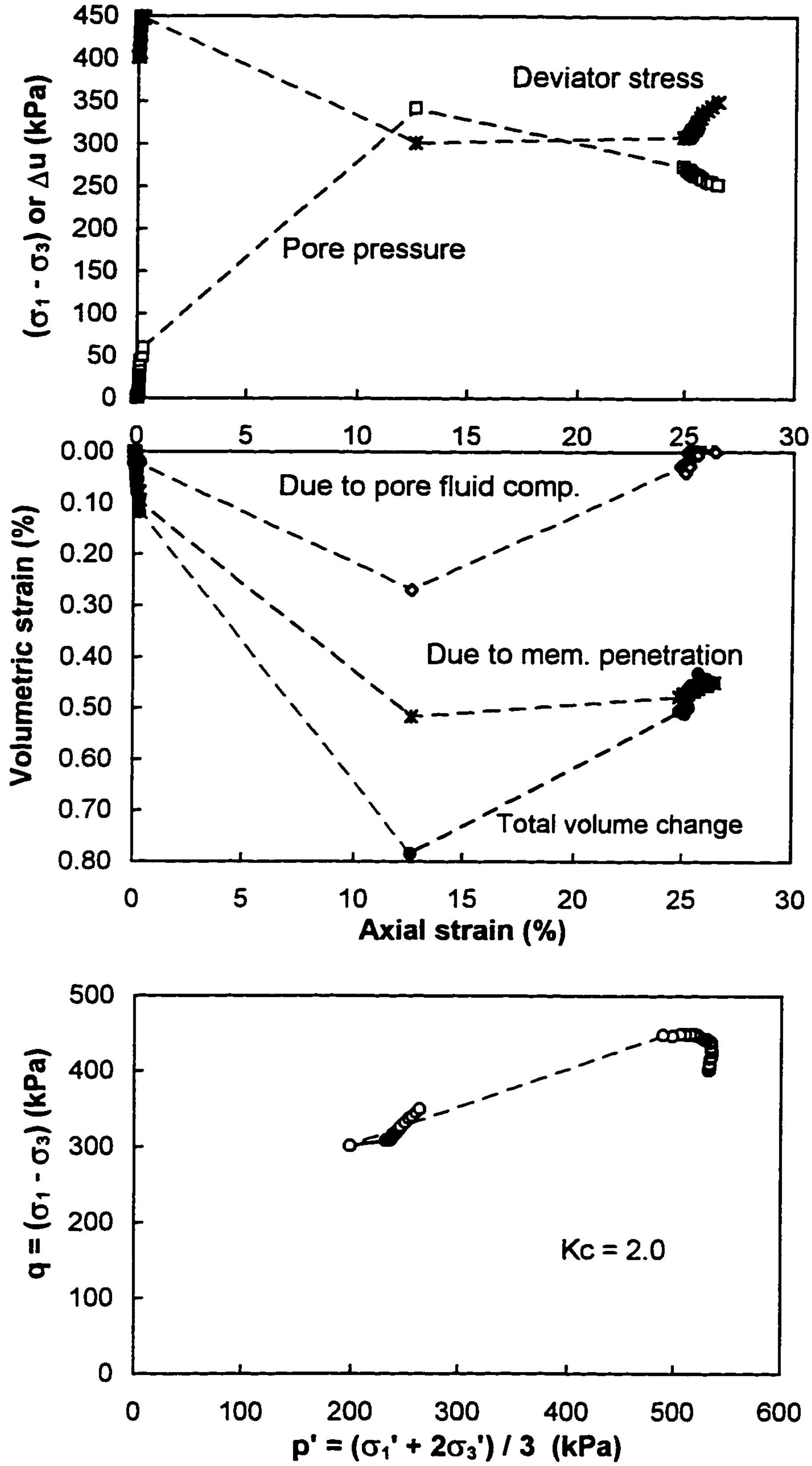

Fig. A.37 Group 2, CAU test, Dr_c = 45.5%, σ_{3c}' = 399 kPa

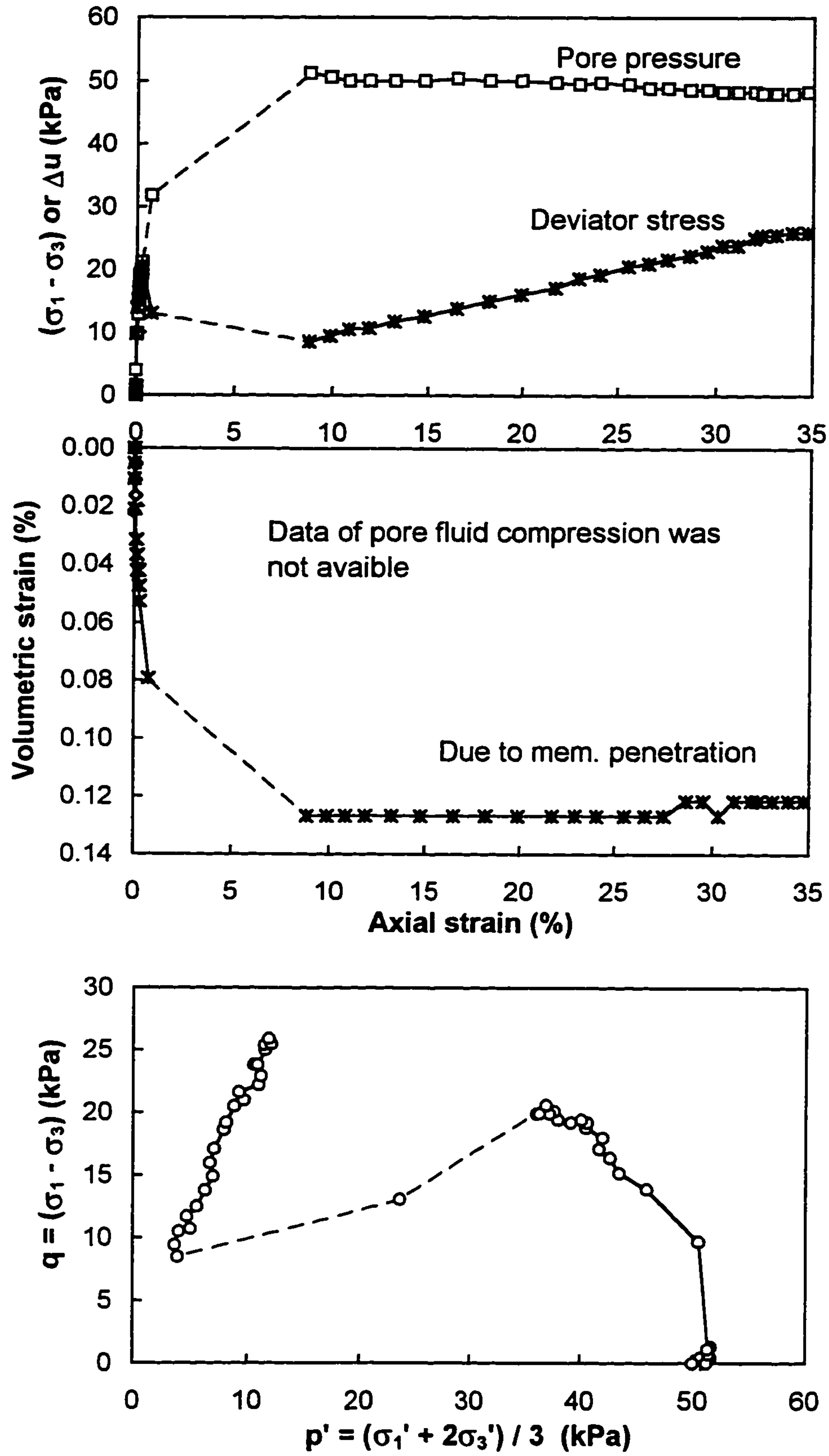

Fig. A.38 Group 2, CIU test, Dr_c = 25.6%, σ_{3c}' = 52 kPa

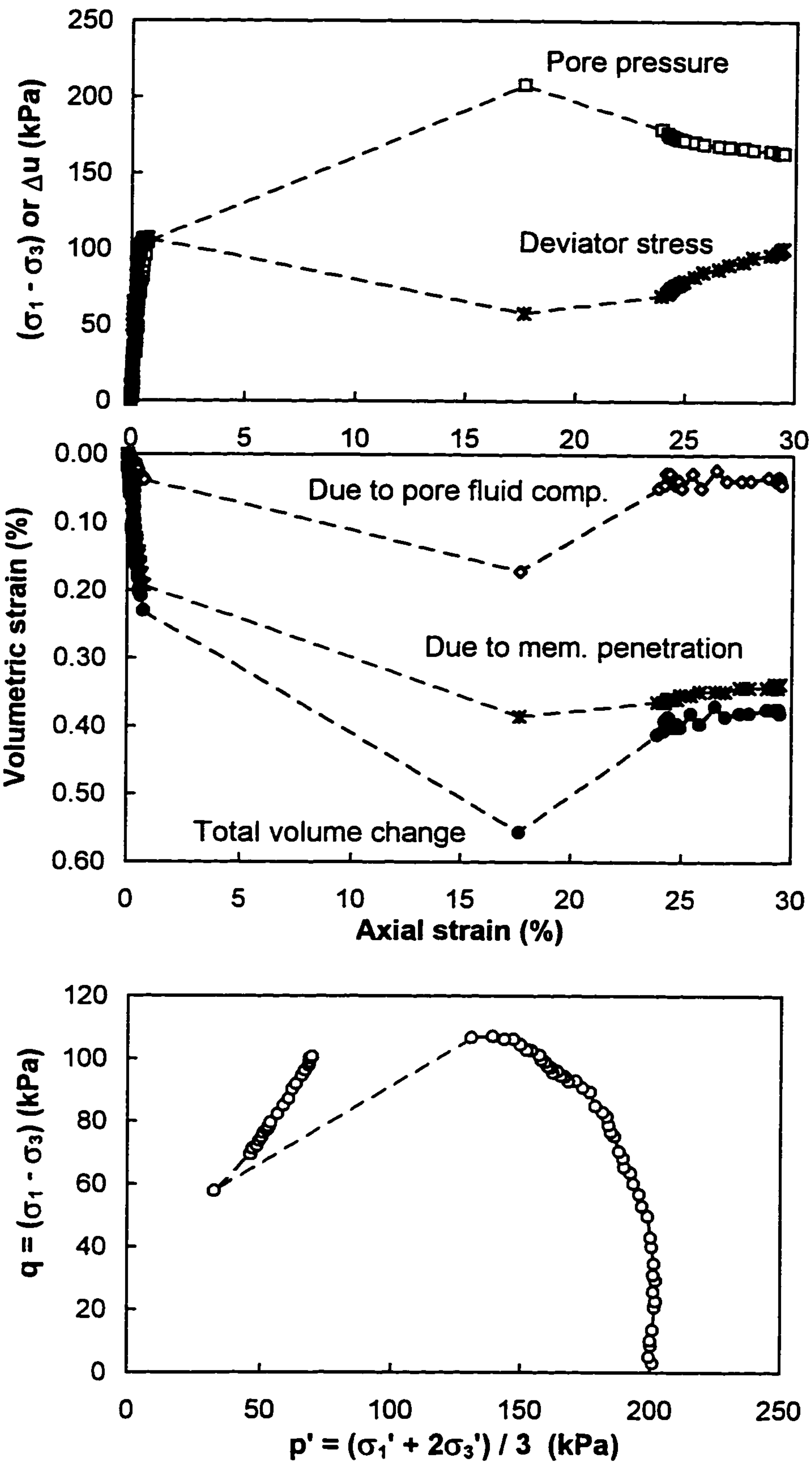

Fig. A.39 Group 2, CIU test, Dr_c = 31.5%, σ_{3c}' = 200 kPa

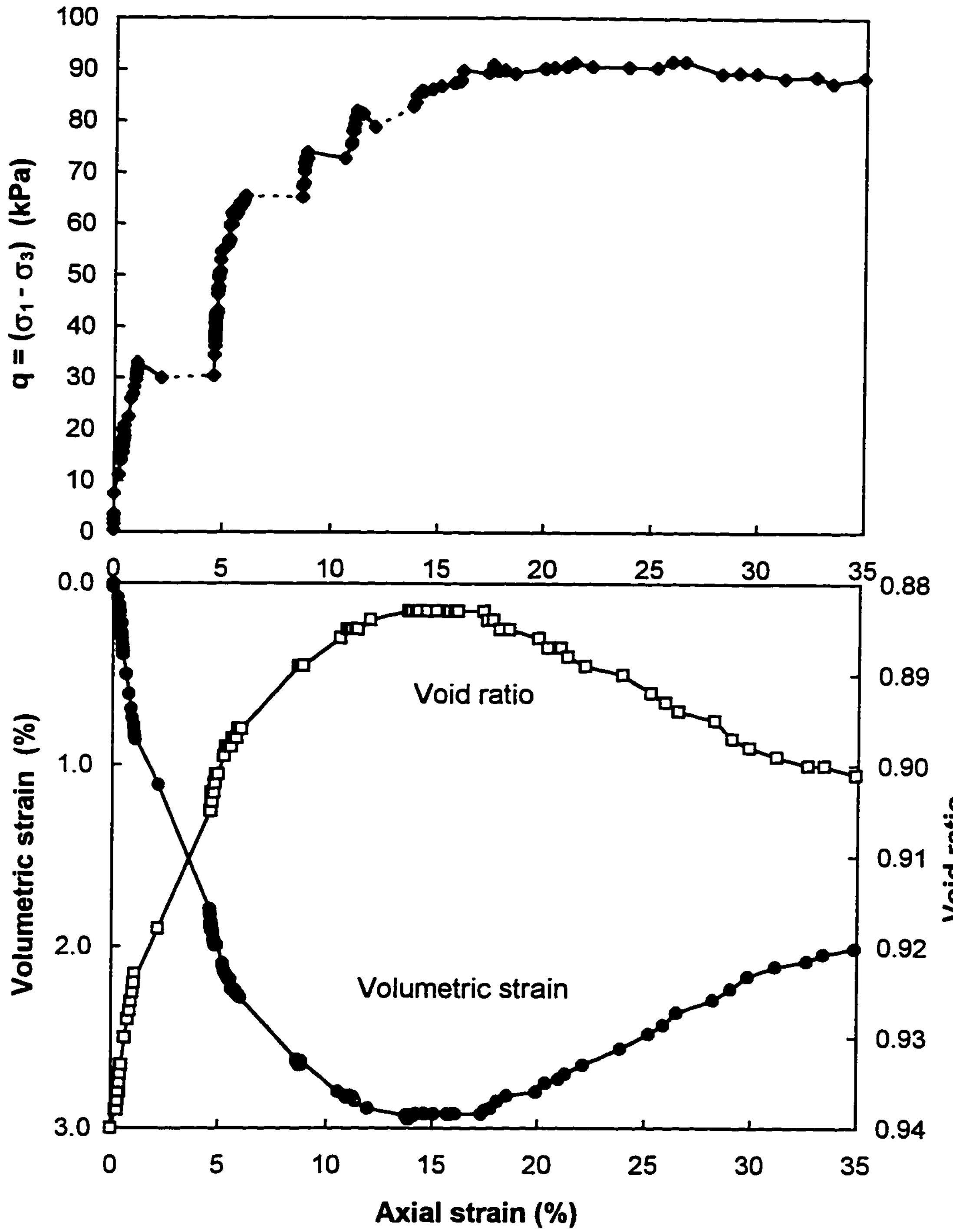

Fig. A.40 Group 2, CD test, Dr_c = 25.6 %, σ_{3c}' = 30 kPa

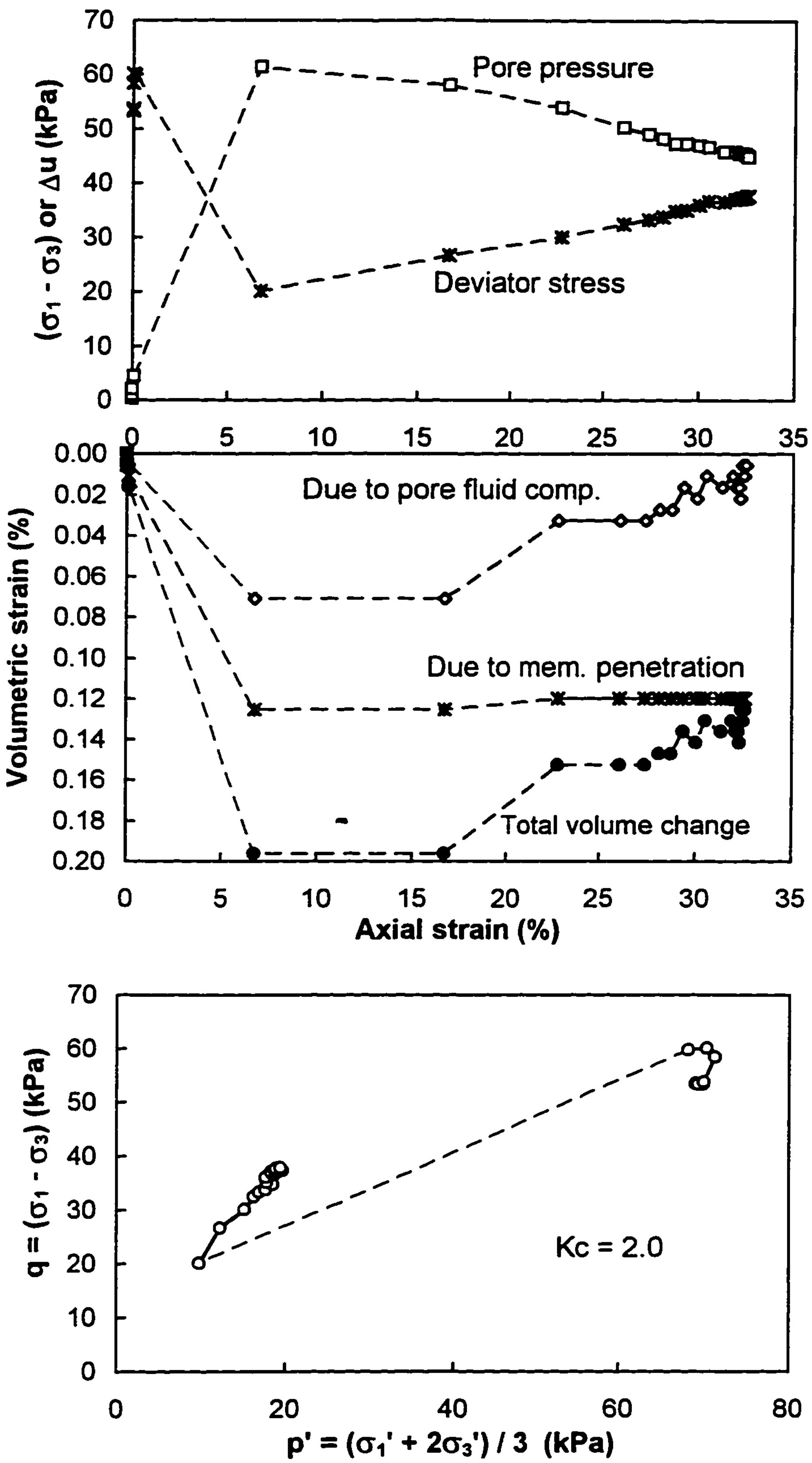

Fig. A.41 Group 3, CAU test, Dr_c = 15.8%, σ_{3c}' = 52 kPa

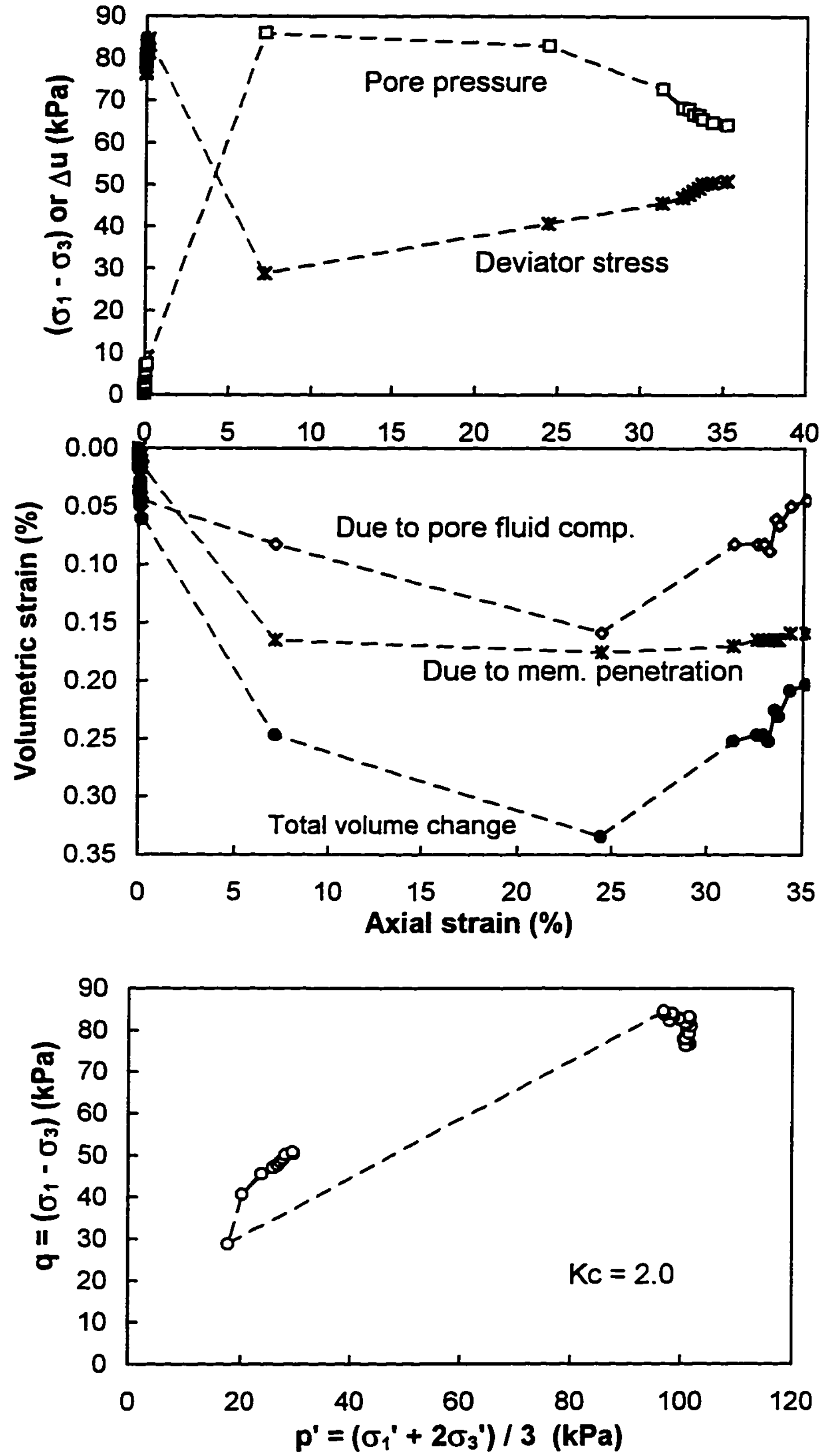

Fig. A.42 Group 3, CAU test, Dr_c = 19.3%, σ_{3c}' = 76 kPa

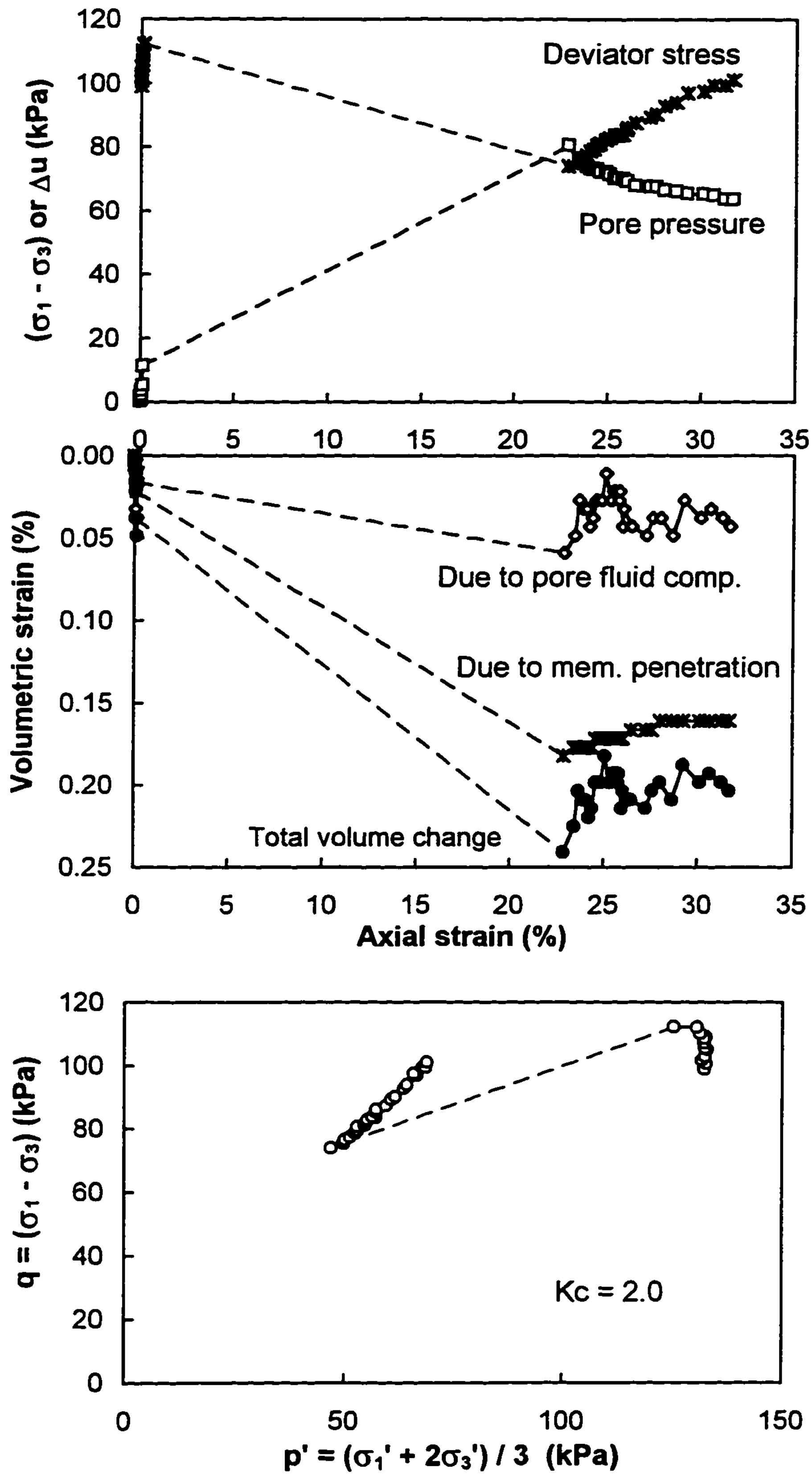

Fig. A.43 Group 3, CAU test, Dr_c = 22.6%, σ_{3c}' = 100 kPa

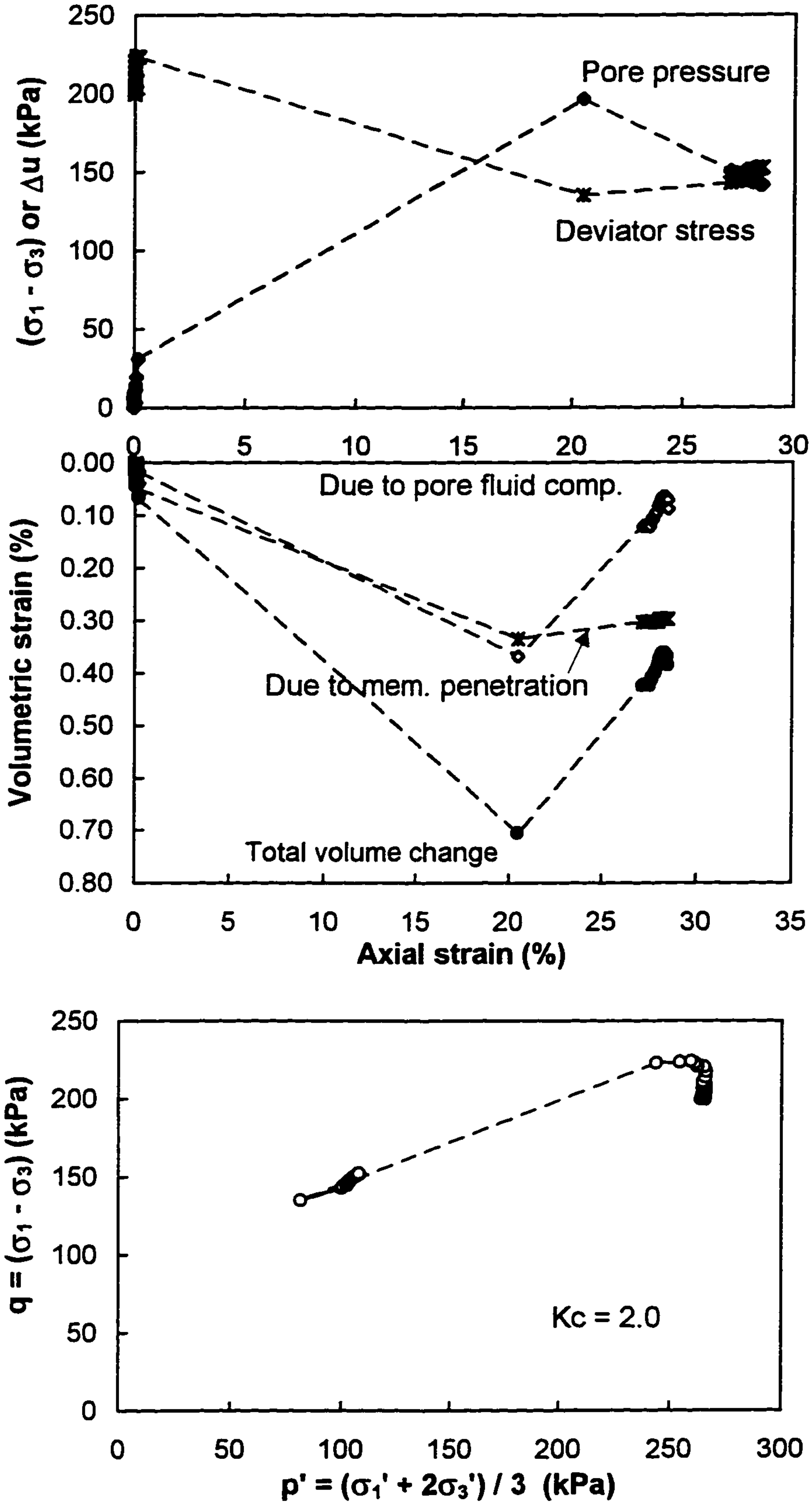

Fig. A.44 Group 3, CAU test, Dr_c = 26.7%, σ_{3c}' = 199 kPa

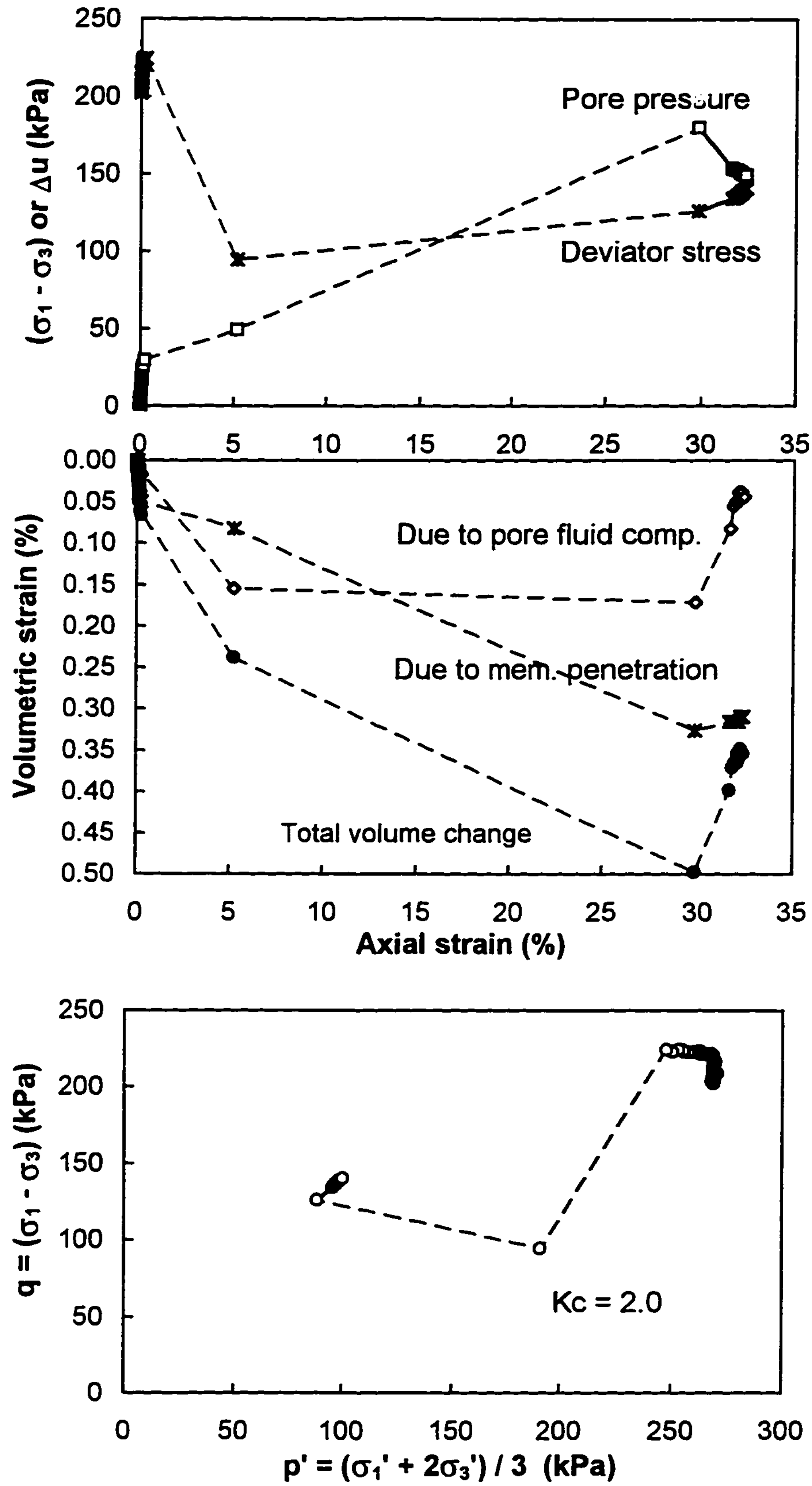

Fig. A.45 Group 3, CAU test, Dr_c = 28.5%, σ_{3c}' = 202 kPa

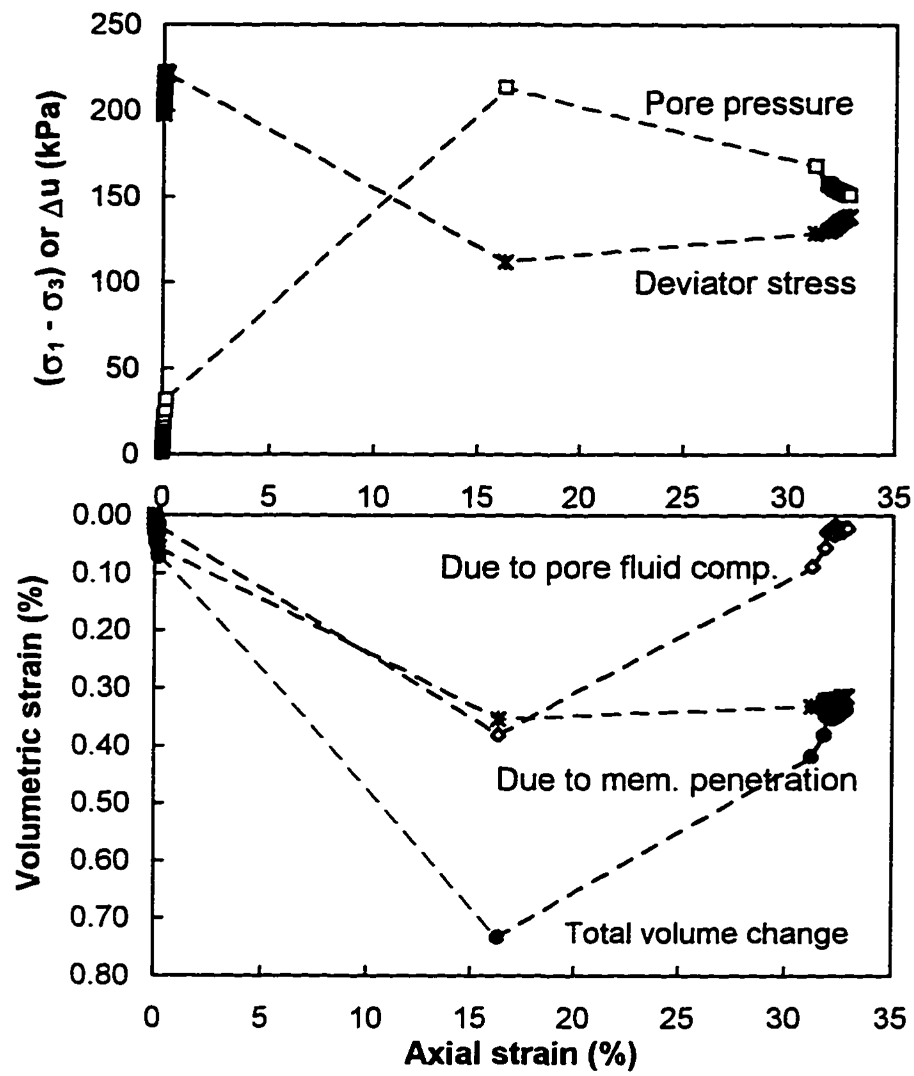

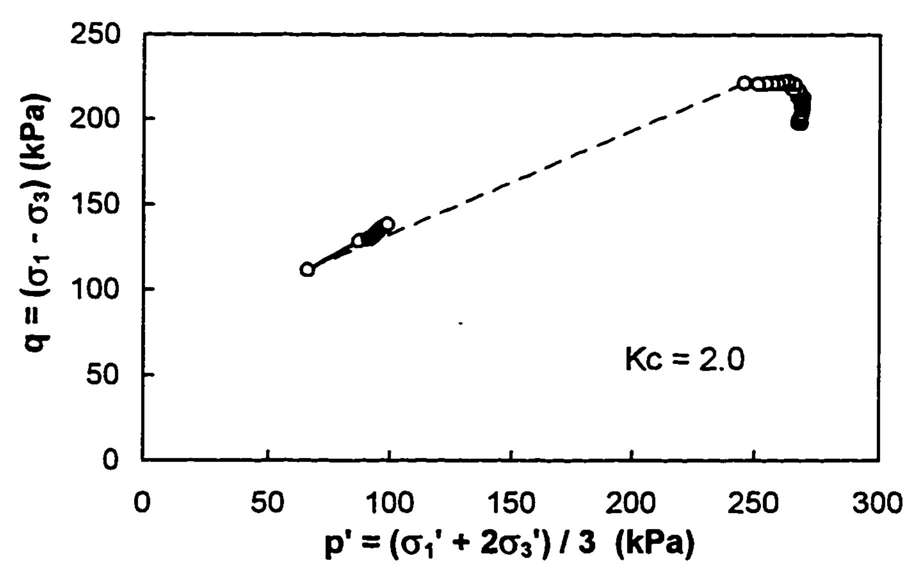

Fig. A.46 Group 3, CAU test, Dr_c = 26.7%, σ_{3c}' = 202 kPa

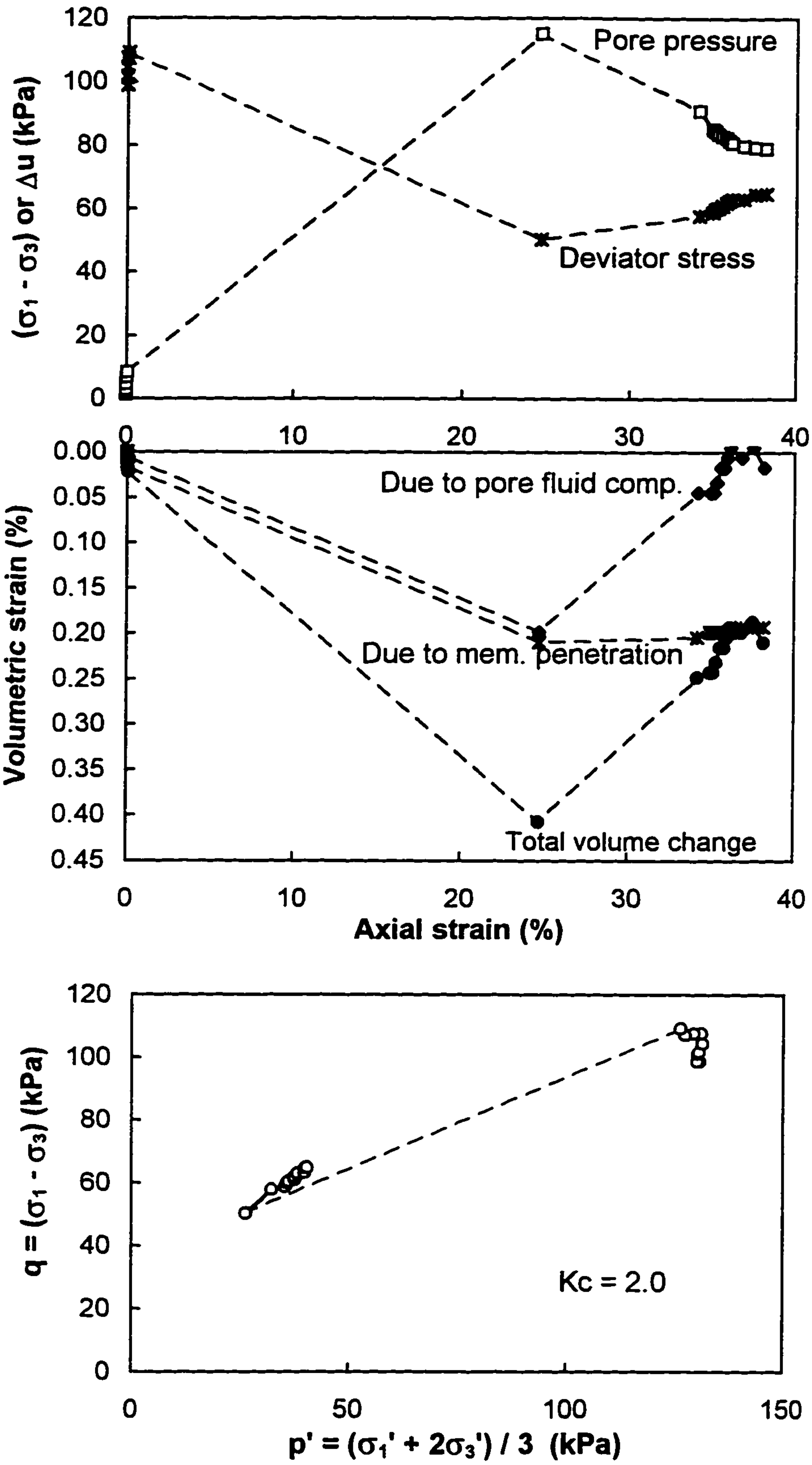

Fig. A.47 Group 3, CAU test, Dr_c = 20.8%, σ_{3c}' = 98 kPa

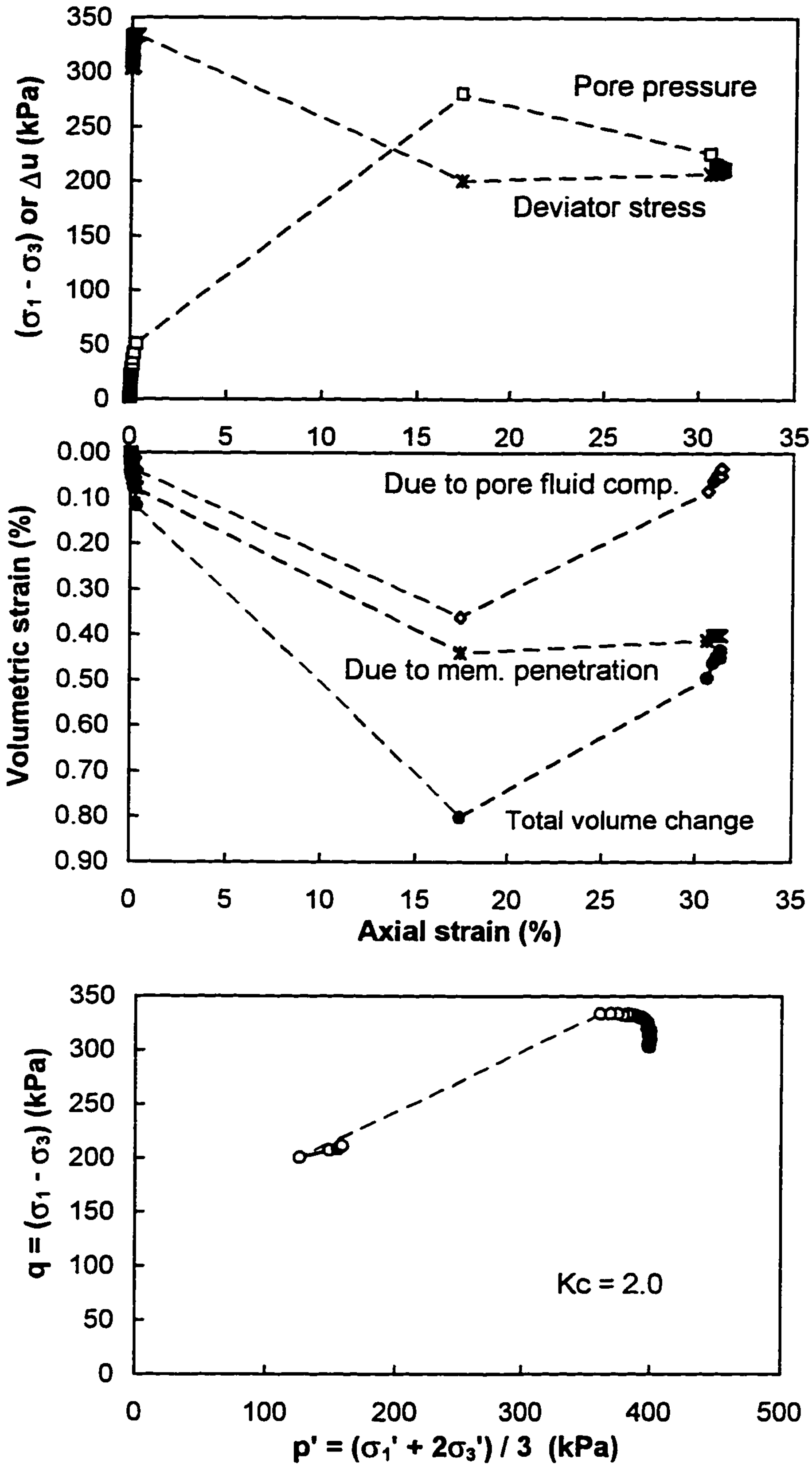

Fig. A.48 Group 3, CAU test, Dr_c = 32.2%, σ_{3c}' = 298 kPa

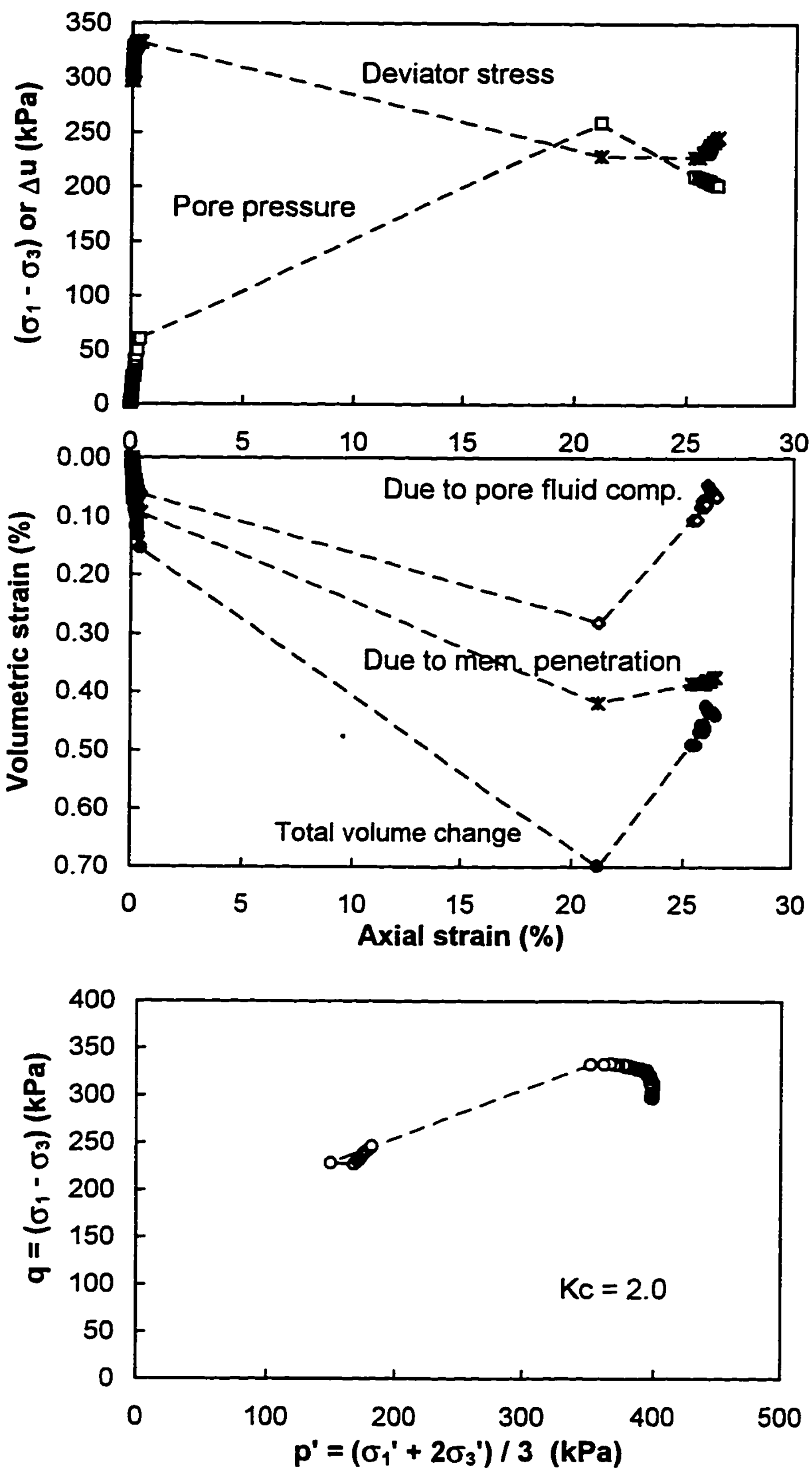

Fig. A.49 Group 3, CAU test, Dr_c = 35.4%, σ_{3c}' = 300 kPa

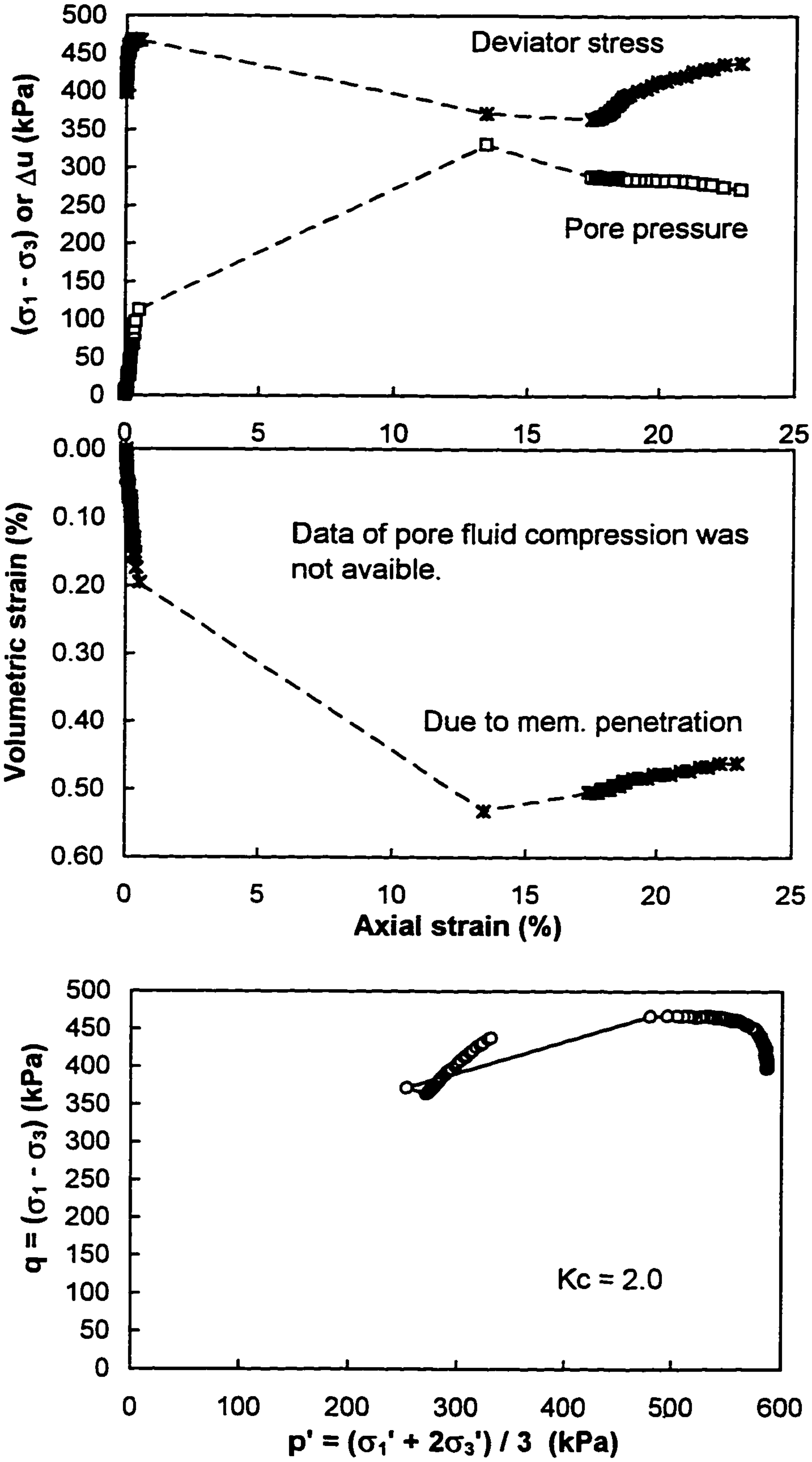

Fig. A.50 Group 3, CAU test, Dr_c = 38.2%, σ_{3c}' = 455 kPa

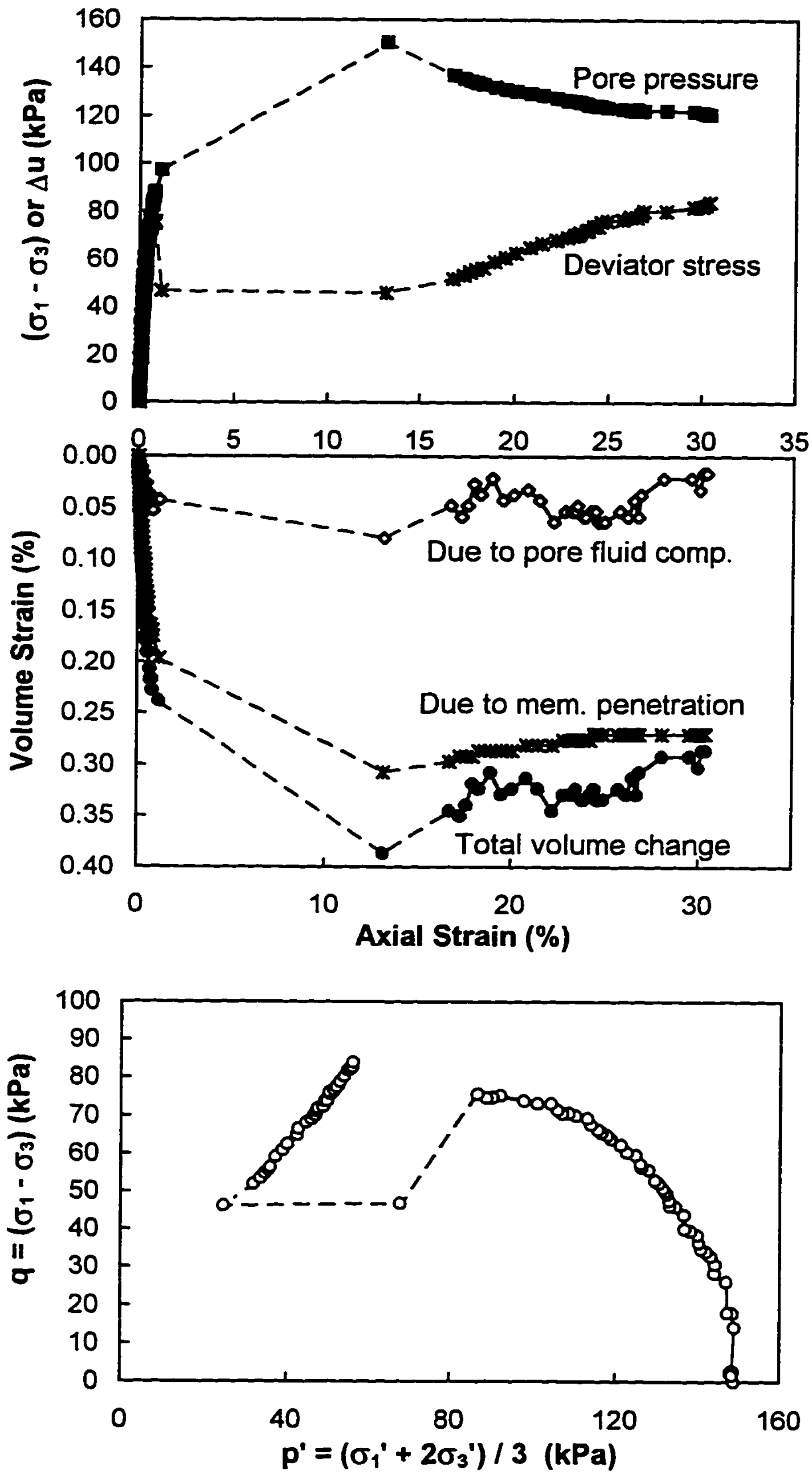

Fig. A.51 Group 3, CIU test, Dr_c = 22.3%, σ_{3c}' = 149 kPa

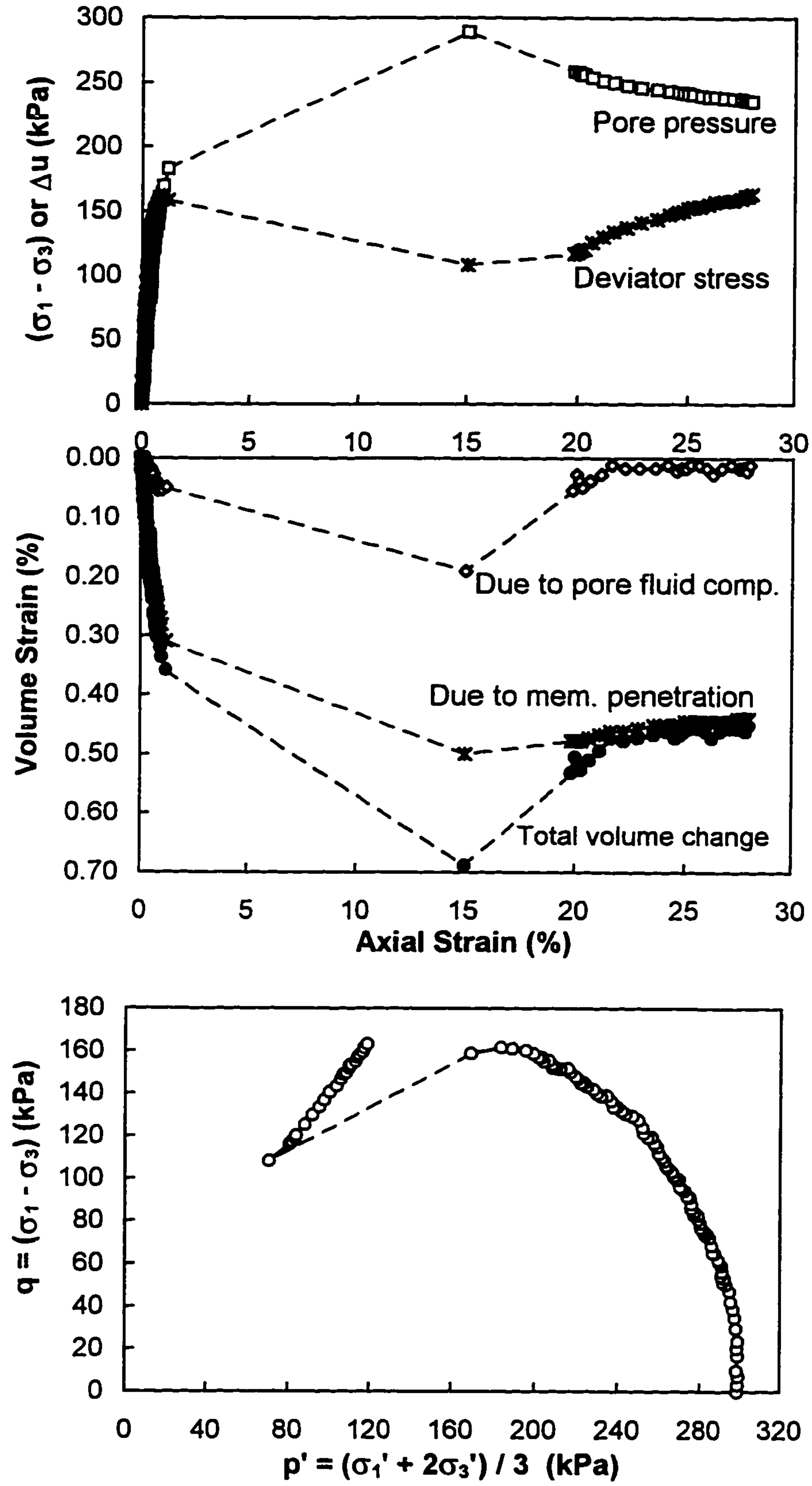

Fig. A.52 Group 3, CIU test, Dr_c = 28.9%, σ_{3c}' = 299 kPa

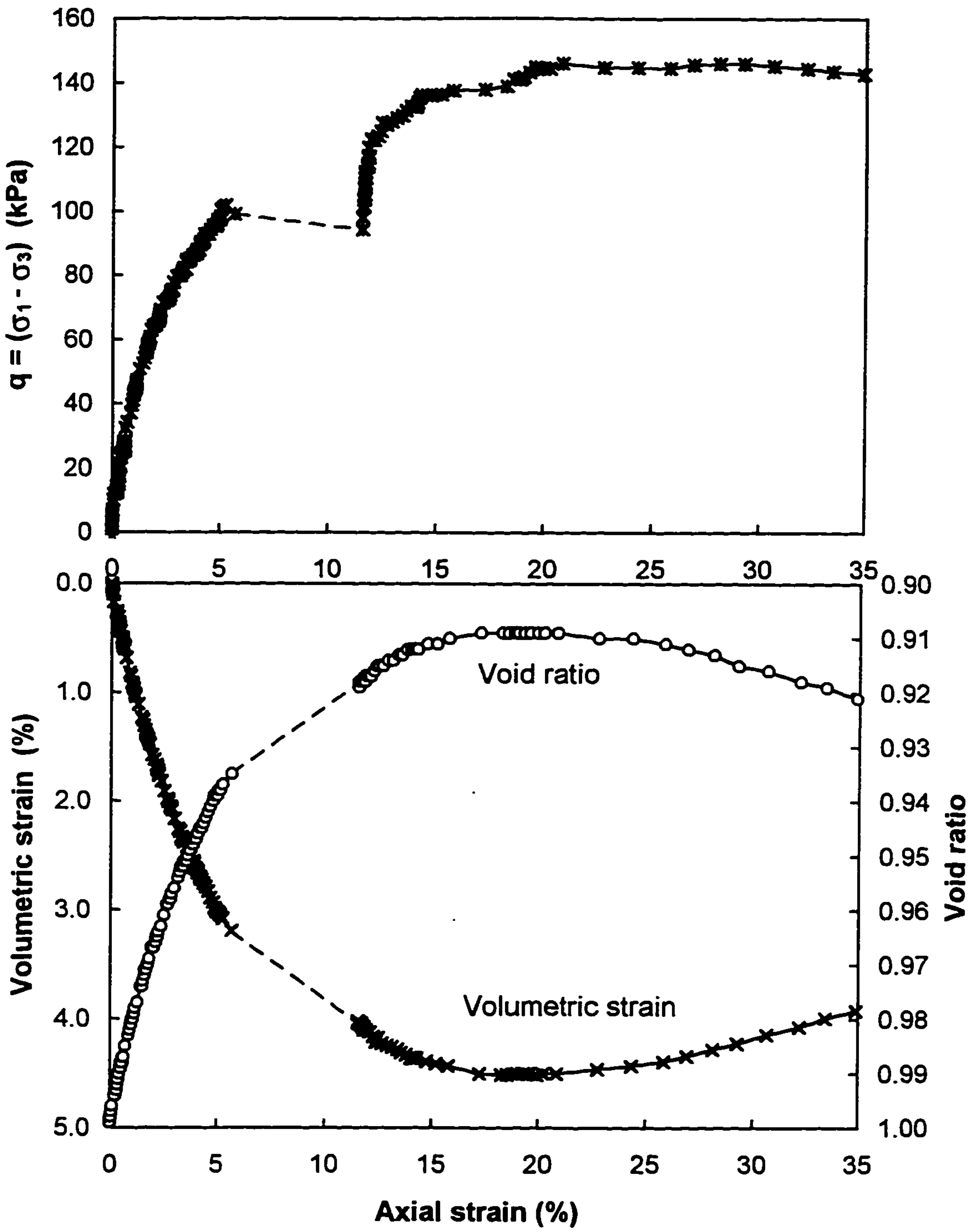

Fig. A.53 Group 3, CD test, Dr_c = 10.0 %, σ_{3c}' = 52 kPa

APPENDIX B:

PHOTOGRAPHS OF APPARATUS

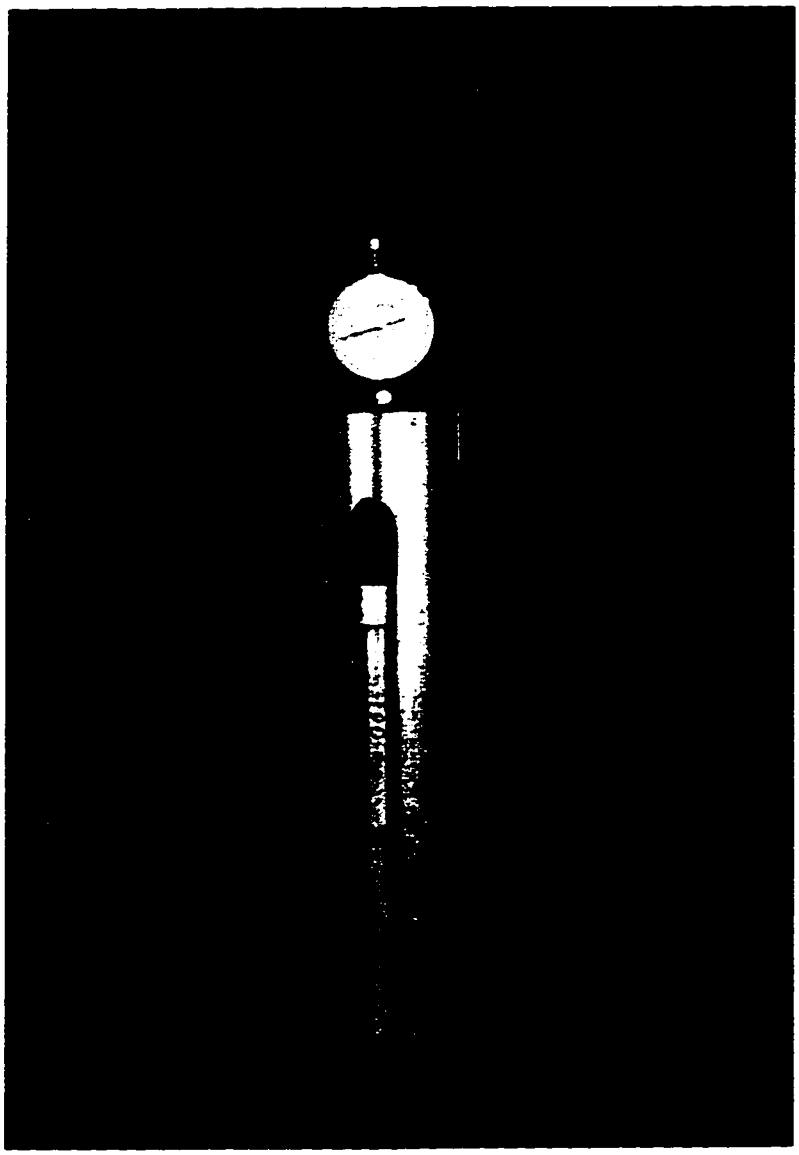

Photo. A.1 Height gauge

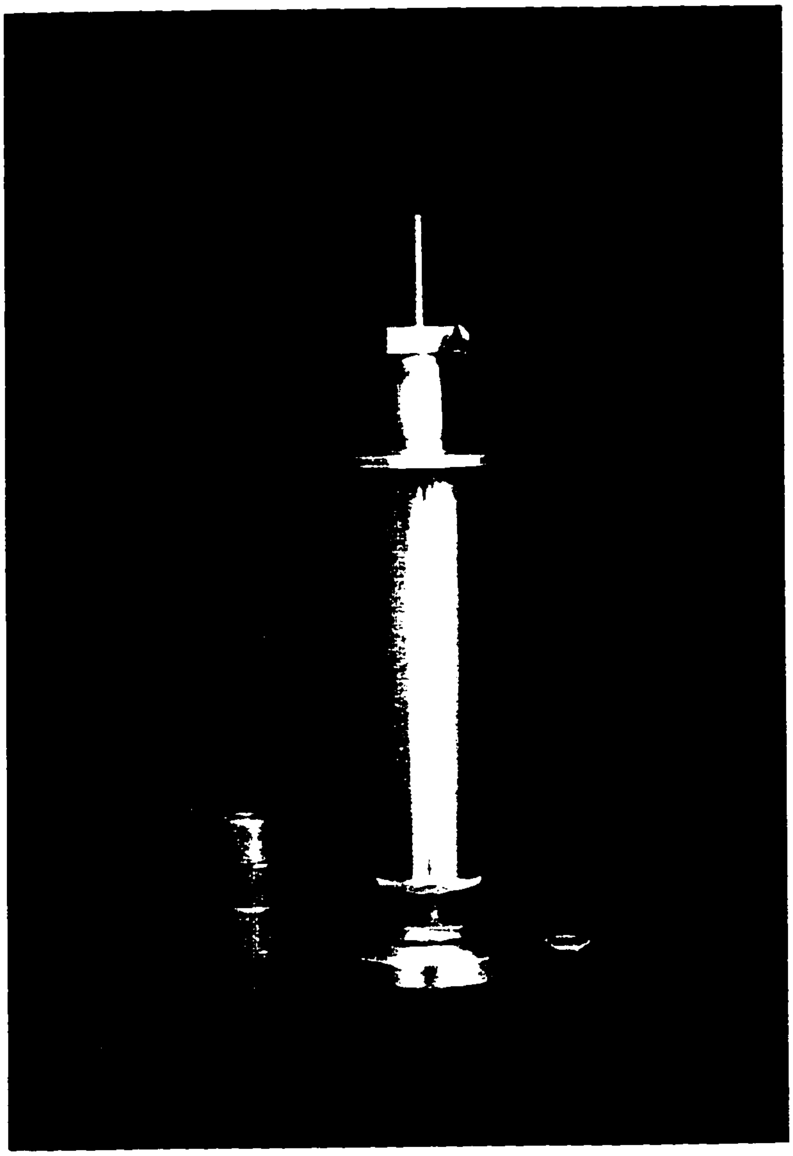

Photo. A.2 Tamping device

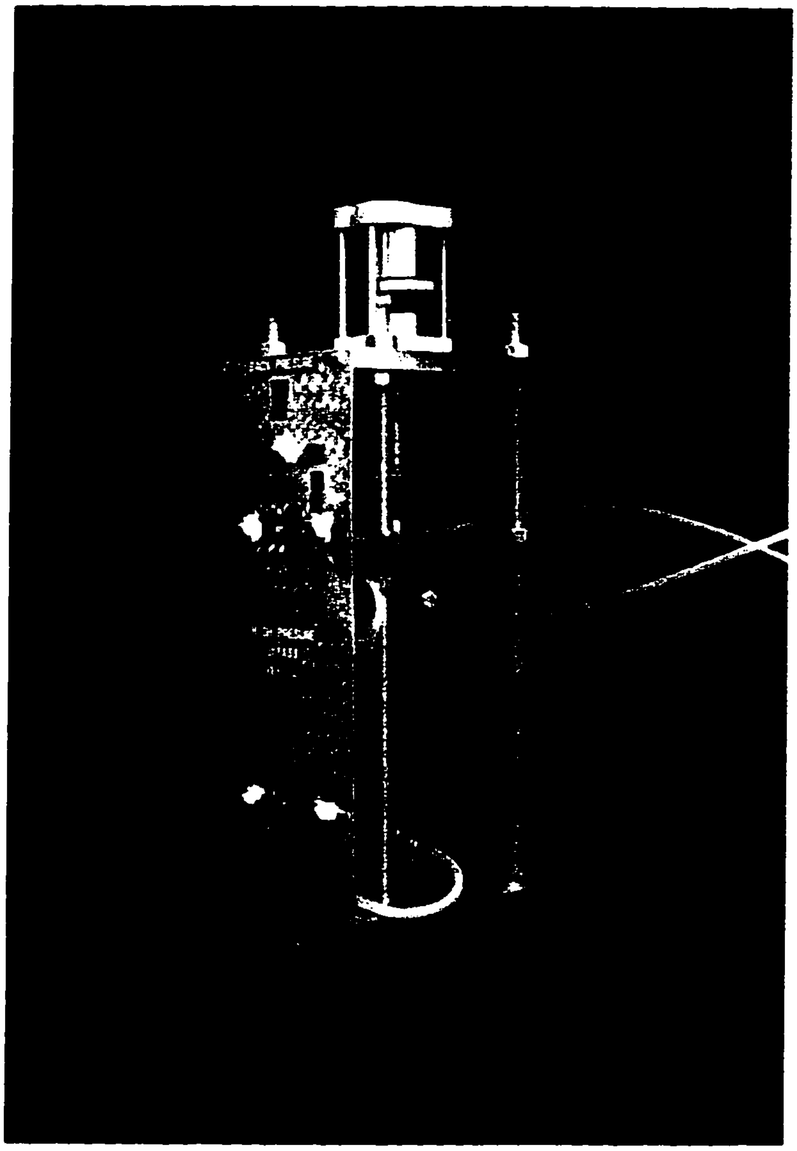

Photo A.3 Pressure booster

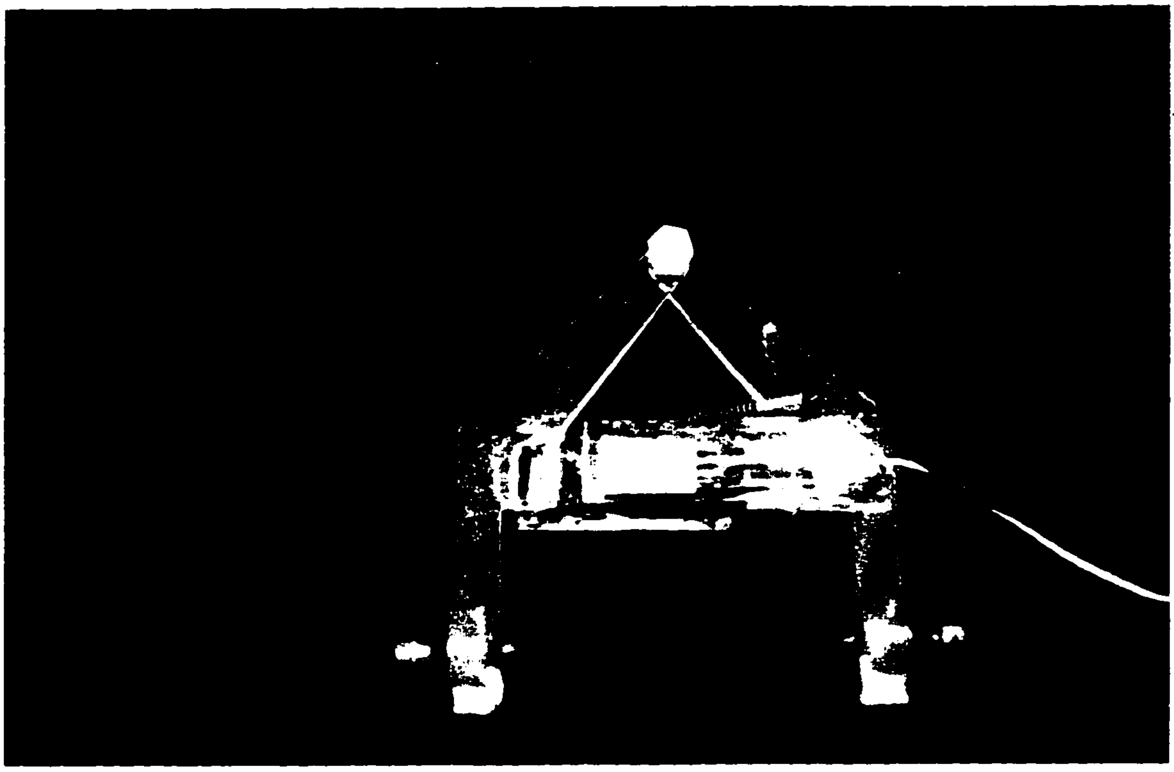

Photo. A.5 Hall Effect radial displacement transducer (HRDT)

Photo. A.5 Membrane checker

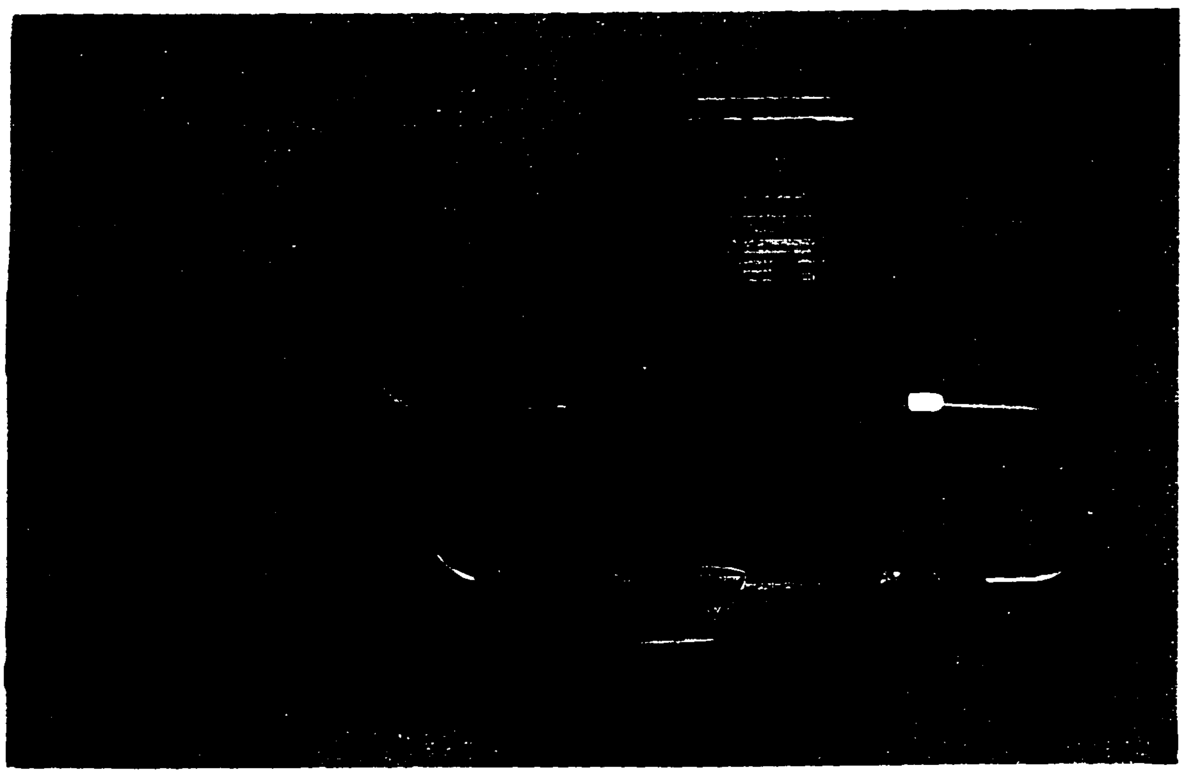

Photo. A.6 Air pressure amplifier